D5.2: Experimentation results

Revision: v.0.7

Work package	WP5
Task	Task 5.2, T5.4 and T5.5 (and updates to tasks 5.1 and 5.3)
Due date	31/12/2025
Submission date	15/12/2025
Deliverable lead	Nokia
Version	1.0
Authors	VTT's team: Olli Apilo, Mikko Uitto, Seppo J Rantala, Mikko Hongisto. UOULU's team: Hamid Malik, Juho Markkula, Faheem Shahid, Erkki Harjula, Jaakko Sirviö (Nokia)
Reviewers	Arne Erdmann (Raytrix), Javier Fernandez Hidalgo (i2CAT), Mohammed Al-Rawi (IT), Jonathan Rodriguez (IT)
Abstract	This final report details and summarizes experimentation results of the WP5 Energy Self-sustainable Network and Base Station with 3GPP gNB. Applied technical infrastructure was presented in D5.1 report "Description of sustainability experimentation framework". This report focuses on autonomous base station energy conservation technologies and their usage in test setups and trial runs. In addition, new sensor-based methodologies and AI tools for 48 h Energy Weather, and solar yield prognoses were developed to enable forecast-based control and energy efficiency optimization of the end-to-end (E2E) data transmission system containing adaptive RAN-components and video streaming. A methodology was developed to produce key performance indicators (e.g., energy-, CO2-, and € -savings), and it was applied to practical validation trials of the developed demonstrated system.
Keywords	Proposals: Energy measurement framework, Energy Weather forecast, Dynamic Energy Storage System, Radio Access Network, Open Air Interface, Next Generation Node B, Photovoltaic systems, PV yield prognoses, end-to-end data-pathway.

Co-funded by the European Union
6GSNS
WWW.6G-XR.EU
Grant Agreement No.: 101096838
Call: HORIZON-JU-SNS-2022
Topic: HORIZON-JU-SNS-2022-STREAM-C-01-01
Type of action: HORIZON-JU-RIA

Document Revision History

Version	Date	Description of change	List of contributor(s)
V0.1	06/11/2024	1st version of the template (ToC)	Hamid Malik (UOULU), Mikko Hongisto (VTT)
V0.2	27.05.2025	Interim report	VTT's team: Olli Apilo, Mikko Uitto, Seppo J Rantala, Mikko Hongisto. UOULU's team: Hamid Malik, Juho Markkula
V0.3	18.11.2025	Chapter 5.2	Faheem Shahid, Erkki Harjula (UOULU)
V0.4	20.11.2025	Finalizing all chapters	Hamid (UOULU), VTT's team: Olli Apilo, Mikko Uitto, Seppo J Rantala, Mikko Hongisto
V0.5	21.11.2025	External reviews	Arne Erdmann (Raytrix), Javier Fernandez Hidalgo (i2CAT
V0.6	05.12.2025	External reviews comments resolved	Hamid Malik, Olli Apilo, Mikko Uitto, Mikko Hongisto
V0.7	09.12.2025	Technical reviews	Mohammed Al-Rawi (TM) and Jonathan Rodriguez (TM-Deputy)
V0.7	11.12.2025	Reference and numbering corrections	Olli Apilo, Mikko Hongisto
V1.0	12.12.2025	Final version	All

DISCLAIMER

Co-funded by the European Union

6GSNS

Project funded by

Schweizerische Eidgenossenschaft
Confédération suisse
Confederazione Svizzera
Confederaziun svizra

Swiss Confederation

Federal Department of Economic Affairs, Education and Research EAER
State Secretariat for Education, Research and Innovation SERI

6G-XR (*6G eXperimental Research infrastructure to enable next-generation XR services*) project has received funding from the **Smart Networks and Services Joint Undertaking (SNS JU)** under the European Union's **Horizon Europe research and innovation programme** under Grant Agreement No 101096838. This work has received funding from the **Swiss State Secretariat for Education, Research, and Innovation (SERI)**.

COPYRIGHT NOTICE

Project co-funded by the European Commission in the Horizon Europe Programme		
Nature of the deliverable:	**to specify R, DEM, DEC, DATA, DMP, ETHICS, SECURITY, OTHER***	
Dissemination Level		
PU	*Public, fully open, e.g., web (Deliverables flagged as public will be automatically published in the CORDIS project's page)*	✓
SEN	*Sensitive, limited under the conditions of the Grant Agreement*	
Classified R-UE/ EU-R	*EU RESTRICTED under the Commission Decision No2015/ 444*	
Classified C-UE/ EU-C	*EU CONFIDENTIAL under the Commission Decision No2015/ 444*	
Classified S-UE/ EU-S	*EU SECRET under the Commission Decision No2015/ 444*	

* R: Document, report (excluding the periodic and final reports)

DEM: Demonstrator, pilot, prototype, plan designs

DEC: Websites, patent filings, press & media actions, videos, etc.

DATA: Data sets, microdata, etc.

DMP: Data management plan

ETHICS: Deliverables related to ethics issues.

SECURITY: Deliverables related to security issues

OTHER: Software, technical diagram, algorithms, models, etc.

EXECUTIVE SUMMARY

This deliverable summarizes the work done in WP5. Solar energy production and battery energy storage are integrated for 5G radio access networks (RAN) whose energy consumption is accurately monitored using the developed energy measurement framework. The system also includes AI tools for predicting green energy production, which helps to proactively set guidelines on how the base station energy consumption and associated video clients should be controlled by energy-saving features. The system is validated against the defined key performance indicators (KPI) in long end-to-end (E2E) energy optimization tests, where the RAN power saving states and the video traffic resolution are adapted according to the solar energy availability.

For base stations, significant energy saving improvements were demonstrated. Techniques such as discontinuous transmission (DTX), multiple-input multiple-output (MIMO) muting, cell blocking, and sleep modes reduced power consumption by up to 51% in idle conditions and 26% under typical traffic patterns. A RAN controller was developed to enable external control of power-saving states and integrated into an end-to-end optimization framework.

The energy weather forecast developed to enhance the prediction of photovoltaic (PV) production and guide the consumption pattern of the base station sites delivers highly accurate results on an hourly basis, showing strong correlation of 0.974 with real PV outputs, RMSE of 27%, and daily aggregated accuracy staying within ±8%. The accuracy of the forecasting APIs was tested and validated using multiple test runs.

Adaptive control of both RAN and video applications based on solar energy availability achieved notable gains. Video optimization through reduced resolution and bitrate delivered 43% energy savings per client with minimal impact on user experience. Validation tests confirmed that combined adaptive strategies lowered overall energy consumption by 36.8%, while grid-intake depended effective operational costs and indirect CO_2 emissions dropped by 86.9% and 84.6%, respectively. Additionally, trials with a solar power supply system (a PV-hybrid with battery energy storage) indicated that 70-80% of grid energy could be replaced by local solar energy (in Oulu region, during sunny periods) using advanced multifunctional inverter technology and $LiFePO_4$ battery, further enhancing sustainability and resilience.

In parallel, the ORAN setup was used to validate energy-saving methods while using different combinations of RAN configurations. Overall, RAN optimization inside the OAIBOX reduced total gNB and USRP N310 power consumption by 15.4%, lowered daily CO_2 emissions by 55–72 g, and delivered measurable cost savings when aligned with dynamic electricity pricing.

TABLE OF CONTENTS

LIST OF FIGURES

LIST OF TABLES

ABBREVIATIONS

5GNR	5G New Radio
AC	Alternating Current
AI	Artificial Intelligence
API	Application Programming Interface
APP	Application
BBU	Baseband Unit
BESS	Battery Energy Storage System
CAPEX	Capital expenditure
CC	Central Controller
CN	Core Network
CSI-RS	Channel State Information Reference Signal
DASH	Dynamic Adaptive Streaming over HTTP
DC	Direct Current
DESS	Dynamic Energy Storage System
DL	Downlink
DM	Decision Making
DRX	Discontinuous Reception
DSO	Distribution System Operator (electricity supply)
DTX	Discontinuous Transmission
DU	Distributed Unit
E2E	End-to-End
ELSPOT	Electricity Spot Market
FDD	Frequency Division Duplexing
FIFO	First In, First Out
FMI	Finnish Meteorological Institute
gNB	Next Generation NodeB

GSM	Global System for Mobile communications
GSMA	GSM Association
HTTP	Hypertext Transfer Protocol
IP	Internet Protocol
KPI	Key Performance Indicator
KVI	Key Value Indicator
LFP	Lithium Iron Phosphate, also LiFePO4
LTE	Long Term Evolution, 4G
MetCoOp	Meteorological Corporation
MIMO	Multiple-Input Multiple-Output
ML	Machine Learning
mMIMO	massive-MIMO
MCS	Modulation and Coding Scheme
MPPT	Maximum power point tracking
MQTT	Message Queuing Telemetry Transport
MU-MIMO	Multi-User MIMO
NG	Next Generation
OFDM	Orthogonal Frequency Division Multiplexing
O&M	Operation and Management
OPEX	Operational Expenditure
PDSCH	Physical Downlink Shared Channel
PRB	Physical Resource Block
PV	Photovoltaic system
QoE	Quality of Experience
QoS	Quality of Service
RAN	Radio Access Network
RES	Renewable Energy Sources

RRC	Radio Resource Control
RRH	Remote Radio Head
RSRP	Reference Signal Received Power
RTSP	Real-time Streaming Protocol
RTMP	Real-time Messaging Protocol
RU	Radio Unit
SA	Standalone
SDR	Software-Defined Radio
SoC	State of Charge (%)
SoH	State of health (%, battery)
SSB	Synchronization Signal Block
TCP	Transmission Control Protocol
TDD	Time Division Duplexing
TSO	Transmission System Operator (National Electricity Grid)
Tx	Transmitted
UE	User Equipment
UL	Uplink
USRP	Universal Software Radio Peripheral
VAT	Value added tax
VRM	Victron's cloud based Remote Monitoring -system
XR	Extended Reality

1 INTRODUCTION

This final report details and summarizes experimentation results of the 6G-XR Work Package 5 “Energy Self-sustainable Network and Base Station with 3GPP gNB”.

In the first phase of the project, technical research infrastructure was developed, and key elements of it were documented in the D5.1 report “Description of sustainability experimentation framework” [13]. Since the publication of D5.1, the North-Node research infrastructure was further developed, and energy measurement framework was also enlarged to cover O-RAN installations. Generated data streams were successfully applied in several 6G-XR’s collaborative open-call projects. Substantial methodological improvements, as well as integration work, were done after the D.5.1 publication, and that work was also documented in this report.

Especially, this final report focuses on autonomous base station energy conservation technologies (T5.2) and their usage in wider E2E test setups and trial runs. The report contains 6G-XR project progress for tasks T5.2: Autonomous base station energy conservation technologies. It also provides long-term follow-up results related to applied energy production systems, validates forecasting methodologies and presents results of T5.3 AI tools for 48 h Energy Weather (focusing solar yield prognoses of real installations). In addition, new sensor-based methodologies and AI tools for 48 h Energy Weather and solar yield prognoses are presented to enable forecast-based control of the entire E2E-system.

The report also describes the progress and integration efforts made in putting technical pieces and multidimensional data together to cover the entire end-to-end (E2E) data pathway in Task 5.4 E2E Energy Efficiency.

In addition to this report, an E2E-demonstration system was created and presented to make it more understandable how developed building blocks in the various WP5-tasks were applied together (data monitoring, external data-pipes, prognoses information, traffic profiles, control systems etc.). The created E2E-controller enabled communication with the dynamically adaptive RAN-elements and video transfer systems over the entire E2E-scope to achieve better system level energy efficiency and other KPI-dimensions.

Technical demonstration of the entire system was necessary to enable execution of the last integrative task T5.5: Validation and KPI & KVI assessment of self-sustainable network, where the first results of the savings and key performance indicators (energy-, CO_2-, and €-savings) were generated. T5.5 completes the work with validation activities. However, experimentation’s performance results in this report should be treated as preliminary results in applied data-context and trial periods and as a starting point for the practical usage of the entire E2E-system infrastructure, as well as developed methodologies. However, room for further improvements remains in every module of the E2E-control system.

1.1 BACKGROUND

In the entire 6G-XR context, WP5 was planned to be responsible for intensive research to create valuable assets and perform validation of a self-sustainable and energy-efficient wireless network. WP5 concentrated on the electricity consumption challenge. We also provided a framework and solutions for energy production and consumption measurements, investigated methods for reliable solar energy forecasts for sustainable energy, and expected energy needs based on traffic profiles. Energy consumption and viable solutions for the reduction of energy were studied with intelligent

control of the E2E data path components and services, including adaptive applications, Radio Access Network, as well as edge processing. Energy saving methods were investigated and developed to optimize the communication service considering expected energy weather. Measurement-based KPI results are provided covering energy-harvesting, storing, and consumption for a gNB site. Energy production and the overall measurement frame is defined in T5.1 (publication D5.1). Mechanisms for improving energy efficiency on the element level were investigated in T5.2 and advanced methods for forecasting and charging/discharging energy are investigated in T5.3. T5.4 examines E2E energy efficiency improvement techniques for mobile networks, and finally T5.5 completes the work with validation activities.

1.2 OBJECTIVES

The objective of this Deliverable is to compile most of the results obtained and achieved through the extensive usage of constructed experimentation facilities at the North Node of the 6G-XR project. Although D5.1 captures most of the specifications and framework issues, and part of T5.3 was accomplished up to the document's production. This document focuses more on the experimental results and was developed to final (public) deliverable D5.2.

The specific objectives of WP5 were:

- O5.1: Research and development of wireless communication networks towards autonomous, energy-optimized, and sustainable communication solutions.
- O5.2: Introduce a sustainability experimentation solution, including energy forecasting, production, storage, and consumption.
- O5.3: Research and develop energy optimization methods, including energy production and consumption with advanced methods aiming to boost the decarbonization of the runtime of the mobile networks and services.

2 UPDATES TO THE ENERGY MEASUREMENT FRAMEWORK AND DATASETS

A comprehensive real-time measurement and data-infrastructure was seen as a prerequisite for the research and development work aiming to gain energy savings and other indirect sustainability improvements. By means of this kind of infrastructure, more flexible demand-based control of telecommunication systems and even the entire end to end data-pathways were developed and tested. To achieve higher levels of self-sufficiency in the balanced system, both consumption and production side's electric and monitoring infrastructure was constructed. In addition to solar energy production units, the framework consists of electricity storage devices, controllable grid interface and distribution cabinets with protection.

We identified a need to improve methodologies, and quantitative understanding should be improved about the origin of electricity consumption in the complex E2E-system, as well as about factors, choices, and conditions affecting it. The operational environment as well as demand for services is fluctuating, and many external factors should be considered simultaneously when controlling these systems energy efficiently, smarter and more sustainable way. Accurate information showing the run-time impacts of various test trials in sufficiently standardized laboratory conditions, with a limited amount of confounding factors, was needed to develop the usage of energy-saving measures and automate the control of E2E- and power system devices. In the end, a monitoring system is also needed to validate and follow up on overall performance during the trials and in the longer term. Performance improvements are also multidimensional: e.g. QoS, direct energy savings, indirect costs and indirect CO_2 emissions. Saved kilowatt-hours must be determined against some reference baseline. Changes in the amount of procured electricity (grid-intake) has impact on effective "run-time" costs (€/time period) and indirect external environmental burden (e.g. kilograms of CO_2-emissions). To estimate that, information is needed from the market area-wide power production system by means of interlinking external data services to the platform.

Steps towards more sustainable energy usage and materialization of various aspects of sustainability can be taken by means of integrating real-time consumption measurement data with external services' information to create quantitative estimates for e.g. emissions or final impacts. Specific system-wide external services can estimate complex output consequences and feed inputs to control systems to enable adaptation and anticipation of the fluctuating conditions and partly random things (like behavior and weather). This all requires more intelligent control of production and consumption systems, which are both aware of numerous aspects at present but are also capable of forecasting, anticipating, and adapting to the coming conditions to overcome challenging situations.

The first deliverable (D5.1) of WP5 [13] described a comprehensive sustainability experimentation framework built and implemented within the north node of the 6G-XR-project on a quite detailed level. Framework covers both VTT's and the University of Oulu's experimental laboratories and MQTT-based real-time data-exchange solutions between these organizations. The same solution was used to interlink open-call project participants to the energy measurement framework of the north-node. In this section, some updates and experimental results achieved during the project work, as well as longer-term follow-ups, are presented to complete the work done in T5.1.

In this section, we present long-term data sets, which were used to e.g. estimate necessary scale-up factors for the existing PV-production systems, enabling self-sufficient electricity usage at various sufficiency levels (% of longer-term consumption levels) in the North-Node's real conditions. In addition to that, also impact of small-scale wind power production as an auxiliary power source supporting PV yield was estimated by means of the weather station's data and production curve.

In Section 6.1.1 we also provide long-term run-time performance results of the implemented multifunctional power supply system integrated with external consumption and yield forecasts, and in Section 5.3.3.1 we propose a preliminary methodology paving the way towards automated load control of the entire E2E-chain.

The energy measurement framework specified in D5.1 was implemented, and the following key datasets were stored to be applied in the other tasks of the project. The following sections introduce these datasets briefly for further usage.

2.1 ELECTRICITY CONSUMPTION MEASUREMENT DATA AND APPLIED TIME RESOLUTIONS

Carlo Gavazzi's electricity measurement devices (EM-series and ET-series transducers) were installed in distribution cabinets to measure power supply cables to system- and radio modules and video servers ("device level real-time measurements"). On the scale of few watts, also Otii-ACE measurement systems were used to measure end-user equipment (modems, laptop). These were the "primary sources" of the power and energy consumption data on 1/s time resolution.

In addition to this, the aggregated power output circuit of the PV-Hybrid's inverter was monitored separately as an entity. To achieve a flexible system, device, and unit-specific data were aggregated to an E2E-wide monitoring window for research usage (Figure). This "power aggregator panel" was also used to produce the overall energy consumption data for various matching purposes, e.g., related to dimensioning of the battery and PV-system components. Data from the power aggregator was also utilized for control purposes. E.g., scale-up or -down factors were applied to create "virtual PV-production data", which was used to match energy balance, i.e., production and consumption during the desired trial periods. Visualization panels were constructed in Grafana. The "Total" real-time data-stream was used to investigate energy needs of all devices in the E2E-scope.

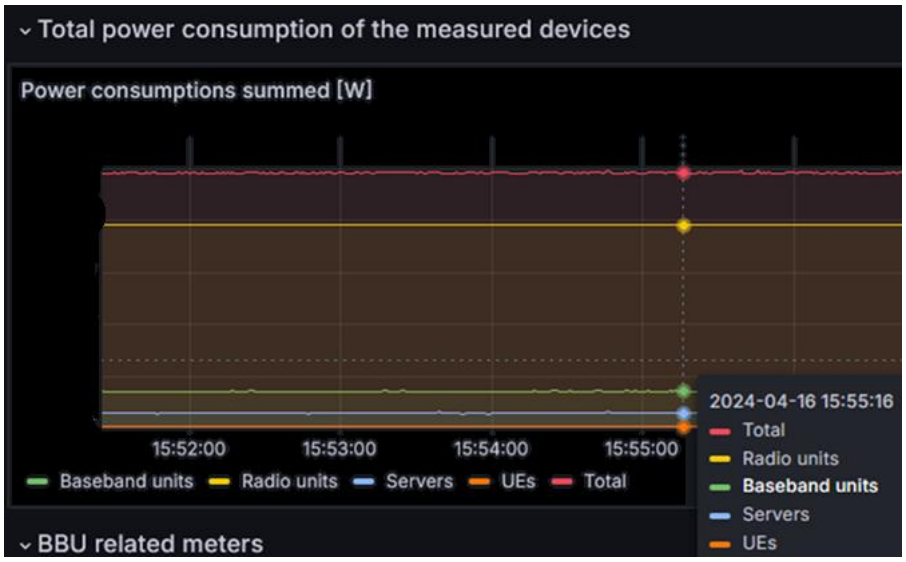

Figure 1: Aggregated power monitoring window of the E2E-scope operating on 1/s time resolution.

Impact of triggered changes for the investigated device -groups' power consumption was made visible by means of this real-time measurement setup and visualization tool on the 1/s sampling time resolution. It enabled characterization of power level changes because of modified configurations,

other parameters or settings, i.e., estimation of impacts of shifting energy saving states (one by one) in the measured devices.

This data was then stored to Influx-DB at least 2 weeks. During that time, researchers were able to download trial datasets from the R-T database to other applications if necessary (e.g., directly to Excel). Typical range of E2E measurement needs started from the few watts -level up to a few kilowatts -level, depending on the connected devices.

In addition to device-specific measurements, total consumption in the PV-hybrid's in- and output feeders was measured by means of Gavazzi's ET112 transducers, and 1/s results were stored to Influx-DB (very long retention time). However, part of that consumption relates to the distribution and monitoring system itself and the installed O-RAN devices.

The third level of consumption measurements was based on internal sensors of the inverter and data logged (from the real-time data) on 1/min level by the VRM-cloud service to formulate monthly 1/min datasets (widget in the Figure 2). This 1/min energy data (Wh) was then aggregated into 15-minute timeslots to construct project-wide multi-year datasets.. For the validation task, the consumption meters' data retention time was prolonged.

Figure 2: An example of 1/min AC-OUT-1 circuit's active power (W) time-series from the Multiplus-II inverter supplying the subset of connected devices.

The last 6 months' data was also directly available in the VRM-cloud service, and it was used to create useful widgets showing all necessary electrical details of the power supply and storage system, enabling fine-tuning of control parameters. Longer period datasets were then constructed from monthly datasets to Excel files on a 1/15min basis and were then inspected to enable power supply side's KPI -calculations presented in Section 6.1.1. Raw 1/min, monthly data was not used in practical trials, due to the time shifts in data-logging processes.

In the end, validation trials together with the developed E2E-controller were executed based on aggregated 1/s power measurement results stored in the Influx-DB (and visualized in the "power aggregator" panel), which was then processed to an hourly energy consumption data-stream (i.e., using 1/h time resolution). The set of devices and their measurement units was larger than the sub-group, which was directly connected to the PV-Hybrid's AC-out circuit. Thus, the data originated from the real PV-hybrid had to be upscaled and re-modelled in the short-term validation trials.

Consumption profile of the connected devices (in their normal usage in the laboratory environment) was considered not to reflect real base station's electricity consumption and underlying traffic patterns or profiles, and thus it was understood that the development of a specific test profile for traffic generation activities for the test setups is an inevitable step forward. In Section 3.3.1 "Traffic model for evaluation," the applied reference profile is presented, and the same profile was also taken as a

guideline for the consumption profile when developing energy availability-based load controlling methods. In practice, the variation of the test-consumption profile was also matched to range 0,6 – 1,8 kW (average near 1 kW) when PV setups' scale-up factors were determined for the specific trialing or certain test periods applying a specific dataset about external factors. This range of power levels was also selected to match the control system capable of changing energy-saving states in the entire E2E system.

2.2 OBTAINED PV-YIELD DATA (VTT'S PV-HYBRID)

PV yield data was collected by the VRM cloud service, Influx-DB, and MQTT-based data exchange system to the central controller from the solar-charger unit. Data was read from the internal voltage and current sensors or the cumulative energy counter of the DC-Solar Charger unit through VENUS-GX's Modbus-TCP register. MPPT solar charger (we used Victron 250/60-device) converts fluctuating PV module's current and voltage optimally to a 48V DC system (to a busbar where batteries, inverter/charger unit, and monitoring devices are connected). We decided to collect "PV-power to 48V busbar" data on 1/s level. Cumulative counter, PV to busbar-power (W), and PV-modules power (W) registers were also logged, and data is stored to 1/min monthly data files (kWh, +2 decimals). This data was then used to process 1/15min energy data to support analysis of longer periods. Also, 1/h PV-yield data was formulated to support the generation of energy availability-based guidelines for the E2E controller. It was processed from the "user yield" data stream (a cumulative PV-yield counter, all available datapoints were listed in the appendix of D5.1 [13]).

Long-term solar yield datasets are very valuable because they enable accurate modular scale-ups (for similar types of installations) to various power levels as well as comparative research and validation against various PV-yield forecasts. The obtained results also provide a reliable base to follow up on the energy balance-based efficiency of the entire power supply unit containing the battery system. Datasets (e.g. in Figure 3) made it possible to analyze the impacts of PV-hybrid's control pattern (battery usage) on various KPIs, also during the longer-term follow-up periods in North-Node's environmental conditions.

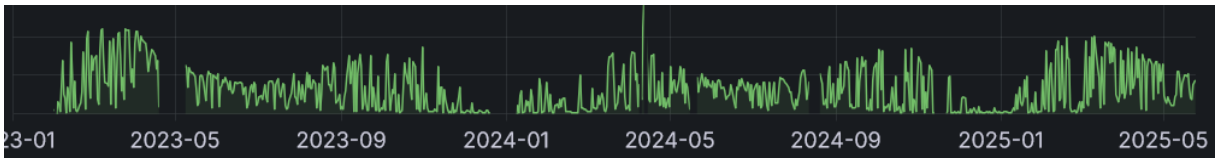

Figure 3: Solar power yield data stream in VTT's vertically wall-mounted PV setup in Oulu during 1.1.2023-20.5.2025.

Notably, the vertical southward wall setup produces well in early spring and autumn periods, when prices on electricity markets are typically higher than during the mid-summer holiday season. It also captures reflections from snow and ice surfaces efficiently, even under winter conditions without significant snow or ice accumulation. However, in the North-Node's conditions, solar irradiance is very weak for four months of the year and thus alternative power supply systems are required. This is why our laboratory setup is grid-connected, and energy deficit can be filled by means controllable flexible power intake.

We aggregated the obtained PV yield data to a project-wide 1/15 min dataset to match it to the coming electricity market reformation, and on the other hand, enable comparisons with other datasets (Figure 4). Parts of this extensive dataset were used to find the optimal scale-up factor for the electricity supply system and battery sizing against a relevant "test consumption pattern" which also

took traffic profiles into account. When the demand for the service is low (especially during nighttime), remarkable energy savings could be obtained by means of changing RAN states dynamically. Some amount of adaptation was thought to be possible also during the daytime, based on realized irradiation and short-term forecasts about it.

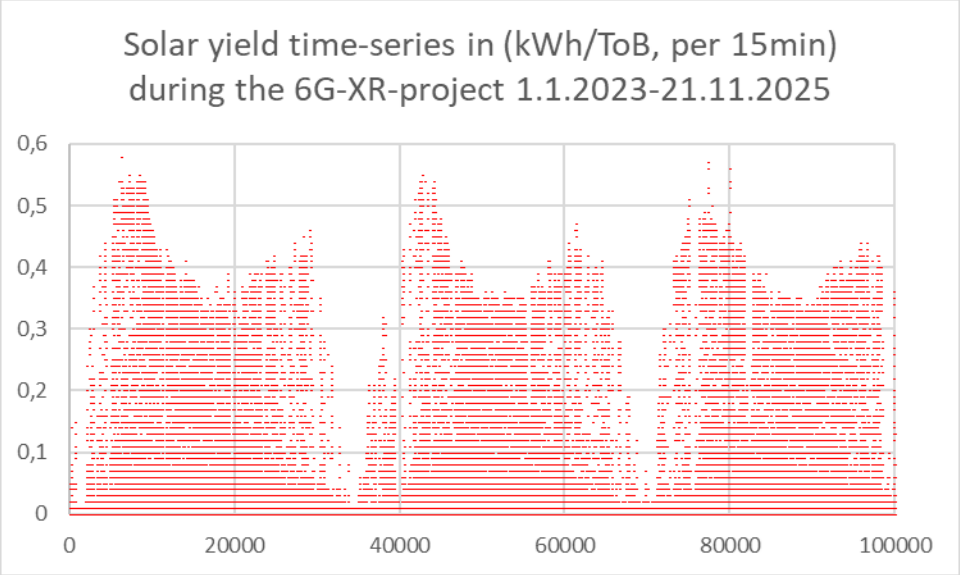

Figure 4: This figure shows an annual pattern of PV-energy/15min collected by a 48VDC system on the southward PV-module setup on the wall of VTT's HVAC room.

The monthly dataset (processed from the 1/15 data and averaged in the monthy level, Figure 5) was a very useful starting point to estimate energy-positive usage periods with various scale-up factors for PV-module set-up. The figure shows how much energy our PV-system has produced to 48V system in practice per 1 installed kWp of PV-modules. kWp refers to the sum of modules' nominal power figures (W) in their background plates and datasheets in standardized test conditions, STC).

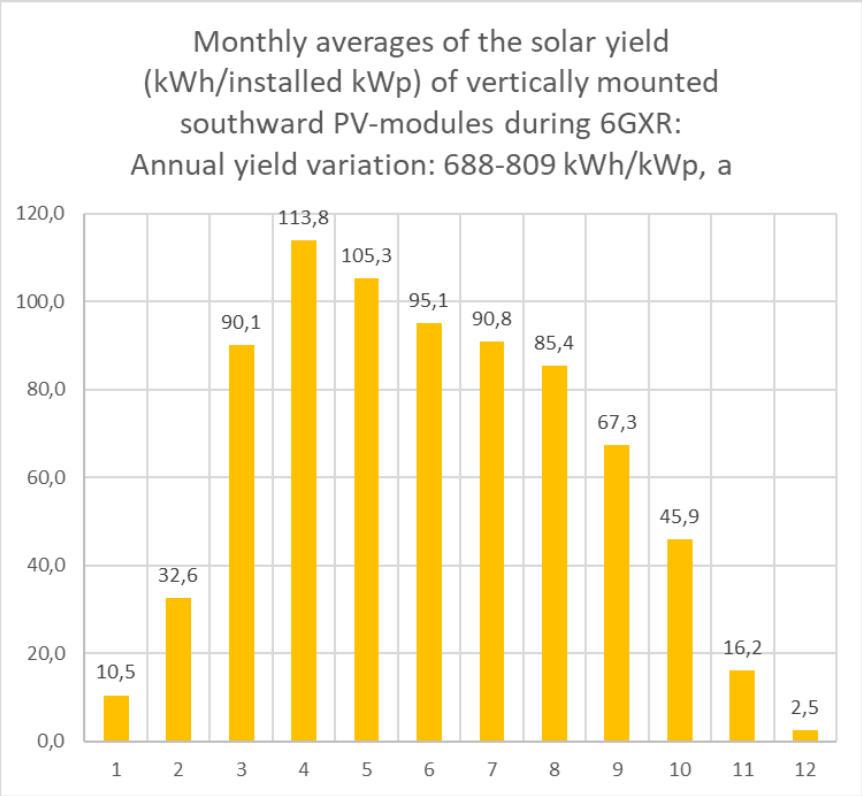

Figure 5. Specific monthly Wh/Wp -PV-yield levels for an average year.

In the Oulu area, it was possible to apply a 7-8 month energy-positive “usage or dimensioning period” for bi-directional wall-PV-hybrids targeting high self-sufficiency levels.

Monthly 1/min and 1/15min datasets were stored, and data was updated regularly to follow up on monthly variations and energy efficiency and gains of the overall power supply system.

In the early phases of the E2E controller development, we decided to use 1/h PV yield data derived from the solar charger’s cumulative user yield datapoint together with various 1/h-level PV yield prognoses. Both datasets were then scaled up “virtually” to match for investigated consumption level (and typical daily consumption profile during the trial periods.)

2.3 VIRTUAL WIND POWER YIELD AND OUTDOOR AIR TEMPERATURE - DATASETS

To overcome the low solar irradiance period during the winter season, auxiliary local power supply systems were assessed as an add-on option. Local wind power yield was estimated by means of the nearby weather station's 1/min data. A real power profile (W/wind speed) of a domestic wind turbine producer was then applied to that dataset. Figure 6 below shows the obtained dataset from the weather station. Few data-gaps appeared due to service breaks and unintended events. It is typical for this kind of systems that 100% operation time is difficult to achieve. In case of critical data streams, and to improve resilience, integration of complementary and redundant systems may be useful.

Figure 6. A captured 1/min dataset from Vaisala WXT536 weather station was used to understand the role of the local wind power setup as a background power source.

Wind speed m/s was characterized in the previous figure by means of averages, min, and max during 1 min measurement period. Wind direction was determined in degrees.

Data gaps during the period (August-September) did not affect the winter 24/25 analysis. Virtual wind power yield time series was derived from the wind speed data, start-up and close-down thresholds and it is presented in next Figure 7.

Figure 7. Time series of a virtual small-scale wind-power unit thought to be located on the roof of the VTT's facilities in Oulu.

Data was downloaded from Grafana and processed into a duration curve. Due to the threshold/start-up level of the WP unit and rare windy days, the output seemed to be quite low.

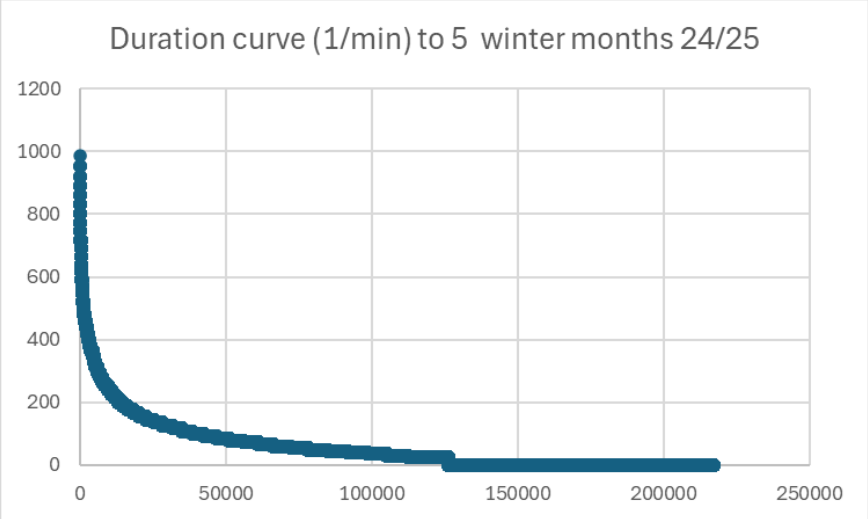

Figure 8. Duration curve of the power (W) of virtual small-scale wind power unit during 11/24-3/25 covering 5 winter months.

The analysis indicates that the local conditions are not suitable for effective small-scale wind power production. Median power of the 5 winter months follow-up period based on 1/minute data was only 30,7 W. Average power of simulated 1/min timeslots was 58 W and averaged monthly energy production i.e., "wind power yield" was 42 kWh/month. During 5 winter months, total production would have been only 210 kWh based on this preliminary analysis with realistic thresholds and measured wind speed data. PV and wind power results suggests that also other power supply technologies should be considered in future work to overcome winter challenges. E.g. methanol fuel-cell integration as a back-up power source could be one promising alternative, especially if high level of self-sufficiency or even off-grid usage would be targeted during winter months or challenging arctic conditions.

Outdoor air temperature data (1/min + 1 decimal, Figure 9) was also stored to enable analysis of maximum PV-module's voltage-peaks and outdoor temperature interaction.

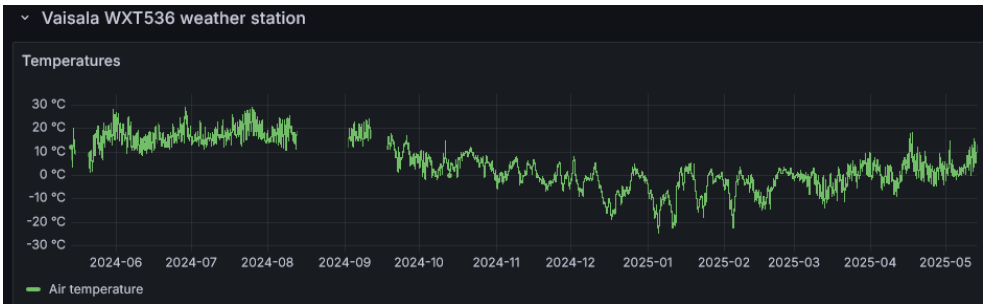

Figure 9. Stored temperature data (1/min) from the nearby Vaisala WXT536 weather station.

There were a few data gaps during the last year. Accurate outdoor temperature data was also used to find out PV-modules DC-voltage peaks (the recording of this time series started 27.1.2024). For the time-being (during the 7 year's usage period) highest voltage peak registered by the installation's DC-solar charger has been 39,71 V (if scaled down to 1 module). Corresponding nominal open circuit

voltage V(oc) of the modules is 38,5 V (plate-value). In the newer datasheet for this module type (Trina-Solar TSM-275, PD05) V(oc) is 38,1V [30]. Thus, at least +4,2 % safety margin (for the time being an experimental minimum) should be applied above the data sheet's V(oc) figures in STC, when designing serial string voltages in Oulu's conditions. Even the use of a +5% margin would be well grounded to avoid overvoltage damage in DC-solar chargers.

2.4 INDIRECT EMISSION FACTORS RELATED TO POWER CONSUMPTION FROM THE GRID

Specific emission factor (gCO_2/consumed kWh) data stream was interlinked into a Grafana panel "6G data from external sources, where various streams from several open data services' APIs were combined to the operative framework (Figure 10). This data source was linked to both VTT's and UOULU's systems (on 1/3min basis), and it was used to estimate indirect CO_2 emissions of auxiliary "remaining" power intake from the grid, which is needed after the prioritized usage of local PV production and BESS. Grid intake is needed to fill the balance when the energy deficit is unavoidable by means of other local systems. For the time being, it was not possible to utilize emissions as a criterion for adaptation, although forecasting of the emissions on an hourly basis was too difficult. However, this was utilized together with the grid-intake data in KPI evaluations.

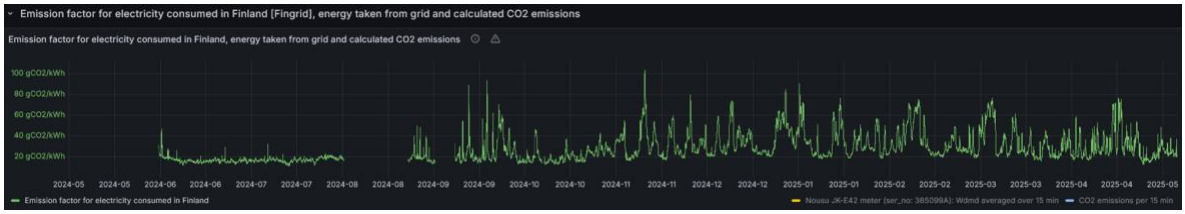

Figure 10. gCO_2/kWh time-series was processed to fit to 1/15 min KPI-follow-up resolution based on FINGRID's open data service (FINGRID is the Finnish transmission system operator, TSO).

This data stream is also considered in Section 4.2.3. Using the estimated almost real-time CO_2 emission factors on 1/3min level brings seasonal impacts to the KPI framework. In the short-term test setups (few days to weeks) and control system validation task, we decided to utilize standardized datasets for all external factors related to grid-intake to minimize their confounding impact in E2E-controller trials.

2.5 DAY-AHEAD PRICES OF ELECTRICITY AND USAGE OF OTHER EFFECTIVE COST COMPONENTS

The official ENTSO-E transparency platform's hourly (and later 1/15min) data-stream was integrated into the framework since 10/2024 (Figure 11). Observed data gaps were substituted from auxiliary data sources, if necessary (recording of this dataset from alternative services started 13.12.2023). During the validation phase, some comparisons were made to other data sources to find discrepancies in ELSPOT data. Some potential time-shift errors were found even in the ENTSO-E's data or data pipes related to the data processing, but their impact on analyses was negligible.

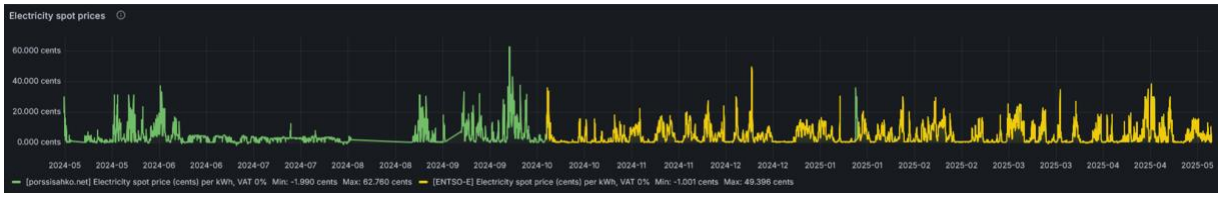

Figure 11. ELSPOT time series integrated into the framework and KPI calculations. (When there is no data in certain periods, Grafana interpolates a line between the last and first numbers).

Operative "run-time" costs of procured electricity were calculated from ELSPOT-data stream. We applied the principle €/time slot=average energy intake from the grid or direct consumption (kWh/time slot) x effective costs €/kWh + €/time slot taking both ELSPOT and distribution service's fees and taxes into account. This was done to enable "cost-counter" as a one KPI-perspective for trials and long-term follow up of the PV-hybrid power supply unit. Relative or absolute €-savings were then calculated from the difference of amount of power intake 1) in case with the PV-hybrid power supply (realized power intake data) and 2) in case without it assuming that loads would have been traditionally connected directly to the grid. In this case data from the consumption metering system was used together with cost factors. In performance evaluations estimating this kind of operative expenditure costs (or OPEX-savings compared to the reference case) a local grid-service tariff and a simple market-based energy procurement contract model's cost components were used with ELSPOT and measured or simulated kWh/h data. Value-added tax was not included in the analysis, but other (Finnish) taxes and fees were included. Usage of the ELSPOT data stream is also considered in Section 4.2.2.

2.6 APPLIED SOLAR YIELD PROGNOSES (IN VTT'S APPLICATION)

At the beginning of the E2E controller development work, several PV forecasting systems (APIs and data sources) were integrated into the framework. The aim was to obtain sufficiently accurate prognoses for the next hour or much longer periods of "the forecasting horizon" and then select the best data source for the validation phase. These issues are considered in Section, Energy Production: AI tools for 48 h Energy Weather. Here, we present some alternative approaches we used in interim phases of the development work. In the first step, we applied localized forecasts provided by Victron Energy's VRM-cloud service [31] related to the DESS system [32]. These prognoses were originally based on Solcast's services, but they were localized by means of monitored data and learning algorithms linked to the performance of the installation. Figure 12 reveals the relationship between irradiance and irradiance forecasts (W/m2) as well as localized PV-yield forecast vs. realized production to the 48VDC busbar system during May 2025.

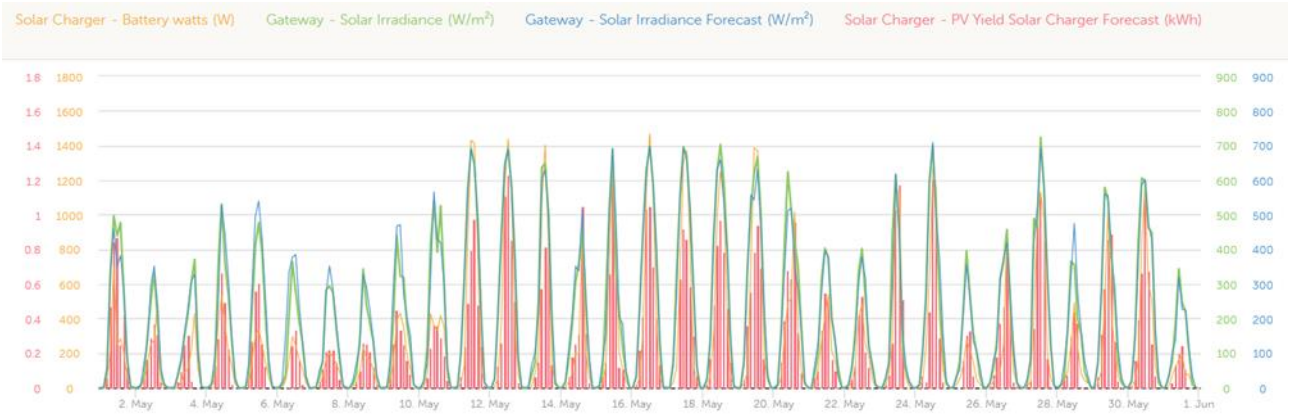

Figure 12 Victron's Solcast service-based irradiance forecast and localized prognoses (a custom widget created in the Victron's VRM-service).

Forecast data (Figure 12) seemed to be sufficiently accurate for E2E-controller development work. A slightly larger deviation between forecasted and measured yield (in Wh/h) was observed for localized predictions than for irradiation-based ones. There may be numerous underlying reasons for this, which cannot be determined with certainty. Next Figure 13 visualizes the same time-series in Grafana. This data was stored to InfluxDB and was used to develop energy availability prognoses for the E2E-controller.

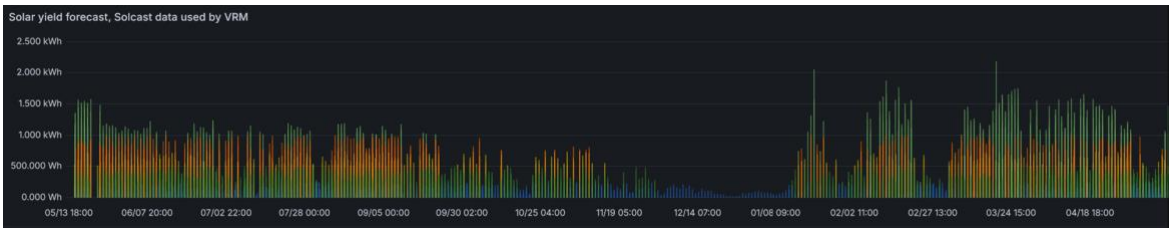

Figure 13. Collected and stored solar yield forecast -time series (by Victron Energy/Solcast services).

AI/ML has been applied to monitored real data to localize prognoses for the installation. One full (intact) yearlong year-long dataset was captured to support further analyses.

In the next Figure 14 our second alternative, solar yield forecasts from the Finnish Meteorological Institute's (FMI's) service, is presented and compared to realized daily yields of the installation. FMI's prognoses were integrated also into the framework (this time series started 26.3.2025).

Figure 14. Hourly FMI forecasts collected via FMI's API into the Influx-DB and a comparison of daily forecasts against realized PV-yield data from the solar charge controller.

In the final integrated validation phase of the E2E-controller's development work (T5.5), IR-sensor-based PV yield prognoses developed in WP5 task 5.3, as well as UOULU's PV yield data, were utilized. Forecasting methodologies and the generated prognoses finally applied in the E2E-controller trials are evaluated and discussed in greater detail in Section 4.4.

3 AUTONOMOUS BASE STATION ENERGY CONSERVATION TECHNOLOGIES

According to the GSM Association (GSMA) Energy Efficiency Benchmarking project, 76% of energy consumed by mobile operators is consumed in base stations and their supplementary functions, such as air conditioning and alternating current (AC)-to-direct current (DC) conversion [1]. This indicates the importance of minimizing the base station energy consumption while keeping the required quality of service (QoS) for the services it is running. Traffic in mobile networks is typically bursty in nature and varies significantly during a day [2]. In order to keep the satisfactory service level at all times, mobile networks are typically dimensioned based on the busy hour load. In addition, even during the busy hour, the traffic flow fluctuates, and it is common that some of the time slots are not scheduled for traffic. This temporal variation of traffic calls for energy-saving methods that can adapt to traffic variation at different time scales.

In this section, we summarize the results from T5.2 'Autonomous Base Station Energy Conservation Technologies'. First, the base station energy saving methods from the literature are reviewed. Some of these methods are evaluated using the energy measurement framework from Section 2 and commercial base stations at VTT's test network. Based on the measurement results, the most promising energy-saving methods are proposed for end-to-end assessment. We also present a framework for controlling the base station energy saving features from an external controller that considers not only the traffic variations but also energy availability and price. Finally, we present the practical energy savings achieved in T5.2 using the control framework against typical daily traffic patterns.

3.1 BASE STATION ENERGY SAVING CAPABILITIES

This section identifies the most promising energy-saving methods and features for modern base stations and evaluates their potential power savings. The evaluation is done at VTT's 5G standalone (SA) test network with the latest commercial network equipment. The radio access network (RAN) architecture is defined to be hierarchical, with cells at different carrier frequencies having partially overlapping coverage areas. The choice of the reference architecture reflects the situation in many commercially operated networks where extra carriers and capacity can be enabled when needed.

3.1.1 Proposed energy saving methods

The current state-of-the-art methods and approaches on RAN energy saving methods are reviewed in this section. We go through the latest advances and the most promising proposals from scientific literature and standardization. This provides a clear understanding of which methods have the greatest potential for achieving significant energy savings.

The best potential for base station energy savings is expected to be achieved by dynamic switching of cells and carriers, by fully utilizing the lean carrier design via discontinuous transmission (DTX), and by dynamic switching of massive MIMO transmitters [3]. The idea of DTX is to temporarily turn off the unused RF components at base station radio units for short durations when there is no signal to be transmitted. The smallest supported time granularity for DTX is an orthogonal frequency division multiplexing (OFDM) symbol. However, due to lean carrier design in 5G New Radio (5GNR), DTX is also efficient when operating at time slot granularity because, unlike in 4G Long Term Evolution (LTE), there are no more cell-specific reference signals transmitted in every slot. In addition, there is obvious potential in applying machine learning (ML) techniques for RAN energy optimization. The most common use cases for ML are traffic and cell load forecasting, as well as optimization of sleep modes. A recent survey on the 5G evolution towards 6G [4] also emphasizes the importance of base station

scheduling in combination with DTX. If the served traffic load is low and it can tolerate small delays, it is a prudent strategy to buffer DL data such that the base station can enter longer sleep modes.

When looking at RAN from a wider perspective, there is great potential for energy savings in RAN sharing and slicing between different operators [5]. This would reduce the number of overlapping cells and reduce the number of redundant network infrastructures. Technically, this is feasible and even relatively simple, but the business agreements and regulations for competitions among the operators may hinder the widespread use of multi-operator RAN sharing.

From the standardization point of view, 3GPP has completed a Rel-18 study on network energy savings where both the energy saving potential and the required standardization changes are evaluated [6][6]. The methods can be divided into time-, frequency-, spatial-, and power-domain methods. According to the study, the most promising energy savings, which are included in the normative work items in Releases 18 and 19 [7], are

- Aligning base station DTX and discontinuous reception (DRX) patterns to the DRX patterns used by the connected UEs. This would save energy on both the base station and the UE sides.
- Reducing the amount of common signaling. This could be achieved, e.g., by increasing synchronization signal block (SSB) periodicity and transmitting SSB/SIB1 only on demand by the UE.
- More dynamic adaptation of the number of base station transmitters. Currently, only semi-static adaptation of the number of gNB transmitters is possible using the Radio Resource Control (RRC) reconfiguration procedure towards the UEs.
- Dynamic DL transmission power adaptation. Currently, only semi-static adaptation of SSB transmitted (Tx) power and its offset to channel state information reference signal (CSI-RS) Tx power, as well as the offset between the CSI-RS and physical downlink shared channel (PDSCH) Tx power, is possible.

In addition to the scientific literature and standards, we also studied the features available in the commercial base stations deployed to our test network. Based on the study, the available energy-saving methods align well with the ones discussed earlier in this section. The selected set of energy-saving methods evaluated for D5.2 are

- DTX
- Turning off some of the base station transmitters (MIMO muting)
- Reducing the DL transmitted power
- Cell blocking, i.e., no signals transmitted
- Radio unit sleep mode

3.1.2 Reference architecture for measuring the base station power consumption

In order to quantify the gains from energy-saving features, we define a reference base station architecture that corresponds to a single multi-layered sector of a site. The architecture consists of a single frequency division duplex (FDD) cell providing always-on coverage for the UEs requesting service, and two time division duplex (TDD) cells providing high capacity when needed. The reference

architecture is shown in Figure 15. The base station equipment was upgraded during the project. Figure 15 illustrates the current status of the network, and all the results presented in Section 3 are measured using this architecture.

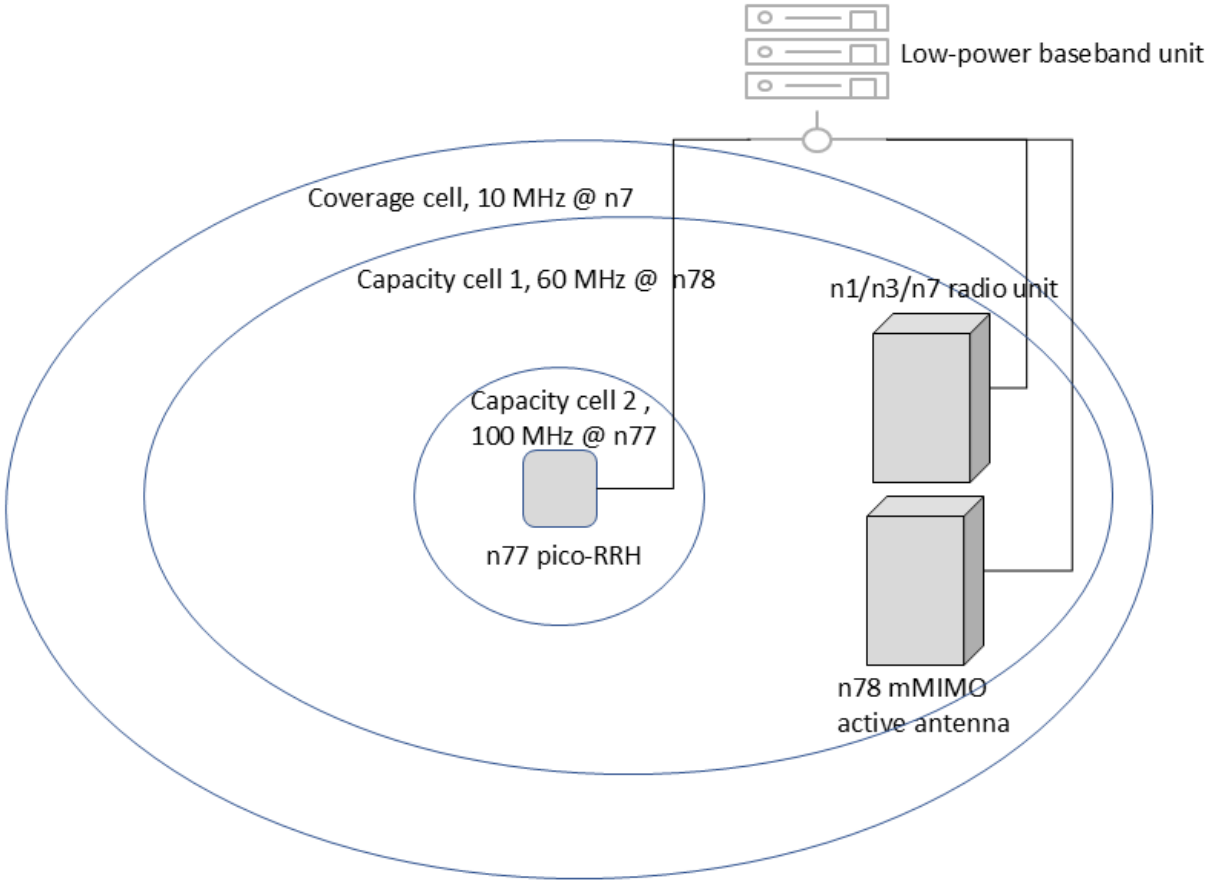

Figure 15: Reference base station architecture for measurements.

In order to evaluate the relative energy savings from different energy-saving features, we need a baseline configuration for comparison. As a baseline, all the cells in the reference architecture are switched on, and no energy-saving features are enabled. The baseline configuration is summarized in Table 1 for each cell.

Table 1: Baseline configuration for energy saving measurements.

	Coverage cell	Capacity cell 1	Capacity cell 2
Technology	NR5G SA FDD	NR5G SA TDD	NR5G SA TDD
Band	n7	n78	n77
Max. DL Tx power (W)	126.5	320.8	0.8
Number of transmitters	4	64	4
Bandwidth (MHz)	10	60	100
TDD time slot ratio (UL/DL)	-	1/4	1/4

3.1.3 Measured base station power consumption with the energy-saving features

The power consumption measurements were done using the energy measurement framework presented in Section 2. In practice, the baseband unit and the radio units are all measured separately using accurate Carlo Gavazzi meters that collect the AC power fed to the units. The sampling rate of these meters is 4096 samples/s, which is enough to capture the effect of short-term variations that take place when DTX is enabled. We considered two different cases: Full load in DL (all physical resource blocks (PRB) scheduled and idle cell (no RRC connected UEs), which represent the upper and lower limits for power consumption. Each case was measured for 5 minutes.

The results of the baseline power configuration measurements relative to the maximum power consumption (full load in DL) are shown in Table 2. The relative power consumption with no RRC-connected UEs is considerable for hardware units, which indicates that there is great energy-saving potential under low load.

Table 2: Relative baseline power consumption.

	Full DL Load	No RRC connected UEs
Baseband unit	100%	96%
Radio unit for the coverage cell (n7 cell only)	100%	68%
Radio unit for capacity cell 1	100%	76%
Radio unit for capacity cell 2	100%	85%
Total power consumption	100%[1]	75%

The radio unit power consumption reduced nearly linearly with the maximum configured Tx power in our measurements, making it a potential energy-saving method for cells with no UEs near the cell edge. Unfortunately, the changes in the DL Tx power level triggers a base station reset. During the reset, the network is not available for several minutes. This makes adaptation of the DL Tx power level for any of the cells infeasible because the energy saving mechanisms should not affect the network service availability.

The relative power consumption results for the other energy saving methods selected in Section 3.1.1 are collected in Table 3. Power consumption values are presented relative to the baseline configuration with the same traffic assumption, i.e., empty cell values are compared to empty cell values with the baseline. The energy-saving methods had no notable effect on the baseband power consumption, which is why it has been excluded from Table 3. In practice, to ensure network availability, cell blocking or sleep mode cannot be allowed for the coverage cell. Thus, the minimum power consumption in the empty system can be reached by turning on MIMO muting for the coverage cell and putting the radio

[1] Full DL load in all cells

units for capacity cells into sleep mode. In this case, the power consumption is 49% of the baseline consumption with no RRC-connected UEs.

Table 3: Relative power consumption with energy saving features.

	DTX		MIMO muting		Cell blocking	Sleep mode
	Full DL load	No RRC connected UEs	Full DL load	No RRC connected UEs	No RRC connected UEs	No RRC connected UEs
Radio unit for the coverage cell (n7 cell only)	100%	73%	65%	59%	43%	29%
Radio unit for capacity cell 1	100%	66%	75%	57%	37%	25%
Radio unit for capacity cell 2	100%	81%	93%	89%	72%	-
Total power consumption	100%	74%	75%[1]	65%[2]	49%[2]	39%[2]

It is important to consider not only power consumption but also the reduction in system capacity when the energy-saving features are enabled. DTX has no negative impact on the capacity, and it can be configured to be on all the time. Cell blocking and radio unit sleep mode completely prevent cell access, significantly reducing the system capacity. Entering and exiting the radio unit's sleep mode takes several minutes, and thus it should be used only when the traffic load is expected to be low for a long time.

MIMO muting is expected to reduce the cell capacity. To give an example of what the effect can be in practice, we generated full DL buffer traffic for a single UE and measured its DL throughput in different cells. These results are collected in Table 4. The UE was located in good coverage (reference signal received power (RSRP) between -85 and -90 dBm) in capacity cell 1 and in coverage cell while in capacity cell 2, the UE was in excellent coverage (RSRP -65 dBm). In the coverage cell and in capacity cell 2, the radio units have a one-to-one mapping between the transmitters and the antennas. MIMO muting is implemented by halving the number of transmitters at the radio units. Thus, MIMO muting reduces the maximum rank from 4 to 2, which explains the clear throughput reduction in this example. In capacity cell 1, there are 32 transmitters even after activating the MIMO muting, and thus, the

[2] Energy saving in all cells

maximum rank is not restricted by MIMO muting. However, the beamforming gain is reduced with MIMO muting, and this can have a negative effect on the achievable rate at some UE locations. In our example, the throughput reduction was so significant because we had an outdoor-to-indoor link and the UE was located at the backlobe of the mMIMO antenna.

Table 4: Example of the effect of MIMO muting on the single-UE DL throughput.

	All transmitters active	Half of the transmitters active
Coverage cell	140 Mbps	80 Mbps
Capacity cell 1	680 Mbps	130 Mbps
Capacity cell 2	1500 Mbps	760 Mbps

3.2 CONTROLLING THE ENERGY SAVING FEATURES

MIMO muting and cell blocking can be controlled autonomously by the gNB using pre-configured traffic load thresholds. These load-based energy saving features have been tested to be working as expected. However, they are not directly suitable for the 6G-XR E2E energy optimization approach, where not only the traffic load but also other factors such as energy price and local green energy availability should be taken into account. This motivated us to define a set of RAN power saving states and study the possibility of controlling them externally. The external control has the benefit of having arbitrary triggers for performing any energy-saving actions.

3.2.1 Power-saving state-based control

Based on the findings from Section 3.1.3, we define four different per-cell power saving states mapped to the most promising energy saving methods. A capacity cell can be in four different states: **A) DTX-only, B) MIMO muting, C) Cell blocked, D) Sleep mode**. A coverage cell should guarantee network availability and thus only power saving states A and B are allowed for it. When there are one coverage and *N* capacity cells per coverage area, the number of different power saving states becomes $2 \cdot 4^N$.

The relative power consumption and the theoretical maximum capacities in different power saving states in the reference architecture are collected in Table 5. The states are denoted with three-character strings such that the leftmost character corresponds to the coverage cell and the rightmost character to capacity cell 2. For example, state BDC corresponds to the case where MIMO muting is enabled for the coverage cell, capacity cell 1 is in sleep mode, and capacity cell 2 is blocked. The sleep mode was not supported by the pico-RRH of capacity cell 2, and thus, states xyD are excluded from Table 5. Power consumption is presented relative to the maximum power consumption (at state AAA). The minimum level corresponds to the case with no RRC-connected UEs, while the maximum level is for the case when all PRBs in all available cells are scheduled. The theoretical capacities are calculated using [8][8] with parameter values from Table 1, assuming that multi-user MIMO (MU-MIMO) is not used.

Table 5: Power saving states with their relative power consumption levels and theoretical capacities at the VTT reference architecture.

Power saving state	Maximum power consumption	Minimum power consumption	Maximum DL capacity	Maximum UL capacity

AAA	100%	55.9%	3200 Mbps	520 Mbps
AAB	99.8%	56.2%	2260 Mbps	520 Mbps
AAC	98.7%	55.7%	1588 Mbps	270 Mbps
ABA	87.4%	52.7%	3200 Mbps	520 Mbps
ABB	87.2%	53.0%	2260 Mbps	520 Mbps
ABC	86.1%	52.5%	1330 Mbps	270 Mbps
ACA	64.4%	45.3%	2090 Mbps	370 Mbps
ACB	64.2%	45.6%	1150 Mbps	370 Mbps
ACC	63.1%	45.1%	220 Mbps	120 Mbps
ADA	60.1%	41.0%	2090 Mbps	370 Mbps
ADB	59.9%	41.2%	1150 Mbps	370 Mbps
ADC	58.8%	40.7%	220 Mbps	120 Mbps
BAA	87.4%	52.3%	3090 Mbps	520 Mbps
BAB	87.2%	52.6%	2150 Mbps	520 Mbps
BAC	86.1%	52.1%	1220 Mbps	270 Mbps
BBA	74.9%	49.1%	3090 Mbps	520 Mbps
BBB	74.6%	49.3%	2150 Mbps	520 Mbps
BBC	73.6%	48.9%	1220 Mbps	270 Mbps
BCA	51.9%	41.7%	1980 Mbps	370 Mbps
BCB	51.6%	42.0%	1040 Mbps	370 Mbps
BCC	50.6%	41.5%	110 Mbps	120 Mbps
BDA	47.5%	37.4%	1980 Mbps	370 Mbps
BDB	47.3%	37.6%	1040 Mbps	370 Mbps
BDC	46.2%	37.1%	110 Mbps	120 Mbps

As seen from Table 5, the power saving states in the reference architecture provide flexibility in controlling both the energy savings and available capacity. We'll emphasize that the capacity values are only the theoretical maxima, and the available system sum rate strongly depends on the locations of the UEs and their channel state. For example, even if the 100-MHz bandwidth capacity cell 2 can theoretically provide very high capacity with low energy cost, in practice, its coverage is very small and, in many cases, it provides no capacity increase because all the UEs are located elsewhere in the coverage area. This emphasizes the importance of having knowledge of UE locations available when making decisions about the power-saving states.

In practice, a power-saving state can be changed by providing new gNB configuration parameter values using the manufacturer-proprietary operation and management (O&M) interface. However, due to security concerns, it is not advisable to open the gNB configuration interface to RAN-external actors. There are thousands of gNB configuration parameters whose values should be changed with care. For this reason, we implemented a RAN controller that converts the external commands for changing the RAN power saving states into gNB configuration changes. In addition, the RAN controller also checks if the requested state transition is allowed and reports the state changes for the system monitoring.

RAN controller interacts with the gNB, central controller (centralized decision making), and centralized database. The related RAN controller interfaces are listed below:

- Towards gNB
    - Manufacturer-proprietary

- Outgoing
  - Requests to change gNB configuration parameters
  - Requests to get gNB status reports
- Incoming
  - Response to the requests, success/failure
  - gNB status reports for verifying the current RAN power saving state

- Towards central controller
  - MQTT-based
  - Publish (outgoing)
    - Current RAN state
    - Response to the state change commands, success/failure
  - Subscribe (incoming)
    - Commands to change the RAN power saving state

- Towards the centralized database (InfluxDB)
  - Python API
  - Outgoing
    - Current RAN state

The RAN controller interfaces with the related functional components, are shown in Figure 16.

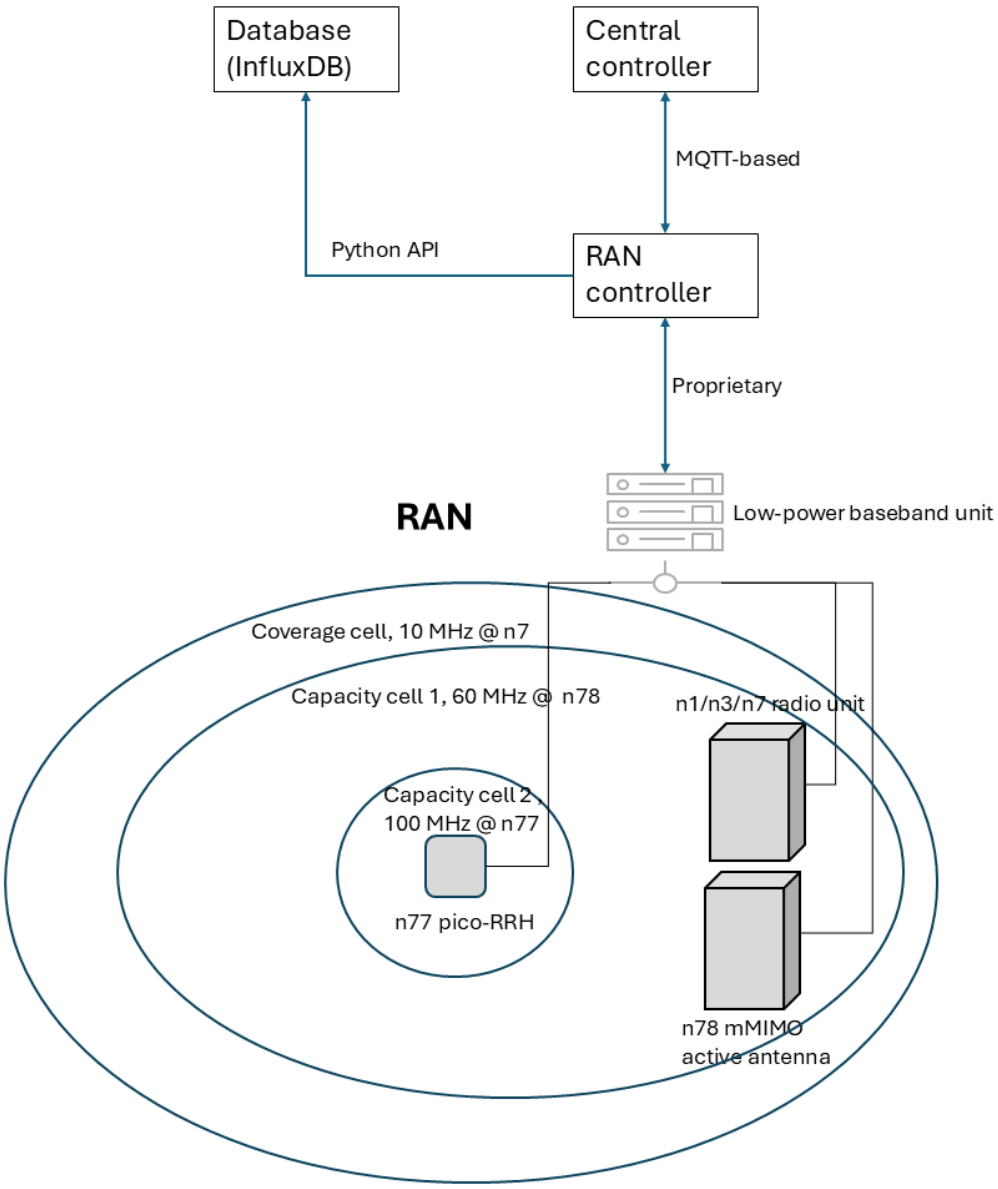

Figure 16: RAN controller and its interfaces.

3.2.2 State transition effects

The number of possible state transitions becomes very high even with only a few capacity cells, which complicates decision-making. The complexity of selecting a suitable power-saving state can be reduced by carefully selecting assumptions and restrictions. We could e.g., assume that

- Power saving state is changed only for a single cell at a time, e.g., direct state transition AAA -> ABC is not allowed.
- State D is entered only from State C, i.e., radio sleep mode should be triggered only after the cell has been first blocked.
- The cell states with very little power saving gain are excluded from the decision-making. In our example, the gain from MIMO muting in capacity cell 2 is very low. Thus, only states A and C are allowed for capacity cell 2.

Taking into account the above assumptions, the set of possible state transitions is given in Table 6. State transition time refers to the time it takes before the power-saving state is enabled and the change is visible in power consumption.

Table 6: Set of considered state transitions.

State transition	Average transition time	Max. DL capacity change
xxA -> xxC	< 5 s	- 1870 Mbps
xxC -> xxA	< 10 s	+ 1870 Mbps
xAx -> xBx	~30 s	-
xBx -> xAx	~30 s	-
xAx -> xCx	~15 s	- 1110 Mbps
xCx -> xAx	< 5 s	+ 1110 Mbps
xBx -> xCx	~15 s	- 1110 Mbps
xCx -> xBx	< 5 s	+ 1110 Mbps
xCx -> xDx	> 1 min	-
xDx -> xCx	> 1 min	-
Axx -> Bxx	~30 s	- 110 Mbps
Bxx -> Axx	~30 s	+ 110 Mbps

In addition to the state transition times and potential changes in the cell capacity, it is also important to evaluate the effect of state transition on connected UEs. In practice, the cell selection priorities have to be selected such that the UEs in RRC-Idle and RRC-Inactive prefer the capacity cells in their cell reselection processes. This guarantees that any new RRC connections will be established to the capacity cells if the UE is within their coverage area. The UEs in RRC-Connected can also be steered to the wanted cells by properly configuring different handover thresholds and priorities. This is illustrated in Figure 17, Figure 18, and Figure 19. Frequency priority-based handover to the capacity cells can be configured by properly setting the frequency priorities and by setting the A4 measurement parameters such that handover to the capacity cell is triggered even when the signal levels from the coverage cell are higher. This ensures that the traffic is steered to the capacity cell when available [9]. An example of successful frequency-priority-based handover is shown in Figure 20, where the DL throughput time series is shown for a DL iperf3 transfer. After the UE is forced to make a handover to the coverage cell, it successfully returns to the capacity cell even though its signal levels are lower. As can be seen from Figure 20, there is no notable gap in the throughput curve during the handover.

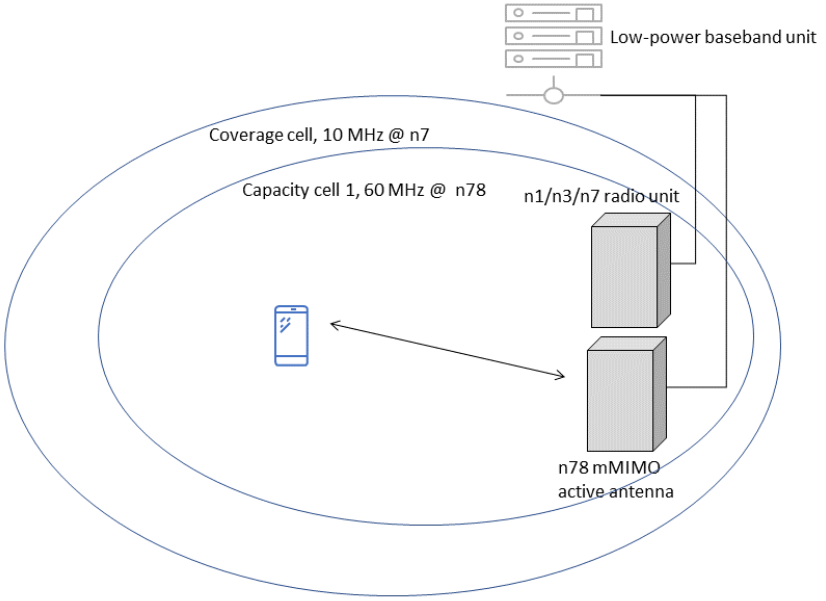

Figure 17: RAN initially in state AAC. Traffic load in capacity cell 1 is low.

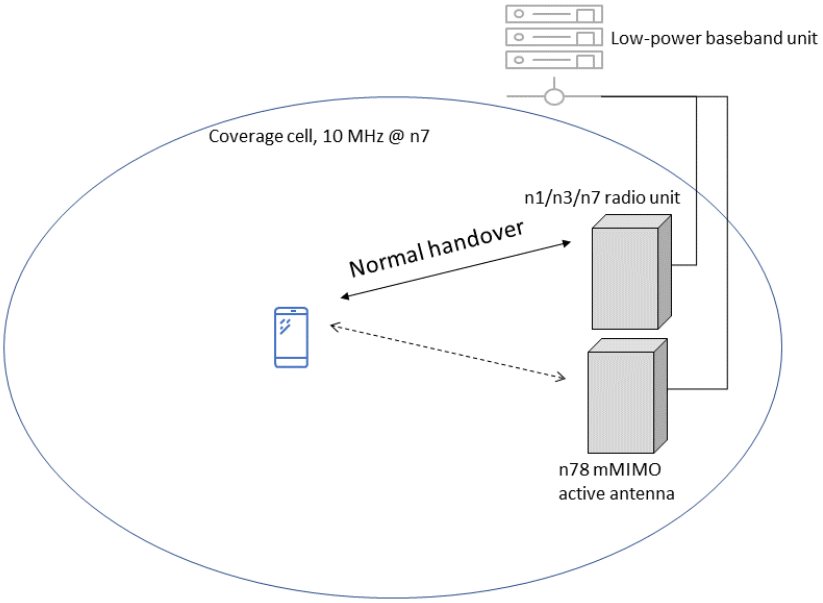

Figure 18: RAN enters state ACC. Handover to the coverage cell is triggered.

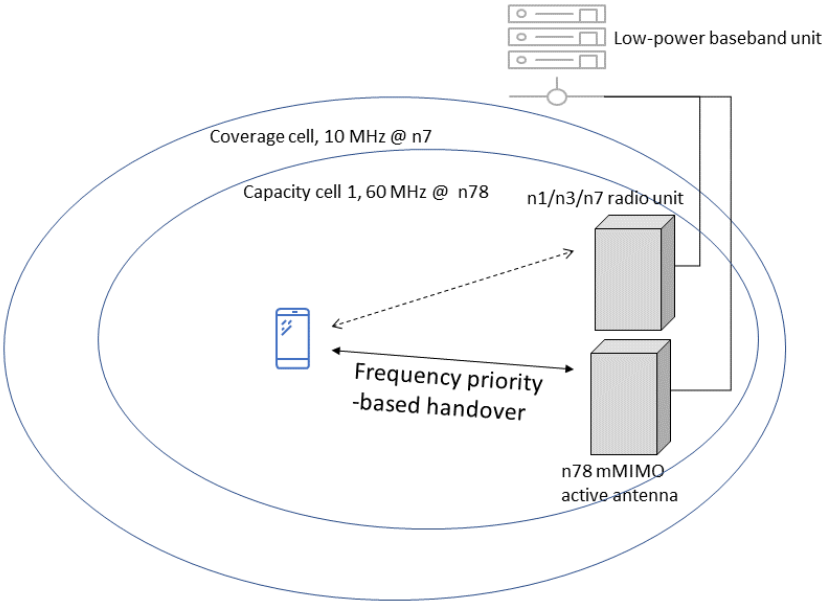

Figure 19: Traffic load in the coverage cell is high. RAN enters back to state AAC. Frequency priority-based handover is triggered to the capacity cell.

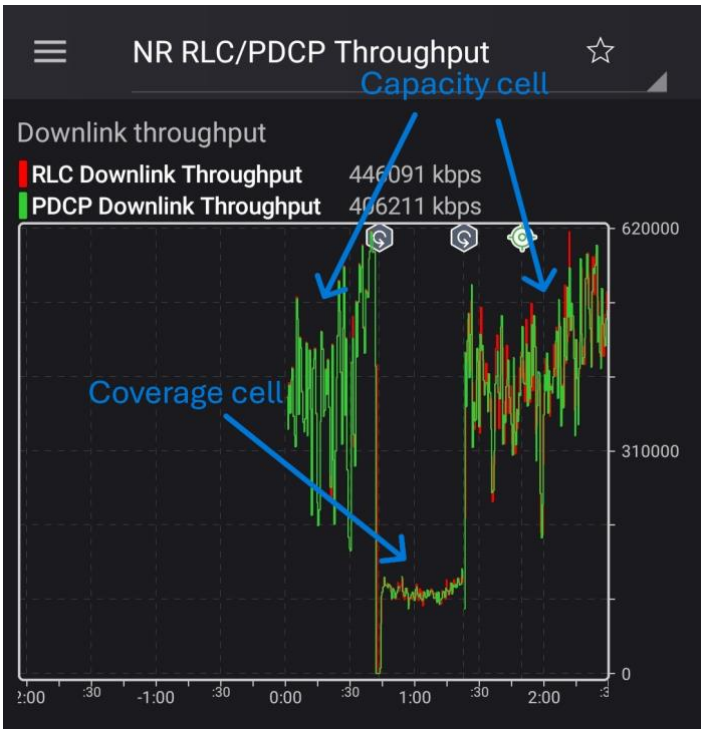

Figure 20: DL throughput time series while the device is making handovers to the coverage cell and back to the capacity cell.

3.3 EVALUATION OF ACHIEVABLE ENERGY SAVING GAINS

Base station power consumption with the selected energy saving features and under the power saving states has been reported in Sections 3.1.3 and 3.2.1, respectively. These results were given for either

full load or for empty cell, which provide upper and lower bounds for energy consumption. However, the dynamics of traffic were not considered, making it hard to draw any conclusions about the practical energy saving gain. To better understand the achievable energy saving gain, there is a need to make longer measurements against realistic traffic models.

3.3.1 Traffic model for evaluation

Traffic in mobile networks is typically bursty in nature and highly concentrated during the busy hours of the day [2]. The typical daily traffic profile has its busiest hours in the evening, while late night and early morning are quiet. The typical daily variation of the traffic load relative to the busy hour load is shown in Figure 21 [10]. In addition, there is also significant short-term variation in traffic load, resulting in empty time slots even during the busy hour.

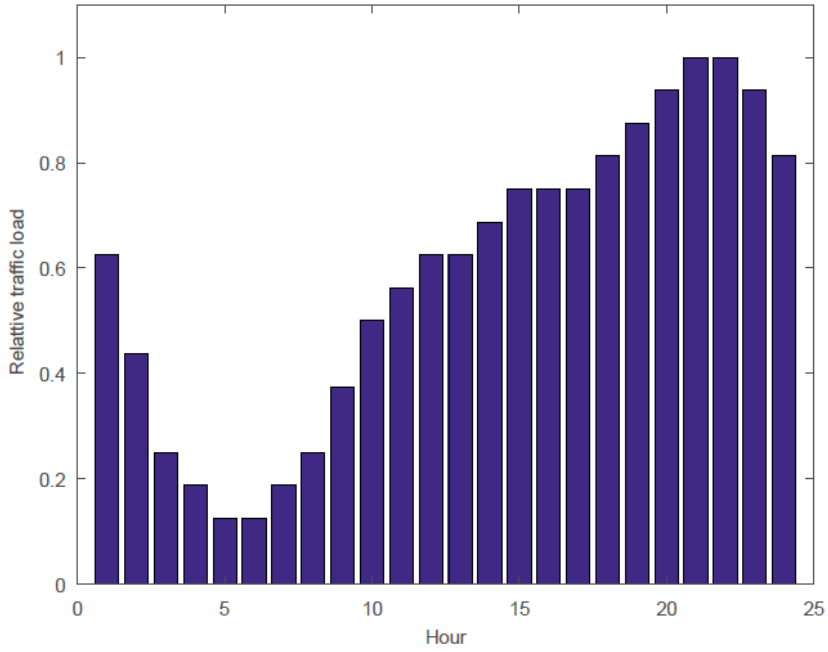

Figure 21: Typical daily load profile in a base station. The busy hour load is normalized to unity.

Recommendations on how to generate traffic for RAN energy consumption or energy efficiency evaluation have been given by both 3GPP [6] and ETSI [11]. These recommendations are very accurate, assuming the use of the UE emulator. At the time of writing, VTT's Keysight UeSIM UE emulator system can be attached to either FDD or TDD cells, but not both. This prevents its usage in the reference architecture with an FDD coverage cell and TDD capacity cells.

As a simplified approach to traffic generation, we used three Telewell USB modem devices with system- and band-locking capabilities (5GSA n7, n77, and n78, in this case). DL traffic was generated using iperf3 such that both the session duration and the inter-arrival times were exponentially distributed, which is a common assumption when modelling mobile traffic [12]. The target data rate for a session was scaled according to the daily traffic profile in Figure 21 such that the per-UE target rate was 100 Mbps during the busy hour. The average new session arrival time and session duration were both exponentially distributed with means of 60s and 40s, respectively. The resulting sum rate for 24-h and 1-h periods is shown in Figures 22 and Figure 23, respectively. It can be seen that the time series for the 24-h period follows the targeted daily profile in Figure 21. As intended, there are also occasional periods of a few seconds during which there is no traffic at all, as can be seen from Figure 23.

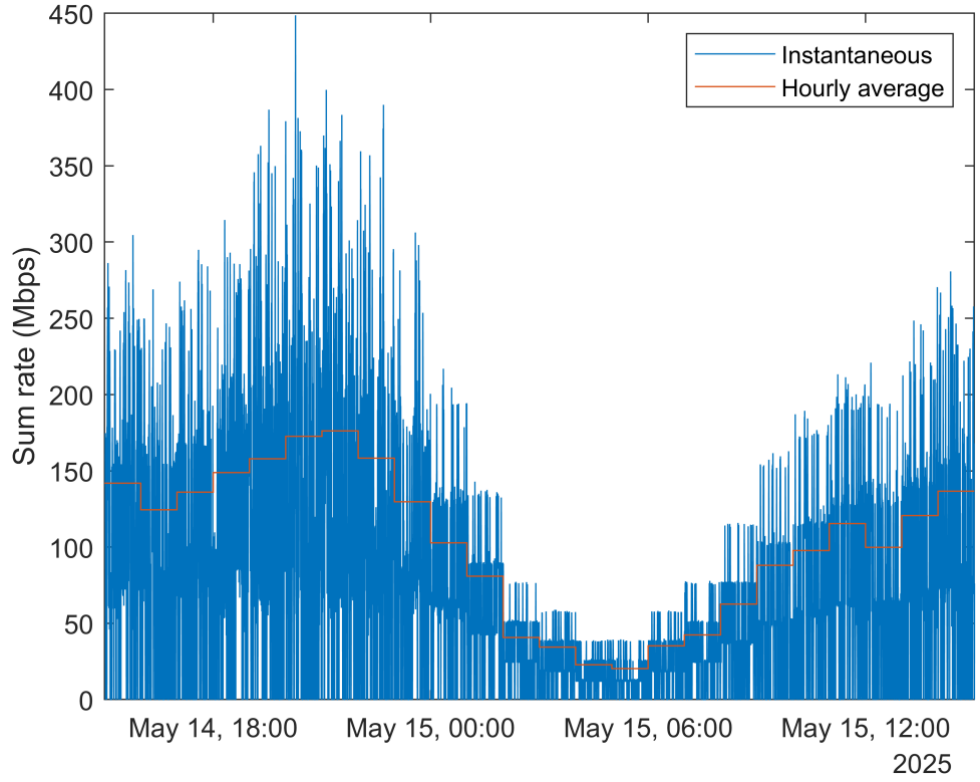

Figure 22: Sum rate of the generated traffic over 24-h period.

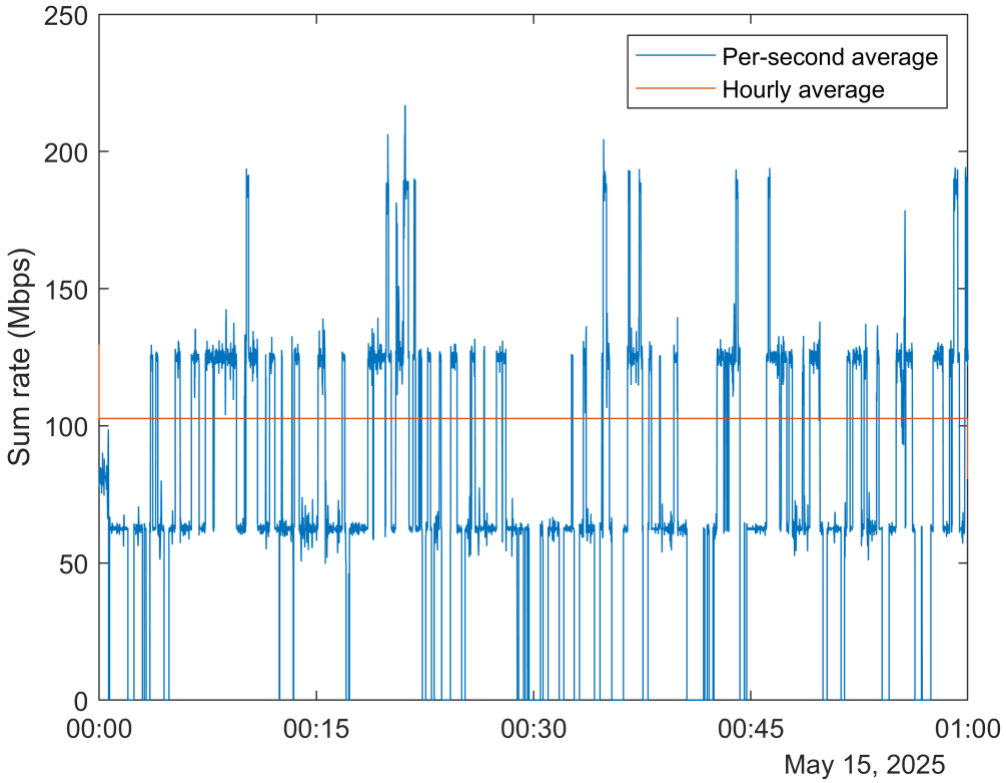

Figure 23: Sum rate of the generated traffic over a 1-h period on May 15, 00:00-01:00.

3.3.2 Measured energy saving gain from power saving states

To quantify the energy saving gain from adapting the power saving states, we measured the power and energy consumption over two 24-hour periods using the traffic generation approach presented in Section 3.3.1. In the first measurement, the reference RAN system (Figure 15) was configured according to the baseline presented in Section 3.1.2, with all cells unblocked and no energy saving methods enabled. In the second measurement, the RAN power saving state was selected for each hour such that the expected peak sum rate can be served without QoS degradation and such that the energy consumption is minimized. Telewell 5G modems were deployed at the same location that was used for measuring the example capacities in Table 4. This location was outside the coverage area of capacity cell 2, and thus the UEs were connected only to the coverage cell or to capacity cell 1.

The time series for the relative RAN power consumption and the PRB usage for the baseline measurement are shown in Figure 24 and Figure 25, respectively. The power consumption is presented relative to the fully loaded system. The PRB usage for the coverage cell and capacity cell 2 is 0% during the baseline measurement, because the cell selection priorities and frequency priority-based handover (see Section 3.2.2) are configured such that all the traffic is steered to the capacity cells. In addition, none of the UEs were within the coverage area of capacity cell 2. It can be seen from Figure 24 and Figure 25 that the power consumption correlates well with the PRB usage, as expected.

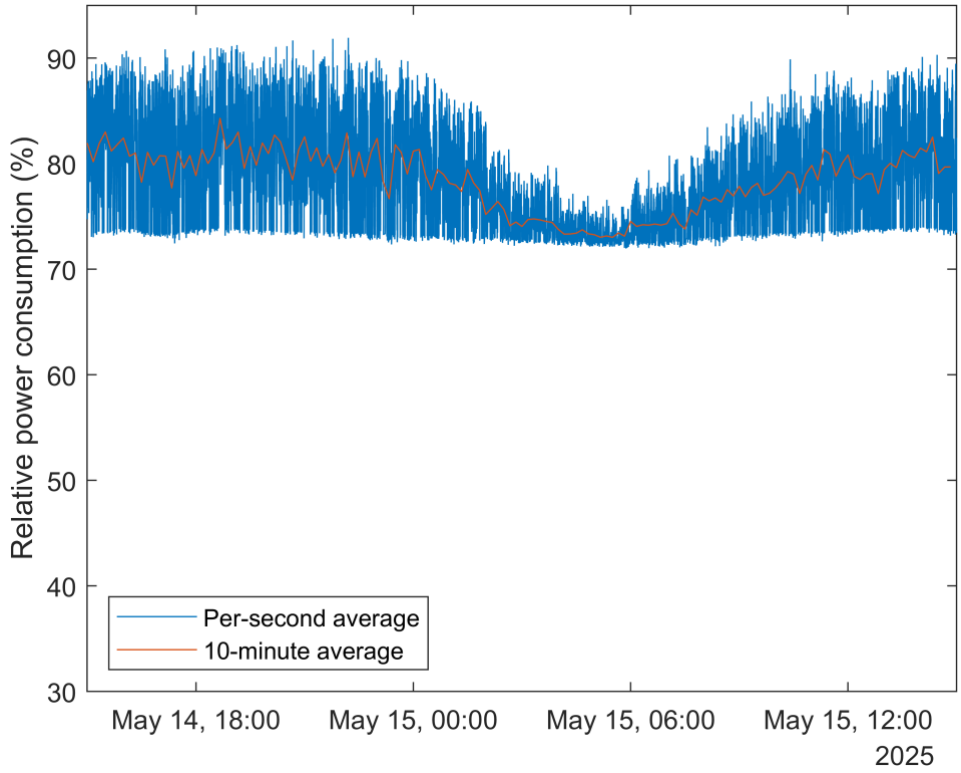

Figure 24: Relative RAN power consumption for the baseline measurement.

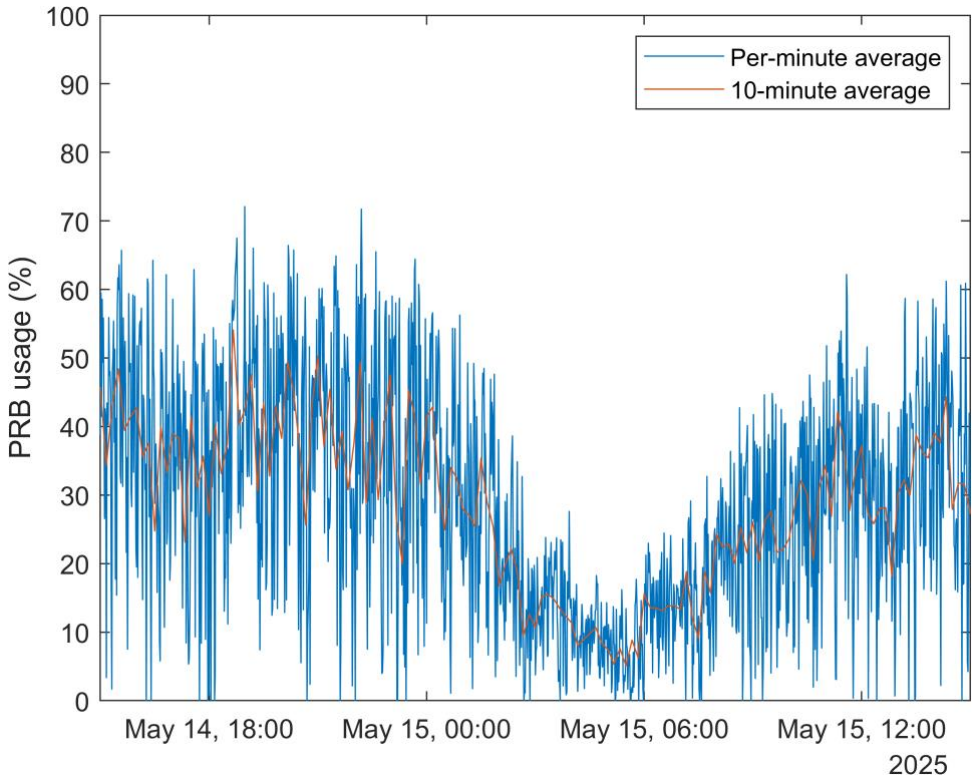

Figure 25: PRB usage in capacity cell 1 for the baseline measurement.

In the second 24-hour measurement, the RAN state was selected once per hour such that it can fulfil the capacity requirements for the given hour while minimizing the power consumption. The set of RAN

states used during the measurement is given in Table 7. The time series for the relative RAN power consumption and the PRB usage for the energy saving measurement are shown in Figure 26 and Figure 27, respectively. When comparing Figure 24 and Figure 26, it can be seen that by adapting the RAN power saving states according to traffic demand, the power consumption can be decreased considerably. For example, during the lowest traffic, the power consumption is only ~40% of the power consumption of the fully loaded baseline system. Based on the results from the 24-hour measurements, switching the RAN states on an hourly basis reduces the daily energy consumption by ~26% compared to the baseline. It can be seen from Figure 27 that the PRB usage in capacity cell 1 was somewhat higher during the energy saving measurement than during the baseline measurement (see Figure 25), even within the time range 14:00 – 00:00 when MIMO muting was not active. One potential explanation for this is that during the baseline measurement in May, the weather was sunny and clear, whereas during the energy saving measurement in June, the weather was rainy and cloudy. It seems that the rainy weather negatively affects the channel quality necessitating the use of lower modulation and coding scheme (MCS) indices and rank. Thus, we expect that under similar channel conditions, the daily energy gain from RAN state adaptation would be even higher than 26%.

Table 7: RAN states used during the energy saving measurement.

Time range	RAN state	Expected sum rate at the measurement location
00:00 – 01:00	BBC	214 Mbps
01:00 – 02:00	ACC	139 Mbps
02:00 – 03:00	ADC	139 Mbps
03:00 – 07:00	BDC	83 Mbps
07:00 – 08:00	ADC	139 Mbps
08:00 – 09:00	ACC	139 Mbps
09:00 – 14:00	BBC	214 Mbps
14:00 – 00:00	BAC	761 Mbps

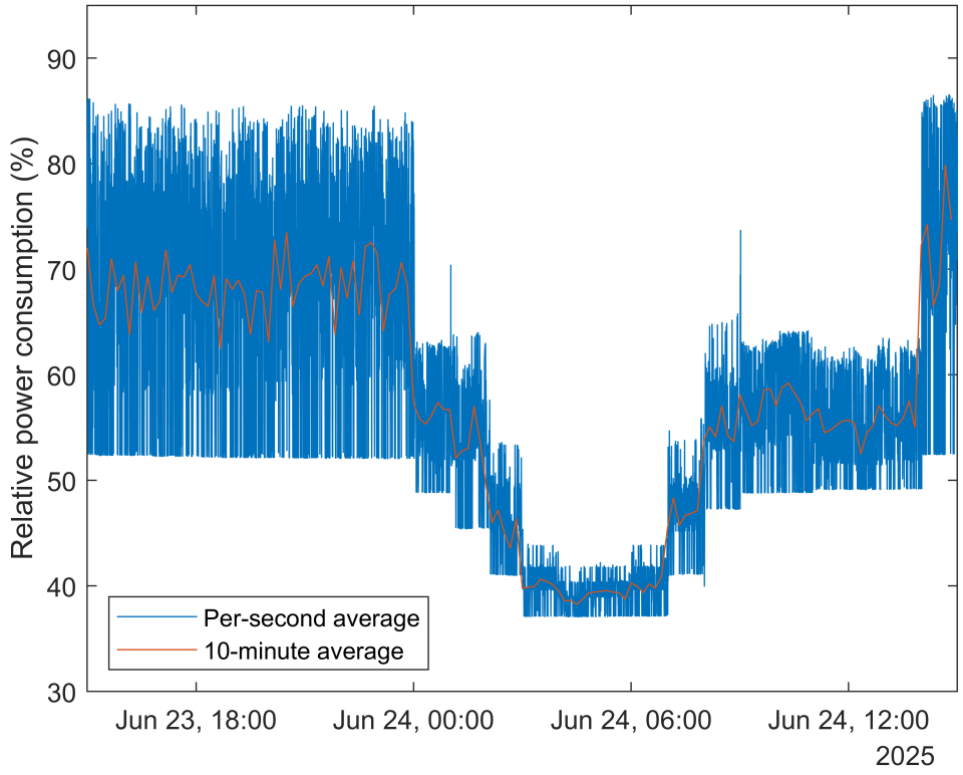

Figure 26: Relative RAN power consumption for the energy saving measurement.

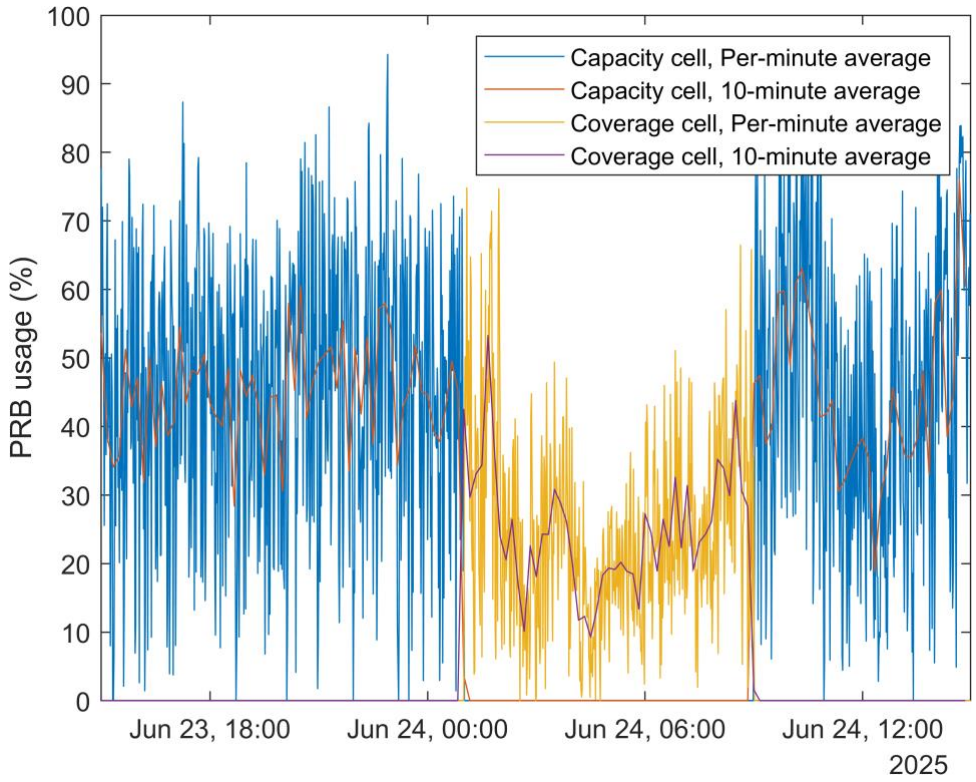

Figure 27: PRB usage for the energy saving measurement.

4 ENERGY PRODUCTION: AI TOOLS FOR 48 H ENERGY WEATHER

The energy measurement framework discussed in D5.1 [13] provides the foundation for performing sustainability experimentation and site analysis, sizing and selection of the right equipment for renewable energy sources (RES) and determining self-sustainable 3GPP gNB and Radio Units with linked carbon emissions and cost counters. The energy weather forecast gives us insight into the forecasted energy availability which is produced every 3 hours and extends to 66 hours, based on the size and orientation of the equipment (PV modules). It also analyzes how different solar radiation impacts the PV installation and generates the total sum of energy in kWh. In the 6G-XR project and UC5, the energy weather forecast provides us with a platform to adjust our energy consumption and energy storage behavior according to the prediction accuracy and 2 days ahead energy production estimates. This section examines the accuracy of the prognosis made by the energy weather forecast for the next 2 days and evaluates it against the real-time observed PV yield by the 24 PV modules at UOULU rooftop. It also describes the updates in the energy measurement framework pipeline since D5.1 [13], and how different forecasting APIs are integrated into the framework using the central controller.

The energy systems are transitioning mostly towards RES, smart grid technologies, and local energy trading. This will introduce new opportunities but also challenges, such as a volatile energy profile. Therefore, critical infrastructure components such as ICT system elements need to be constantly available regardless of energy generation status [20]. The North Node arctic gNB sites are located in one of the harshest regions in the world and the energy availability during the polar nights, especially in winter times when the sun does not rise for more than 50 days goes to almost zero with only PV installations. This creates a challenging environment and hence forecasting becomes crucial. In addition, there are vast areas in arctic regions where grid connectivity is not an option therefore developing a self-sustainable solution through RES becomes essential. To make such an energy mix as efficient as possible, ML algorithms can provide accurate energy production estimates and hence better energy balancing strategies [20].

4.1 UPDATES ON ENERGY WEATHER FORECASTING APIS SINCE D5.1

The energy measurement framework, as described in detail in D5.1 [13], was integrated with a previous version of the FMI-based energy weather forecast API. These APIs were accessed using the requests library in Python. A python script ran as a nohup background process inside the central controller to automatically fetch energy and weather-related data frames as .csv files using the API provided by FMI updated every 3 hours. The data was then stored in the central database, which was configured in Grafana for real-time visualization. These FMI predictions were based on HARMONIE-AROME-based weather model system MEPS (Mesoscale Ensemble Prediction System) [21], and instead of a single forecast, they utilized 8 MetCoOp runs, as shown in Figure 28 and Figure 29 Figure 29. The ensemble forecasts (in different colors) represent dynamic atmospheric conditions. The extent to which they are spread apart indicates the level of unpredictability in the energy weather under Nordic conditions. Figure 28 illustrates the highly dynamic weather conditions in April, as evidenced by the widely spread ensemble forecasts across all estimates [21]. In contrast, the weather conditions in July are more stable and less variable, resulting in less spread among the fractals, as shown in Figure 29.

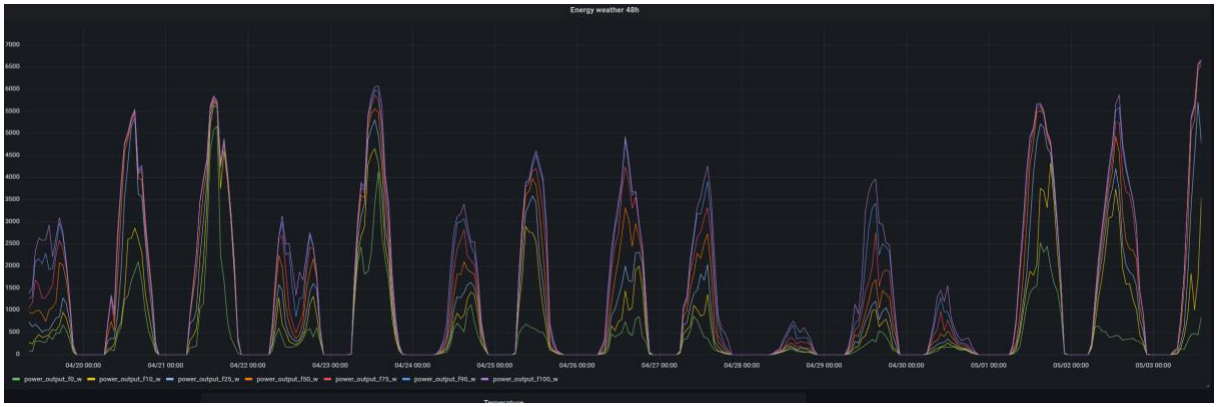

Figure 28: Probabilistic solar PV forecast last week of April 2024

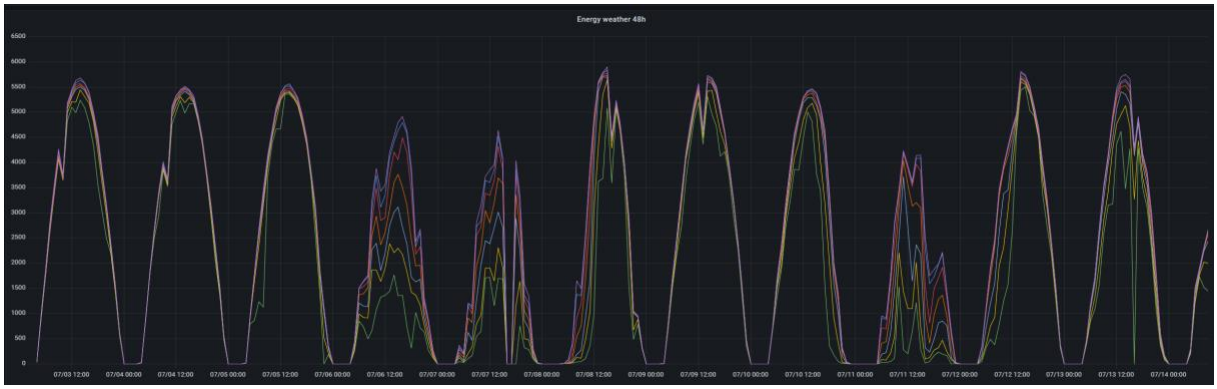

Figure 29: Probabilistic solar PV forecast first week of July 2024

Since January 2025, the energy measurement framework deployed at the 5GTN site has been updated with the enhanced version of the FMI Open PV forecast. This version uses numerical weather predictions from FMI and combines them with PV-related tools available in the PVlib Python package. The updated Python script fetches energy and weather-related dataframes, which are not ensemble estimates; instead, they provide a single estimation for predicting the output from a solar PV installation at given coordinates [24]. This prediction is based on panel angles, inverter capacity, solar irradiance, and all relevant weather data such as wind, albedo, temperature, absorption, losses, scattering, and cloud coverage. Following the integration of the FMI forecast into the energy measurement framework, several module integration and testing activities were conducted to validate the newly developed feature. These activities are described in detail in the next section.

4.2 FORECASTING APIS INTEGRATION WITH THE ENERGY MEASUREMENT FRAMEWORK

This section covers the use of forecasting APIs, which enable energy budgeting scenarios for the North Node gNB sites to utilize energy efficiently among the entire E2E network components. The forecasting APIs deployed inside the central controller includes the enhanced site-specific FMI energy weather forecast (up to 66 hours ahead), ELSPOT electricity spot pricing (24-hour ahead), and real-time grid-linked CO2 emissions estimates from FINGRID. The data is stored in a central database as described in earlier sections and visualized for the user through a Grafana dashboard.

Steps: The following steps were performed to integrate and validate the forecasting APIs into the deployed energy measurement framework at 5GTN sites.

- **FMI Energy Weather Forecast:** The main.py Python script is scheduled every 3 hours and executed via a nohup background process as shown in Figure 30, storing outputs in fmigitoutput.log. The script successfully simulated 3-day-ahead PV generation forecasts.
- **ELSPOT Electricity Spot Pricing:** The ELSPOTrequests.py script fetches hourly electricity prices for the next 24 hours using the API from https://api.porssisahko.net/v1/latest-prices.json.
- **FINGRID grid-linked CO_2 emissions estimates:** The Fingrid_Open_data.py script is scheduled every 3 minutes via nohup and fetches real-time grid-linked CO_2 estimates using the API from https://data.fingrid.fi/api/datasets/266/data.

Result: All three forecasting APIs (FMI energy weather forecast, ELSPOT pricing, FINGRID CO_2 estimates) were successfully called, parsed, and validated. Output data is correctly formatted from JSON, time-aligned to Finnish local time, stored in the central database, and visualized in Grafana as real-time dashboards for energy budgeting. The central controller publishes this data for the North Node sites using the MQTT bridge broker, allowing each component (energy and network) to subscribe to these forecasting APIs.
Visual Studio Code is used to run the scripts and connect to the host server (central controller). The Python scripts perform the following tasks, also shown in Figure 30.

1. Fetch energy weather forecast data from FMI (66 hours ahead, updated every 3 hours), publish relevant data via the MQTT bridge, store it in MySQL, and visualize it in Grafana in real time.
2. Fetch electricity spot pricing data from ELSPOT (24 hours ahead), publish it using the MQTT bridge, store it in MySQL, and visualize it in Grafana.
3. Fetch real-time CO_2 estimates from FINGRID's API (updated every 3 minutes for gCO_2 per kWh), publish it using the MQTT bridge, store it in MySQL, and visualize it in Grafana.
4. Collect external meter data, on-site sensor data, and PV-hybrid system data (including BESS) and store it using Venus GX at VTT and the central database at UOULU.

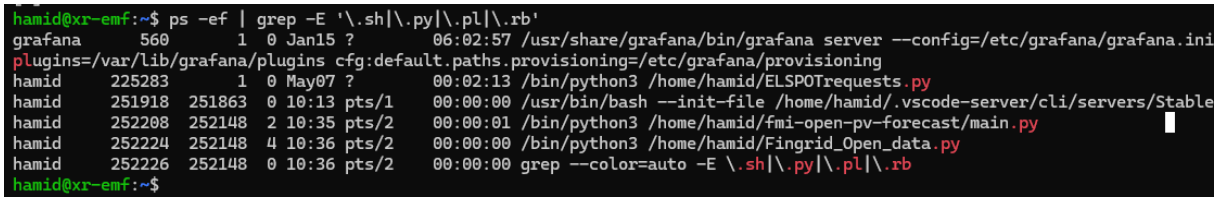

Figure 30: Forecasting APIs integration with central controller

4.2.1 Enhanced FMI Open PV forecast for next 66 hours

As mentioned in Section 4.1, the FMI Open PV forecast was updated using the latest FMI-provided APIs [24]. The Python code that runs the FMI model against the PVlib is based on a clear sky PV output forecast in kWh. As shown in Figure 31, the FMI Open Data-based weather forecast-aware energy output was generated for the next 3 days and plotted against the PVlib-based model. Figure 31 highlights the performance of theoretical maximum generation and the weather model-based generation side by side. The dataframes were obtained after inputting the configurable parameters based on the UOULU site-specific coordinates and specifications of 24 PV modules. The bar chart shown in the Figure 31, contains a comparative analysis between PVlib-based cloud-free and theoretical clear sky PV output versus the energy weather modelling, where the dark blue lines indicate the weather model-based generation in both lines and bar charts. The estimated output on day 1 prediction is 40 kWh, which is equivalent to 90% of the 6 kW inverter capacity of 24 solar panels on a clear sky. The second day estimation for a cloudy day is 27.2 kWh, which is about 60 percent of the theoretical maximum PV generation. Similarly, on day 3, the output estimate is 8kWh on a cloudy day.

The comparison analysis is further highlighted in Figure 32, which shows how these predictions, which are indicated by green lines, behaved against the real-time PV productions by 24 PV modules represented as yellow lines. All the estimated and real-time energy production values are stored and compared, and used for testing and validation of requirements and KPI metrics with a sampling rate of one hour [21] [24].

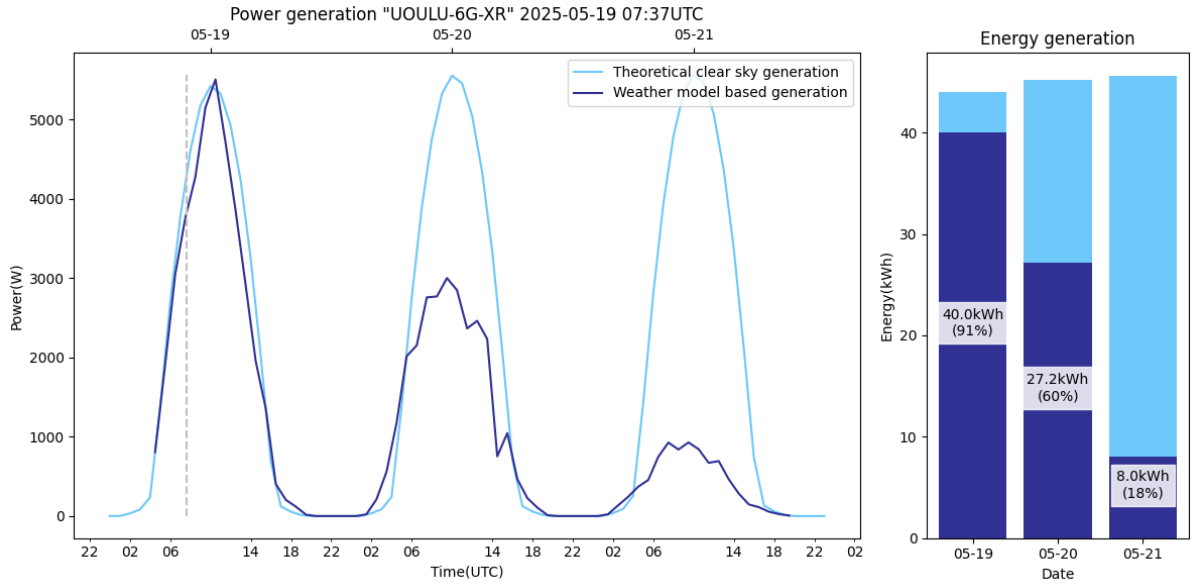

Figure 31: Simulating clear sky and weather model-based PV generation for the next 3 days using FMI forecast

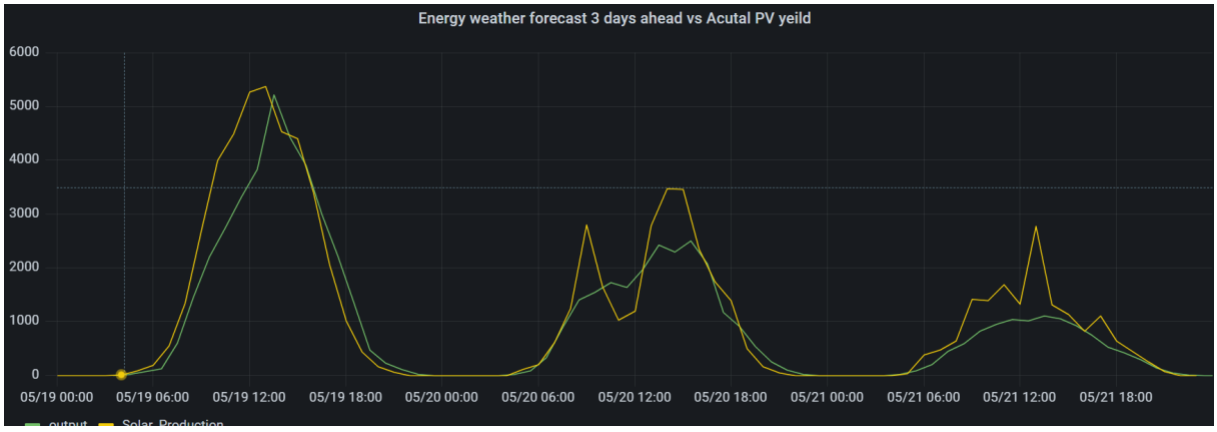

Figure 32: FMI model-based forecast (green) versus observed PV yield (yellow)

4.2.2 ELSPOT electricity pricing for the next 24 H

The second forecasting API integrated into the energy measurement framework is the ELSPOT electricity market feed, also known as the Nord Pool day-ahead market. It provides hourly electricity spot prices based on bids submitted by producers and consumers across the Nordic and Baltic regions [22]. This pricing data is essential for enabling energy-aware operation of a self-sustainable base station, supporting decisions such as when to rely on grid power, activate power-saving measures, or

switch to backup batteries. In Finland, day-ahead electricity price forecasts play a key role in energy budgeting and cost optimization. By using forecasted hourly prices for the next 24 hours, it becomes possible to strategically schedule energy use and select the most cost-effective energy source to power the base station. To retrieve ELSPOT pricing data, a Python script deployed at the central controller, as shown in Figure 33, queries the API endpoint at https://api.porssisahko.net/v1/latest-prices.json using the requests library. The script parses the JSON response and extracts the relevant timestamps and prices. As the timestamps are in UTC, they are converted to Finnish local time (EET or EEST) using the pytz library to align with local scheduling requirements. This data can then be used to plan energy-intensive operations during periods of lower electricity prices, improving both cost efficiency and energy resource management. After the API is called, the hourly data fetched for the next 24 hours is saved to the central database for KPI validation and visualized in Grafana panels, as captured in Figure 34.

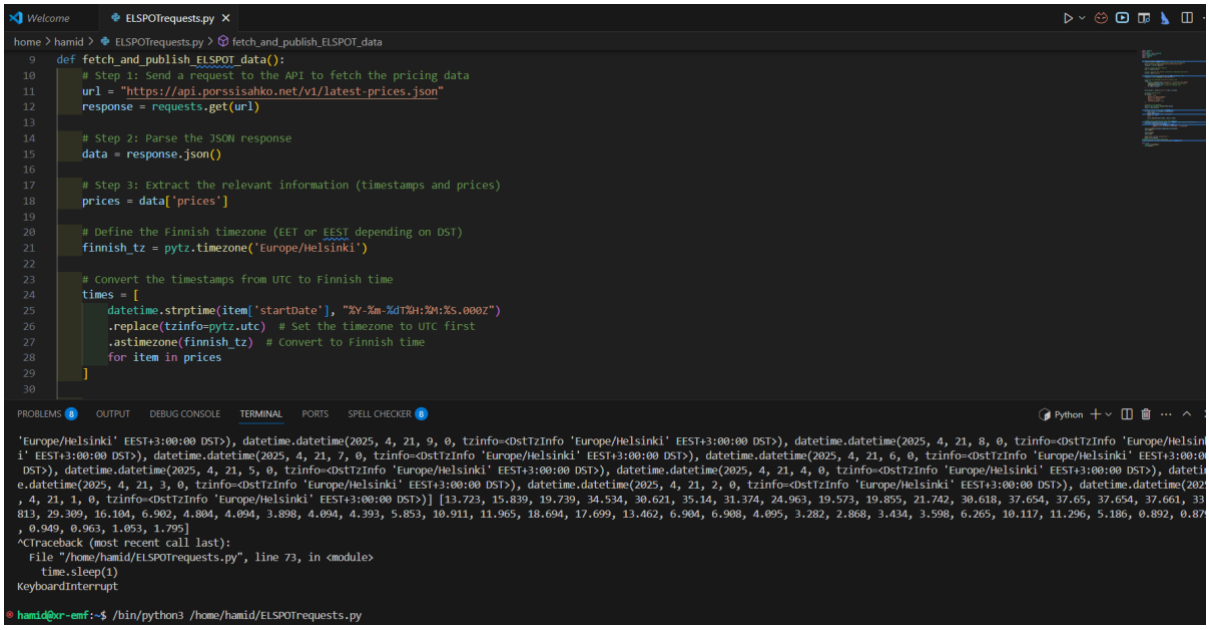

Figure 33: ELSPOT electricity pricing 24-hour ahead API validation.

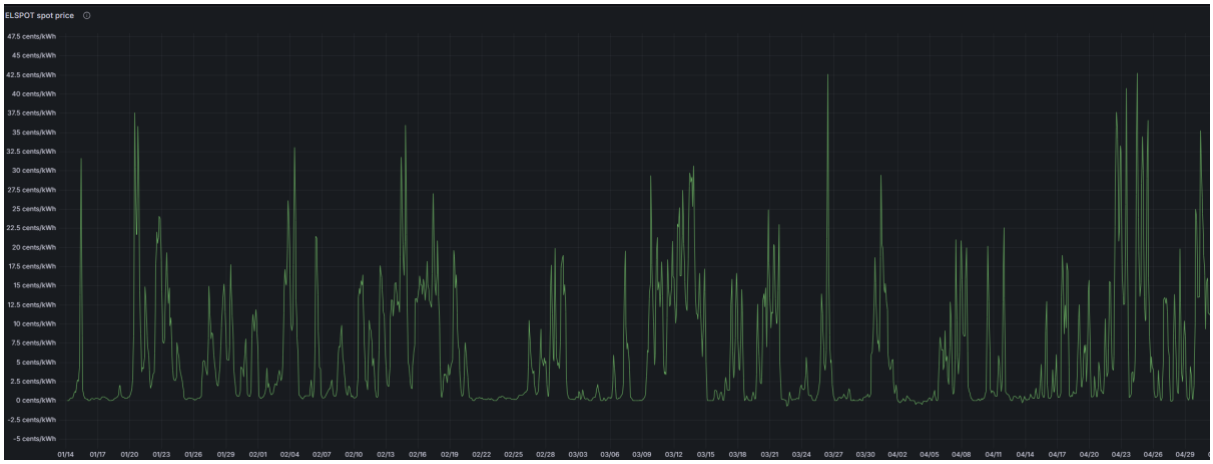

Figure 34: Grafana visualization of ELSPOT electricity pricing on an hourly basis.

4.2.3 FINGRID CO2 real-time estimates

The third forecasting API enabled by the deployed energy measurement framework is from the Finnish national electricity transmission grid operator, FINGRID, which provides estimates of CO2 emissions per kilowatt-hour of electricity consumed. This plays a crucial role in energy budgeting and avoiding periods of high CO2-linked grid generation. For example, in Finland, the transmission system operator (TSO) provides specific emission estimates in the form of gCO2/kWh to the consumed average electricity in Finland with a refresh rate of 5 minutes. When this emission data is processed and combined with the measured energy consumption data, absolute indirect emissions related to energy exchange through the grid interface can be estimated [23]. Similarly to the ELSPOT API acting as a cost counter, a CO2 counter was also created by combining the energy consumption data from the energy measurement framework with CO2 emission data from FINGRID APIs, as shown in Figure 35.

By integrating this data into our decision-making and energy budgeting, the mitigation of cumulative CO2 emissions as an objective may change the targeted consumption patterns, as the objective of energy budgeting can be to minimize the carbon footprint of the gNB site. This allows us to allocate resources in a way that reduces emissions while using a central controller for guiding power-saving measures at gNB sites. In this way we perform sustainable operations and also minimize the carbon footprint using the linked CO2 information from the grid intake. In addition to avoiding base station power usage from the grid during the periods of high CO2-linked estimates, as shown in Figure 36, the FINGRID open data API managed by the central controller can also assist in determining the periods of battery charging times, which align with the low CO2 estimate periods.

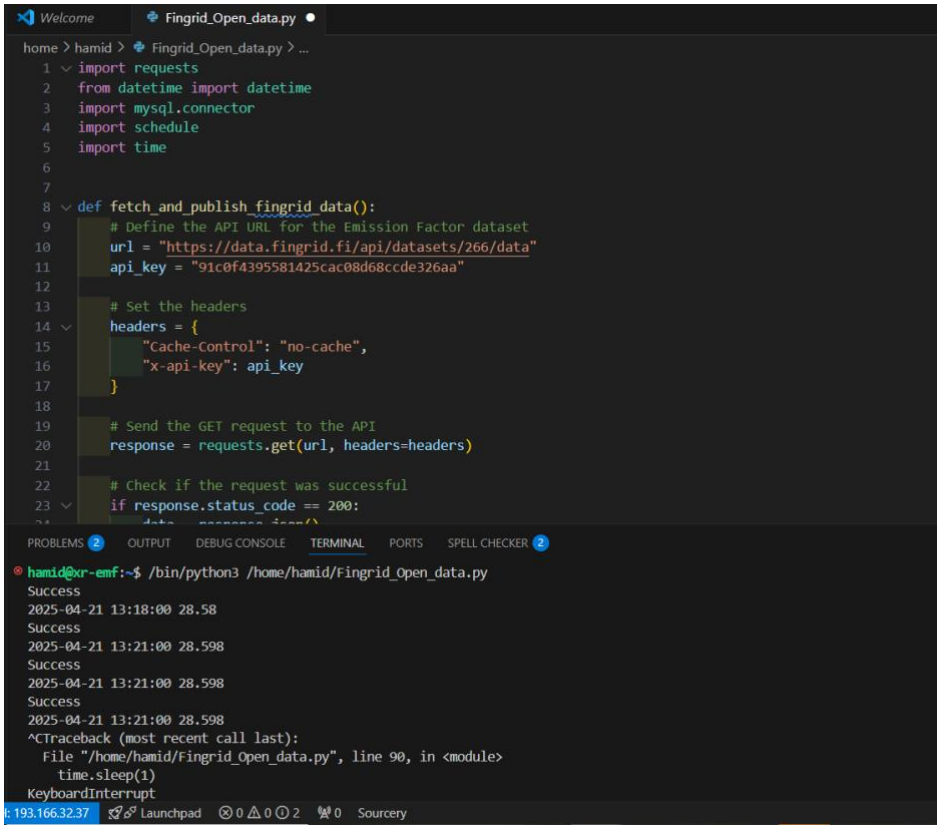

Figure 35: FINGRID Grid-Linked CO2 estimates API validation

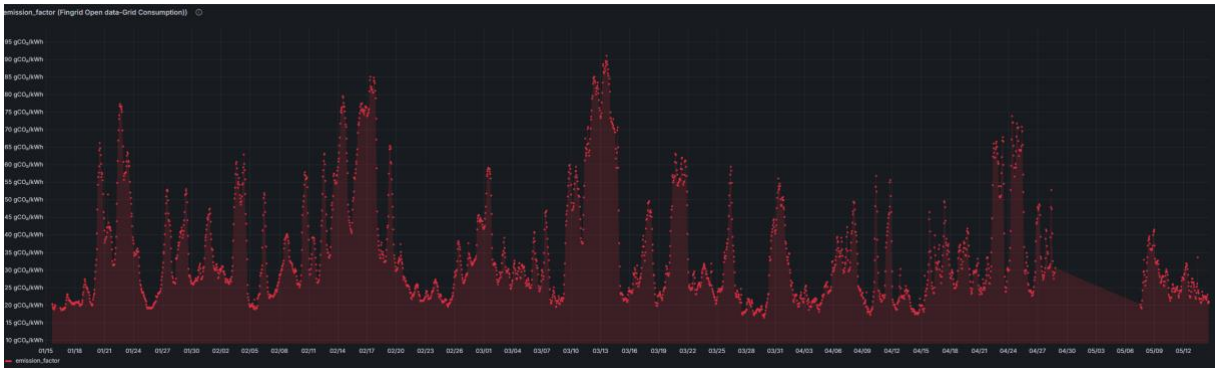

Figure 36: Grafana visualization of real-time FINGRID CO2 estimates.

4.3 UPDATED FMI OPEN PV FORECAST 66H

As described in previous sections, the enhanced and improved FMI open PV forecast is integrated with the central controller and has facilitated site-specific predictions, enabling energy budgeting for the upcoming 66 hours. There are new features integrated with the energy measurement framework as described in the following sections, which help with a better understanding of the weather-based modelling in harsh Finnish conditions. The features added to the forecast include adjustable simulation parameters, which are discussed later in the section. This section explores the weather-based parameters and radiation sources that the model takes into account before providing the output in kWh for the next 3 days. These radiation sources produced by the FMI-based model are as follows [24]:

- **Direct Radiation:** Modeled using DNI (Direct Normal Irradiance).
- **Atmospheric Scattered Radiation:** Modeled with DHI (Diffuse Horizontal Irradiance).
- **Ground-Reflected Radiation:** Modeled using GHI (Global Horizontal Irradiance).

These radiation sources are available in dataframes for the next 3 days, as shown in Figure 37, and provide valuable insights on how much solar PV output will vary based on the direct, scattered, and ground-reflected radiation. In addition, these radiation sources are further modelled with the weather-based conditions like wind speeds, clouds, snow, rain, reflections, transposition, and absorption of panels, etc. These parameters are updated by the FMI weather model every 3 hours. After executing the main.py file, the FMI-based API fetches all the required parameters and produces hourly based dataframes for the next 3 days as follows [24]:

- **[index (Time)]:** Meteorological time. In meteorology, a timestamp for 13:00 represents the time 12:00-13:00.
- **[time]:** This is the time index shifted by 30min. More useful than the meteorological time for physics.
- **[dni, dhi, ghi]:** Irradiance types, these can be used for estimating radiation from direct radiation, atmosphere-scattered radiation, and ground reflected radiation, as shown in Figure 37.
- **[albedo]:** Ground reflectivity near installation. This is retrieved from the FMI open data service. It should be between 0 and 1 as shown in Figure 37.
- **[T]:** Air and panel temperature updated by FMI as shown in Figure 37.
- **[wind]:** Wind speed updated by FMI is shown in Figure 37.
- **[cloud_cover]:** Cloudiness percentage, between 0 and 100 as shown in Figure 37.

- **[dni_poa, dhi_poa, ghi_poa]:** Transpositions of dni, dhi, and ghi to the plane of array (POA). These values are always positive and lower than their non poa counterparts as captured in Figure 37.
- **[poa]:** Sum of dni_poa, dhi_poa, ghi_poa. Represents the amount of radiation reaching the panel surface. This does not account for panel reflectivity as shown in Figure 37.
- **[dni_rc, dhi_rc, ghi_rc**]: Transpositions of radiation types with reflection corrections. These are lower than their '_poa' counterparts as shown in Figure 37.
- **[poa_ref_cor]:** Sum of dni_rc, dhi_rc and ghi_rc. This represents the amount of radiation absorbed by the solar panels as shown in Figure 37.
- **[output]:** System output in watts as shown in the right most side of the Grafana dashboard in second row with label Energy-weather FMI 3 days ahead as shown in Figure 37.

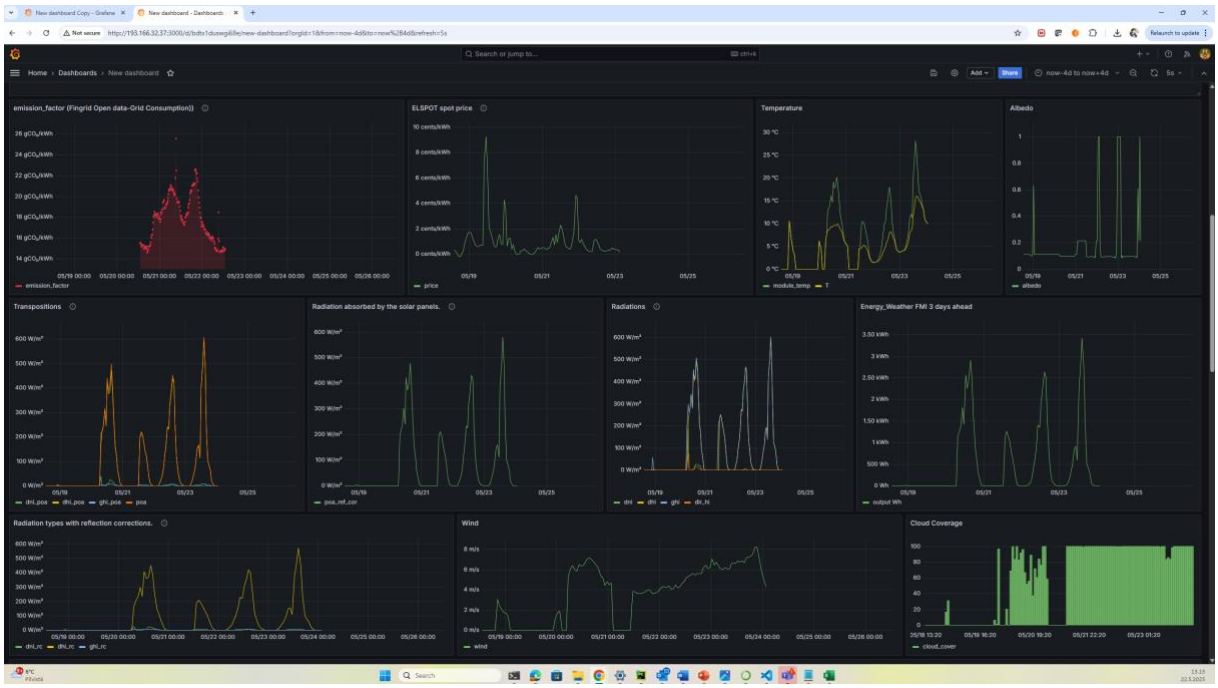

Figure 37: Grafana Visualization of all the collected datasets from forecasting APIs updated 22.05.2025

4.4 EVALUATION OF ENERGY WEATHER FORECAST ACCURACY

This section evaluates the accuracy of the energy weather forecast fetched from the FMI Open PV forecast API. The Python code deployed at the central controller inside the energy measurement framework includes adjustable simulation parameters in the config file as shown in

Figure 38. These adjustable parameters are based on site-specific coordinates and features of the PV modules located on the rooftop of Biolongintie, University of Oulu, Finland, and are presented in Table 8. The inverter capacity is 6kW, installed by third-party SolarEdge. In addition, there are three on-site sensors and one consumption meter. Based on the solar installation parameters by SolarEdge, these FMI parameters were adjusted based on the comparison between forecasted values versus the actual PV yield and real-time values from solar irradiance and module temperature sensors.

Table 8: Adjustable simulation parameters

Adjustable parameters	Values
Coordinates (UOULU)	latitude = 65.0599 longitude = 25.4651
Rated installation power in kW	6 kW
Module elevation in meters	3m wall-mounted, 1m horizontal
Panel angles (UOULU site mixed panel angles)	tilt = 45 # degrees. A panel flat on the roof would have a tilt of 0. Wall-mounted panels have a tilt of 90. azimuth = 180 # degrees, north is 0 degrees, east is 90. Clockwise rotation
Albedo	Real-time update by FMI between 0 and 1
Wind Speed	Real-time update by FMI
Air Temperature	Real-time update by FMI
Cloud Coverage	Real-time update by FMI

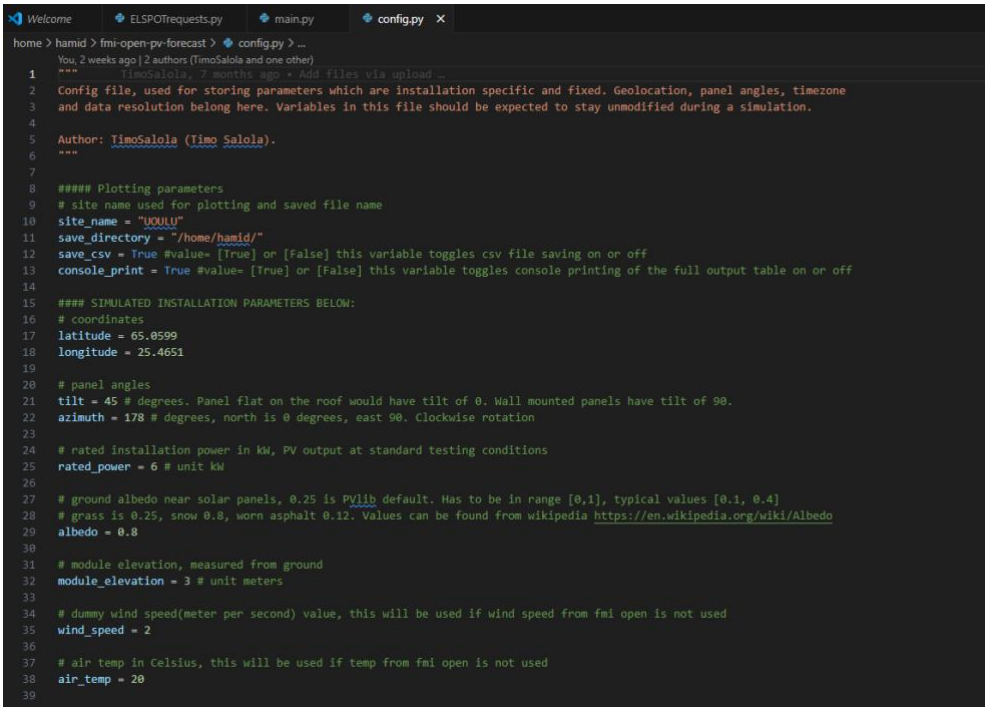

Figure 38: Config.file for adjusting PV installation parameters

The central controller automates the API provided by FMI and uses a nohup background process inside the edge server to automatically fetch the API every 3 hours. The script is able to then store the data to the central database and use the MQTT bridge broker to rely on the energy weather forecast at the other gNB site inside the North Node energy measurement framework. Figure 38 shows the configuration file used to refine the accuracy estimates of FMI's energy-weather forecasts for the next 66 hours.

4.4.1 Observed data vs FMI energy weather forecasts for the next 48 hours

WP5, Task 5.3 is responsible for production and for enabling the energy measurement framework with the measured vs predicted performance of the FMI-based site-specific energy weather forecast for the 24 PV modules at UOULU's rooftop. Figure 39 presents a 7-day period (May 12, 2025, until May 19, 2025) comparison of the hourly PV output forecasts from the forecasted energy prognosis for the next 48 hours (orange lines) against the actual measured data from the PV modules (blue lines). The two lines closely correlate with each other, especially on clear sunny days, but some underestimation and overestimation can be seen due to unpredictability in cloud movement, shadowing, and scattering of radiation. Further reasons for the mismatch are discussed in 4.4.3. This prediction of PV yield production over the next 66 hours forms the basis of energy budgeting scenarios for battery storage (BMS) and network element consumption. The validation activities were carried out both at the VTT and UOULU sites using the dataset generated in Figure 39 and provided in Chapter 7.

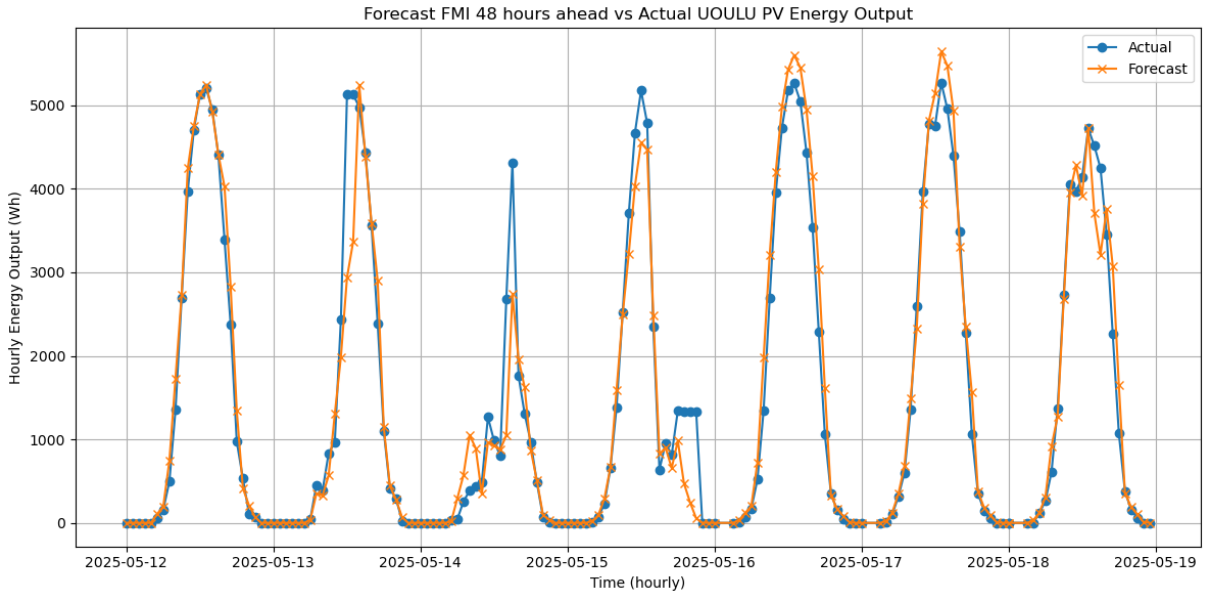

Figure 39: Actual Output from SolarEdge vs FMI-based 66 h ahead forecast accuracy comparison

Figure 39 shows the performance evaluation of the site-specific energy weather forecast with respect to the observed PV yield. The forecast starts to deviate significantly from the measured PV output when the prediction is more than 48 hours (third-day forecasts). The model achieves an MAE of 217.25 and an RMSE of 413.71, corresponding to a percentage RMSE of 27.86%. The high MAPE of 77.97% indicates large relative errors during some hours, mostly caused by rapid weather conditions or unpredictable cloud coverage from low to high layers. The correlation coefficient of 0.974 shows that the forecast still follows the overall trend and temporal shape of the actual production very closely, which is why the energy budgeting scenarios can be tuned reliably based on the available forecast with minor adjustments on a real-time basis using on-site sensors like solar irradiance. Overall, the FMI forecast captures the pattern well but significantly underestimates or overestimates the PV production sometimes due to uncontrollable factors.

4.4.2 Daily Accumulated Energy Forecast vs. Actual Daily accumulated PV yield with Percentage Deviation

Figure 40 highlights the comparison analysis in percentage when using the hourly energy outputs and aggregating them into daily accumulated PV yield versus the daily accumulated energy weather forecasts. This percentage of deviation is shown in Figure 40, with some days showing deviations exceeding ±15%. The average daily accumulated accuracy of the FMI weather-based forecasting for the next 48 hours was within the range of ±8%, with the model performing very well during clear sky days, thus providing a solid platform to adjust the daily energy consumption pattern for base stations. The energy weather forecast model assumes a uniform panel tilt of 40 degrees and has a limitation of not accounting for the mixed angle installation at the UOULU site. This leads to structural bias in the forecast preventing it from achieving highest levels of accuracy. The FMI energy weather forecast API deployed at the central controller was scheduled to run every 3 hours, updating the dynamic conditions like albedo, wind speed, and temperatures. In addition, accuracy is also dependent on local conditions, frost, snow, shading, and other factors which are currently not modeled.

In the VTT pilot, a +24-hour PV-production prognosis was selected as the basis for constructing the energy availability estimate used in the E2E demonstration (section 5.3). This time horizon was chosen to provide adequate reaction time for network adaptation relative to the anticipated PV-yield levels of

the following day, particularly when considering continuous operation supported by virtual battery dimensioning and the available range of RAN power-consumption options. Multiple forecasting horizons were evaluated using a simplified moving-average simulation model. Forecasts exceeding 48 hours exhibited excessive smoothing and stability, resulting in insufficient responsiveness to day-ahead fluctuations. Conversely, horizons shorter than 24 hours produced overly dynamic behavior, triggering adjustments that were too frequent for practical operational planning. The +24-hour horizon therefore represented the most balanced option, enabling meaningful adaptation decisions while avoiding high-frequency oscillations in RAN power-state control.

Furthermore, the +24-hour horizon aligns well with the availability of ELSPOT day-ahead market prices, which become accessible after 15:00. This alignment supports potential future optimisation features that combine energy availability with electricity market signals, including the possibility of 15-minute energy budgeting in later development stages. In the current implementation, the emphasis was placed primarily on demonstrating achievable energy-saving percentages.

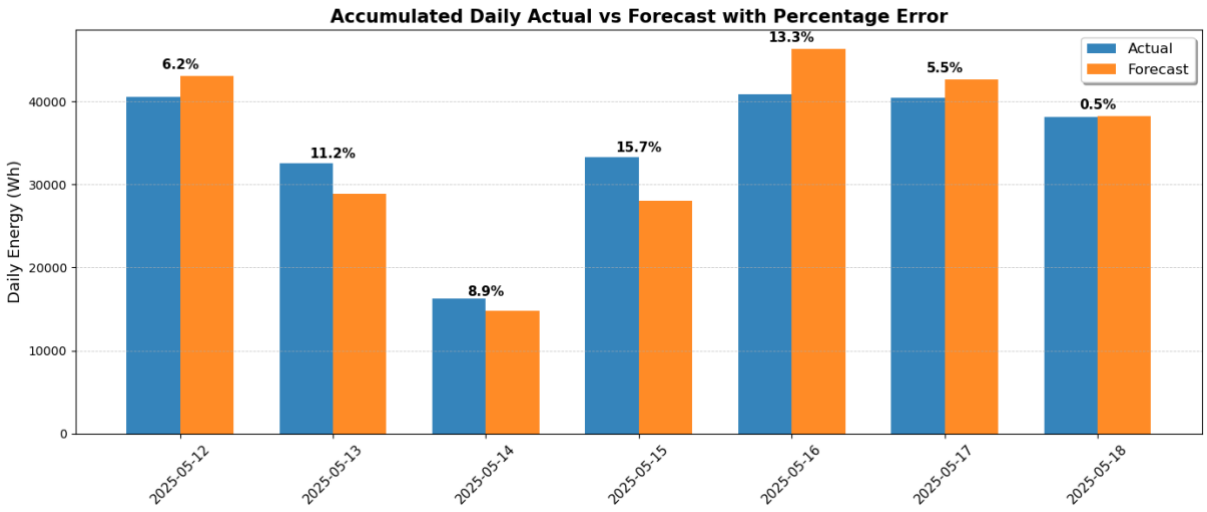

Figure 40: Daily Accumulated Energy Forecast vs. Actual with Percentage Deviation

4.4.3 Underestimation and overestimation of the forecasted parameters

The accuracy of the forecast described in section 4.4.1 depends on controllable and uncontrollable factors. As shown in Figure 39, the forecast is sometimes underestimated, while in other hours it is overestimated. The reasons behind these inaccuracies are described in this section. The forecast simulated in our system represents a somewhat ideal monofacial PV system, with a perfect open horizon, standard assumed losses, and no snow accumulated on the panels. Real PV systems may deviate from this for various reasons, including, for example:

- Shadows cast by trees and other structures.
- Snow on top of the panels decreases the PV production.
- System-specific losses aren't accounted for properly.
- Weather forecasts are always uncertain to some extent due to their complexity.

- FMI Open Data values are expected hourly averages.

The FMI-based simulated generation often exceeds or falls short of the actual PV output due to several compounding factors. The underestimations and overestimations by the FMI weather-based model have many uncertainties, but the following are the observed reasons identified after careful examination of daily forecasting comparisons with real-time PV output.

4.4.3.1 Simulated generation is higher than the real output:

- Ideal conditions assumptions like optimal panel cleanliness, no panel degradation due to harsh weather conditions.
- Mixed-angle site not accounted for by FMI-based models. The sun tracking is not enabled in real installations and impacts the real PV yield, especially during the last hours of the day, as shown in Figure 41.
- PV panels degrade over time. Adjust *rated_power* in *config.py* to be a lower value.
- Panels may be dusty. Wash panels or wait for rain to do it for you.
- Wind may cool the panels less than the model suggests, and the increased temperature may be decrease efficiency. This means setting a lower than actual module elevation in config.py to adjust the PV generation.

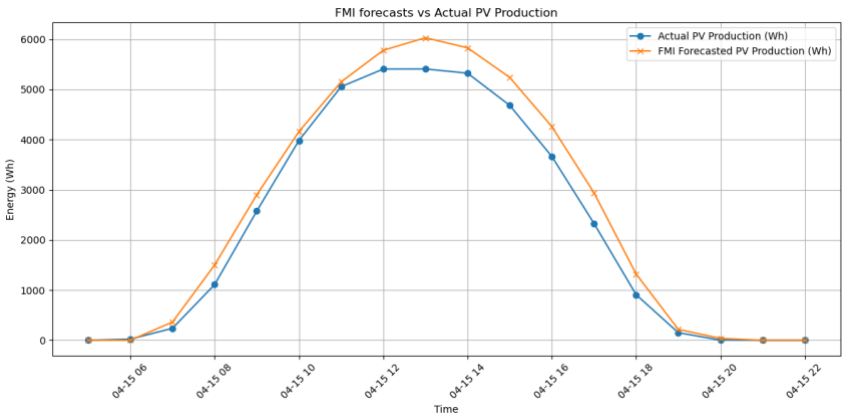

Figure 41: Overestimation of the forecasted parameters

4.4.3.2 Real generation is higher than simulated output.

- Verify that system power rating and panel tilt/orientation are correctly defined in config.py (Figure 38)
- Cloud-edge reflections can temporarily boost PV output even when direct irradiance is partially blocked as shown in Figure 42. No changes are required as this effect is difficult to adjust in the configuration parameters and occurs rarely.

- Actual panel temperature (can also be observed using an on-site sensor, as shown in Figure 43) might be lower than the estimated panel temperature by the forecasting model. Adjusting this would require integration with the on-site sensor (PV module temperature) and would require enhanced model adjustments.

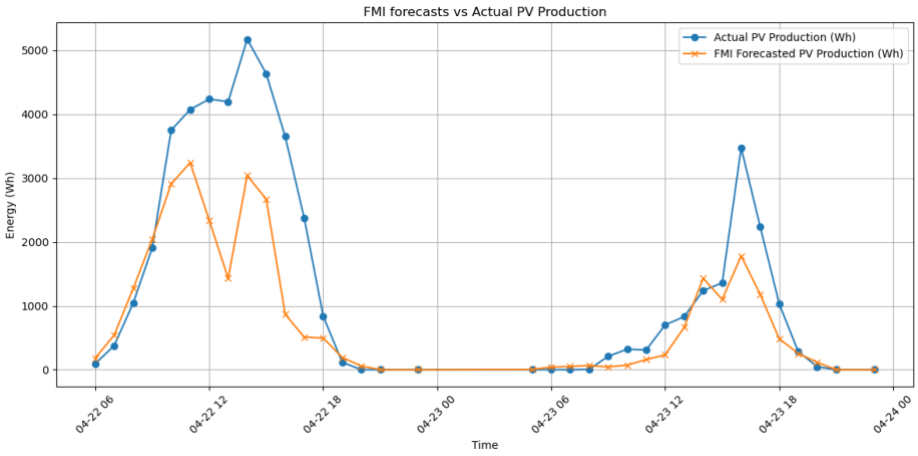

Figure 42: Underestimation of the forecasted parameters

4.4.4 Accurate 66-Hour Solar PV Forecasting Without Physical Deployment: Harnessing FMI Data

Using the FMI open data API, it is possible to forecast solar PV production for the next 66 hours without requiring any physical solar panel deployment or historical PV production data. The PV forecast API allows us to adjust key environmental and installation parameters such as geographic coordinates (UOULU: latitude 65.0599, longitude 25.4651), rated PV system size (6 kW), panel elevation (3 m wall-mounted, 1 m horizontal), and orientation (tilt 45°, azimuth 180°), Thus, we can simulate the energy output dataframes of a virtual PV system with high temporal granularity and accuracy as shown in Figure 39. This approach is particularly beneficial for energy budgeting strategies as it utilizes highly sophisticated site-specific energy weather modelling. This stands in contrast to traditional third-party forecasting methods, which typically rely on historical solar yield data and often struggle to capture short-term weather dynamics. In contrast, the FMI-based method dynamically adjusts and computes real-time atmospheric conditions like irradiance, temperature, wind speed, albedo, and cloud cover (every 3 hours). allowing it to estimate actual production potential for any arbitrary site setup. This makes FMI-powered forecasting not only more adaptable and cost-effective but also ideal for scenarios where physical panels have not yet been installed or for evaluating new locations and configurations before investing in hardware.

4.4.5 On-site sensor data

The on-site sensors are crucial for real-time energy monitoring, particularly for enhancing forecasting model accuracy through nowcasting capabilities and AI tools used in energy budgeting strategies. These on-site sensors, shown in Figure 43, located at the gNB sites, provide valuable datasets for training, forecasting, and analyzing PV array and wind turbine sizes. The on-site sensors located near the gNB and PV installation site include solar irradiance and temperature, humidity sensors, which are also integrated within the energy measurement framework with an interval rate of 3 minutes per sample.

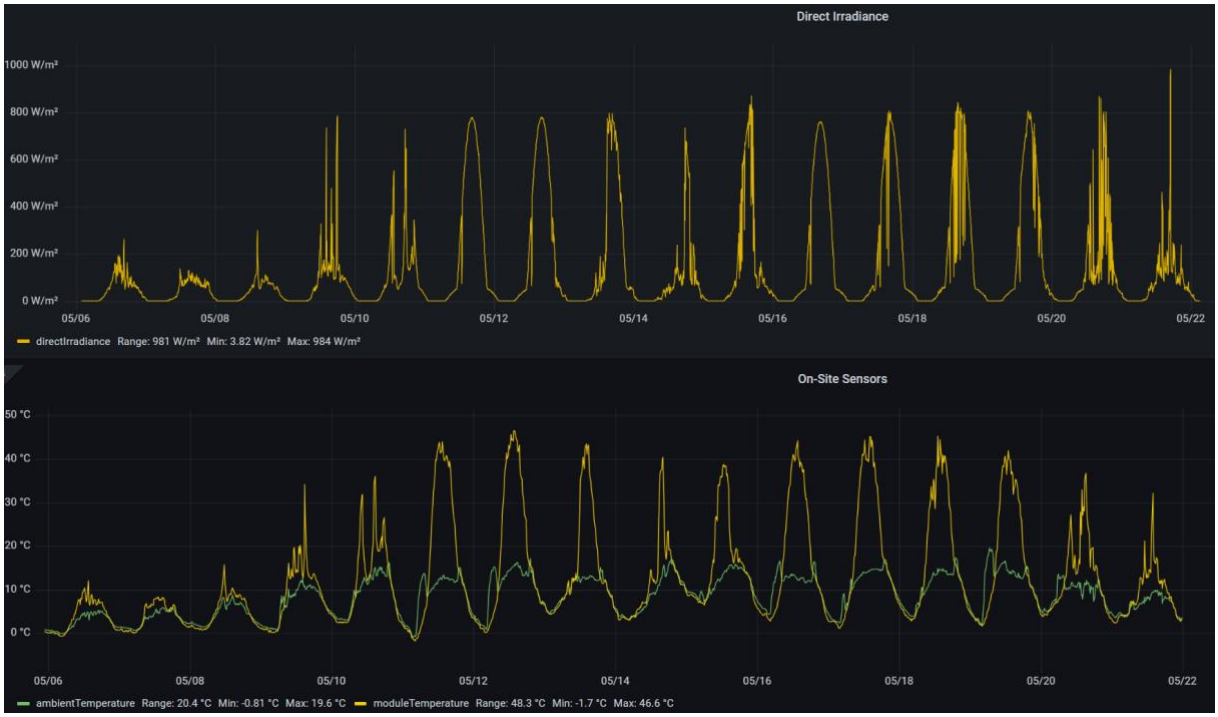

Figure 43: Solar irradiance and temperature, on-site sensor data at UOULU gNB site

4.4.6 Recurrent Neural Networks: Long Short Term Memory (LSTM)

For time series data recurrent neural networks are recognized for their superior performance in machine learning or deep learning algorithms [33]. Using the deep learning model for the UOULU PV yield dataset, in particular LSTM, is our proposed model to guide short-term energy forecasting. The goal of this model is to assist in mitigating underestimation and overestimation in the energy weather forecast produced by the central controller using the APIs from FMI. We implemented the LSTM model using PV yield data from 24 panels, following the configuration detailed in Table 9. The collected dataset was used for training the LSTM model starting from July 2021 until January 2025. The training dataset spans from July 2021 to January 2025, as shown in Figure 44. The data was first cleaned and normalized before training. As shown in Figure 45, the LSTM model effectively captures the temporal patterns in the dataset and provides accurate short-term predictions, achieving an RMSE of 7%. The collected datasets are divided into training and test data. The dataset was split into 90% for training and 10% for testing. The blue lines shown in Figure 45 represents LSTM model predicted values overlaying on the original training data. The LSTM shows promising results during the training and testing splits, but its ability to predict the future PV yield output remains limited. This is mainly because real-time weather conditions depend on many dynamic variables, while FMI forecasts rely on advanced models such as astronomical calculations, irradiance transposition, panel temperature estimators, reflection estimators, solar irradiance estimators, and satellite-based scattering information regarding albedo, wind and snow, which cannot be accounted for by LSTM models. This LSTM model can only help in correcting underestimation and overestimation of the output estimators and simulated solar PV yield.

- Data Cleaning & Preprocessing Steps
- Resampling, Interpolation, NaN handling, positive enforcement
- Normalization, Scale Solar Production between 0 and 1 using MinMaxScaler for LSTM input.
- The model will look at the past 72 hours (3 days) of solar production as input and training.

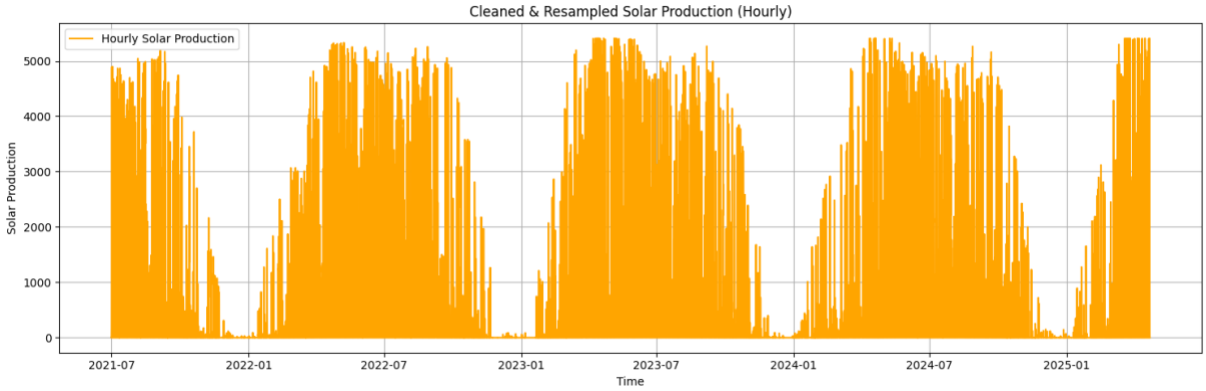

Figure 44: Four years of historical PV yield data from the OULU site, used to train and validate the LSTM model for short-term solar energy forecasting

Table 9: LSTM Model Configurations

Area	Current
Look-back Window (input_steps)	72 hours
Forecast Length (output_steps)	240 hours
Features	Solar_Production at UOULU site 24 PV modules
Model Complexity	Basic LSTM
Scaling	MinMaxScaler (0-1)
Neurons layer	64, adam, epochs = 100, batch size = 252
Loss Function	**Normalized RMSE = 7.01%**

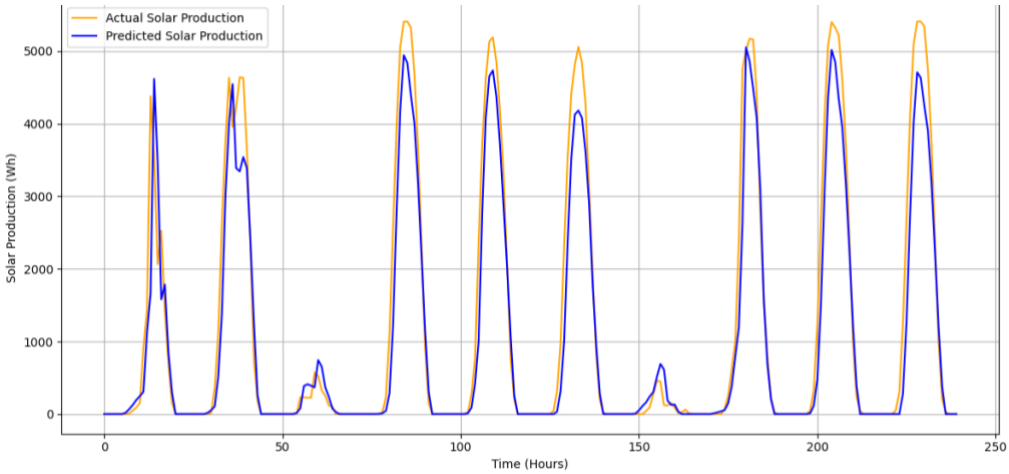

Figure 45: LSTM based short term forecasting for trained data for provided PV yield dataset

5 E2E ENERGY EFFICIENCY

In this section, we summarize the results from T5.4 “E2E ENERGY EFFICIENCY” with the entire E2E network components connected to external meters and holistic solutions focusing on enabling energy efficiency across the full E2E data path. The North Node 5GTN sustainability experimentation infrastructure was used to validate the results, focusing on local private networks infrastructure such as ORAN and commercial gNB, USRPs, Radio Units, Video servers, and UEs/Modems. The E2E energy efficiency activities were carried out using an open source 5G ORAN environment at the UOULU site and a commercial gNB baseband unit, n78 mMIMO radio, n7 macro radio, and video server at the VTT site. This section further defines the activities listed in D5.1 [13], the energy saving methods based on RAN configuration at both North Node sites, and the role of the centralized controller in optimizing E2E energy consumption profiles among the network components.

5.1 OPEN-SOURCE 5G ENVIRONMENT E2E ENERGY CONSUMPTION

5.1.1 5G indoor RAN (UOULU)

As described in D5.1 [13], the 5G indoor ORAN environment is the UC5 enabler at UOULU for test case specification, KPI validation, and assessment. Using various RAN configurations from the OAIBOX UI, the validation methodology was applied for the assessment of KPI metrics listed in D1.1 [17]. The set of radio and RAN configurations is changed using the gNB RAN configuration panel provided by OAIBOX MAX UI, as shown in Figure 46. Using this configuration panel, the user can change the various RAN configurations to implement and validate energy-saving methods and full power modes based on energy budgeting strategies developed during the 6G-XR UC5 research activities. The OAIBOX dashboard has already been explained in D5.1 [13], and in this section we discuss the impact of different RAN configurations when OAIBOX, USRPs, and UEs are connected to external meters and power consumption values are stored in the central database with one sample per second.

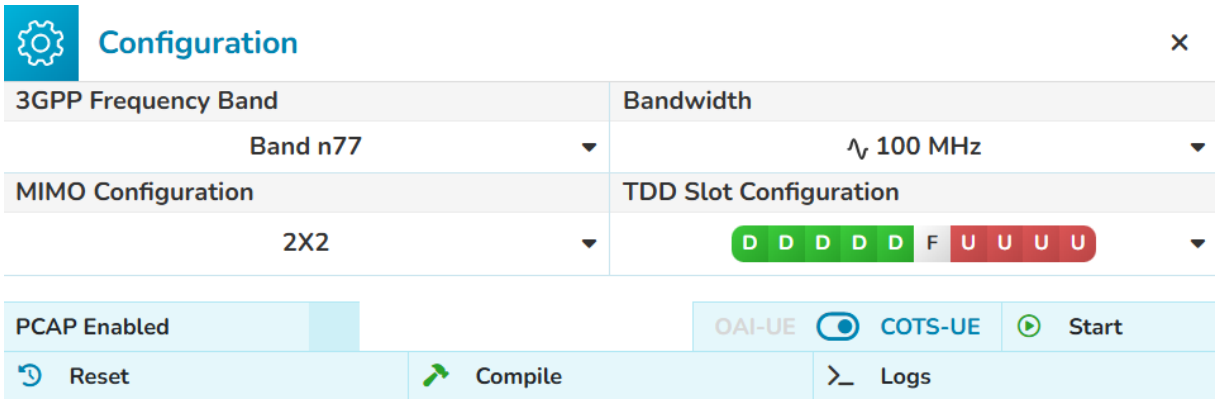

Figure 46: OAIBOX MAX gNB RAN configuration panel

The experimentation results include various radio configuration changes to potentially save energy, which were tested in UOULU 5G indoor test environment using a single OAIBOX MAX device and a software-defined radio (SDR): USRP models B210 and N310 supporting bandwidths up to 40 MHz and 100 MHz, respectively [28]. For tests using the USRP B210, the UE consisted of a 5G Quectel modem and a Raspberry Pi 5 (Linux). For trials using the USRP N310, the UE comprised a 5G Quectel modem and a Windows laptop. The radio configuration changes tested including limiting the used bandwidth, restricted the modulation constellation, time division duplex (TDD) slot configuration selection, and

MIMO mode selection. The purpose of these experimentation trials was to study whether these radio configuration changes are reasonable to be used for conserving energy in the UOULU O-RAN setup. iPerf3 was used to generate UDP and TCP traffic with the UE functioning as the client and the OAIBOX acting as the server. This set up was setup to carry on validation activities, which are presented in Chapter 7.1.

The power consumption was measured separately for the OAIBOX MAX device, SDR device (USRP B210 or N310), and 5G Quectel modem/Raspberry Pi5. Monitoring the energy consumption separately for USRPs provides information for individual radio units of the gNB. The UE comprises a communication component (5G Quectel modem) and a computing device (Raspberry Pi 5 or Laptop), both of which were monitored for energy consumption. MQTT enabled (using central controller) NetioPowerBox was used as an alternating current (AC) power meter for measuring separately current (I), voltage (V), and true power factor (TPF). These values were used to calculate power (P), P=I·V· TPF, with an accuracy of 0.1 W. These energy-related parameter values are stored in the central database and then delivered to the Grafana dashboard for visualizing the results and for data analytics.

5.1.2 Received traffic with different radio configurations

Table 10 was used to present seven different radio configurations (Conf. 1 - Conf. 7) that were tested in the UOULU 5G indoor test environment (using USRP B210) with 10 min test runs. Maximum TCP traffic was generated separately in DL direction (from gNB to UE) and in UL direction (from UE to gNB) using iPerf3 speed test tool and received average traffic values ranging between 64Mbps (20MHz) and 133Mbps (40MHz). Two different bandwidth sizes were used (20 MHz, 40 MHz), three different maximum modulations (QPSK, 64-QAM, 256-QAM), and three different TDD frame structures with different slot configurations (3D-F-1U, 2D-F-7U, 7D-F-2U), providing distinct ratios for DL and UL communication as shown in Table 10. Conf. 2 was used as a default configuration where other configurations were compared. Conf 2 uses a bandwidth of 40 MHz, allows all possible modulations (max. modulation up to 256-QAM), and applies a TDD frame structure of 3 DL and 1 UL slots (F is a flexible slot used as a guard time between DL and UL periods). USRP B210 applied only the SISO (1x1) antenna configuration with one transmitting and one receiving antenna. Mean power consumption and received data per energy unit with all seven configurations were monitored and used for validation activities and performing an energy conservation-based combination of RAN configurations.

Table 10: Different configurations with applied radio parameters and received average DL and UL traffic (using USRP B210 with SISO antenna configuration)

Configuration #	*RAN configurations for USRP B210*
Conf #1	*Bandwidth 20 MHz, MCS = 256 QAM (max_mcs=28), TDD= 3*DD-F-1*UU, SISO 1x1*
Conf #2	*Bandwidth 40 MHz, MCS = 256 QAM (max_mcs=28), TDD= 3*DD-F-1*UU, SISO 1x1*
Conf #4	*Bandwidth 40 MHz, MCS = 64 QAM (max_mcs=19), TDD= 3*DD-F-1*UU, SISO 1x1*
Conf #4	*Bandwidth 40 MHz, MCS = QPSK (max_mcs=4), TDD= 3*DD-F-1*UU, SISO 1x1*
Conf #5	*Bandwidth 40 MHz, MCS = 256 QAM (max_mcs=28), TDD= 2*DD-F-7*UU, SISO 1x1*
Conf #6	*Bandwidth 40 MHz, MCS = 256 QAM (max_mcs=28), TDD= 7*DD-F-2*UU, SISO 1x1*
Conf #7	*Bandwidth 20 MHz, MCS = QPSK (max_mcs=4), TDD= 2*DD-F-7*UU, SISO 1x1*

In addition, corresponding measurements shown in Table 11 were performed with all different radio configurations (Conf #1 to Conf # 18) when using USRP N310 instead of USRP B210. The purpose of the Conf. 1-18 was to measure the effect and relation of MIMO (2x2) and SISO(1x1), TDD slots, MCS, and bandwidth selection for communications performance and power consumption. The purpose of these various configurations was to measure the effect of increasing the bandwidth up to 100 MHz with MIMO 2x2 and comparing it with 20MHz bandwidth with SISO 1x1 for communications performance and power consumption test cases and validation activities for the energy saving KPI metric. The seven different configurations with applied radio parameters and received average DL and UL traffics are shown in Table 11.

Table 11: Different configurations with applied radio parameters and received average DL and UL traffics (using USRP N310 with SISO and MIMO antenna configuration).

	RAN configurations for USRP n310
Conf #1	*Bandwidth 100 MHz, MCS = 64 QAM (max_mcs=19), TDD= 5*DD-F-4*UU, MIMO2x2*
Conf #1.1	*Bandwidth 80 MHz, MCS = 256 QAM (max_mcs=28), TDD= 3*DD-F-1*UU, MIMO2x2*
Conf #1.3	*Bandwidth 60 MHz, MCS = 256 QAM (max_mcs=28), TDD= 3*DD-F-1*UU, MIMO2x2*
Conf #2	*Bandwidth 40 MHz, MCS = 256 QAM (max_mcs=28), TDD= 3*DD-F-1*UU, MIMO2x2*
Conf #2.1	*Bandwidth 20 MHz, MCS = 256 QAM (max_mcs=28), TDD= 5*DD-F-4*UU, SISO 1x1*
Conf #2.2	*Bandwidth 100 MHz, MCS = 256 QAM (max_mcs=28), TDD= 5*DD-F-4*UU, MIMO2x2*
Conf #7	*Bandwidth 100 MHz, MCS = QPSK (max_mcs=4), TDD= 3*DD-F-1*UU, MIMO2x2*
Conf #8	*Bandwidth 100 MHz, MCS = 256 QAM (max_mcs=28), TDD= 2*DD-F-7*UU, MIMO2x2*
Conf #9	*Bandwidth 100 MHz, MCS = 256 QAM (max_mcs=28), TDD=7*DD-F-2*UU, MIMO2x2*
Conf #10	*Bandwidth 100 MHz, MCS = 256 QAM (max_mcs=28), TDD=7*DD-F-2*UU, SISO1x1*
Conf #11	*Bandwidth 80 MHz, MCS = 64 QAM (max_mcs=19), TDD= 3*DD-F-1*UU, MIMO2x2*
Conf #12	*Bandwidth 80 MHz, MCS = QPSK (max_mcs=4), TDD= 3*DD-F-1*UU, MIMO2x2*
Conf #13	*Bandwidth 60MHz, MCS = 64 QAM (max_mcs=19), TDD= 3*DD-F-1*UU, MIMO2x2*
Conf #14	*Bandwidth 60MHz, MCS = QPSK (max_mcs=4), TDD= 3*DD-F-1*UU, MIMO2x2*
Conf #15	*Bandwidth 80MHz, MCS = QPSK (max_mcs=4), TDD= 7*DD-F-2*UU, MIMO2x2*
Conf #16	*Bandwidth 60MHz, MCS = QPSK (max_mcs=4), TDD= 7*DD-F-2*UU, MIMO2x2*
Conf #17	*Bandwidth 80MHz, MCS = QPSK (max_mcs=4), TDD=3*DD-F-1*UU, SISO1x1*
Conf #18	*Bandwidth 60MHz, MCS = QPSK (max_mcs=4), TDD= 3*DD-F-1*UU, SISO1x1*

5.1.3 Power consumption with different radio configurations

Mean and standard deviation (StdDev) of power consumption and received data per energy unit (kilobits per Joule) with different radio configurations and traffic profiles are presented for the OAIBOX MAX device in Table 12 (using USRP B210) and Table 13 (using USRP N310). Additionally, results for the USRP B210 are presented in Table 14. It must be noted that power consumption values with the different SDRs (USRP B210 and N310) are not comparable because the level of power consumption is remarkably higher (about 45 W) with USRP N310 than with USRP B210 (about 4 W).

Table 12: Mean and standard deviation (StdDev) of power consumption and received data per energy unit (kilobits per Joule) with different configurations and traffic for the Quectel modem when using the USRP B210

	No Traffic		DL Traffic			UL Traffic		
	Mean	StdDev	Mean	StdDev	Kilobits per Joule	Mean	StdDev	Kilobits per Joule
Conf. 1	118.6 W	8.2 W	127.4 W	8.6 W	503.9 kb/J	130.0 W	8.8 W	66.9 kb/J
Conf. 2	120.0 W	7.8 W	129.7 W	9.1 W	1029.3 kb/J	132.2 W	7.0 W	139.2 kb/J
Conf. 3	118.2 W	5.6 W	125.9 W	4.8 W	737.1 kb/J	129.2 W	4.2 W	143.2 kb/J
Conf. 4	118.4 W	4.9 W	122.8 W	4.3 W	179.2 kb/J	122.2 W	3.4 W	65.5 kb/J
Conf. 5	116.4 W	6.4 W	124.6 W	7.8W	321.8 kb/J	127.7 W	3.8 W	134.7 kb/J
Conf. 6	121.3 W	8.9 W	128.0 W	6.6 W	953.1 kb/J	129.2 W	4.8 W	106.0 kb/J
Conf. 7	117.7 W	7.7 W	120.1 W	8.5 W	27.5 kb/J	125.1 W	7.5 W	27.2 kb/J

Table 13: Mean and standard deviation (StdDev) of power consumption and received data per energy unit (kilobits per Joule) with different configurations and traffics for OAIBOX MAX (when using USRP N310).

	No Traffic		DL Traffic			UL Traffic		
	Mean	StdDev	Mean	StdDev	Kilobits per Joule	Mean	StdDev	Kilobits per Joule
Conf. 2	119 W	7.2 W	130W	6.5 W	1007.7 kb/J	133 W	5.3 W	139.8 kb/J
Conf. 2.1	128 W	4.0 W	136W	4.9 W	1727.9 kb/J	139 W	6.3 W	235.3 kb/J
Conf. 2.2	133 W	6.1 W	149 W	9.2 W	2510.1 kb/J	150 W	6.2 W	154.0 kb/J

Table 14: Mean and standard deviation (StdDev) of power consumption and received data per energy unit (kilobits per Joule) with different configurations and traffic profiles for USRP B210

	No Traffic		DL Traffic			UL Traffic		
	Mean	StdDev	Mean	StdDev	Kilobits per Joule	Mean	StdDev	Kilobits per Joule
Conf. 1	3.6 W	0.1 W	3.8 W	0.1 W	16894.7 kb/J	3.6 W	0.1 W	2416.7 kb/J
Conf. 2	4.1 W	0.1 W	4.4 W	0.1 W	30340.9 kb/J	4.2 W	0.1 W	4381.0 kb/J
Conf. 3	4.1 W	0.1 W	4.4 W	0.1 W	21090.9 kb/J	4.2 W	0.1 W	4404,8 kb/J
Conf. 4	4.1 W	0.1 W	4.4 W	0.1 W	5000.0 kb/J	4.2 W	0.1 W	1904.8 kb/J
Conf. 5	4.1 W	0.1 W	4.2 W	0.1 W	9547.6 kb/J	4.2 W	0.1 W	4095.2 kb/J
Conf. 6	4.1 W	0.1 W	4.3 W	0.1 W	28372.1 kb/J	4.2 W	0.1 W	3261.9 kb/J
Conf. 7	3.6 W	0.1 W	3.6 W	0.1 W	916.7 kb/J	3.6 W	0.1 W	944.4 kb/J

5.1.3.1 Restricting the bandwidth used

The difference between Conf. 2 and Conf. 1 is that the bandwidth was lowered from 40 MHz to 20 MHz (when using USRP B210) which approximately halved the data rates. Mean power consumption seems to be lower with all traffic conditions (No Traffic, DL Traffic, UL Traffic) and for all measured devices (OAIBOX MAX: Table 12) when the bandwidth was halved in Conf. 1 than in Conf. 2. For OAIBOX MAX the decrease in power consumption was about 1.2%, 1.8%, and 1.7% for No Traffic, DL Traffic, and UL Traffic, respectively. For USRP B210 the decrease in power consumption was about 12.2%, 13.6%, and 14.3% for No Traffic, DL Traffic, and UL Traffic, respectively, as listed in Table 14. However, the data received per energy unit (kilobits per Joule) illustrates that about twice as much traffic was received with Conf. 2 per Joule when compared to Conf. 1 with a smaller bandwidth. Thus, reducing the bandwidth could be used to save energy during low traffic periods, but when there is high traffic in the network, then the higher bandwidth should be used.

Some decrease in power consumption was also seen when reducing the bandwidth from 100 MHz to 20 MHz between Conf. 2.2 and Conf. 2.1 (when using USRP N310) radio configurations defined in Table 11. For OAIBOX MAX (Table 13) the decrease in power consumption was about 3.8%, 8.7%, 7.3% for No Traffic, DL Traffic, UL Traffic, respectively. The percentage reduction for the USRP N310 device was low because its high baseline power consumption (~45 W) dominates the total, making the dynamic power savings from bandwidth reduction relatively small and the maximum transmission power allowed by OAIBOX MAX (maximum effective Isotropic radiated power (EIRP) from antenna was limited to 10 mW).

Figure 47 presents power consumption as a function of time with 20 MHz bandwidth for OAIBOX MAX, USRP N310, and Quectel Modem, and the total sum of all network components. Figure 48 presents power consumption as a function of time with 40 MHz bandwidth for OAIBOX MAX. Results in these figures, obtained from the Grafana dashboard, illustrate how the power consumption varies as a function of time when there is 10 min DL and 10 min UL traffic periods for USRPB210 and one hour measurement for USRP N310. For the validation of KPI metrics, USRP N310 was chosen with its more stable connectivity performance and despite the small percentage, the absolute power savings in this case are high when changing the bandwidth from 100MHz to 20MHz.

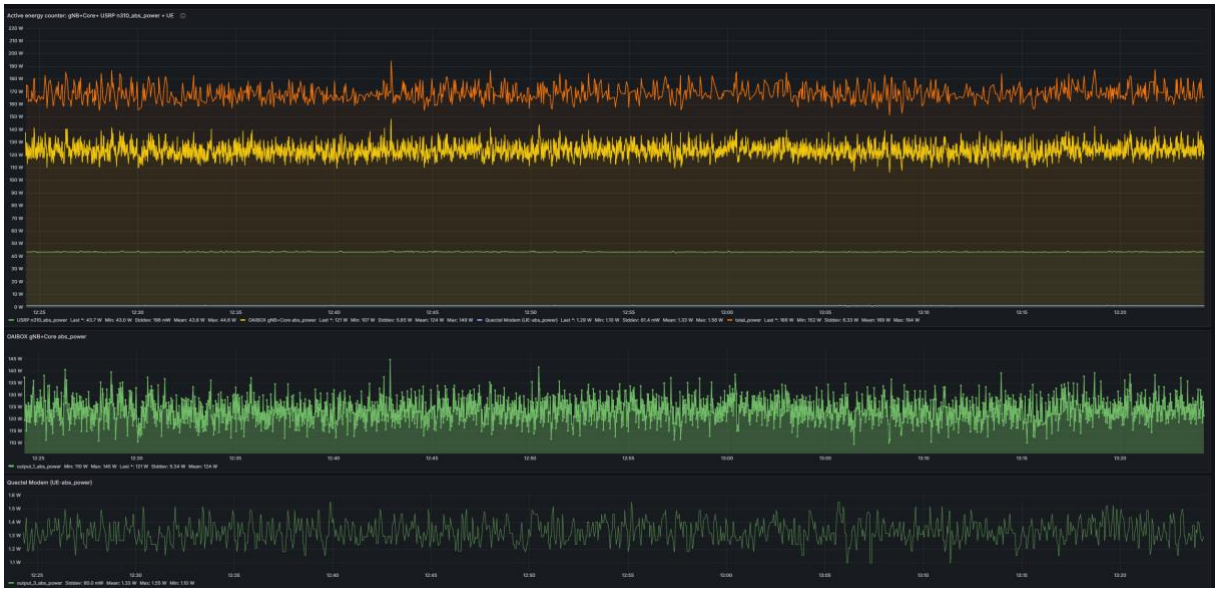

Figure 47: OAIBOX MAX, USRP N310, and Quectel Modem power consumption as a function of time with 20 MHZ bandwidth

Figure 48: OAIBOX MAX power consumption as a function of time with 40 MHz bandwidth with B210.

5.1.3.2 Restricting the modulation constellation

The difference between Conf. 2, Conf. 3, and Conf. 4 presented in Table 10 is that the MCS was restricted (when using USRP B210) to allow at maximum 256-QAM, 64-QAM, and QPSK modulation, respectively, and the bandwidth was kept the same (40 MHz). Results in Table 12 illustrate that a lower modulation order decreased the amount of received traffic remarkably, except for received UL traffic, which was approximately the same with Conf. 2 and Conf. 3 because 64-QAM was the maximum modulation constellation that was obtained for UL traffic based on MCS. A decrease in power consumption for OAIBOX MAX was observed when lowering the maximum modulation constellation: Between Conf. 2 and Conf. 3 (from 256-QAM to 64-QAM) power consumption decreased by about 1.5%, 2.9%, and 2.3% for No Traffic, DL Traffic, and UL Traffic, respectively. Between Conf. 3 and Conf. 4 (from 64-QAM to QPSK) power consumption decreased by about 0%, 2.5%, and 5.4% for No Traffic, DL Traffic, UL Traffic, respectively. Thus, between Conf. 2 and Conf. 4 (from 256-QAM to QPSK) power consumption decreased by about 1.5%, 5.4%, and 7.7% for No Traffic, DL Traffic, and UL Traffic, respectively. USRP B210 power consumption stayed the same as presented in Table 14 , regardless of the modulation constellation restrictions, probably because modulation and demodulation operations are not performed on the USRP device (are performed on OAIBOX MAX). For the USRP N310 RAN combinations 256 QAM was used to perform validation activities due to the length of the trial runs

being one hour instead of 10 minutes. This way, the test runs were performed without UE dropping the connection with the OAIBOX.

5.1.3.3 TDD frame structure selection

The difference between Conf. 2, Conf. 5, and Conf. 6 (Table 10, when using USRP B210) is that the TDD frame structure was changed to have different numbers of DL and UL slots (different slot configurations): 3D-F-1U, 2D-F-7U, 7D-F-2U, respectively. There are 10 subframes (each 1 ms) in a frame (10 ms). Applied 30 KHz subcarrier spacing provided two slots (each 0.5 ms) per subframe. The slot contains 14 symbols. Thus, with different slot configurations, there are different ratios of UL and DL slots in a frame for communication. Bandwidth was kept the same (40 MHz), and the modulation constellation was not restricted. When the number of DL slots was lowered, and the number of UL slots was increased between Conf. 2 and Conf. 5 (from 3D-F-1U to 2D-F-7U): Power consumption of OAIBOX MAX (Table 12) decreased by about 3%, 3.9%, and 3.4% for No Traffic, DL Traffic, and UL Traffic, respectively. Power consumption of USRP B210 (Table 14) decreased by 4.5% for the DL Traffic and stayed the same for No Traffic and UL Traffic cases. Thus, USRP B210 power consumption was affected only due to changes in the TDD frame structure when the USRP was transmitting traffic (DL Traffic case). When the numbers of DL and UL slots were increased between Conf. 2 and Conf. 6 (from 3D-F-1U to 7D-F-2U): Power consumption of OAIBOX MAX increased slightly by about 1% for No traffic and decreased by about 1.3% and 2.3% for DL Traffic and UL Traffic, respectively. Power consumption of USRP B210 decreased by 2.3% for the DL Traffic and stayed the same for No Traffic and UL Traffic cases. Power consumption of the Quectel modem decreased by 4% for the DL Traffic, increased by 8.7% for the UL Traffic, and stayed the same for the No Traffic case. For the USRP N310 RAN combinations 5*DD-F-4*UU For the USRP N310 RAN combinations 256 QAM was used to perform validation activities due to the length of the trial runs being one hour instead of 10 minutes. This way, the test runs were performed without UE dropping the connection with the OAIBOX.

5.1.3.4 MIMO mode selection and bandwidth

This section analyses power measurement results when using SISO (1x1 20MHz) and MIMO (2x2 100MHz) with Conf. 2.1 and Conf. 2.2 showed the highest difference in energy consumption. These measurements were performed using USRP N310 with radio configurations presented in Table 11. Thus, the difference between Conf. 2.1 and Conf. 2.2 was that the number of transmitting and receiving antennas was doubled for the base station and the bandwidth was also increased from 20MHz to 100MHz, providing about twice as high bitrates and the power delta is a result of both factors combined. A decrease in power consumption for OAIBOX MAX (Table 13) was seen when changing from MIMO to SISO. These two configurations were the default for performing the test cases and KPI validation of the energy saving counter as presented in Chapter 7.3.1.

5.1.3.5 Combined radio configuration changes

This section analyses measurement results of Conf. 7, in which all tested radio configuration changes (with USRP B210) were combined: limiting the used bandwidth, restricting the modulation constellation, and TDD frame structure selection. Radio configuration parameters that provided the lowest power consumption values were selected for Conf. 7. Thus, Conf. 7 used bandwidth of 20 MHz (Conf 1.), allowed only QPSK modulation (Conf. 4), and applied TDD slot configuration of 2 DL and 7 UL slots (Conf. 5). The results show that the average DL and UL traffic received were clearly the lowest when compared to other tested configurations: DL traffic: 3.4 Mb/s and UL traffic: 3.3 Mb/s. In addition, the power consumption values of Conf. 7 were the lowest or equal to the lowest with the most radio configurations and traffic. Only radio configuration Conf. 4 provided lower power

consumption values than Conf. 7 for OAIBOX MAX when UL traffic was generated. This occurred because there was a lower number of UL slots allocated in Conf.4 (3D-F-1U) than in Conf. 7 (2D-F-7U).

For USRP N310, the lowest power consumption value was recorded as 169 W (total power OAIBOX + USRPN310 + Quectel Modem) when using Conf 2.1 and compared to 200 W when using Conf 2.2. This yields a remarkable energy savings of about 15 %.

5.1.4 Conclusion based on the measurement results

Different RAN configurations were used to see the impact of power consumption among the individual network components, which were recorded using the central controller, and the datasets were stored inside the central database. The methods used to evaluate power profiling and the energy saving methods inside the OAIBOX were examined, and iPerf3 was used to generate maximum UDP traffic in order to saturate the network to see its energy efficiency impact.

In most cases, radio configurations that provided higher bitrates caused more power consumption during non-traffic periods and during TCP/UDP speed tests (UL and DL traffic). It seems that all the tested radio configuration changes (restricting the used bandwidth, restricting the modulation constellation, TDD slot configuration selection, and DL MIMO mode selection) have some effect on power consumption. Overall, the lowest power consumption was measured when the radio configuration parameters that provided the lowest power consumption with different tested radio configuration changes were selected for Conf. 7 (bandwidth of 20 MHz, QPSK modulation, TDD slot configuration of 2 DL and 7 UL slots, and SISO antenna configuration for USRP B210). The radio configuration providing the lowest power consumption also caused the lowest average bit rates: DL traffic was 3.4 Mb/s, and UL traffic was 3.3 Mb/s.

Below are described some examples that illustrate how much energy can be saved with certain radio configuration changes:

Combined System Savings (OAIBOX MAX, USRP, and UE):

- During DL traffic, total power consumption was reduced by approximately 15% when switching from a high-performance configuration (MIMO, 100 MHz, 256-QAM, 3D-1U TDD) to a low-power configuration (SISO, 20 MHz, QPSK, 5D-4U TDD).

USRP B210 Component Savings: When isolating USRP B210, the power reduction varied by method:

- Bandwidth: Reducing from 40 MHz to 20 MHz saved 13.6%.
- TDD Slots: Changing from 3 DL / 1 UL to 2 DL / 7 UL saved 4.5%.
- Modulation: Changing from 256-QAM to QPSK resulted in 0% savings.

Based on the measurement results, it seems that the lowering of bandwidth is more effective than other method to reduce power consumption for OAIBOX MAX and changing from MIMO to SISO antenna configuration is the most efficient method to save energy for USRP N310. In addition, the other radio configuration changes can also be used to save energy. Restricting the modulation constellation does not seem to have a notable effect on the power consumption of the Quectel modem and USRP B210, but this may happen due to very low transmission powers and ranges used in the indoor environment tests. The lower modulation constellation should allow the higher transmission ranges with the same transmit power. Thus, the use of lower modulation may reduce power consumption in some other measurement scenarios with higher distances. Reducing the number of DL

slots was noticed to be effective for decreasing the power consumption of a base station by reducing the allowed time for DL transmissions in a frame.

5.2 ENERGY-OPTIMIZED DYNAMIC DISTRIBUTED SERVICE ORCHESTRATION

5.2.1 Introduction

The management and coordination of distributed services across three tiers, edge devices, edge servers, and cloud infrastructure, is referred to as energy-optimized dynamic distributed service orchestration in the three-tier edge-cloud continuum. This strategy aims to reduce energy usage, which ensures effective delivery of service and fulfilling performance requirements across the continuum [34]. Implementation of dynamic distributed service orchestration that is energy-optimized in the edge-cloud continuum is as follows:

5.2.1.1 Extreme Edge Devices:

The orchestration system considers the energy limitations and capabilities of edge devices, such as Internet of Things (IoT) or mobile devices. The dynamic allocation of tasks to edge devices or higher-tier resources is determined based on factors such as energy usage, task requirements, and resource availability. The system's main objective is to reduce the energy consumption of edge devices while maintaining the desired level of service quality through implementing intelligent offloading decisions.

5.2.1.2 Edge Servers:

Edge servers, which have more computation and storage capabilities than edge devices (IoT, edge servers), are found in the edge layer. Based on workload characteristics and energy efficiency measures, the orchestration system optimizes resource distribution and task scheduling among edge servers. In order to reduce energy usage and yet satisfy service-level goals, the number of edge servers is scaled dynamically. In order to arrange edge servers for maximum energy efficiency, the AI system architecture can also make use of workload estimation and data proximity [35].

5.2.1.3 Cloud Infrastructure:

The three-tier continuum's foundation is made up of a cloud architecture that offers huge computing capabilities and scalability. By dynamically assigning resources depending on workload requirements and energy efficiency issues, the orchestration system maximizes the usage of cloud resources. It makes use of strategies including load balancing, virtual machine (VM) consolidation, and power management to reduce energy usage while offering services. To optimize energy utilization throughout the cloud architecture, the system may additionally consider workload offloading and data backup possibilities.

5.2.1.4 Inter-tier Communication and Data Placement:

Energy optimization within the three-tier continuum heavily depends on efficient data transfer and deployment methods. Data location, network bandwidth limitations, latency, and energy costs related to data mobility are all considered by the orchestration system. A distributed AI algorithm takes intelligent decisions about when and how to transmit data between tiers to save energy and guarantee quick and efficient service provisioning [36].

5.2.1.5 Dynamic Optimization and Monitoring:

The energy-efficient dynamic distributed service orchestration consistently monitors the energy usage, performance indicators, and workload characteristics across the three-tier architectural frameworks of the computing continuum. The system utilizes feedback loops, predictive analytics, and machine learning methodologies to dynamically allocate resource allocation, task scheduling, and scale methods in response to evolving circumstances and changes. The system is capable of dynamically optimizing energy use while simultaneously ensuring service quality and adjusting to fluctuating workloads and energy availability [36].

Organizations may increase the energy efficiency of their distributed service infrastructure, minimize operating costs, and maximize resource usage by using distributed service orchestration in the three-tier edge-cloud continuum. This strategy is especially useful in edge computing situations where energy resources may be constrained, and sustainability is a top concern.

5.2.2 Task scheduling

5.2.2.1 Scenario-1: Computational and data intensity of the Tasks

Energy-efficient task scheduling based on constraint requirements in the three-tier edge-cloud continuum involves dynamically assigning tasks to appropriate resources across the edge, server, and cloud tiers while considering energy efficiency and meeting specific constraints or requirements. This approach aims to optimize energy consumption while ensuring that tasks are executed within specified constraints .

5.2.2.2 Task Classification and Constraints:

Classification of tasks based on their features and requirements. Limitations that are implemented on a system may include multiple components such as time constraints (e.g., defined timeframes, executions, or response time), resource constraints (e.g., required resources for CPU or RAM), and geographical constraints.

5.2.2.3 Dynamic Task placement and offloading:

Evaluate if the tasks may be locally completed or offloaded from edge devices to more powerful resources. Consider offloading jobs with special requirements, such as latency-sensitive or resource-intensive tasks, to the edge servers or cloud infrastructure, based on the needs and the resources available [37].

5.2.2.4 Resource Evaluation and Selection:

To reduce the consumption of energy, assess the resources that are accessible in each tier based on their energy effectiveness, capacity, and closeness. When choosing the best task execution resources, consider the energy requirements of edge devices, edge servers, and cloud infrastructure. To make intelligent decisions, analyze characteristics including workload structure, usage of energy, and energy consumption models.

5.2.2.5 Optimization Algorithm:

Optimization AI algorithms are applied to solve the task scheduling problem while considering the constraint requirements and energy efficiency objectives. These AI algorithms can include heuristic-based approaches, mathematical programming, or machine learning techniques. The objective is to find an optimal allocation of tasks to resources that satisfies the constraint requirements and minimizes overall energy consumption.

5.2.2.6 Dynamic Adaptation and Monitoring:

Keep track of how much energy is being used, what resources are available, and how well tasks are being executed. Apply real-time evaluation and input methods to modify task scheduling decisions in response to evolving conditions and requirements. To ensure energy efficiency and follow the given constraints, this includes reassessing the resource allocations and tasks scheduling as appropriate.

5.2.2.7 Load Balancing:

Efficient allocation of resources and optimization of energy consumption may be achieved by evenly distributing the workload across the extreme edge, server, and cloud tiers. Load balancing strategies are often used to achieve equal distribution of tasks and applications, considering both energy efficiency and constraint requirements. This process includes the transfer of workload between different edge to cloud continuum tiers, the enhancement of data placement, and the dynamic management of resource allocations.

Organizations may improve their energy usage and guarantee task deployments correspond to certain limitations and requirements by adopting energy-efficient task scheduling based on constraint requirements in the three-tier edge-cloud continuum. This method is useful in distributed computing applications because it maintains a balance between power consumption, resource usage, and service quality.

5.2.2.8 Minimize Task Blocking Probability:

Another important element of the Key Performance Indicators (KPIs) is the reduction of the probability of tasks being blocked in the network of resource nodes. The primary purpose of the orchestrator is to efficiently allocate a maximum number of tasks while minimizing the blocking probability of these tasks on edge nodes. As shown in Figure 49, the load balancing between the computing nodes is performed using the resource computing in each computing node. The workload balancing is distributed optimally across all the computing nodes.

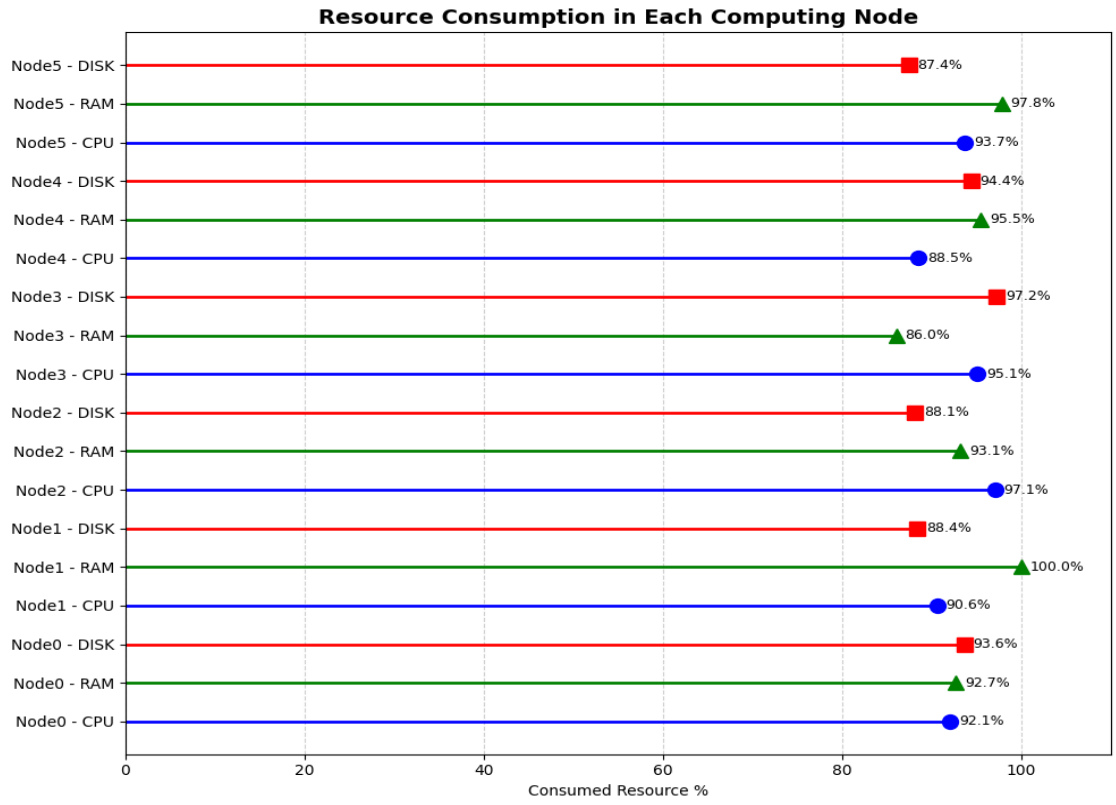

Figure 49: Load Balancing in all the Computing Nodes

5.2.3 Scenario-2: Service Orchestration

5.2.3.1 Scalability of available resources:

Scalable, when provisioning and deprovisioning the resources.

5.2.3.2 Load Balancing:

Load balancing algorithms are used to distribute the workload across available resources, ensuring efficient utilization and minimizing energy waste. Task scheduling mechanisms consider the energy profiles of resources, workload characteristics, and performance objectives to make intelligent decisions about where and when to execute tasks.

5.2.3.3 Energy-aware resource optimization:

An orchestration system actively monitors energy consumption of individual resources, such as servers, data centers, or cloud instances.

5.2.3.4 Dynamic resources provisioning and de-provisioning:

The orchestration system dynamically allocates and deallocates resources based on real-time demand and workload patterns. It leverages workload prediction models, performance requirements, and energy efficiency considerations to determine the optimal allocation of resources at a given time.

5.2.3.5 Cloud Computing:

Cloud computing is a computing paradigm for providing and using computer resources, such as storage space, servers, databases, networking platforms, and more, through the internet. This technology facilitates the ability of organizations and people to conveniently use resources by adopting a pay-as-you-go model, thereby reducing the need to invest in and manage expensive on-site devices and infrastructure. This technique has the advantages of scalability, flexibility, and cost-efficiency, making it an essential element of modern information technology.

Energy-aware service orchestration is an essential component of cloud computing that prioritizes the optimization of energy usage and productivity within the cloud architecture, while simultaneously guaranteeing the provision of necessary services.

Cloud service providers incorporate a range of strategies to implement energy-aware service orchestration, such as:

5.2.3.5.1 Virtualization:

This technical innovation makes it possible to effectively share a real server's resources across many virtual machines. Because virtual machines (VMs) can be dynamically allocated to servers that demonstrate higher energy efficiency, this may decrease the amount of power used by the system.

5.2.3.5.2 Load Balancing:

One potential approach to address the issues of resource provisioning and de-provisioning is implementing a strategy to encourage balanced distribution of workloads across all servers within the system. This load-balancing approach will significantly decrease the quantity of energy that is wasted.

5.2.3.5.3 Dynamic Resource Allocation:

The dynamic approach to allocation of resources, such as the central processing unit (CPU), memory, and storage, is determined by the real-time requirements of applications. This resource allocation process may be adjusted to minimize energy usage by scaling up or down as needed.

5.2.3.5.4 Renewable Energy Integration:

Cloud service providers can mitigate the environmental effects of their data centers through renewable energy sources such as wind and solar energy.

In summary, the purpose of cloud computing that places an emphasis on energy-aware service orchestration is to achieve a balance between the efficient delivery of computing services and a sustainable use of energy. This additionally helps cloud service providers lower their operational costs, but it also makes a beneficial contribution to the sustainability of the environment by reducing the number of emissions that is linked with the operations of data centers. The concept of energy-aware service refers to the consideration and optimization of the use of energy in the provision of services. The importance of orchestration is increasing due to the growing demand for cloud services, as it is the only means to ensure both economic and environmental sustainability in the current technological advancement.

5.2.3.6 Maximize Task Acceptance Ratio:

The concept of energy-aware service implies the consideration and optimization of energy use in the provision of services. The orchestrator is responsible for successfully deploying incoming tasks across the network of Edge Nodes. The primary goal of this Key Performance Indicator (KPI) is to maximize the acceptance ratio of tasks in the system. The important objective of the Orchestrator is to effectively

allocate and execute each task while ensuring minimal loss or misplacement, assuming limited resource availability [38][39].

5.2.4 Requirements specification for energy-optimized AI-based Algorithms

This section outlines the key performance indicators (KPIs) used to evaluate the overall performance of the system. These indicators provide a comprehensive understanding of how effectively the system meets its objectives in terms of functionality, efficiency, and reliability. Table 1 presents a detailed explanation of the functional requirements associated with the system, illustrating how each requirement aligns with the corresponding KPIs to ensure a robust and measurable evaluation framework.

5.2.4.1 Functional requirements

The operating cost and sustainability of AI-driven systems are strongly impacted by electrical supply, which underpins the energy efficiency claims of programmable, virtualized, and open network designs. To guarantee optimal system performance under a range of power situations, AI-based algorithmic needs and specifications must be in line with energy-aware design concepts. AI-based Algorithmic requirements & specifications.

For energy optimization in AI algorithms, several key functional requirements should be considered as follows [39]:

- Current and forecasted energy availability and pricing.
- Energy Efficiency.
- Resource Allocation.
- Task Scheduling.
- Computational requirements.
- Energy Consumption.
- Data Storage.
- CPU.
- Memory.
- GPU.
- Communication requirement.
- Latency.
- Bandwidth.
- Autonomous and Dynamic behavior.
- Optimization Criteria.

- Real-time Decision Making.
- Complexity of an AI-Based algorithm.

SR.	Functional Requirement	Description
1	Local Energy Sources	The evaluation of the accessibility to local energy resources
2	Orchestration Flexibility	It is important to ensure that the system can effectively adapt to the dynamic aspects of evolving tasks and varying loads produced on the system.
3	Algorithm Execution	To optimize the performance of orchestration algorithms, it is important to ensure efficient execution.
4	Real-time data analysis and decision	The process of analysing data and making decisions in real-time is important in the Edge to Cloud Continuum.
5	Energy Pricing	It is essential to actively monitor and consider the current energy pricing.
6	Price Investigation	This analysis aims to examine the present and projected energy costs.
7	Monitor Energy Consumption	The objective is to systematically observe and document the total energy use during the whole process for tasks execution in different circumstances.
8	Energy Availability Analysis	Conduct an analysis of the present and projected energy accessibility.
9	Develop AI-based approaches	Define and develop an AI-based dynamic distributed service orchestration approach with an emphasis on energy efficiency.
10	Task Deployment Algorithms	Develop task deployment algorithms for the energy orchestration component
11	Task Computational Analysis	The computational and data intensity of the tasks must be considered.
12	Task execution timing	Manage when tasks and algorithms will be executed.
13	Dynamic task Placement	Manage how and where tasks are executed in real time using an edge-cloud service architecture.
14	QoS/QoE Requirement Analysis	Determine dynamically changing application QoS/QoE requirements.
15	System Load Analysis	Examine the current system load as it is increasing in real-time.
16	Communication Links	Edge-cloud continuum architecture communication connection quality should be taken into consideration

17	Computing Architecture	Consider the load of processing units in different tiers of the edge-cloud architecture.
18	Optimization Problem	Define the complex and continuously varying optimization problem.
19	Scalability	Verify that the system has the capacity to accommodate the potential requirements of the tasks.
20	Fault Tolerance	Implement fault tolerance mechanisms to handle failures.
21	Reporting and Documentation	Maintain comprehensive documentation for system components and configurations.
22	Computational requirements	• Energy Consumption (exp) • Data Storage • CPU • Memory • GPU
23	Communication requirement	• Latency • Bandwidth

The following rules can be used as an AI-based task deployment based on orchestration by FMI Energy-weather forecast and ELSPOT Pricing:

- Energy-Efficient Orchestration.
- Urgent Tasks: Schedule immediately (e.g., VoIP, Video Streaming).
- Non-Urgent Tasks: Schedule during low energy pricing and PV peaks.
- Energy Forecast: Prefer high energy forecast periods if prices are favorable.
- PV Yield: Exclude tasks from energy cost calculations during periods with PV yield > 4000 watts.
- Optimal Times: Choose periods with both low pricing and high energy forecast for non-urgent tasks.
- PV Yield Threshold: Set a threshold of 4000 watts for determining high PV yield periods.

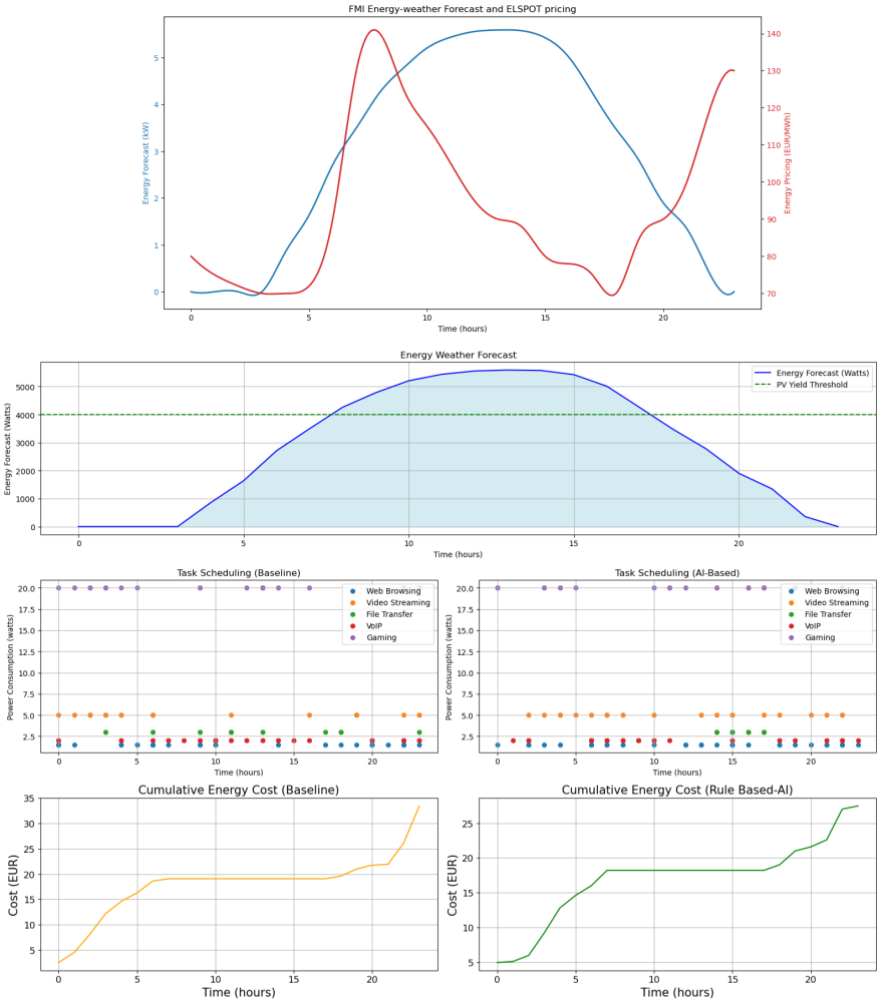

Figure 50: Task deployment based on Orchestration by FMI Energy-weather forecast and ELSPOT Pricing

A rule based AI was used in this simulated environment of 100 randomly selected urgent and non-urgent tasks, such as Gaming, video streaming, and file transfer (heavy computation), and two more light computational tasks, such as web browsing and VoIP. The heuristic rule-based AI will perform task scheduling based on strategically scheduling the non-urgent tasks during the periods of high PV production and lower electricity pricing. As shown in Figure 50, the tasks are mostly scheduled between 6am to 6pm due to high PV yield. We extended the rule-based AI approach to use file transfer as a non-urgent task only, and all file transfer tasks are scheduled only when PV yield is at peak value. Finally, the cost estimation was calculated (baseline vs Rule-based AI) based on day ahead ELSPOT pricing API, as shown in Figure 50. As a result, the AI-based scheduling strategy significantly reduced the estimated cumulative cost of deploying 100 tasks based on forecasting APIs versus the baseline cumulative energy cost of random distribution of tasks.

5.3 OPTIMIZING E2E ENERGY CONSUMPTION VIA CENTRALIZED CONTROL

5.3.1 Introduction

This section presents our work on energy efficiency, where we have developed an autonomous E2E system able to adapt to the volume of local green energy availability by adjusting RAN and application states according to the available energy budget. This work combines excellently the efforts done in T5.1 – T5.3 related to energy measurement framework infrastructure, base station energy saving mechanisms, and green energy availability based on accurate energy weather prognosis. In addition to these tasks, T5.4 has investigated the use of adaptive, energy-efficient video applications since they form the most energy-hungry portion due to video processing (decoding and playback) in the client, as presented in the first deliverable of WP5 [13]. Furthermore, mobile streaming is the most data-consuming factor today, used not only in entertainment applications but also in a large variety of industries ranging from remote surveillance to low-latency control mechanisms. During the project, the focus has been set on adaptive HTTP streaming, which is widely used in the majority of the nowadays video service platforms. The selected open source video player has been integrated as a part of the E2E system with full controllability. Finally, we have also developed a central AI/ML-ready controller which is in charge of deciding the next states of the system based on green energy budget originating from solar yield and application needs as quality of service (QoS). With the efforts made, we have developed the basis for sustainable communication.

5.3.2 System architecture

The high-level architecture diagram is presented in Figure 51, which shows all the essential blocks of our system running in the North Node. The far left and right of the diagram illustrate the video UE and the video server, respectively. Video UE comprises the actual device, selected video application, and 5G modem, which interconnects to the video server as a streaming host over 5G. In our system and measurements, we consider the location of the video client fixed. It is notable that the server can function either as a video content (origin) server or an edge server and host both video-on-demand or live content.

The Next Generation RAN (NG-RAN) system is based on a hierarchical 5G SA architecture where there is an always-on coverage cell (FDD) providing service availability and an on-demand capacity cell (TDD) providing additional capacity, for example, when needed by demanding video applications. The frequencies and specifications used can be found in Section 3. Both coverage and capacity cells share the baseband unit (BBU) and run under the core network (CN) Open5GS.

The PV energy production system currently connected to the test environment's multi-RAT BBU consists of a hybrid infrastructure able to switch the energy source between solar panels, battery storage, and the electricity grid. This approach allows the hybrid energy production system to be part of the end-to-end optimization, as the gNB component responsible for the majority of the user data processing can be fed flexibly from different energy sources based on the targeted optimization criteria.

The depicted components are connected to the North Node energy measurement framework, which is able to report 1/s power values. In addition, the video UE and server can provide 1/s network KPIs such as throughput, delay, jitter, and packet loss, which provide essential data to the decision-making (DM) process of the Central Controller (CC) in order to maintain the application QoS at an acceptable level.

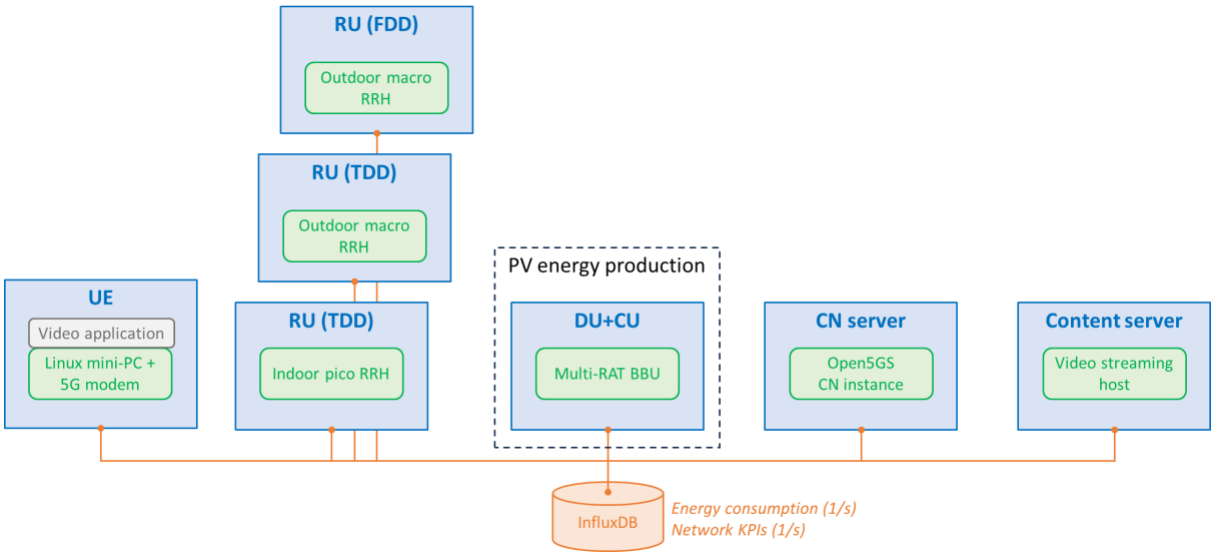

Figure 51: High-level E2E system architecture.

5.3.3 Implementation

Next, we deep dive into the actual implementation, which targets adapting the RAN and applications to green energy availability while maintaining QoS at an optimal level. The architecture in more detail is depicted in Figure 52, which outlines the whole E2E chain. CC oversees the overall DM fed by Energy production and Measurement database blocks and interconnects using MQTT messaging. Generally, the first one provides the prognosis of green energy availability for the next hour, and the latter one stores both network QoS and energy consumption KPIs in 1/s accuracy needed in the DM of the CC. All the KPIs seen by the CC are illustrated in Table 15. As an output, the CC instructs the application and RAN sub-controllers, which will be presented in more detail in the following subsections.

Ther E2E transmission is considered to range from the edge server (video content origin) to the video UE through 5G RAN. In a live streaming context, the edge server and its associated live encoder and packetizer can also take inputs from the application controller in terms of desired bitrate or resolution, but this technique is more suitable for RTSP/RTMP-based streaming, which is not yet in our focus.

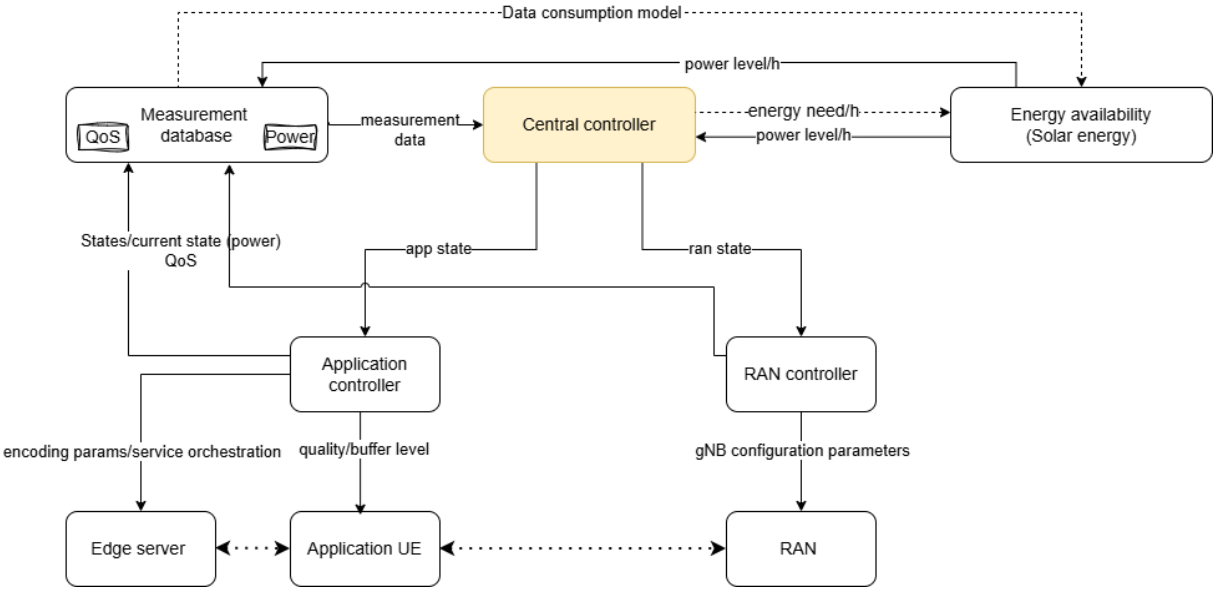

Figure 52: E2E implementation architecture for energy and QoS optimization.

Table 15: Parameters taken into account by the CC in the final implementation stage (Q4-2025).

KPI	Unit	Input	Output	Implementation status
Energy budget	kWh	X		OK
RAN state	1-7 (int)	X	X	OK
RAN power consumption	W	X		OK
App. state	1-4 (int)		X	OK
App. power consumption (separately for modem & client)	W	X		OK
App. throughput	Mbit/s	X		OK
App. delay	ms	X		OK
App. cache size	s	X		OK
Cell throughput/utilization rate	%	X		OK

5.3.3.1 Energy availability

Figure 53 presents the energy availability block in detail. Inside this block, the energy availability guide (EA-guide) provides a power budget for the CC for the next hour. At the final development stage, "energy availability" was interpreted as a sum of stored usable energy in the storage and PV yield prognoses in various time periods. For example, using the next 24 h PV yield forecasts together with

realized hourly energy storage change (originated from measured solar yield and realized consumption based on meter readings during the last hour), a new power setpoint can be calculated as an average power of total energy availability for the next hour by means of hourly steps. The method reacts smoothly to the potential deviation between the proposed guide and realized consumption and allows a lot of freedom for the controller to select suitable states for E2E system components.

The system was first simulated using Excel (to find operative principles), and then it was programmed to enable the usage of R-T data-streams, auxiliary external datasets, and scale-up or scale-down parameters and conversion efficiency factors. From the energy content of the virtual battery, which is calculated once per hour, it was possible to calculate the capacity needed for the battery energy storage as well as match PV-scale up factors to the applied consumption profile. From the fluctuating curve of the usable virtual energy storage content also timing, and average hourly power levels for the power intake from the grid were extrapolated.

Firstly, we used Victron Energy's Solcast-based localized forecasts and upscaled VTT's PV yield data, and linked UOULU's sensor-based forecasts and downscaled PV-yield data to be applied in weekly integrated trial runs. Figure 53 shows the energy content of the virtual battery during the weekly trial run.

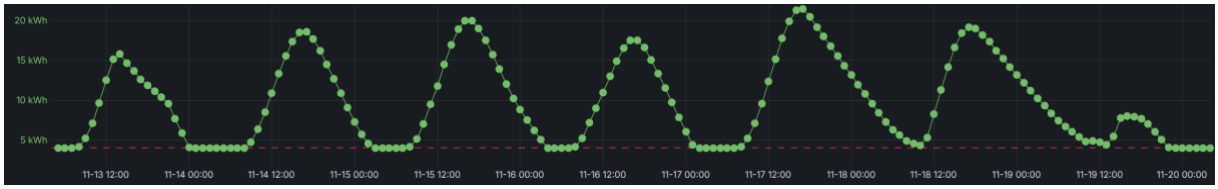

Figure 53. Available energy content of the virtually well-balanced PV-system and virtual battery for 1 week trial-period.

The previous figure was based on UOULU's PV prognoses and PV yield data (captured from week 20, 2025), and a 4kWh minimum energy level was set for the virtual battery simulation. This minimum level triggers energy intake from the grid directly to the loads. Week 20 data context was also used to standardize external conditions in various trials using real-time consumption and control systems. On the other hand, validations were made during late autumn 2025 outside the dimensioning period of the real-PV-hybrid system, making partly virtualized simulations necessary due to extremely low daily irradiation levels.

The forecast provided through the HTTP REST by the Victron VRM API uses internal AI logic inside Solcast to determine the accuracy of the availability for the next hour. The realized solar yield is fetched from the Venus-GX PV-hybrid site controller into Influx, making it available for the EA-guide. Alternatively, data sources such as energy price, FMI forecast, and UOULU energy weather can be used as secondary options for DM by the CC.

EA-guide calculates the next hourly power level estimate using the forecast and realized solar yield as inputs and adjusts the output with DC to AC inverter loss (8%). Using this value as an input, a small Python script adjusts and scales it to our system and outputs it to InfluxDB and MQTT broker as a JSON-formatted value:

{"E2E_power_setpoint": "<float>"}

In the final quarter of the project, the EA-guide evolved to include a virtual battery model for the battery reserve, which is now factored into the estimation of the upcoming hourly power level.

In future phases of this implementation, we plan to provide the data consumption forecast (e.g., for the next hour) and the energy needs to the Energy Production block, which can then take these values into account for its internal decision-making. This is seen as dashed lines in the next figure.

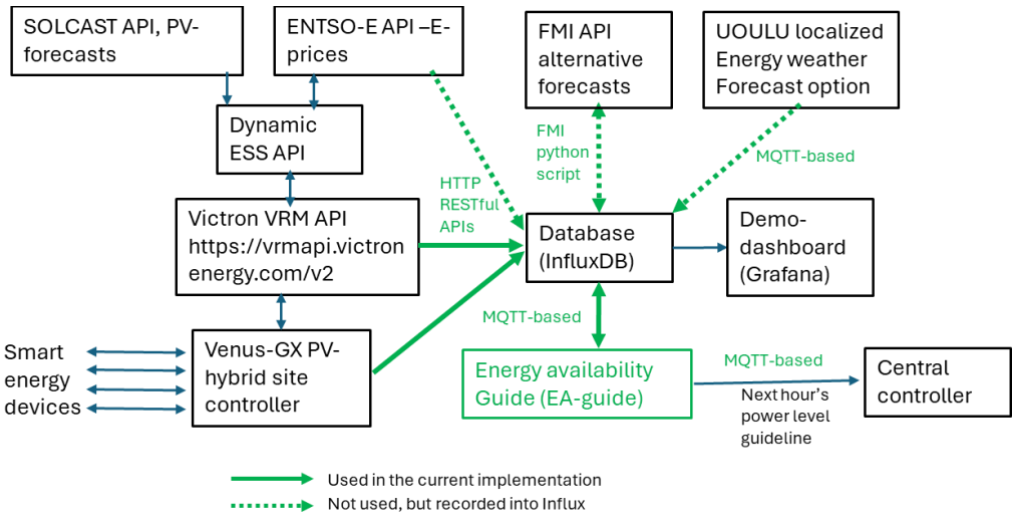

Figure 54: Energy availability guide and its interfaces

5.3.3.2 Dynamic RAN

The selected RAN states for E2E evaluation are presented in Table 16, which are originally illustrated in Table 5. For simplicity, we assume that the UEs are located outside the coverage area of capacity cell 2. Thus, capacity cell 2 can be excluded, reducing the number of states in Table 5 to one third (24 -> 8). These states are decided in the CC and passed in operation through the RAN controller, as shown earlier in Figure 16. The state transitions in our current implementation are considered once every hour according to the available energy budget, and the selection for the next hour's state is done based on the cell's power consumption and its associated DL capacity to fulfill the application needs. Furthermore, multi-hop state transitions are possible if direct state change is not possible, but naturally, this requires more transition time as shown in Section 3.2.2.

Before applying for the new RAN state, the RAN controller first makes a sanity check to see if the state transition is allowed. This requires retrieving the current state through the proprietary base station O&M interface. Notably, CC can send multiple state transition commands if a multi-hop state transition is needed. These commands are piped into the RAN controller queue and activated accordingly with the base station. Finally, after completion, the new RAN state is recorded into the Influx database.

Table 16: Selected power saving states for E2E RAN evaluation.

Power saving state	Maximum power consumption	Minimum power consumption	Maximum DL capacity	Maximum UL capacity
AAC	98.7%	55.7%	1588 Mbps	270 Mbps
ABC	86.1%	52.5%	1330 Mbps	270 Mbps

ACC	63.1%	45.1%	220 Mbps	120 Mbps
ADC	58.8%	40.7%	220 Mbps	120 Mbps
BAC	86.1%	52.1%	1220 Mbps	270 Mbps
BBC	73.6%	48.9%	1220 Mbps	270 Mbps
BCC	50.6%	41.5%	110 Mbps	120 Mbps
BDC	46.2%	37.1%	110 Mbps	120 Mbps

5.3.3.3 Adaptive video application

For the adaptive DASH application implementation, we selected the open-source mpv video player[3] according to earlier energy-aware studies [14],[16], compiled it from scratch to support demuxer buffering and caching, and added a Python API to support receiving external commands from the application controller. The application controller receives state transition commands from the CC via the MQTT broker at any time due to the threaded implementation. Usually, such commands occur in the context of new energy budgets every hour, but they can also arrive at random times if network capacity drastically changes due to, for example, other users. For the demonstration purposes, we have set the application buffer level very low to enable faster adaptation, but parallel long-term studies have identified several benefits of using longer buffer levels during streaming (i.e. enabling sleep modes in modem and RAN).

The application controller can accept state transitions 1-4 according to the evaluated pre-defined states (resolution @ bitrate) for the video application. Those states were encoded with the libx264 encoder into a constant bitrate H264 video-on-demand format with 30 frames per second, as shown in Table 17. Furthermore, we averaged the power consumption for these streams when receiving and playing back the streams over 5G. In the E2E experiments, we use a DASH-compliant stream where all 4 resolutions introduced in Table 17 are encapsulated into a single multi-representation stream, enabling adaptivity. In the experiments, we use a 10s video cache (network/demuxer buffer) with 5s hysteresis, which means that the cache should always contain 5-10s of content in case of a good network connection. This caching technique can enable power savings, especially in 5G modems and RAN by the use of sleeping modes.

Table 17: Used video streams (states) and their measured power consumptions in video UE.

State	Acronym	Resolution	Bitrate [Mbit/s]	Avg. Power consumption (modem)[mW]	Avg. Power consumption (Terminal)[W]
1	720p	1280x720	4	1060	29
2	1080p	1920x1080	10	1073	30
3	4K	3840x2160	40	1098	45

[3] https://mpv.io/

4	8K	7680x4320	100	1152	78

These states are aligned with the recommendations by ETSI for XR video [15]. It is notable that especially 8K streaming to small mobile phones is extremely wasteful in terms of power vs quality, but its usage is extremely beneficial for testing purposes in our system. Thus, 8K usage is useful for large UHD displays as well as displaying small artifacts and details. It is notable that the perceptual power consumption increase from state 1 to state 3 is 55%.

Once the application controller receives the appropriate state transition through MQTT, it unifies this value as the wanted representation of DASH and interconnects with the actual video player through the Python keyboard API in case for live streaming. The keyboard API functionality enables easy dynamic switching to the desired video representations without intervening in the decoding or playback. In addition, the application controller can also queue state transition requests and apply them when starting the player next time (video-on-demand streaming). During the application state transition, the new state is also recorded into the Influx database.

For the application side, Qosium[4] is used for monitoring the network KPIs between the edge server (video origin) and the video UE. The essential parameters, throughput, delay, and jitter, are monitored and taken into InfluxDB through the Qosium Listener API implemented in Python. By using a 1/s recording interval, sudden collapses in the network can be observed and reacted to quickly, for instance by lowering video quality. For the power consumption, the 5G modem is measured separately from the Sierra industrial board with an accurate Otii Ace measurement device, as presented in Section 2.

One essential metric for assessing video QoS or QoE over HTTP-based streaming is identified as the number of video stalls, which depicts how often video freezes during playback, leading to an annoying quality of experience. This is retrieved from the mpv as *cache size* and recorded into Influx.

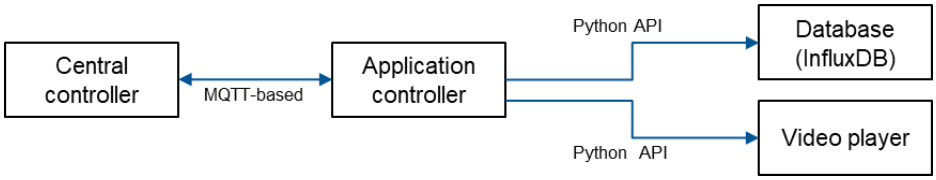

Figure 55: Application controller and its interfaces.

5.3.3.4 Central controller

The CC, implemented in Python, is the brain of our centralized system, as shown in Figure 52, and it interconnects with the energy-, RAN-, and application sub-controllers. The CC takes the green energy availability as an input of its DM process since the main purpose is to minimize the grid power consumption of our system. On the other hand, with this energy budget, we are trying to maximize the QoS for the video user, which is the second target of our work.

Once CC has subscribed to the new energy budget topic from the MQTT broker, it first checks the current RAN and app states using recall from the Influx database. These are needed especially when

a) The CC is started

[4] https://www.kaitotek.com/qosium

b) The previous RAN/Application state command has failed or not activated properly (exception state, which should not usually occur)
c) Application state is changed manually (e.g., for demonstration purposes)

After this, the new RAN state for the next hour is selected by fitting the energy consumption sum of video UE+RAN within the provided energy budget. For this, we exploit the pre-measured power consumption and DL capacity values for the RAN (see Section 3.1.3) and a single video client (see Table 17). At the final phase of this project, we added two more UEs with their respective power consumption to the system. Once the CC finds a good candidate for the next RAN state, it checks if the next state is allowed with 1 hop. If not, the CC determines the sub-RAN state, which is placed first in the MQTT-publish transmission queue, followed by the final state. As stated earlier, the intelligence in the RAN controller can handle multiple commands with a FIFO queue buffer. In case multiple RAN states can be used as the next state, the CC will select the best one in terms of DL capacity to enable the best available QoS for the users. Once the next RAN state is determined by the CC, it will publish this to the MQTT broker fetched by the RAN controller.

After the new RAN state is selected and published, the CC will check if the video application can cope with the DL capacity of the next RAN state. If not, it will select a suitable video application state and publish it to the MQTT broker fetched by the application controller.

In case it is a cloudy day or at nighttime, there will not be enough green energy available. For those situations, the CC will set the lowest energy-consuming state in RAN and the application in order to minimize grid power usage.

Evaluation and results

5.3.3.5 Long-term measurements

The majority of the long-term measurements with results are presented in Section 7.3 with associated KPIs shown in Table 15. In addition to those, we record and visualize RAN and APP states as well as network (5G) delays with a special focus on downlink, as the video traffic is pull-based DASH over HTTP. This delay also serves as one of the objective quality indicators for the video.

During the 48h-long baseline and adaptive test cases, the users (video clients 1, 2, 3) stream on average 1530 video clips according to the traffic model introduced in Section 3.3.1. The measurements and in-depth result analysis are focused on those times when streaming occurs.

Delay examples for one of the clients are illustrated in Figures 56 and 57. As seen, the adaptive delay stays mostly under 50ms, whereas the baseline peaks several times over 50ms. As an average delays for all three clients during the times of the video clips we calculated

- baseline: **33.2ms**
- adaptive: **15.2ms**

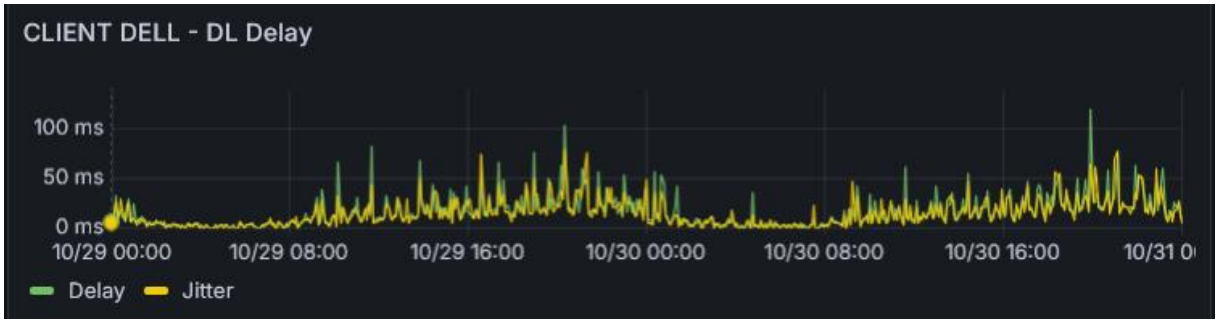

Figure 56: Measured 48h downlink delay and jitter for the baseline test case (UC5.BL).

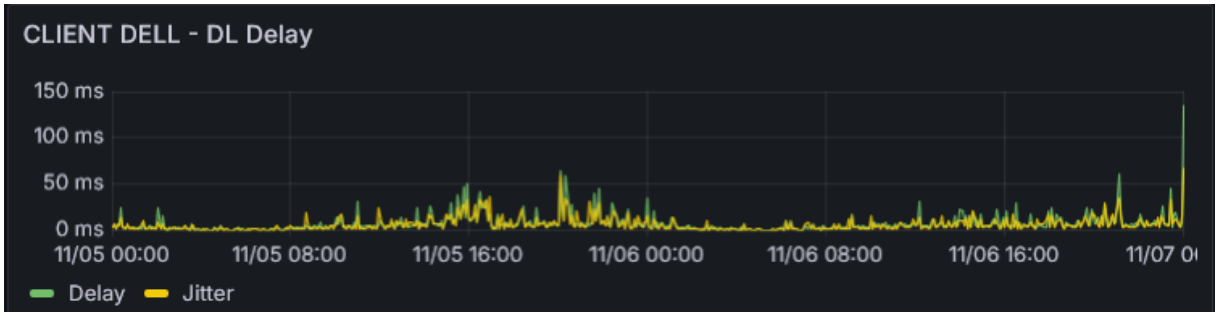

Figure 57: Measured 48h downlink delay and jitter for the adaptive test case (UC5.AD).

RAN and application (APP) state transitions for the adaptive case can be seen in Figure 58 and Figure 59. During the 48h period, RAN enters 4/7 pre-defined states and video APP 3/4. As the power vs capacity limits are quite close to each other and as the power budget is not high enough, entering to remaining states has not been possible by the logic in the central controller.

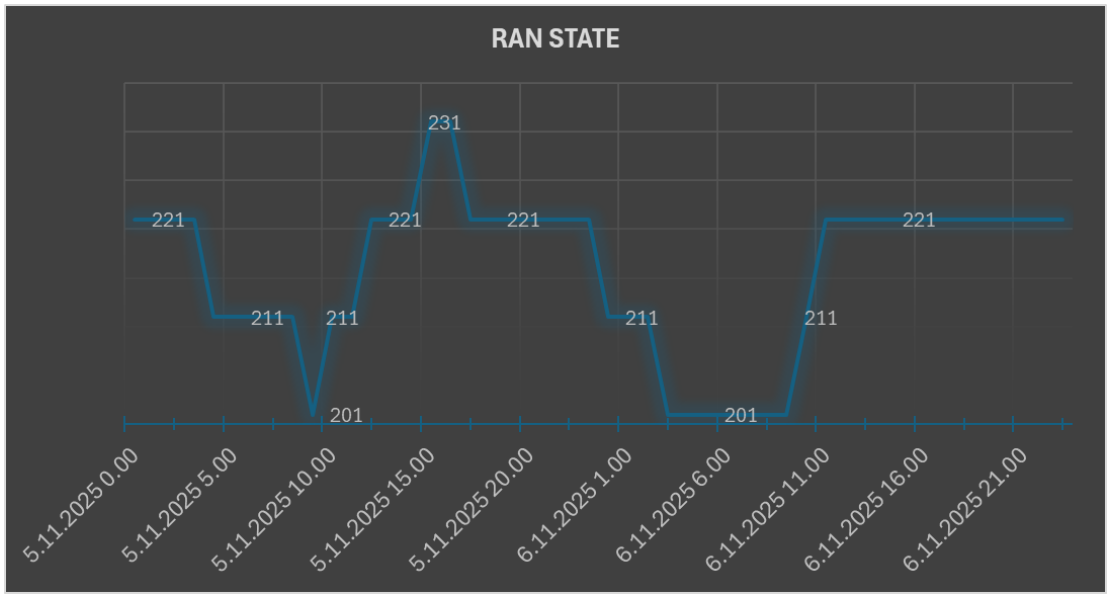

Figure 58: RAN state transitions for the adaptive test case (UC5.AD).

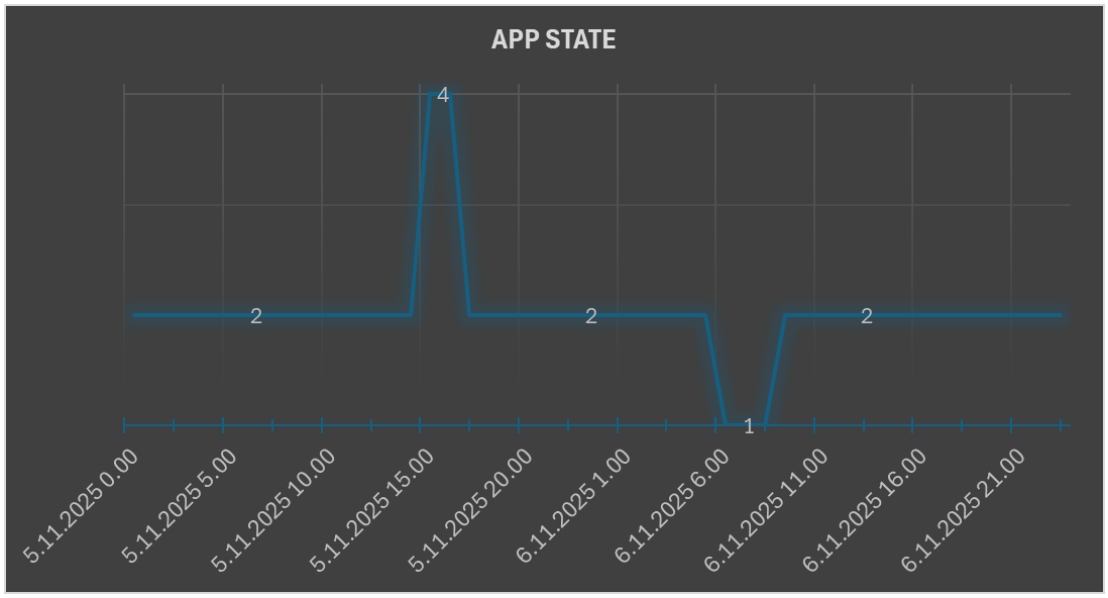

Figure 59: APP state transitions for the adaptive test case (UC5.AD).

5.3.3.6 Public demonstrations

The first version of the E2E implementation, namely as "*Joint Video and RAN Optimization based on Green Energy Budget*" was showcased in VTT Democompo'25[5] in 6th of May. In the event, we showed the daily pre-recorded run statistics (Figure 60) of our system in action, as well as the manually triggered RAN and application state transitions. The demo (Figure 61) had excellent visual impact, where the visitors could see the immediate change in RAN and application power consumption with fluent handovers without interruptions in the video UE. The second version of the E2E implementation was shown at the VTT's demo booth in EuCNC'25, Poznan, Poland, 3-6th of June[6]. It demonstrated a similar behaviour to the first version, only this time we formed a remote connection to VTT's 5G laboratory environment, where the actual demonstration was running.

Finally, the third and final public demonstration took place at the 6G-XR final event in Madrid,[7] 28th of Oct., where the evolved E2E demonstration was called "*E2E application and 5G RAN optimization based on green energy availability*". As we entered the final quarter of the project, we conducted long-term measurements concurrently with the event and presented the results in real time, comparing the adaptive system's performance against the baseline. The demo booth of this event is presented in Figure 62.

[5] https://www.cnl.fi/democompo-2025/

[6] https://www.eucnc.eu/2025/www.eucnc.eu/

[7] https://6g-xr.eu/event/6g-xr-impact-day/

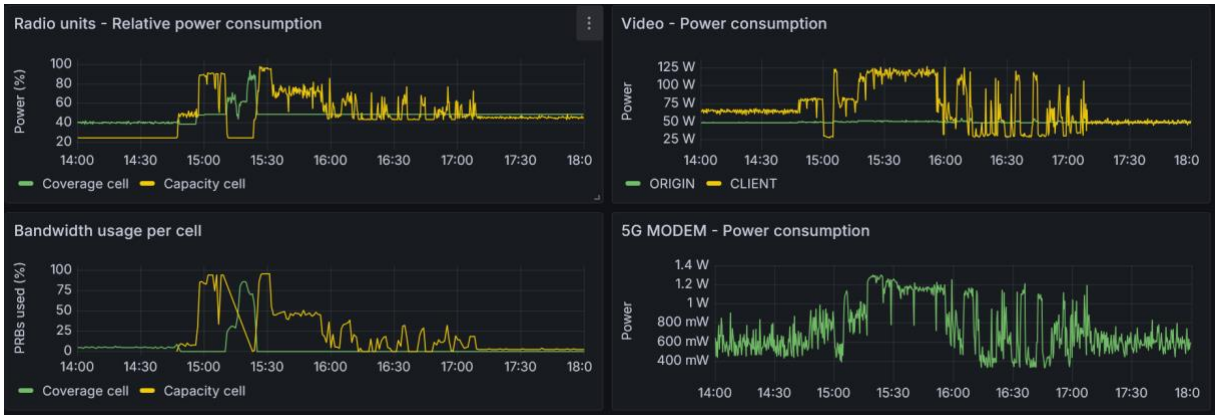

Figure 60: Snapshot of Grafana illustration with selected meters during the Democompo'25.

Figure 61: Demo setup at Democompo'25 (left) and EuCNC'25 (right).

Figure 62: Demo setup at the 6G-XR Final Event.

6 KPI & KVI ASSESSMENTS OF THE SELF-SUSTAINABLE NETWORK

This chapter presents the follow-up information on WP5 measurement-based KPIs throughout the project period. Presented long-term KPIs focuses on the PV hybrid-based real power supply system and its automated dynamic energy storage control system. Also, demonstrative key value indicators will be presented, although their usage is in early stages.

Validation efforts based on the implementation of test setups, comparisons, and test case experiments and short trial runs containing short-term KPI results are presented in a separate Chapter 7.

6.1 KEY PERFORMANCE INDICATORS

Starting point for these KPI-assessments was given in the 6G-XR-project's deliverable D1.1 (Table 18). More specifically applicable KPIs and their groundings have also been specified in the deliverable D1.2 [18] Section 3.3.1.3 "Energy KPIs".

In this chapter, the focus is on a multifunctional PV hybrid system supplying AC power to distribution cabinets where load devices (RAN elements + other E2E appliances) could be connected by means of feeder cables. In this chapter KPI-based follow-up methodology is applied from the long-term perspective (mostly on a monthly or annual level to highlight seasonal environmental variations in the north-node's conditions). In practice, not all E2E devices were yet connected to the AC-OUT circuit of the PV hybrid. Thus, the generated information is preliminary in its nature and will be utilized to construct an up-scaled virtual PV hybrid model to be used in E2E-controller trials together with measured real consumption data.

The results of detailed calculations are captured here as an example. In the next Chapter 7 methodologies have been adapted for the shorter periods and "integrated E2E-trial runs" where the usage of these KPI's and results related to savings will also be presented.

Table 18 Potential KPI's for the use-case UC5 (D1.1 [17])

No.	Category	Reference point
1	Density	Low
2	Active energy counter	The total energy consumed (KWh)
3	Cost counter	The electricity prices to calculate the cost of operating the system
4	CO2 counter	The amount of carbon dioxide (CO2) emissions produced because of energy consumption based on indirect emissions estimates from Transmission System Operator (TSO)
5	Energy savings	The amount of energy saved
6	Self-sufficiency proportion	The proportion of local energy yield per grid intake during a certain follow-up period of time
7	Energy efficiency of power supply unit	Efficiency as a whole

By means of measurement-based KPI's multidimensional impacts of improvements in the system performance can be made visible.

6.1.1 Long-term KPI's for the power supply system

A list of KPIs' interpretations:

1. **Active energy counter**: refers to the real-time active energy consumption measurements (or as well to production measurements in case of power supply unit) or bi-directional measurements in the system boundaries ("of the investigated scope") and e.g. covering all E2E-network elements and devices. These counters can capture cumulative energies of the real or simulated power transmission resulting from the use of traffic-generators or applicable "test-consumption profiles".

2. **Costs counter**: Focuses on runtime electricity costs and substitution costs & savings related to grid intake of the system with and without PV-hybrid based power supply system and active control system, and taking day-ahead electricity spot-market prices, DSO's fees, taxes and other "cost components and fees" into account. However, we excluded the impact of value added tax and presented only VAT 0% values.

3. **Counters for indirect CO_2 emissions and energy & CO_2-savings**: Measures the reduction in CO_2 emissions and energy consumption during the defined period(s) against some baselines. A method to calculate indirect emissions of grid intake was developed. A comparative test set-up was used to estimate relative savings for a certain period.

4. **Self-sufficiency proportion**: Indicates the proportion of energy self-sufficiency of the connected consumption. Methodologies were developed for follow-up purposes. Results depend on the dimensioning of the system components as well as on power levels (time profiles) and the applied control pattern.

5. **Energy efficiency of the power supply unit**: Evaluates the efficiency of the power supply system containing the entire PV hybrid system and its sub-components, like dynamically controlled batteries.

These KPIs were calculated from stored and supplemented time series data and are essential when assessing the longer-term energy efficiency of the power supply system, as well as achieved cumulative savings (**-€, -kWh intake from the grid, -kgCO_2**).

In this analysis, "the scope" is located between the feeder cable measurement unit supplying the PV hybrid and the inverter's AC-OUT circuit's total consumption measurement unit. Thus, changes in the end-consumption were not yet analyzed, because AC-PSU must adapt to them as a "slave". Instead of that, power intake from the grid -savings were analyzed. However, changes in the end-consumption (consumption savings) were analyzed as a primary impact-category related to the developed E2E-demo-controller, which is a specific type of "load controller" capable of changing energy consumption levels based on the anticipated energy availability horizon. Validation of the E2E controller is presented in Section 7.4.

6.1.2 Active energy consumption vs. lengths of the KPI-periods

Applied measurement devices can measure both momentary power components (sampling 1 Hz) as well as registering their time integrals to internal active and reactive energy counters. This data was read from the transducers' Modbus registers to Influx-DB and visualized by means of Grafana panels or customized widgets in Victron's VRM-cloud service. This data formulates the groundings for all KPI analyses. Both the input (grid intake and feed-in) and output side (towards consumer devices) of the grid-connected PV hybrid are equipped with these independent Carlo-Gavazzi transducer units, enabling the formation of the energy balance for certain time periods. In addition, internal data of the PV hybrid was stored on a 1/min level and active energy transfers between sub-elements (grid, battery, PV, and consumption) on 1/15min time slots, which were then used to create a long-term follow-up system. The system was developed so that it can produce all desired KPI's for the interesting periods.

Figure 63 shows the connected active energy consumption data aggregated from 15 min time slots during 2 years.

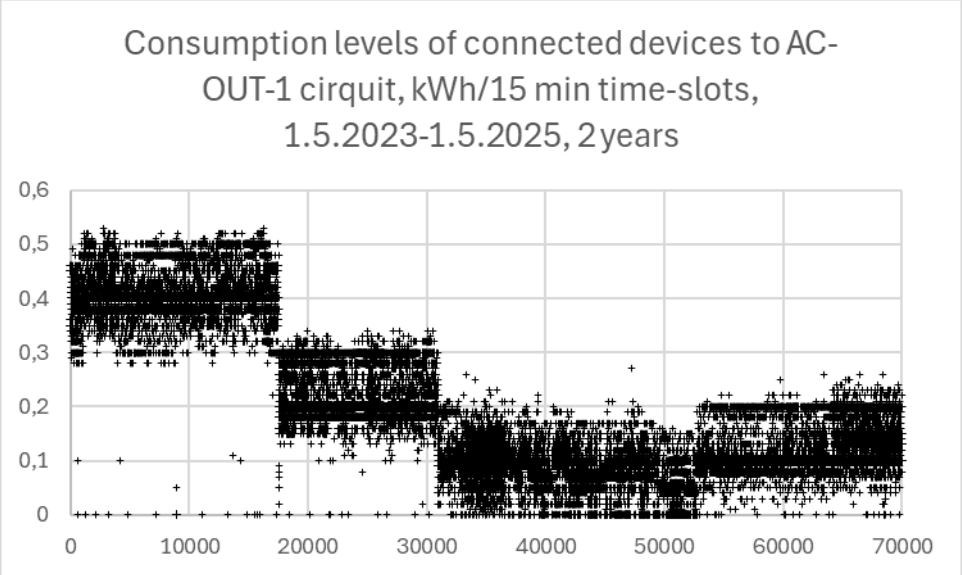

Figure 63. A two-year inventory of inverter's AC-OUT-1 circuits' consumption based on 1/15 min data.

Only a few service breaks and consequential data gaps occurred during 6G-XR's 3-year research period. Their impact on data quality was estimated to be negligible. In most cases, it was also possible to derive data from redundant measurements or other data sources.

Due to the scale of the PV hybrid system presented in the Figure 64 and especially the small, aggregated power of its PV modules (installed total nominal power 2,2 kWp), scale-up factors were needed to match PV-production to the consumption of the real E2E system (not the consumption of the previous Figure 63.)

Figure 64. A picture of VTT's PV installation targeted to long-term research. The pole of Vaisala weather station is on the left side of the installation.

Vertical PV-module setup in the North-Node's conditions can harvest reflections from the snow and ice surfaces in front/south side of the roof, especially during spring-winter.

Figure 65 describes the length of the energy-positive usage or dimensioning period in months per year as a function of the scale-up factor.

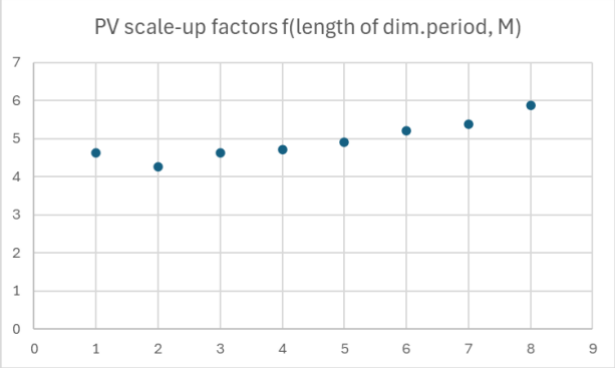

Figure 65. Scale-up factors for existing small wall-mounted PV-module installation as a function of dimensioning period in months per year based on empirical PV-yield and efficiency data and usage of the "test consumption profile".

An example about interpretation: factor 5,5 x real yield from VTT's PV-module setup, would enable even > 7 months energy positive usage periods annually in the north-node conditions with vertical southward module installation. In detailed dimensioning trials, the real-time PV-yield data (Wh/time slot) could be multiplied by 5,5 to simulate various energy transfer situations in the PV-hybrid system. The use of scale-up factors together with real experimental time series about PV-yield/15 min enabled flexible simulations to match the sizing of the PV array to measured or simulated consumption (with a certain daily consumption profile), battery size, and inverter/charger capacities.

If much shorter test trial periods are needed based on time triggering (UTC "epoch" time), then it is easy to utilize and read the nearest active energy counter readings, which can be subtracted from the counter's value representing the end of the trial to get consumed energy during the trial.

However, the accuracy of the active energy measurement results of such a trial also depends on power levels: the smaller the power of the load is, the longer the trial period is needed. Carlo Gavazzi's EM 111 meters accuracy is shown in the next Figure 66.

Also, the data processing capacity of the transducer unit itself could be utilized by means of DMD settings: typically, we have configured devices to calculate 1 minute or 15-minute average and maximum power values and store them in the DMD registers until the next period updates them. The device calculates the average values for the DMD-period from 4096 samples/s according to the applied standards.

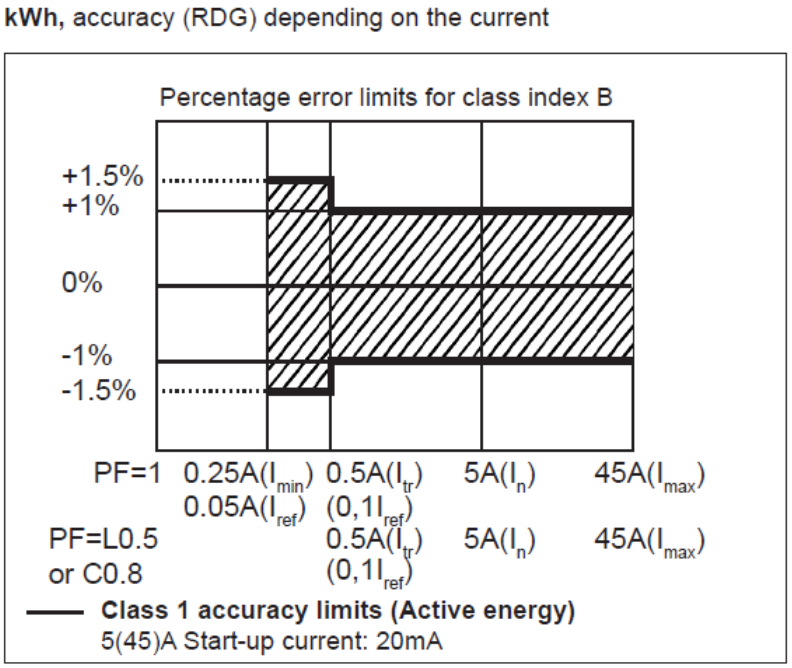

Figure 66. Accuracy as a function of 1-phase current (according to EN50470-3 and EN62053-23) EM111 AV8-model's datasheet [27])

The consequence is that less than 5W loads cannot be measured by means of EM111s due to the start-up current (20mA). In those cases, the OTII-ACE system is needed. Between 57-115 W, the accuracy is in the +-1,5% area, and above 155W, the best level <+-1% of readings is achieved. In practice kWh counter of the EM111 has 1 decimal in its Modbus register (corresponding to 100 Wh of energy). The consequence is that if we measure 500 W average loads and want to get active energy results with 1% accuracy level, the duration of a comparative trial should be circa 20 h long. To a 1kW load, 10 h would be enough, and 2kW 5 h would be enough. If trials focus on comparative active energy savings and standardized results are desired, quite long trial periods are needed (e.g., 1 week was selected to be suitable target length for short-term trials).

If shorter trials must be executed du eto practical reasons (which is not sure), one option would be to reset the energy counter before the start of the trial to activate a 0,001 kWh reading area in use. Then already 1 Wh corresponds to 1% of 0,1 kWh reading, and differences in, e.g., 100 W level trials can be easily detected directly from the counter readings. This may be useful in trials where the active energy consumption is less than 9,999 kWh. In these cases, 1 h long measurements for more than 100W could be long enough. During the longer periods (e.g., on a monthly scale), these accuracy issues are not problematic, and energy results can be obtained in a standardized way.

6.1.3 Energy savings

Energy saving studies and test setups typically require some kind of pre-defined comparative arrangement or baseline to compare obtained results (with activated measures). Alternatively, at least two trial-measurement periods are needed: 1st without energy saving measures and the 2nd with the measures to be validated or verified. The impacts of confounding factors should be eliminated. As a result, both proportional or relative (%) or absolute active energy (kWh) savings per investigated period can be extracted. The same comparative methodology can be utilized to determine kWh, CO_2, and € -based savings.

Achieved energy savings, in case of PV-hybrid based power supply, can be calculated by means of comparing realized net energy intake from the grid with the "traditional situation" where all devices would have been connected directly to the grid. Savings can be presented in absolute or relative units or as a proportion to some meaningful subject (In Figure 67 against installed PV-modules kWp). Net energy intake refers to the equation "power intake minus feed-in" to the grid. In the case of the PV-hybrid-based power supply system, the subtraction energy of consumption and net energy intake was obtained from the PV system. It is important to notice that the control system of the battery energy storage (BESS) has significant impact on the results due to timing and losses. Longer term trials are needed to make it visible. Additional savings (not yet considered) occur in the entire electricity distribution system, but those are site dependent and difficult to estimate without detailed data about the entire distribution system (both facility's internal, DSO's and TSO's grid).

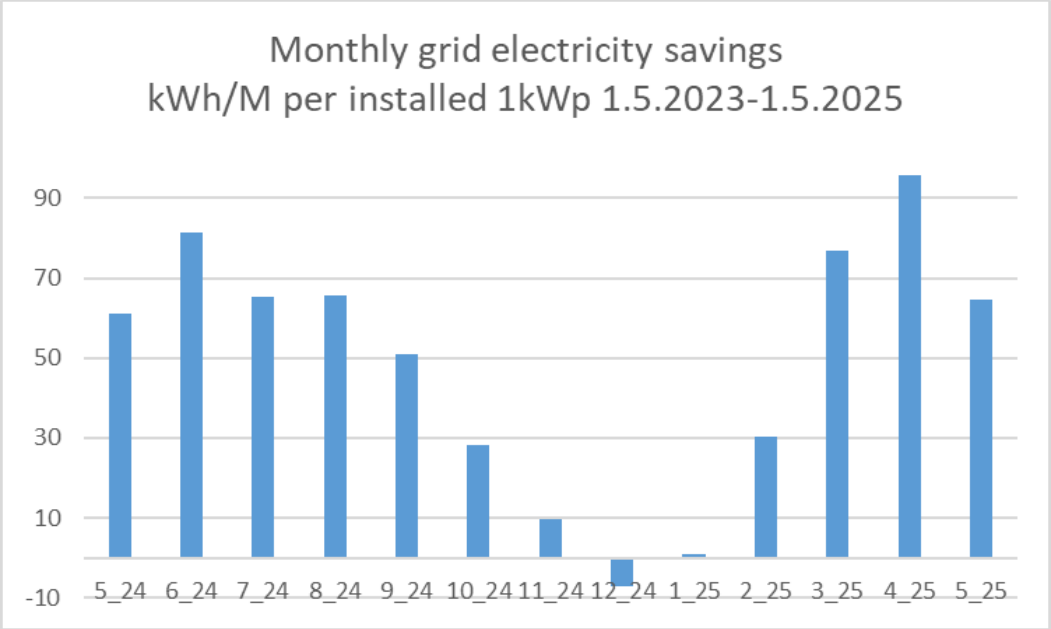

Figure 67. Downscaled *monthly grid*-intake energy *savings (kWh/Month) gained for* every installed *1kWp* of *PV modules in the PV hybrid-based PSU system when supplying energy to consumption devices.*

In this case, a figure shows the realized monthly net electricity intake (intake – feed-in energy counter's difference) from the grid was compared to measured energy output to consumer devices, and the difference is the gained savings, which were achieved by the PV-hybrid. Negative figures indicate that the electricity consumption of monitoring, control, and communication devices and losses of PV-hybrid during dark December were bigger than the captured solar yield. On the other hand, these numbers also depend on the load levels, consumption profiles, and the applied bidirectional inverter-charger's control logic. We utilized Victron Energy's dynamic energy storage control system (DESS-cloud service) as a primary controller of the system in this period. It was capable to take battery costs (and losses) and ELSPOT prices into account. It is also expected that battery degradation speed will also slow down.

6.1.4 Indirect CO_2 emissions and runtime cost savings

Active energy measurement data (grid intake of the PV-hybrid, kWh/15 min slots) was linked to time series obtained from FINGRID's open data service (CO_2-estimates for the Finnish consumption 1/3min and new 1/15 min time series [23]). In first long-term calculations older 1/3 min datasets were applied to formulate averages to 15 min slots.

In the Figure 68 indirect CO_2 emissions of "traditionally grid connected" total consumption are estimated on monthly bases. Emission levels seemed to alternate annually.

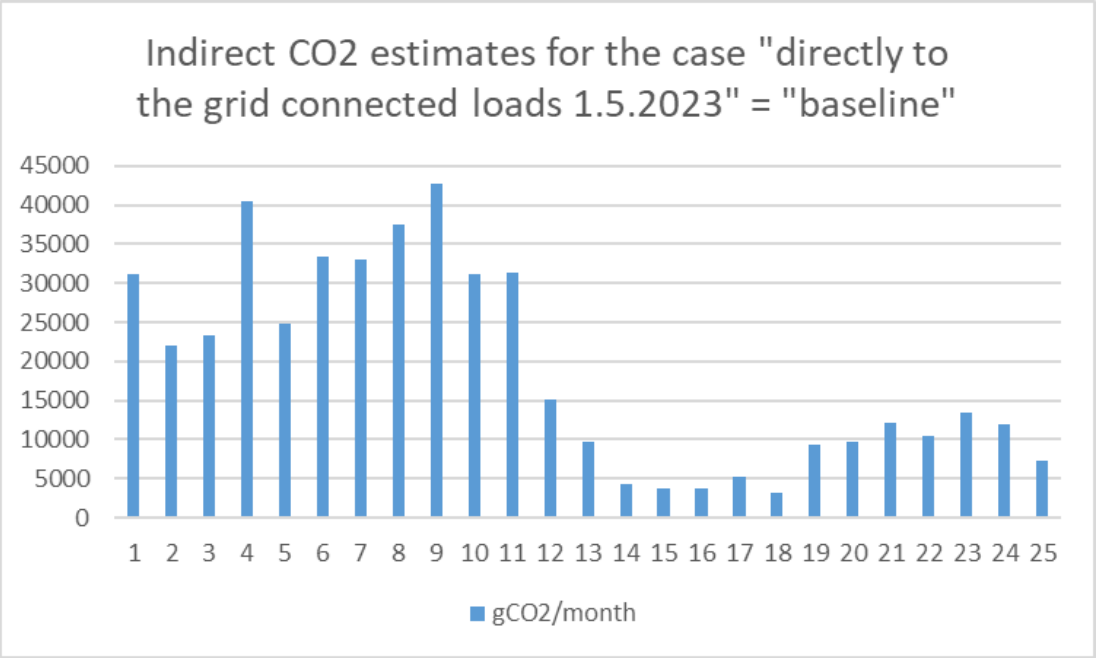

Figure 68. Baseline emissions gCO_2/month related to traditional grid-connected consumption during the project (this contains numerous changes in system setups, circumstances and entire energy system).

Figure 69 shows that the long-term follow-up of CO_2 KPI for the subset of connected devices can be implemented based on 1/15 min matched datasets. This also reflects significant changes in the electricity markets and average emission factors for consumed electricity in Finland.

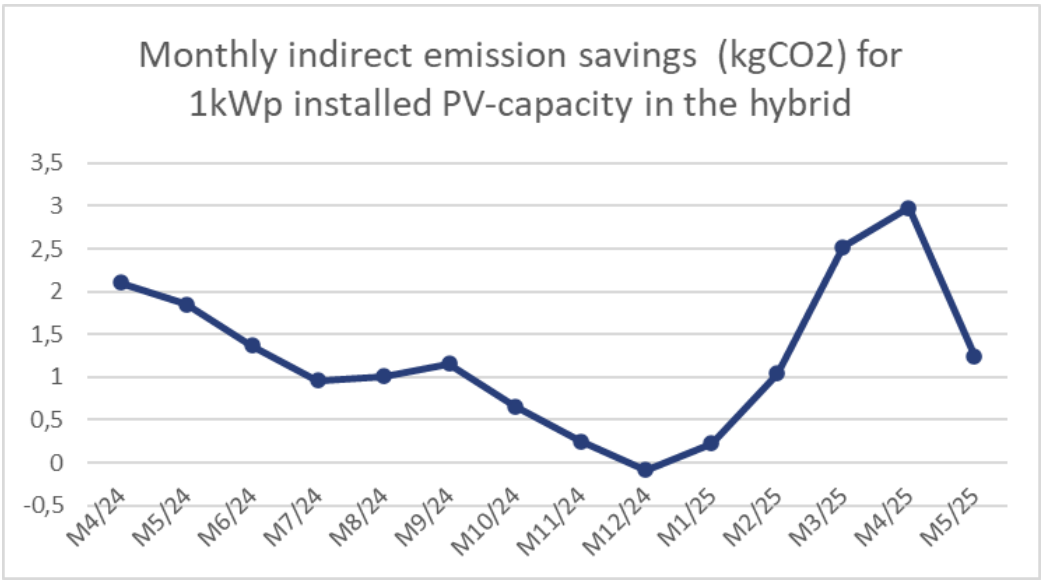

Figure 69: Monthly CO_2 savings based on substituted grid-intake by the PV-hybrid and scaled down to match a 1kWp PV module setup.

Figure 69 reveals the obtained CO_2 savings by means of DESS-controlled PV-hybrid installation. During the 4 winter months, CO_2 and energy savings are nearly negligible (or even negative due to battery losses and minimal PV-yield), but the applied control system enabled price-based optimization and thus economical and resiliency benefits can still be gained.

In the next Figure 70. economic benefits, i.e., € based savings per month are presented in case of PV-hybrid power supply system compared to direct grid-consumption (a reference case).

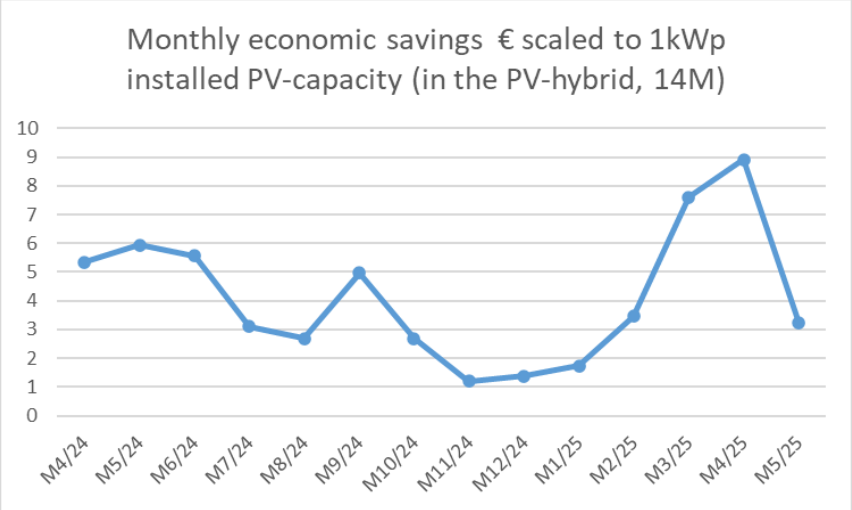

Figure 70: Gained monthly cost savings per 1 kWp installed PV modules under the DESS control.

In this methodology realized runtime electricity costs (intake of the hybrid) were subtracted from the cost of summarized "direct" electricity consumption costs of connected devices to get savings (for every 15 min time slots during the period).

This examination is not yet able to capture economic value of stochastically increased PV-hybrid based energy-storage "as a back-up power reserve". This value may be significant e.g. when batteries are fully charged according to storm warnings.

6.1.5 Price vs. CO_2-emissions correlation

Similarities in the previous curves took up the need to check the correlation of ELSPOT prices and indirect specific CO_2 emission factors (Figure 71). It may reveal what may happen to emissions if more consumption is transferred to cheaper hours.

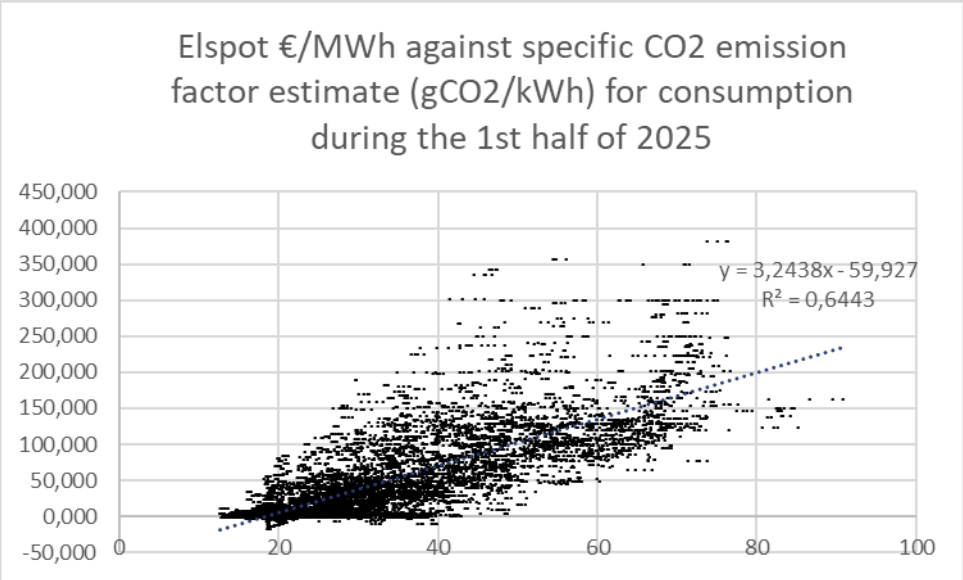

Figure 71: Correlation of ELSPOT day-ahead prices (Y) against emission factors (X) during the first half of 2025.

There was a weak correlation (R^2=0,64) between prices and CO_2 emissions between 1.1.2025-1.6.2025. In further work, it would also be important to separate the winter period (1.11.-31.3) from the other seasons when the Nordic electricity system is operating on lower power and price levels.

6.1.6 Self-sufficiency proportion of the consumption in the case of a bidirectional system

There may be use cases where 100% self-sufficient off-grid systems are needed. However, in harsh northern conditions, the dimensioning of the round-the-year operating off-grid unit would require large multi-day energy storage capable of surviving several days of dark and rainy weather conditions on the required QoS-level and sufficiently high probability.

The PV -energy yield captured in December is on average only 0,3% and the share of the 5 darkest winter months (October to February) has been only 13,6% of the long-term annual specific yield, which is 760 kWh/installed 1kWp or 760 h/a as a “peak power time”. These production statistics are based on our southward vertical PV module installation in Oulu and without any maintenance or service operations).

During December and January, there have been more than 10-day periods when the daily PV yield has been c. 10-50 Wh/kWp (i.e., less than the monitoring and control equipment of the hybrid consumers). Thus, auxiliary energy sources like small-scale wind power units and supplementary fuel cells (or other generators with related dependencies) would be needed to achieve off-grid operation in the northern conditions. In critical IoT-use cases, even very small daily energy yields could be utilized, and in such a case, real experiments are needed to ensure proper functioning of a system.

On the other hand, energy balance-based survival is a stochastic phenomenon, and a consequence of the arbitrary behavior of the users (traffic) and alternating weather conditions (reflecting energy yield containing rare anomalies). During the winter season, inspections and/or services are also needed to keep systems up and running. Also, the number of PV modules increases, and then, on the other hand, overproduction during the sunny days must be curtailed if there are no useful “energy sinks” inside the scope. This creates economic losses and lowers the peak power time (h/a) of the entire system. Our focus in this study was to investigate annually feasible self-sufficiency levels between 15-70 %.

Level 70% was previously found to be difficult and expensive to exceed. Based on realized PV-yield time series and Figure 5 and Figure 65, it was found that longer than 7 months started to increase PV's scale-up factors rapidly. Thus, optimal system dimensioning length in Oulu's conditions seem to be nearly 7 months/year. If we then use this factor 5,5 (Figure 65) and selected 7 month dimensioning period for our existing 2,2 kWp PV-module setup, we get 0,4 kW average level for continuous consumption (this was one design principle enabling intended islanding and round the clock test-runs during sunniest weeks [29]). If we use 90% DC to AC conversion efficiency (Figure 73), the installation would be able to supply 0,36 kW average consumption. These dimensioning principles were previously presented in D5.1 (Sections 3.3.3 – 3.3.5, [13]). During 7-month period, total energy consumption of loads would then be 7/12a x 8760h/a x 0,36kW = 1839,6 kWh. At the same time, PV-yield was 1448 kWh. Thus, self-sufficiency from the consumption perspective would be for 7-month dimensioning period: 1448kWh x 0,9 / 1839,6 kWh = 70,84% (corresponding annual level is much lower, around 50%, due to local conditions in Oulu region). Usage of the shorter summer periods increased self-sufficiency % upto 73,5. During the sunny weeks comparative self-sufficiency level may be 70-80%.

The lower area (below 15% self-sufficiency level) is typically achievable by means of grid-tie inverter solutions without energy storage and load control systems. 15% refers to a non-controllable inverter and a case where PV-inverter's max power would have been dimensioned to exceed average (constant) power of consumption according to factor 1,2 x. In that kind of situation, periodical self-sufficiency % remains below 15% for 4-12 months (corresponding range is 14,5 - 9,5%).

However, by means of active load control systems and connected flexible consumption (controllable loads), matching the production and consumption profiles can be improved even without expensive battery capacity investments with related indirect environmental burden, resulting in higher annual self-sufficiency proportions.

Dimensioning can be done based on determining the energy need firstly during the discharging period(s) (from the assessed break-even point during the evening to the next morning when presumed PC-power exceeds consumption), at least during the start and end of the desired usage period during the early spring and late autumn. In this determination principle, the nighttime consumption time series or some kind of "test profile" or at least default information is inevitable. It has direct impacts on the capacity needs of the energy storage system. Also default efficiencies of power-electronic components and the battery must be considered. In general, the cost efficiency of the power supply system decreases as a function of the self-sufficiency proportion. When the battery size has been determined and decided, then it is possible to conduct "survival simulations" by means of empirical or simulated PV yield time-series against the suitable consumption profiles. Then all the other sub-components, like the size of PV-module setup, power levels of bidirectional inverter charger, and requirements for the busbars and potential load control system can be found for the desired usage period.

Applied practical electrical laboratory setup in this project enabled flexible energy exchange with the grid on various self-sufficiency levels and short runs in islanded mode as an "off-grid system". This functionality was used to enable uninterrupted usage of the connected devices during potential power outages. This functionality could also have been used to isolate test setups from the electrical confounding factors (power quality issues) coming from the internal or external grids of the building and potentially influencing the results of the test measurements. Victron Energy's Multiplus-II technology was selected and found to be compatible with the older and recent grid-code requirements (EN 50549-1). Local protection settings were implemented, enabling full compatibility with the electrical regulations relating to grid-parallel and off-grid usage of the system, including transient states.

A specific "hybrid-diamond" energy-balance methodology was developed to calculate the self-sufficiency of a PV-hybrid containing bi-directional energy storage in grid-parallel operation during a certain trial or follow-up period. The problem was that the origin of the discharged energy from the battery was not known in dynamic usage. We applied energy-based allocation principles for selectable periods. In our system topology, the battery may have been charged from the grid or from the DC-PV system. Stored data in the time slots (the smallest time resolution is 15 min), i.e., active energy transfers between the grid, battery, consumers, and PV-supply were determined, and missing energy transfers between these were calculated by means of the energy balance principle. Practical follow-up periods must be much longer than the storage processes, and in that case, the state of charge (SoC) differences may be neglected. It is also important to note that self-sufficiency proportions (%) are different from consumption (outputs from the PV-hybrid) and production (inputs) perspectives in the case of bi-directional energy transfer with the grid. We chose a consumption-based approach. Demonstrated "hybrid-diamond-energy-balance" methodology can capture the impacts of control operations of the inverter (battery usage) into account. Thus, it is applicable for KPI based follow-up for the cases in which the target is to improve intelligent control principles based on retrospective data. In the future, it may be used for scale-up purposes (and to create digital twins).

The next Figure 72 reveals energy transfers (%), during the 7 months "optimal dimensioning" period in Oulu for the PV-hybrid based power supply. Percentages were calculated from the consumption perspective (=100%). The method is based on 1/15 min calculations through the period.

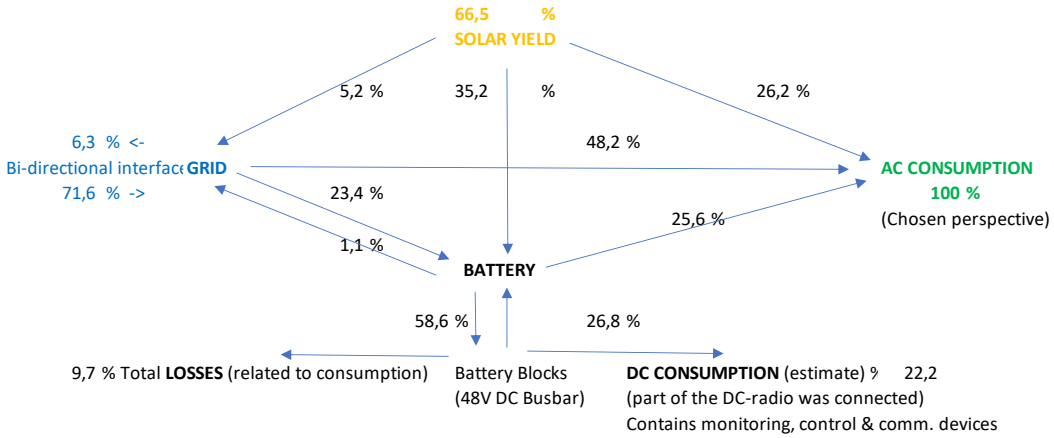

Figure 72: An example of a developed "hybrid-diamond" methodology to show energy transfers between PV-hybrids sub-elements during a selected period (1.3-30.9.2024).

Most of the time, the system was automatically controlled by means of Victron Energy's dynamic energy storage service (DESS) in "green mode" and in a specific configuration in which the system prioritized self-consumption more than economic performance. That choice (by the end user) restricted battery to grid transfers and reduced battery usage during the low-priced hours. For the time being, retrospective indirect CO_2-emission estimates related to grid intake were not considered in the applied control principle.

By means of a created data system and methodology, the following long-term KPIs reflecting the performance of the PV-hybrid-based power supply system were extracted:

- Self-sufficiency (% of total consumption, during a period) 42%
- Solar proportion of net energy inputs (% of E production) 50%

- Solar share of total periodical consumption 0,42
- Overall efficiency of the power supply system (Out/In) 93%
- Sum of energy inputs compared to consumption 108%
- Total losses related to useful consumption 9,7%
- Total losses related to the sum of energy inputs 7,4%
- **Saved amount of electricity, intake from the grid per consumption 57%**

Obtained PV-hybrid's "diamond-calculation results" for sunny periods indicate that even higher than 70% level of energy savings (in relation to procured electricity "grid-intake") is achievable by means of this multifunctional inverter technology and well dimensioned PV-hybrid power supply system with battery energy storage and flexible grid interface.

Previous KPIs were derived from the 7 months "dimensioning period" in which the realized load levels were not so optimal from the inverter's efficiency perspective, and not all the E2E-chain devices were supplied via this PV-hybrid. The average power level of consumption through the previously assessed period was only 385W, reflecting remarkable scale-up needs with the factor 5.5 to PV yield to match the investigated test set-ups in the laboratory and the desired 8M usage period in Oulu. The PV setup, battery sizing, and inverter/charger system were originally optimized to enable 100% self-sufficiency test runs in round-the-clock usage during the short sunniest periods at that average (constant) power level. Scale-up plan of the BESS depends on the controllability of the loads, which was investigated in D5.1.

Originally, VTT's PV-module setup, battery sizing, and inverter/charger systems were optimized to enable 100% self-sufficiency test runs around the clock in off-grid or islanded mode, e.g., due to power outages (back-up power use-case in mind) during April at the consumption level of 400W (continuous load [29]). At that time efficiencies of components were not known. Thus, executed 7 month long test-run with DESS-control verified that the relative dimensioning of PV-hybrids components is quite near the optimum, but the "design power level" of the entire system has proved to be much too small compared to implemented test-setups.

6.1.7 Energy efficiency of the entire power supply unit

Changes in the average power levels of connected loads during the project and obtained data in various situations enabled usage to utilize several methods to reveal energy efficiency of the power supply system, and e.g., inverter/charger. The inverter's efficiency dropped significantly to low power levels, which is illustrated in the Figure 73. This data is based on internal sensors of the converter unit. It is probably specific for the applied converter type with internal isolation transformer. However, it is typical that only maximum efficiencies are presented in datasheets instead of this kind of efficiency curves as a function of power levels. Long-term trials showed that applied converter type achieved highest energy efficiency (energy output/energy input % per timeslot) between 1/3 – 1/2 of its nominal max. power levels. Thus, losses can be minimized by means of careful dimensioning of the units against aggregated power consumption in AC-OUT circuit.

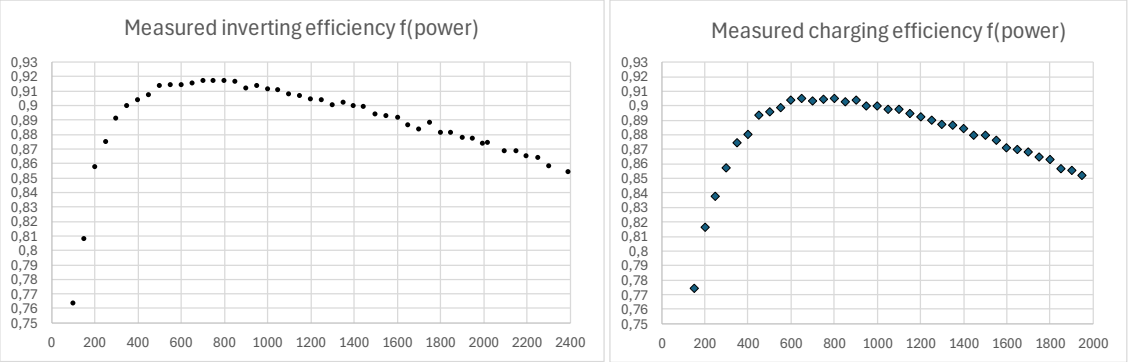

Figure 73: Experimental data-based examination of the efficiency in inverting and charging modes (based on results for the same 3kVA (2,4 kW) inverter type).

The previous figure revealed that high efficiency inverting power (>91% efficiency) is between 500 – 1100 W, and charging efficiency seems to be slightly lower, and >90% can be achieved between 500-1000W. These power levels are between 16-37% of the nominal apparent power level (kVA) of the device. At the maximal active power levels (2400W at 40C) efficiency seems to drop to an 85% level. If the efficiency of the battery is around 90%, the round cycle AC efficiency on the max power level is around 65%. Using the inverter charger near the optimal power level, 74% efficiency is achieved, corresponding to +14% improvement.

Efficiency and power consumption of the PSU itself is an important KPI because losses, i.e., waste heat of the PSU, cannot always be utilized in a valuable way in the southern countries or during the summer in the north. In some cases, surplus heat could be harvested e.g. to domestic hot water circuits by means of air-to-water type of heat pumps. During the cold seasons energy content of heated air could be transferred to use or to input air channels (by means of energy recovery units). During the hot season, heat must be transferred to the environment by means of active cooling systems with additional costs originating from the supplementary electricity consumption.

An energy controller should be able to take efficiencies into account when planning the control policies related to battery usage in parallel with the grid. Unnecessary energy circulation through the battery should be avoided.

Energy efficiency of the PSU (%) can be calculated from the delivered energy to the consumption (output circuits of the PSU) divided by means of the production (inputs of the production units, i.e., AC-grid intake and DC-PV-yield). Storage operations, which are inside the energy balance envelope, can be neglected in case of long enough follow-up “time windows” e.g., 1 month is used. Figure 74 captures the output/input-based energy efficiency of the PSU during the project execution when the amount of connected load power (consuming devices) at a given time have not been optimal from this efficiency perspective.

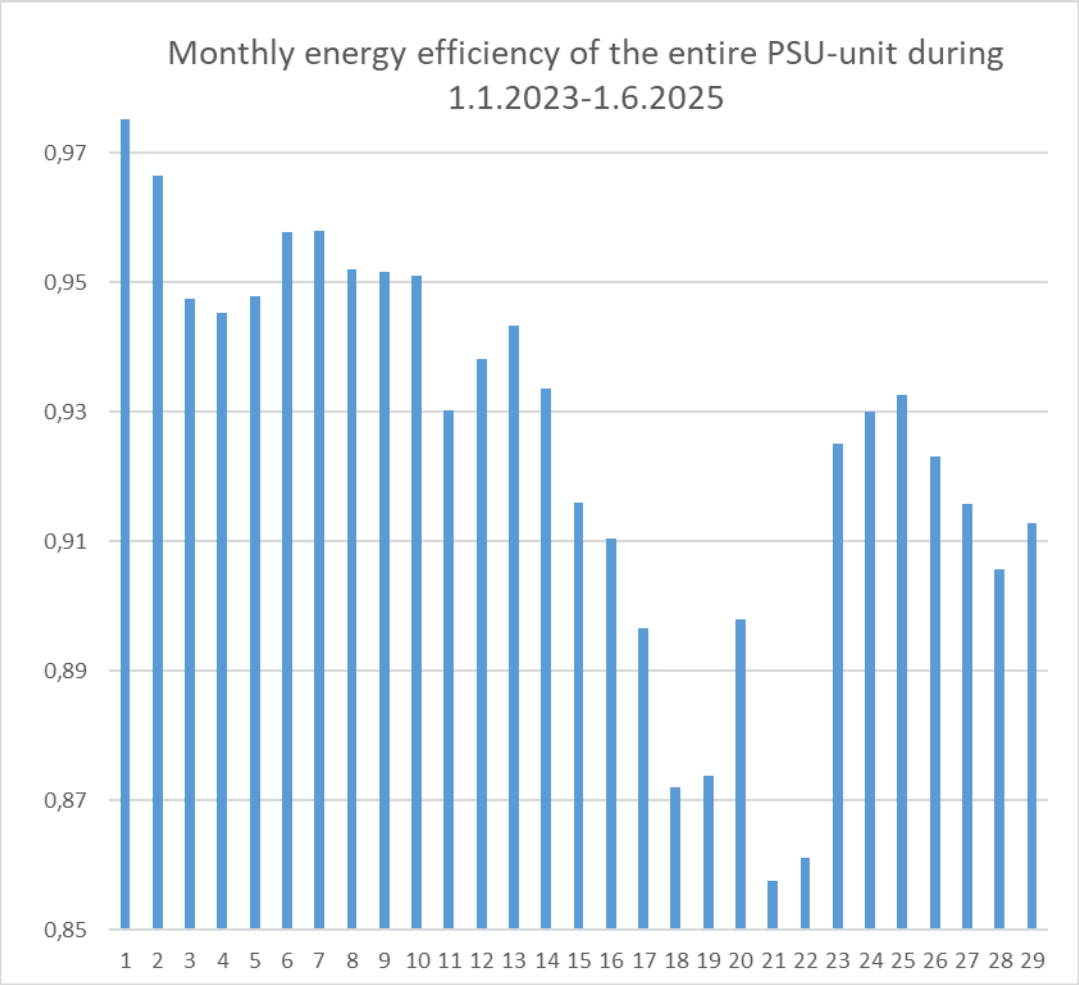

Figure 74: Energy efficiency changes of the PSU on a monthly level during the 6G-XR-project execution.

Decreasing efficiency has been a consequence of changes in average load power levels during the period (numerous changes were made in connected devices). There is free capacity to add additional devices to the system. The share of DC-PV energy in the system also has a strong influence on efficiency. However, impacts of improved control patterns and the system can be monitored by means of energy efficiency KPI and demonstrated follow-up methodology.

6.1.8 Degradation speed of the battery energy storage

When targeting high self-sufficiency levels, sizing of the battery and its investment costs become a significant factor in the energy economics of the system. If effective power procurement costs during the night are smaller than the costs of discharged energy from the battery, then it is not profitable to discharge the battery even if the input energy would be “free of charge” (e.g., surplus from PV-unit). This threshold electricity cost -level can be determined by means of taking investment cost of the battery and its full service-life into account as well as ELSPOT and distribution fees. Service life refers to a promised number of charging-discharging cycles and obtained amount of energy output. One simple way to estimate this threshold is the equation: investment cost divided by the sum of estimated sum of dischargeable energy of cycles (eg. 1000€ / (6000cycles*2,4kWh nominal capacity * 0,8 SoC-range of cycling) = 8,6 snt/kWh from pure investment without costs of electricity losses).

The price level of “LFP-consumer” batteries has decreased a lot to the level 200 €/kWh and below, which would result corresponding threshold level to be around c. 3-4 snt/kWh.

In practice, the usable capacity also decreases over time, and it can be revealed by means of the state of health (SoH) indicator available from battery monitoring systems (BMS). Our experience during 6G-XR-project revealed the ageing equation (related to our type of use) and is presented in the Figure 75 below. Long-term tests made by the ITP Test Centre (Australia, [19][25][26]) capacity degradation of lithium-ion batteries seemed to be quite linear, albeit some variability was observed. VTT applied these reports as a background for battery procurement decisions.

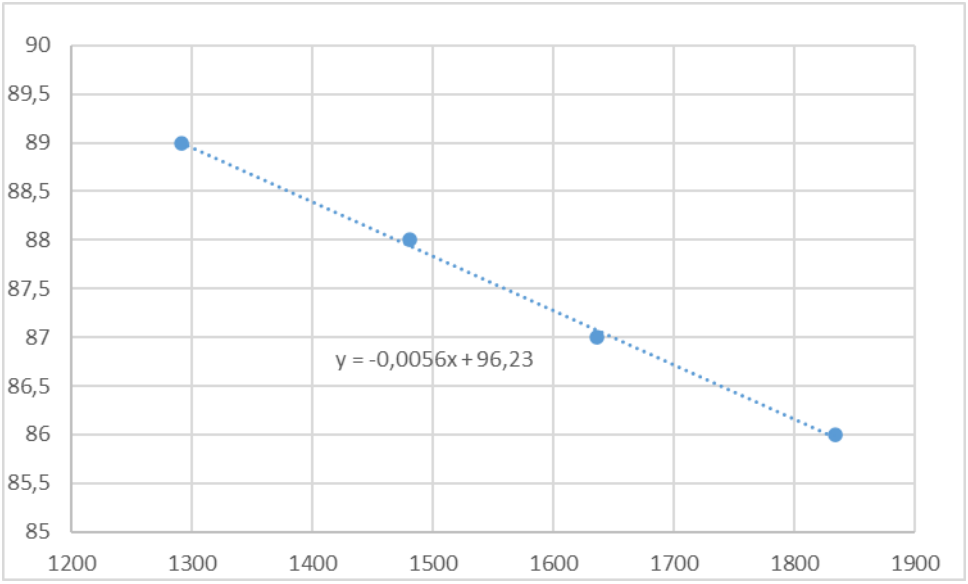

Figure 75: State of health trend of the battery system (degradation trend during 1/2023 to 5/2025, X axis refers to days from the start of the experiment).

According to "currently valid equation" our battery system would reach 50% SoH-level after 22,6 years of service. The service life of the LFP battery seems to be long, and 20 year promises in marketing materials may hold true. However, it depends on control patterns and usage in practice. Minimization of the temperature fluctuations might have slowed down the degradation speed as well as the utilization of the DESS control system, containing battery saving cost parameters.

6.2 KVI ASSESSMENTS

As described in D1.1 [17], the KVIs listed for UC5 are mostly derived from the KPIs linked to UC5. The KVIs listed in D1.1 [17] are mapped to KPIs, and the results were gathered using the validation process of the KPI metrics. These results extend beyond the technical and numeric results obtained during KPI validation and focus on broader societal, operational, environmental, and economic value created by the 6G-XR energy framework. The following sections provide assessments for each KVI relevant listed in D1.1 [17], linking them directly to the results obtained from the KPI evaluations conducted in Task 5.5.

6.2.1 EcoMonitor

This KVI evaluates how effectively the UC5 framework improves stakeholder awareness of energy consumption patterns by collecting the power consumption of the E2E data path and entire network components individually on a one-second basis. KPI results for real-time energy monitoring, active

energy counter, and power readings from external meters such as Carlo Gavazzi's transducers, Otii-ACE devices, and Netio powerbox, and MQTT-based data exchange between gNB sites and collection of measurement streams demonstrate that the EcoMonitor KVI achieved reliable perceptibility into gNB and the entire network level energy consumption.

6.2.2 Energy data sharing

The Energy Data Sharing KVI assesses the North Node network's capability to exchange energy-related information securely and efficiently. The data exchanged is enabled through a secure MQTT bridge broker and authentication within the UC5 framework. The framework successfully facilitated multi-stakeholder sharing (e.g., between UOULU and VTT gNB sites and with several open-call project partners around Europe), demonstrating that the essential data flows for optimization and decision-making were enabled, such as optimization of E2E energy consumption via a centralized controller using RAN parameters.

6.2.3 Energy efficiency

This KVI measures the improvement in overall energy efficiency enabled by UC5. KPI outcomes such as energy saving counter and active energy counter, which calculate the power consumption reductions under different RAN configurations, optimization based on energy weather forecasts, and MQTT-driven control logic, show measurable energy savings across multiple test cases. Inside the ORAN 5G setup, when comparing 100 MHz vs 20 MHz operation or evaluating energy balancing strategies, the UC5 results confirm that intelligent metering and adaptive RAN control produce noticeable energy efficiency gains and energy savings. E2E-demo-controller trials confirmed that remarkable energy efficiency improvements can be achieved.

6.2.4 Affordable and clean Energy

This KVI relates to the ability of the UC5 framework to lower operational costs and promote the use of renewable energy. KVI is derived from cost counter day-ahead market pricing for electricity (hourly ELSPOT API), solar production forecasts (FMI + PVlib), and cost computation models, showing that the system can utilize the estimates and minimize energy expenses by shifting operations when renewable availability is high or electricity cost is low. Integrating solar generation and forecast APIs further reduces reliance on fossil-fuel-based electricity.

6.2.5 Measurement accuracy

It quantifies the level of precision achieved in measuring the E2E energy measurement framework, expressed as a percentage of accuracy. Root Mean Squared Error (RMSE) and Mean Squared Error (MSE) are commonly used metrics to quantify the accuracy of measurement models. The evaluated ML/DL algorithms can minimize these error metrics, ensuring higher accuracy in energy measurements within the E2E framework. These metrics were calculated and yield less than 8 percent of RMSE in LSTM models when trained over the collected PV yield at UOULU rooftop for the last 3 years since the beginning of the 6G-XR project in 2023.

6.2.6 Carbon Cut

It assesses the reduction in grid intake linked to CO2 emissions by using the CO2 counter. The CO2 saving achieved through the use case, promoting a more sustainable and environmentally friendly energy system when applying it to different power saving modes. This KVI is mapped to a KPI that accounts for the use of carbon dioxide (CO2) emissions produced because of energy consumption, based on indirect emissions estimates from TSO. KPI results quantify indirect CO_2 emissions by multiplying energy consumption or grid intake measurements with TSO-provided hourly specific CO_2 emission factors (gCO2/consumed kWh in Finland).

7 VALIDATION METHODOLOGY AND KPI ASSESSMENTS FOR TRIAL RUNS

To validate and achieve the objectives of the UC5, the trial runs and experiments were conducted based on the functional and non-functional requirements and the KPIs defined in [17]. The results highlight the effectiveness of the deployed energy measurement framework in enabling research and development work aiming to gain energy savings and sustainability improvements. The tests are carried out at UOULU and VTT sites under controlled scenarios to analyze and perform validation activities, and specific test cases were designed to align with KPI metrics. The collected data sets were obtained from the deployed energy measurement framework at both North Node sites. The data sets used for analysis were collected from real-time measurements, and checkpoint IDs in the defined test cases were used to evaluate the output of each test case. The approach ensures the evaluation is directly connected to the requirements, KPIs, KVIs, and the corresponding measurement data and logs.

7.1 TESTING FRAMEWORK AND SETUP

The testing framework uses a structured template, included in Annex 1, which is applied throughout the 6G-XR project for each planned test case. This ensures consistency and order in the testing process, as well as systematic recording of the obtained results with the appropriate data presentation. The North Node UOULU and VTT perform the validation and KPI assessment based on real-time datasets collected throughout the 6G-XR project. The final validations were performed using the data values from real-time PV yield, Energy weather forecasts for the next 66 hours ahead, ELSPOT day-ahead electricity pricing, FINGRID grid-linked CO2 estimates, and power consumption values of the entire network components. These gathered values contain data sets for more than two years, but in the validation process, the week 20 of 2025 (May 12- May 18) was used to perform the KPI assessments. The Excel sheet used for the validation activities is also included in Annex 2.

7.2 TEST ENVIRONMENT

To evaluate the sustainability experimentation framework, a dedicated testing setup at both North Node sites has been designed to ensure that all the KPI metrics can be accurately collected. The energy measurement framework enables the real-time measurements of the entire network components at both sites, and a bridge broker enables the data exchange as well. This extraction of real-time values and to capture of the necessary data metrics using multiple sets of tools and measurement methods. This approach ensures that the collected datasets are generated using real-time PV production, forecasting, storing, and consumption processes, accurately reflecting the actual behavior of the system when users are interacting under realistic operating conditions.

7.2.1 UOULU site

UOULU 5GTN lab (as shown in Figure 76) and related components:

- OAIBOX MAX: ORAN 5G environment.
- USRP radios N310, B210.
- Solar Panels: 24 PV modules located on the rooftop of OULU, with 12 vertically mounted and 12 mounted horizontally.
- 5G Quectel RM500Q-GL modems.

- 5G Core Network: The core functions for the 5G network are provided by ORAN 5GC.
- Laptop for connection with UE and generating iPerf traffic.
- Netiopowerbox as external meter, MQTT enabled.
- FMI, ELSPOT, and FINGRID as forecasting APIs.
- Central controller: Server Nokia OpenEdge blade

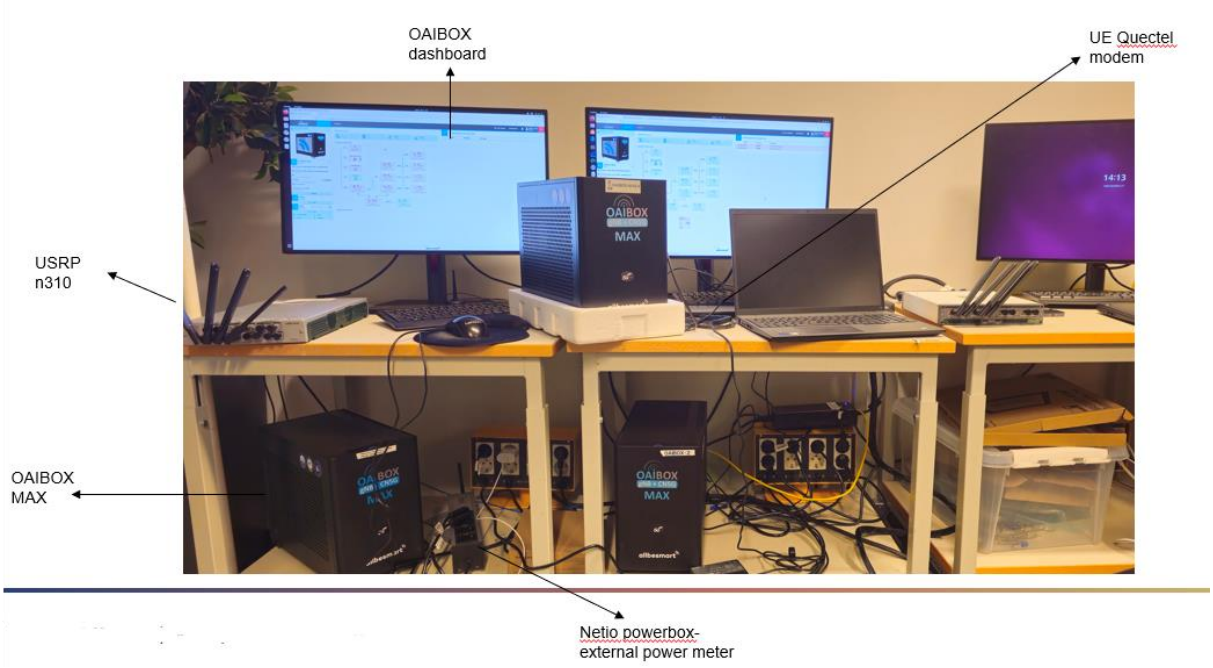

Figure 76: UOULU Lab setup of OAIBOX MAX, USRPs, Modems and Netio powerbox as external meter

7.2.2 VTT site

The following components are integrated or simulated with the E2E implementation running at the VTT B5G lab:

- Solar panels (8 vertically mounted wall PV-modules, which were utilized as a data source for scalable virtual PV-yield used in simulations). In the end, UOulu's data and PV yield prognoses were utilized in validation trials.
- System efficiencies from LiFePO4 battery energy storage and Victron Energy's Multiplus-II inverter/charger's efficiency estimates for energy conversions.
- Open5GS core and commercial carrier-grade 5G RAN with two outdoor macro cells, n7 FDD and n78 mMIMO TDD
- 3 UEs with associated Ubuntu 22.04 laptops as video clients, see Figure 77
- Video (edge) content server

- KPI collectors
    - InfluxDB2
    - Grafana, see Figure 77
- Network performance
    - Qosium
- Power monitoring devices
    - Carlo Gavazzi's transducers and electricity meters
    - Otii ACE, see Figure 77
- + various SW peripherals
    - PTPd time synchronization
    - MQTT broker
    - Central, RAN, application, and EA-guide controllers

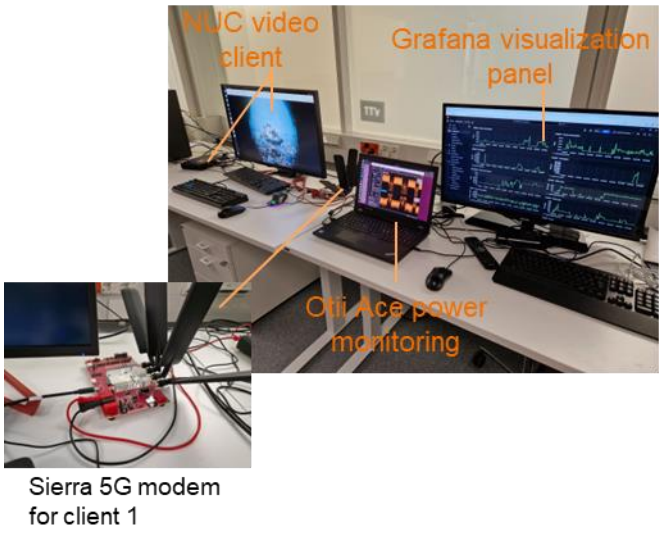

Figure 77: Snapshot of VTT lab setup for the validation tests.

7.3 TEST CASE SPECIFICATION AND VALIDATION AT UOULU SITE

Validation Objective	Test Case	Test ID
Functional Requirements	The overall energy consumption data of the radio access and core network systems shall be sent to a central database by the external meters	UC5.FR2
KPI Metrics	Active energy counter KPI validation: Test Case	UC5. KPI1
	Cost Counter KPI Validation Test Case	UC5. KPI2
	CO2 counter KPI validation Test Case	UC5. KPI3
	Energy saving Counter KPI validation Test Case	UC5. KPI4

7.3.1 Active energy counter and Energy saving counter KPIs validation test case

UOULU	Active energy counter and Energy saving counter KPIs Validation Test Case
Test Case Name	Active energy counter KPI and Test case validation (UC5. KPI1) and UC5.FR2 Energy saving Counter KPI validation Test Case (UC5. KPI4)
Test Case Objectives	Measure the real-time energy monitoring of individual network components, including OAIBOX gNB+Core, USRP n310, and Quectel modem UE (1/s sampling rate), and send to a central database by the external meters. Compute the total energy saved between the OAIBOX gNB RAN using 100MHz and 20MHz based on the collected datasets by the external meters.
Test Case Category	KPI Measurements and functional requirements
Test Environment	5GTN Laboratory UOULU
Test Deployment Setup	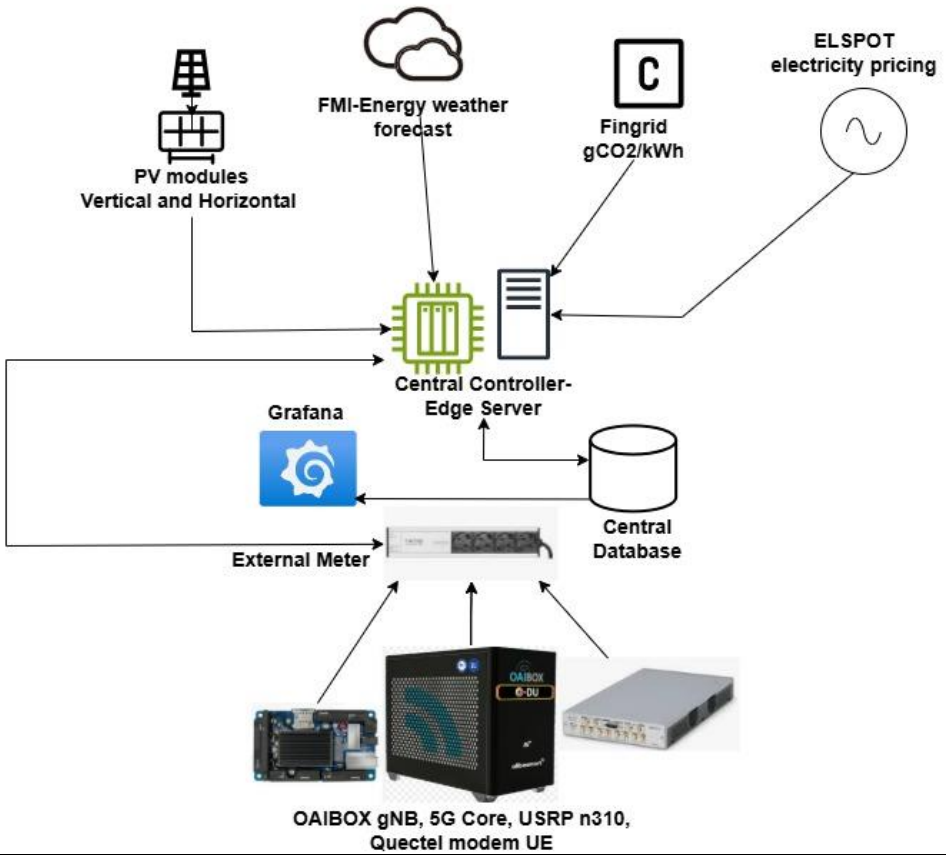

Network Setup	**RAN:**	OAIBOX MAX gNB	**5G Core:**	OAIBOX 5GC- 5G Core Network	**Edge:**	Nokia OpenEdge Blade Server	**Band:** 3.9 - 4.0GHz **Bandwidth:** 100MHz-20MHZ
Test Configuration	**Components Under Test:**	OAIBOX MAX gNB stack, 5GC Core, Radio Unit (USRP n310), UE (Quectel Modem)	**Test Software:**	Mosquitto MQTT broker MySQL Grafana iPerf3	**Test Devices:**	Laptop for UE Quectel Modem Connectivity Edge server for MQTT broker External meter as Netio Powerbox4K	**Testing Payload Data:** TCP and UDP Data streams

Initial Conditions/Prerequisites

1. The energy measurement framework is operational with all of its components running.
2. Central database MySQL is deployed along with the central controller for collecting real-time datasets.
3. The external meter power (Netiopowerbox 4KF) sockets are connected to individual components of the OAIBOX MAX setup.
4. The MQTT broker is running on the edge server as a central controller where the real-time energy monitoring is captured for each module in the OAIBOX setup and stored in the central database.
5. Quectel Modem is used as UE for UDP data traffic with iPerf3 installed on both OAIBOX (server) and the laptop (client) to generate and measure bidirectional UDP traffic between the UE and the 5G core.
6. OAIBOX is able to change the RAN configuration from the dashboard. (bandwidth, MIMO, TDD slots, and MCS).

Test scenario

The purpose of the test is to perform KPI validation and test case validation for active energy counters and energy saving modes of the OAIBOX using a combination of RAN configurations. It also validates the functional requirement of enabling the external meters to store datasets into the central database. The external meter allows real-time monitoring of each network component for the ORAN 5G private network, including gNB, 5G Core, RU, and UEs, and stores each module as a separate dataset with a one-second sampling frequency. Test steps are as follows: 1. Starting energy measurement framework deployed at the central controller, which enables real-time power consumption data from each network component and saves it in a central database automatically. 2. A Quectel modem with a SIM card is used as the UE to connect to the OAIBOX and establish communication with the ORAN 5G network. 3. MQTT broker configured at the central controller enables external meter NETIOPOWERBOX 4KF to publish real-time power consumption data from each socket with individual network components, including ORAN 5G OAIBOX gNB and 5G Core, USRP n310, and UE Quectel Modem. 4. UDP traffic is generated using iPerf3 between the UE (client) and the OAIBOX (server) under varying RAN parameter configurations on the gNB to evaluate performance KPIs (energy saving KPI). 5. The central controller allows real-time E2E network energy consumption data to be visualized using Grafana.
Test variables
1. OAIBOX RAN configurations are being tested for energy profiling. 2. The power consumption profile of each network component is measured once per second
Expected behavior/Target Values
1. iPerf3 traffic was generated using a Quectel Modem as UE over the ORAN 5G network. 2. The number of connected users is 1, and the distance is about 10m to the RU. 3. The energy efficiency of the OAIBOX is evaluated during both idle and active energy counter with traffic 4. All the measurements collected via the central controller have been successfully collected in the central database.

UOULU	**Active energy counter and Energy saving counter KPIs Validation Test Case**
Test Case Name	Active energy counter and Energy saving counter KPIs and Test case validation (UC5. KPI1) and UC5.FR2
Test Execution Date	29/10/2025
Test Executed By	UOULU
Number of repetitions	1
Test's comments	Tests were performed physically in the 5GTN laboratory using a fully operational ORAN 5G private network featuring OAIBOX MAX, USRP n310, and a Quectel modem as the UE connected via a laptop. Due to connectivity and network

	instability issues between the UE and OAIBOX, continuous power consumption data collection for each network component was limited to one hour.

Verification Points (VP)			
Checkpoint ID	**Description of Validation Criteria for the checkpoint**		
ID #1	The external meter successfully transmits power consumption data for individual network components separately to the central controller (edge server) via the MQTT protocol, using port forwarding configured on the Wi-Fi router to enable remote data exchange with the VTT site.		
ID #2	Successful transmission and logging of real-time power consumption data from the OAIBOX gNB, 5GC Core, USRP N310, and Quectel Modem (UE) to the central database for one hour with an interval rate of one sample per second.		
ID #3	Successful fetching of datasets from the central database to the Grafana dashboard for live visualization.		
ID #4	iPerf3 is configured to generate maximum UDP traffic for performance and KPI evaluation		
ID #5	Successful execution of multiple RAN configuration scenarios for KPI validation		
ID #6	Network logs generated during the experimentation trial.		
Test Validation Conditions	Tests were performed with the energy measurement framework central controller, and all checkpoints for each component's validation were checked.		
Test results	**Test run**	**Description**	**Result**
ID #1	1	Mosquitto MQTT broker successfully deployed on the central controller and configured to allow data exchange between the North Node sites.	Pass
ID #2	1	Figure 78, Figure 79	Pass
ID #3	1	Figure 78, Figure 79	Pass
ID #4	1	iPerf3 generated, Figure 80, Figure 81	Pass
ID #5	1	RAN configuration 100MHz, TDD 5D x 4U 5ms, 2x2, MCS adaptive 2025-10-28 12:15:59: 13:14:00 RAN configuration 20MHz, TDD 5D x 4U 5ms, 1x1, MCS adaptive timestamp: 2025-10-29 12:24:16: 13:24:42	Pass Pass
ID #6	1	Figure 80, Figure 81	Pass

Figure 78 represents the real-time power consumption data recorded separately for each network component: the OAIBOX gNB+5GC Core (yellow), USRP n310 (green), and Quectel modem as UE (light blue). Power consumption values for each component were sampled once per second in watts, and each dataset is combined (orange) to illustrate the total power consumption over one hour for the 100 MHz RAN configuration with 2×2 MIMO. For this setup, the average total power consumption during the one-hour test run was approximately 200 W, as shown in Figure 78. Similarly, Figure 79 shows the average power consumption data for the 20MHz RAN configuration with SISO 1x1, which measured 169 W for a one-hour test run. In this setup, the USRPN310 power consumption decreased from 47.1 W to 43.8 W, and UE's power consumption also dropped from 1.97W to 1.33 W. The major difference was recorded in OIABOX gNB+Core, where the power consumption decreased from 151 W to 124 W. This leads to more than 15% in total energy saving when the RAN parameters are changed from 100MHz to 20MHz and antenna selection from MIMO 2x2 to SISO 1x1.

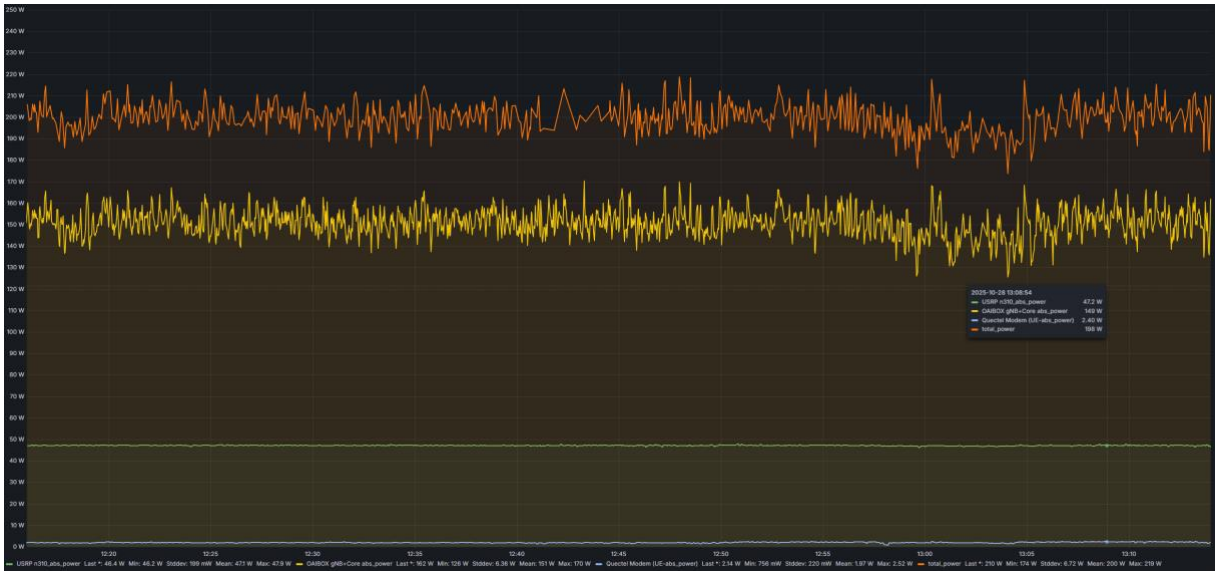

Figure 78: Active energy counter maximum power ORAN setup, OAIBOX MAX; USRP N310, Quectel Modem 100MHZ MIMO 2x2

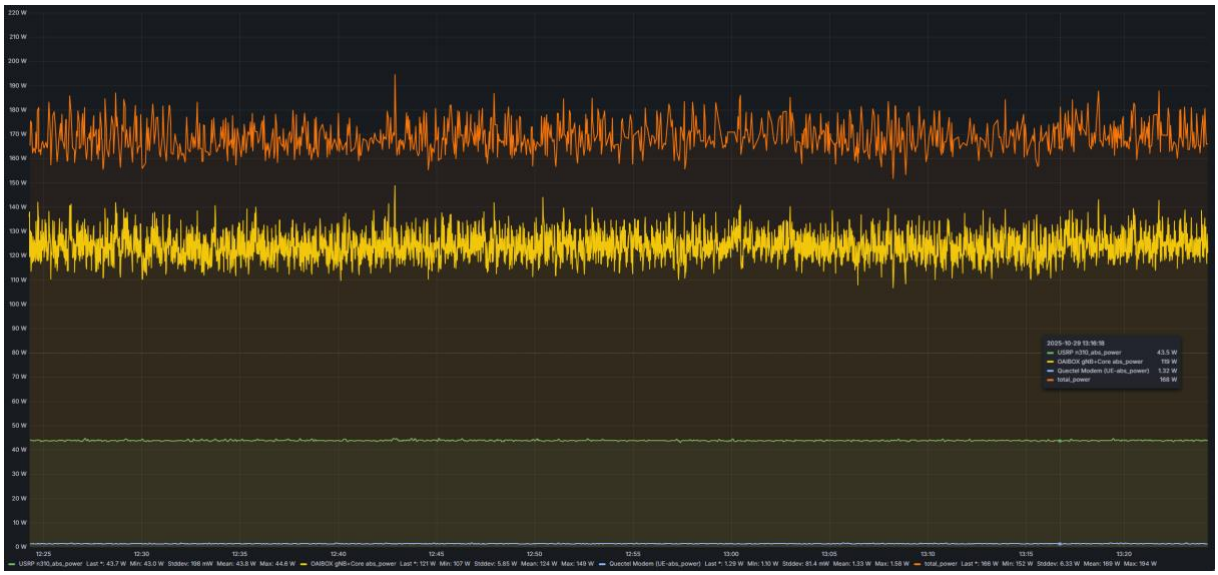

Figure 79: : Active energy counter maximum power ORAN setup, OAIBOX MAX; USRP N310, Quectel Modem 20MHZ SISO 1x1

The network logs were also collected for both power modes to correlate the relationship between power consumption and network performance. Figure 81 shows graphs and logs of the RAN configuration setup of 100MHz bandwidth, which produces the downlink bitrate of more than 500 Mbps during the one-hour test period. The increase in the bitrate correlates with higher power consumption. The adaptive MCS behavior indicates that the connection experienced instability, with MCS values fluctuating significantly, as shown on the right side of Figure 80. Meanwhile, for the RAN configuration setup of 20MHz bandwidth (power saving mode) with active antenna selection of SISO 1x1, the maximum bitrate achieved was 22.2 Mbps, but the MCS remained stable at 27. The gNB logs also show that BLER for the 20MHz SISO configuration was about 0.2% and for the 100MHz configuration was about 3.9% average. The rest of the network logs, compared to both configuration setups, seem to be almost the same.

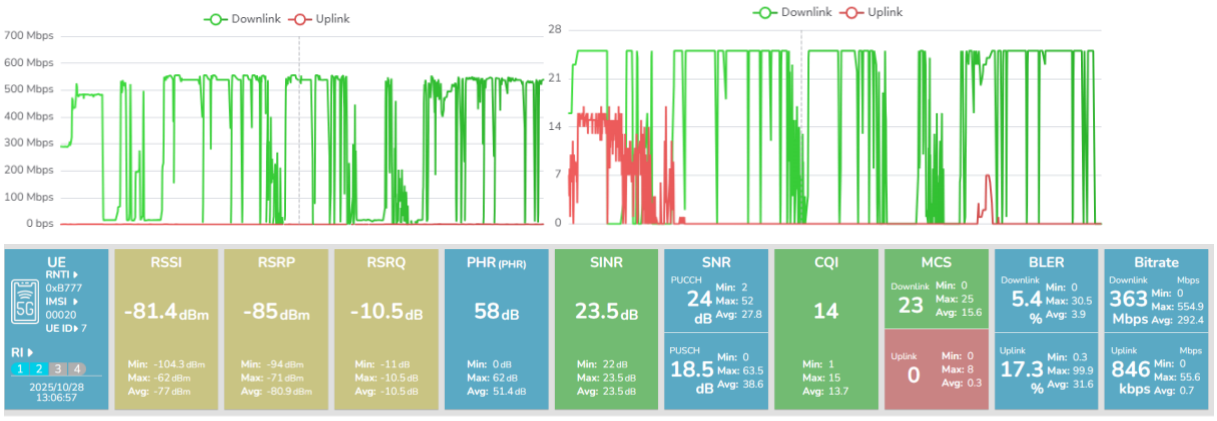

Figure 80: Network logs for 100 MHz MIMO 2x2, UDP iPerf3 traffic with USRP N310(one hour test run)

Figure 81: Network logs for 20 MHz SISO 1x1, UDP iPerf3 traffic with USRP N310(one hour test run)

The energy saving counter produced 15.4% of energy savings when the two RAN configuration setups (full power and power saving mode) energy consumption data were aggregated for the selected validation week (May 12 until May 18, 2025, Annex 2) as shown left side of Figure 82. The energy savings demonstrate promising results, with the two power modes reducing consumption by over 5 kWh during seven days. The first graph on the left shows the total energy consumption for the entire week under the two different power modes, yielding 33.76 kWh and 28.55 kWh, respectively. These results can be combined with the energy weather forecast to predict energy availability for the next two days. The graph on the right in Figure 82 illustrates which power mode should be used based on the 48 hours ahead energy weather forecast, along with ELSPOT pricing, enabling energy-efficient network operation, but at the cost of network performance.

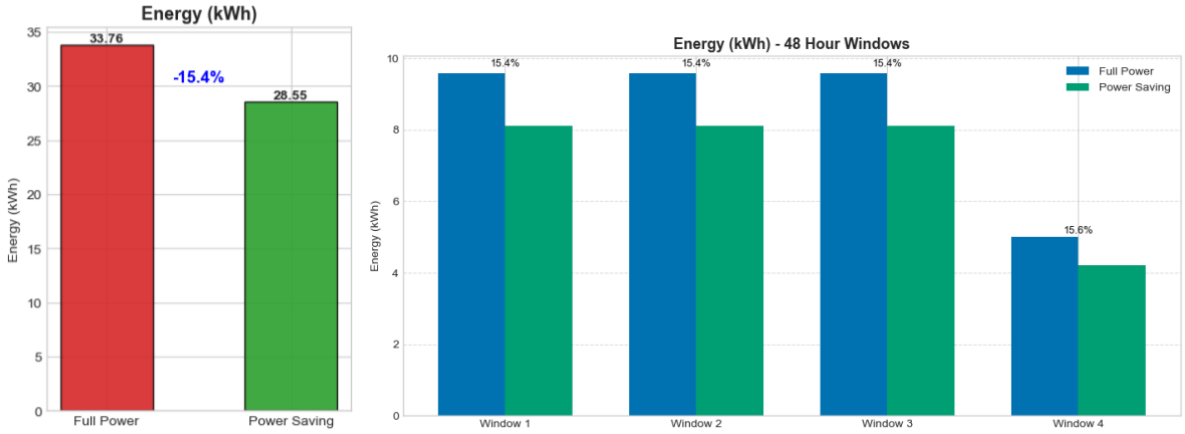

Figure 82: one week energy saving, cost and CO2 counter based on active energy counter

7.3.2 COST COUNTER KPI VALIDATION TEST CASE

UOULU	Cost Counter KPI Validation Test Case
Test Case Name	Cost Counter KPI and Test case validation (UC5. KPI2)
Test Case Objective	Calculate and log the real-time cost associated with the total energy consumption of the entire 5G ORAN testbed, including OAIBOX gNB+Core, USRP n310, and Quectel modem UE (1/s sampling rate), and produce a 24 hour ahead cost forecast.
Test Case Category	KPI Measurements
Test Environment	5GTN Laboratory
Test Deployment Setup	

<table>
<tr><td></td><td colspan="7"> 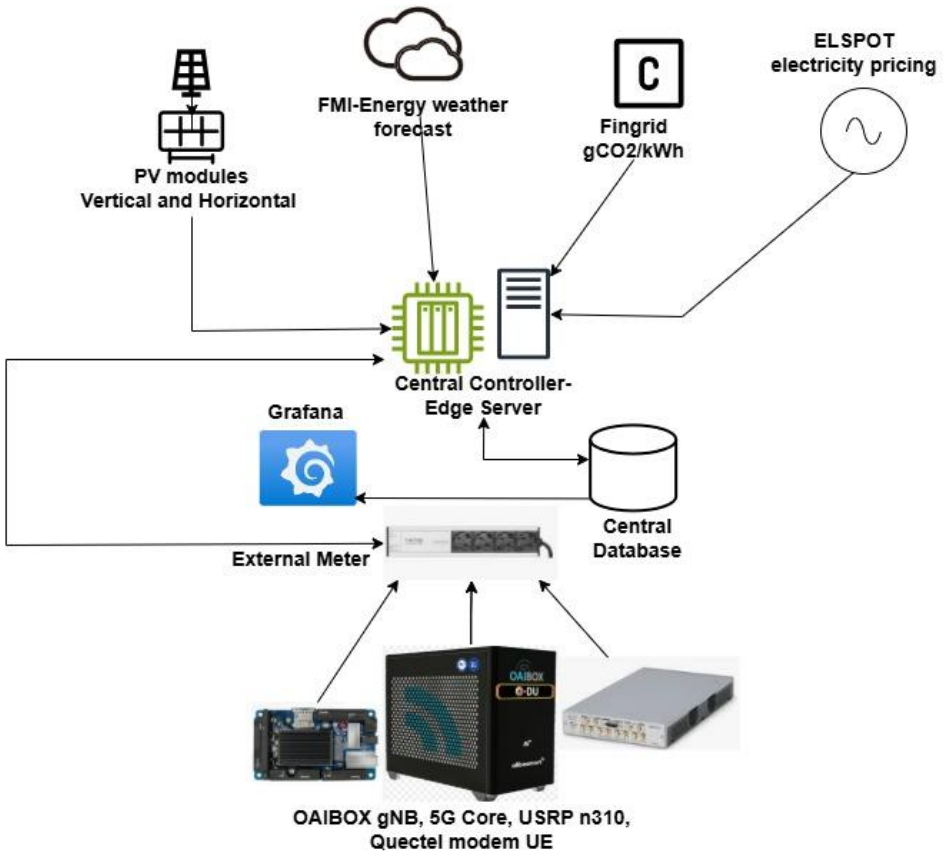
</td></tr>
<tr><td>Network Setup</td><td>RAN:</td><td>OAIBOX MAX gNB</td><td>5G Core:</td><td>OAIBOX 5GC- 5G Core Network</td><td>Edge:</td><td>Nokia OpenEdge Blade Server</td><td>Band: 3.9 - 4.0GHz Bandwidth: 100MHz-20MHZ</td></tr>
<tr><td>Test Configuration</td><td>Components Under Test:</td><td>OAIBOX MAX gNB stack, 5GC Core, Radio Unit (USRP n310), UE (Quectel Modem)</td><td>Test Software:</td><td>Mosquitto MQTT broker MySQL Grafana iPerf3 ELSPOT pricing API for the day head market</td><td>Test Devices:</td><td>Laptop for UE Quectel Modem Connectivity Edge server for the MQTT broker External meter as Netio Powerbox 4k</td><td>Testing Payload Data: TCP and UDP Data streams</td></tr>
<tr><td colspan="8">Initial Conditions/Prerequisites</td></tr>
</table>

The central controller fetches the API every day at 2 PM EET from the third-party ELSPOT pricing for a day-ahead market. The collected data is stored in the central database.
Test scenario
The test is performed using real-time power consumption values from the OAIBOX gNB, Core, RU, and UE, and these values are multiplied by the electricity cost for that hour. In this way, the next-day cost linked to the OAIBOX full-power mode and power saving mode is calculated using different RAN configurations. Test steps are as follows: 1. Request the API from ELSPOT to fetch day ahead electricity pricing. 2. MQTT broker configured at the central controller: External meter NETIOPOWERBOX 4KF real-time power consumption data from each socket with an individual network component. 3. Central controller converts the cost from MWh to kWh and then performs the cost counter on 100 MHz and 20MHz bandwidth with MIMO and SISO 4. For full power mode: df['Cost_full_euro'] = df['E_full_kWh'] * (df['Price_Euro_per_MWh'] / 1000) 5. For power saving mode: df['Cost_saving_euro'] = df['E_saving_kWh'] * (df['Price_Euro_per_MWh'] / 1000) 6. The energy used in kWh is multiplied by the cost of electricity pricing of that hour and then combined for the daily and 48 hour accumulated cost counter.
Test variables
1. OAIBOX RAN configuration 100MHz = full power and 20MHz = power saving mode 2. The power consumption profile of each network component is measured once per second and then aggregated to produce energy data hourly in kWh. 3. ELSPOT hourly pricing is first converted into kWh (€/kWh) from MWh (€/MWh) and then multiplied by the hourly energy consumption data.
Expected behavior/Target Values
1. iPerf3 traffic was generated using a Quectel Modem as UE over the ORAN 5G network. 2. The number of connected users is 1, and the distance is about 10m to the RU. 3. The energy efficiency of the OAIBOX is evaluated during both full power and power saving mode with traffic. 4. All the measurements collected via the central controller have been successfully collected in the central database.

UOULU	**Cost Counter KPI Validation Test Case**
Test Case Name	Cost Counter KPI and Test case validation (UC5. KPI2)
Test Execution Date	29/10/2025
Test Executed By	UOULU
Number of repetitions	1

Test's comments	Tests were performed physically in the 5GTN laboratory with a fully ORAN 5G private network using OAIBOX MAX, USRP n310, and Quectel modem as UE with a laptop and edge server requesting access to the third-party ELSPOT pricing API.		
Verification Points (VP)			
Checkpoint ID	**Description of Validation Criteria for the checkpoint**		
ID #1	Successful transmission and logging of real-time power consumption data from the OAIBOX gNB, 5GC Core, USRP N310, and Quectel Modem (UE) to the central database.		
ID #2	Successful API request and logging of day ahead electricity pricing market from ELSPOT into the central database.		
ID #3	The central controller successfully converts all measurements into a unified unit and uses them to calculate the energy cost associated with different RAN configurations, including full-power and power-saving modes		
ID #4	The central controller successfully automates the daily request to the cost counter API at 2pm EET.		
ID #5	Two methods for validation. One day ahead and 48 hours ahead.		
Test Validation Conditions	Tests were performed with the energy measurement framework central controller, and all checkpoints for each component's validation were checked.		
Test results	**Test run**	**Description**	**Result**
ID #1	1	Mosquitto MQTT broker successfully deployed on the central controller and configured to allow data exchange between the North Node sites.	Pass
ID #2	1	API was successfully requested	Pass
ID #3	1	ELSPOT pricing for RAN configuration 100MHz, TDD 5D x 4U 5ms, 2x2, MCS adaptive 2025-10-28 12:15:59: 13:14:00 ELSPOT pricing for RAN configuration 40MHz, TDD 5D x 4U 5ms, 1x1, MCS adaptive timestamp: 2025-10-29 12:24:16: 13:24:42 Figure 83, Figure 84	Pass
ID #4	1	Using the request library and background job in Linux: nohup /bin/python3 /home/hamid/ELSPOTrequests.py > /home/hamid/ELSPOTrequests.log 2>&1 &	Pass
ID #5	1	Figure 83, Figure 84	Pass

Figure 83 provides the daily accumulated comparison of two power modes of the ORAN system configured with two RAN configurations. The orange bars represent the full power mode with 100MHz bandwidth and MIMO 2x2, while the blue bars represent the power saving mode in which bandwidth is decreased to 20MHz and SISO 1x1. The daily comparisons were calculated for the validation week (May 12 until May 18, 2025, Annex 2). These daily values highlight which configuration is optimal for each day based on day-ahead electricity market prices. On days of negative electricity pricing, using full-power mode is advantageous, whereas on other days, the power-saving mode reduces overall energy costs. Similarly, Figure 84 shows the 48-hour window of the Cost counter for the two energy modes of the OAIBOX ORAN setup.

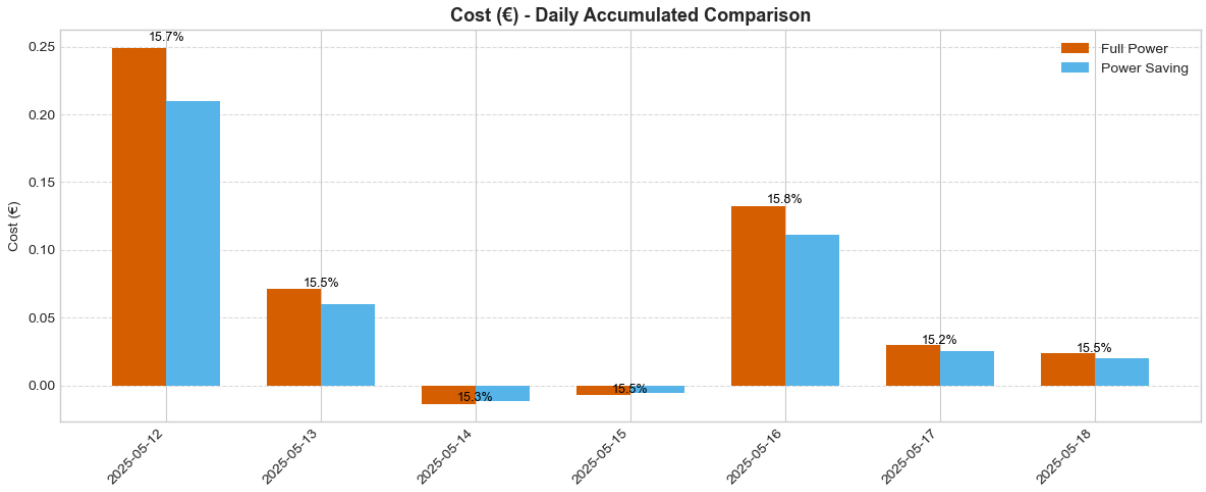

Figure 83: Daily Cost counter for two energy modes of OAIBOX ORAN setup

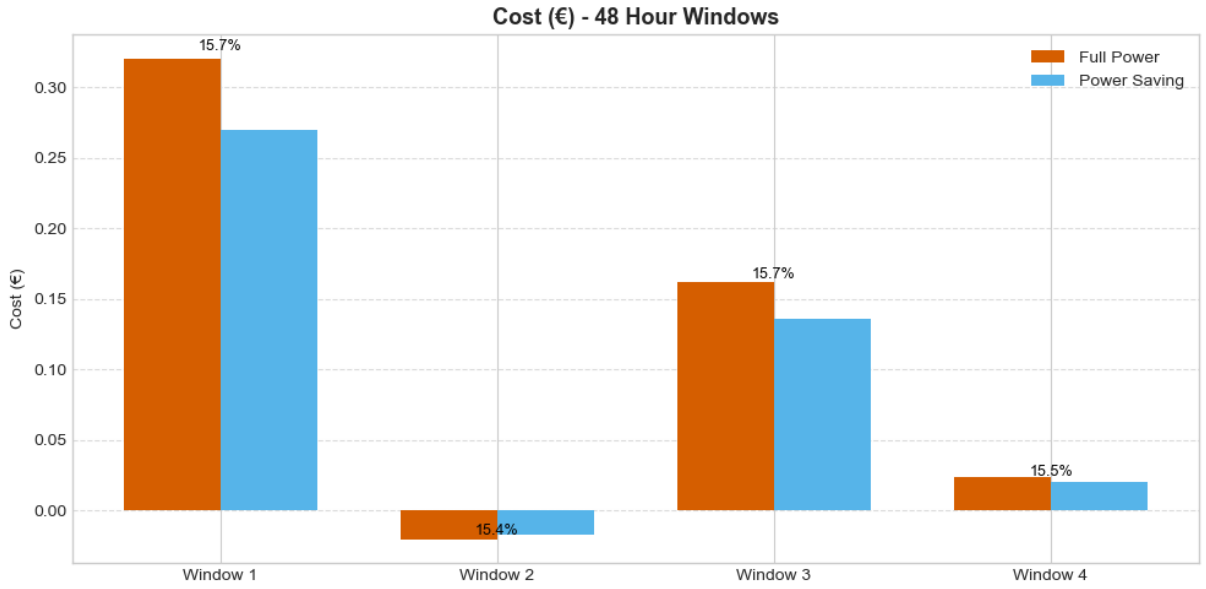

Figure 84: 48-hour window of the Cost counter for the two energy modes of the OAIBOX ORAN setup

7.3.3 CO2 COUNTER KPI VALIDATION TEST CASE

UOULU	CO2 COUNTER KPI VALIDATION TEST CASE
Test Case Name	CO2 Counter KPI and Test case validation (UC5. KPI3)
Test Case Objective	Calculate and log the FINGRID's estimate for gCO2 for consumed kWh associated to the total energy consumption of the entire 5G ORAN testbed, including OAIBOX gNB+Core, USRP n310, and Quectel modem UE (1/s sampling rate).
Test Case Category	KPI Measurements
Test Environment	5GTN Laboratory

<table>
<tr><td>Test Deployment Setup</td><td colspan="7"> 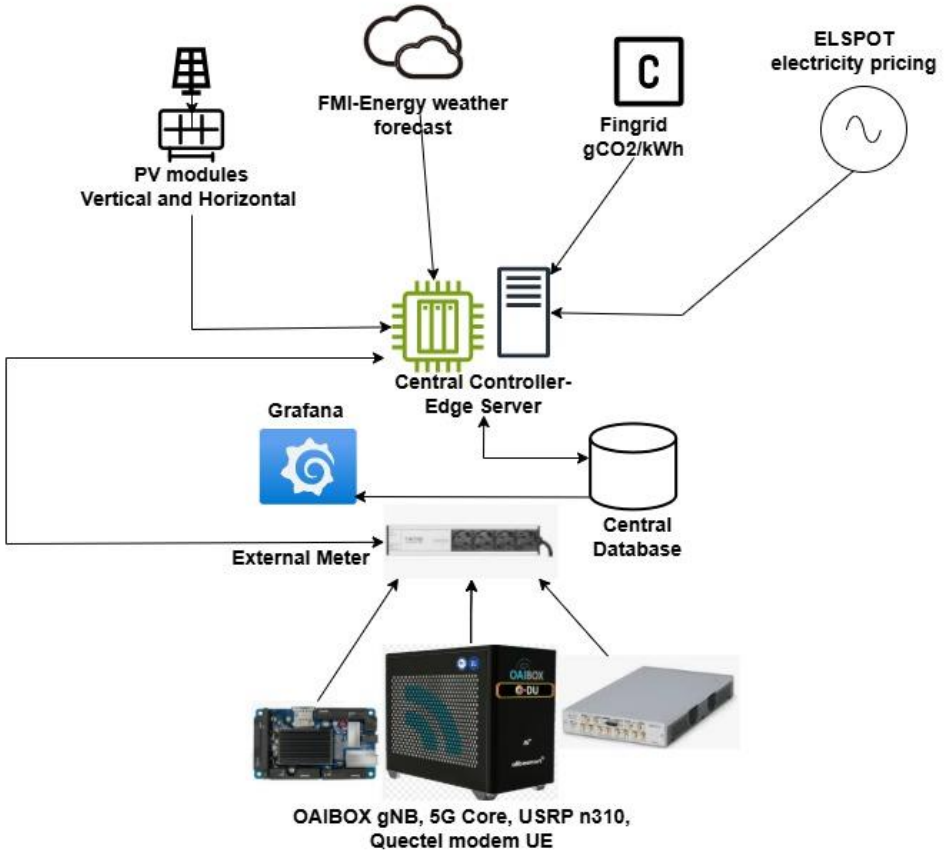
</td></tr>
<tr><td>Network Setup</td><td>RAN:</td><td>OAIBOX MAX gNB</td><td>5G Core:</td><td>OAIBOX 5GC- 5G Core Network</td><td>Edge:</td><td>Nokia OpenEdge Blade Server</td><td>Band: 3.9 - 4.0GHz Bandwidth: 100MHz-20MHZ</td></tr>
<tr><td>Test Configuration</td><td>Components Under Test:</td><td>OAIBOX MAX gNB stack, 5GC Core, Radio Unit (USRP n310), UE (Quectel Modem)</td><td>Test Software:</td><td>Mosquitto MQTT broker MySQL Grafana iPerf3 FINGRIDAPI for gCO2/kWh estimates</td><td>Test Devices:</td><td>Laptop for UE Quectel Modem Connectivity Edge server for the MQTT broker Netio Powerbox 4K</td><td>Testing Payload Data: TCP and UDP Data streams</td></tr>
</table>

Initial Conditions/Prerequisites
The central controller requests the automatic retrieval of the API every 3 minutes from the third-party FINGRID's estimate of gCO2/kWh of energy consumed. iPerf3 packages are present on both the laptop and the core to generate traffic from both ends. The central controller calculates real-time CO2 estimates, which are used for the daily CO2 counter.
Test scenario
The test is performed using real-time power consumption values from the OAIBOX gNB, Core, RU, and UE, and these values are multiplied by the FINGRID estimates to generate a cumulative emission counter for power intake from the grid. In this way, CO2 emissions linked to the OAIBOX full-power mode and power saving mode are calculated using different RAN configurations. Test steps are as follows: 1. Request the API from FINGRID to fetch 1/3 minutes of grid-linked CO2 estimates. 2. MQTT broker configured at the central controller: External meter NETIOPOWERBOX 4KF publishes real-time power consumption data from each socket with an individual network component. 3. Central controller converts the gCO2/kWh into an hourly aggregate and then performs the CO2 counter on 100 MHz and 20MHz bandwidth with MIMO and SISO. 4. For full power mode: df['CO2_full_g'] = df['E_full_kWh'] * df['CO2_g_per_kWh'] 5. For power saving mode: df['CO2_saving_g'] = df['E_saving_kWh'] * df['CO2_g_per_kWh'] 6. The energy used in kWh is multiplied by the CO2 estimate of grid-linked produced electricity aggregated for that hour and then combined for the daily accumulated CO2 counter.
Test variables
1. OAIBOX RAN configuration 100MHz = full power and 20MHz = power saving mode 2. The power consumption profile of each network component is measured once per second and then aggregated to produce energy hourly data in kWh. 3. FINGRID 1/3 minute CO2 emissions original data is first converted into aggregated hourly gCO2/kWh and then multiplied by the hourly energy consumption data.
Expected behavior/Target Values
1. iPerf3 traffic was generated using a Quectel Modem as UE over the ORAN 5G network. 2. The number of connected users is 1, and the distance is about 10m to the RU. 3. The energy efficiency of the OAIBOX is evaluated during both full power and power saving mode with traffic. 4. All the measurements collected via the central controller have been successfully collected in the central database.

UOULU	**CO2 Counter KPI Validation Test Case**
Test Case Name	CO2 Counter KPI and Test case validation (UC5. KPI3)
Test Execution Date	29/10/2025
Test Executed By	UOULU

Number of repetitions	1		
Test's comments	Tests were performed physically in the 5GTN laboratory with a fully ORAN 5G private network using OAIBOX MAX, USRP n310, and Quectel modem as UE with a laptop and edge server as central controller requesting access to third-party FINGRID for CO2 estimates API.		
Verification Points (VP)			
Checkpoint ID	**Description of Validation Criteria for the checkpoint**		
ID #1	Successful transmission and logging of real-time power consumption data from the OAIBOX gNB, 5GC Core, USRP N310, and Quectel Modem (UE) to the central database.		
ID #2	Successful API request and logging of real-time grid-linked CO2 estimates from FINGRID into the central database.		
ID #3	The central controller successfully converts all measurements into a unified unit and uses them to calculate the cumulative CO2 emission counter associated with different RAN configurations, including full-power and power-saving modes.		
ID #4	The central controller successfully automates the daily request to the CO2 counter API every 3 minutes.		
Test Validation Conditions	Tests were performed with the energy measurement framework central controller, and all checkpoints for each component's validation were checked.		
Test results	**Test run**	**Description**	**Result**
ID #1	1	Mosquitto MQTT broker successfully deployed on the central controller and configured to allow data exchange between the North Node sites.	Pass
ID #2	1	API was successfully requested	Pass
ID #3	1	RAN configuration 100MHz, TDD 5D x 4U 5ms, 2x2, MCS adaptive 2025-10-28 12:15:59: 13:14:00 RAN configuration 40MHz, TDD 5D x 4U 5ms, 1x1, MCS adaptive timestamp: 2025-10-29 12:24:16: 13:24:42 Figure 85	Pass
ID #4	1	Using the request library and background job in Linux: nohup /bin/python3 /home/hamid/Fingrid_Open_data.py > fingridoutput.log 2>&1 &	Pass

Figure 85 provides the daily accumulated comparison of CO2 associated with the two power modes of the ORAN system, configured with two RAN configurations. The purple bars represent the full power mode with 100MHz bandwidth and MIMO 2x2, while the green bars represent the power saving mode in which bandwidth is decreased to 20MHz with SISO 1x1. The daily comparisons were calculated for the validation week (May 12 until May 18, 2025, Annex 2). These daily values highlight the difference in CO2 emission between the two power modes, with variations ranging from 55 g to 72 g per day, illustrating how the choice of RAN configuration directly impacts the system's carbon footprint.

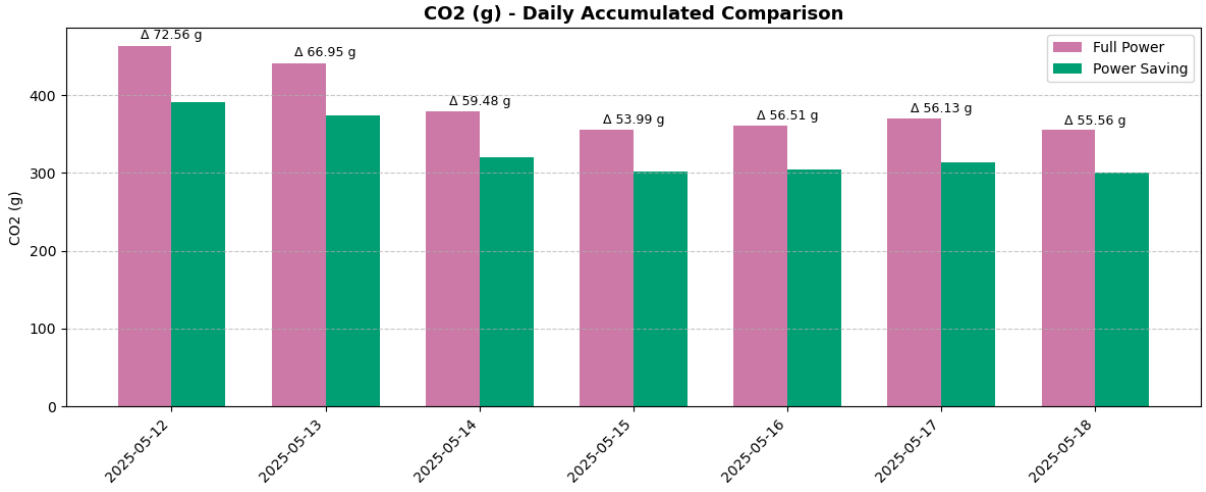

Figure 85: Daily cumulative CO2 counter associated with ORAN energy consumption modes.

7.4 TEST CASE SPECIFICATION AND VALIDATION AT THE VTT SITE

Validation Objective	Test Case	Test ID
Functional Requirements	The overall energy consumption data of the radio access and core network systems shall be sent to a central database by the external meters	UC5.BL, UC5.AD
Functional Requirements	The radio access and core network systems shall be able to change their operational parameters on the fly based on control commands received from a central network resource management entity.	UC5.AD
KPI Metrics	Active energy counter, total energy consumption	UC5.BL, UC5.AD
	Cost counter, OPEX from electricity	UC5.BL, UC5.AD
	CO2 counter, CO2 emissions due to grid energy usage	UC5.BL, UC5.AD
	Energy savings	UC5.AD
	Self-sufficiency proportion	UC5.AD
	Energy efficiency, total transmitted application bits per total energy consumption	UC5.BL, UC5.AD
	Video watching experience, percentage of video clip downloads with near-zero cache (visible as stalling in the video)	UC5.BL, UC5.AD

The purpose of the validation tests at the VTT site is to show the gains in main KPIs (energy savings, cost counter, and CO2 counter) that a private operator could achieve by dynamic E2E control of the energy storage, RAN, and video streaming application. Two long test cases, baseline and adaptive, are executed, and their results are compared for the gain analysis. The baseline case corresponds to the starting point of the 6G-XR project, where RAN was maximized for capacity, the resolution for the video users is maximized, and no green energy production or storage is integrated. In the adaptive case, the E2E optimization framework described in Section 5.3 is taken into use and validated.

It is assumed that users want to download and watch 1-minute video clips at exponentially distributed random moments. The mean video session inter-arrival times follow an hourly pattern shown in Table 19. When the video resolution is kept fixed as in the baseline case, the hourly traffic pattern from video clips follows the one shown in Figure 21.

Table 19: Mean video session inter-arrival times.

Hour	0	1	2	3	4	5	6	7	8	9	10	11	12	13	14	15	16	17	18	19	20	21	22	23
Mean inter-arrival time (s)	47	92	207	296	473	473	296	207	118	73	69	47	47	37	29	29	29	22	16	11	6.7	6.7	11	22

In order to make a fair comparison between the baseline and adaptive cases, we need to use the external data (electricity price and CO2 emission factor) and solar energy yield from the same days for both cases. The test cases were executed in October-November, while the external data and solar yield were taken from the same week 20 as in Section 7.3.

7.4.1 Baseline test case

<table>
<tr><th>VTT</th><th colspan="7">E2E application and 5G RAN optimization based on green energy availability</th></tr>
<tr><td>Test Case Name</td><td colspan="7">Baseline (UC5.BL)</td></tr>
<tr><td>Test Case Objective</td><td colspan="7">To get a baseline for KPI metrics without any green energy production, RAN adaptation or video quality adaptation.</td></tr>
<tr><td>Test Case Category</td><td colspan="7">KPI Measurements</td></tr>
<tr><td>Test Environment</td><td colspan="7">The test was executed at the VTT laboratory over a self-operated 5G SA network.</td></tr>
<tr><td>Test Deployment Setup</td><td colspan="7"> 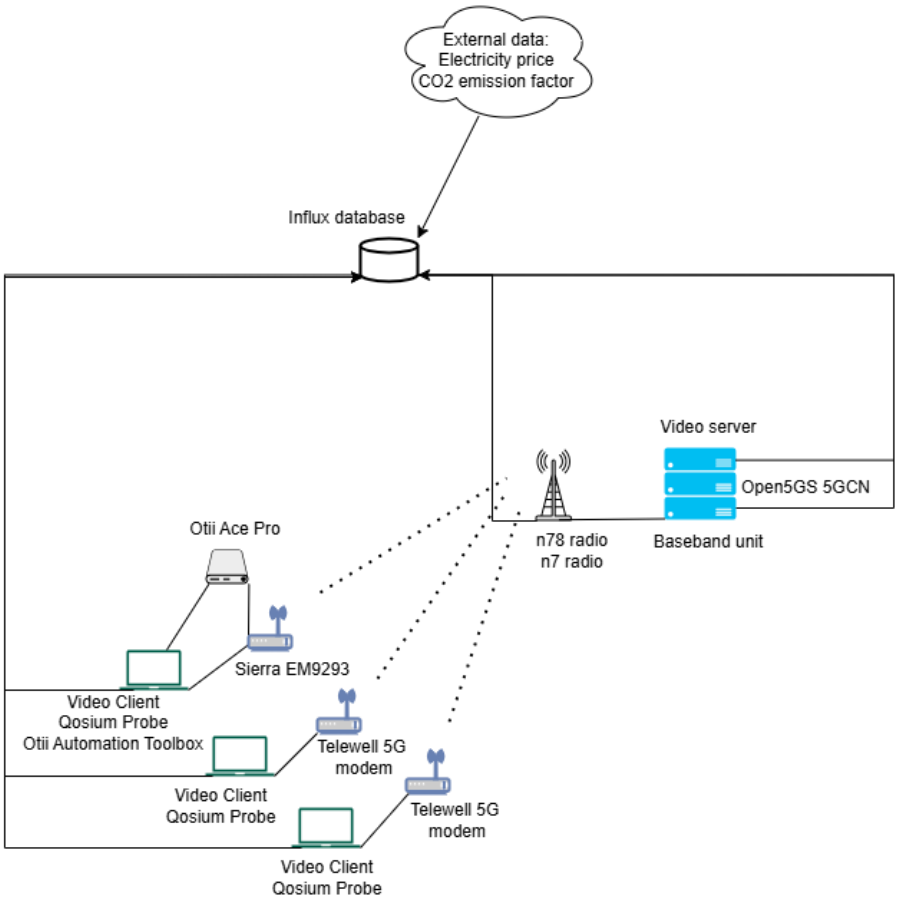
</td></tr>
<tr><td>Network Setup</td><td>RAN:</td><td>Commercial carrier-grade: n78 mMIMO radio, n7 macro radio</td><td>5G Core:</td><td>Open5GS</td><td>Edge:</td><td>Video server</td><td>Band: n78 and n7 Bandwidth: 60MHz and 10MHz</td></tr>
<tr><td>Test Configuration</td><td>Components Under Test:</td><td>Nginx web server (VoD service), gNB baseband unit, n78 mMIMO radio, n7 macro radio, Sierra EM9293 5G module,</td><td>Test Software:</td><td>Qosium, Otii 3, Otii Automation Toolbox, mpv</td><td>Test Devices:</td><td>Carlo Gavazzi energy meters, Otii Ace Pro</td><td>Testing Payload Data: H264-encoded 60 s video clips</td></tr>
</table>

		Telewell 5G modem, Intel NUC mini-PC					over DASH

Initial Conditions/Prerequisites

1. External data, including hourly electricity price and CO_2 emission factors, are available for the selected period of time.
2. InfluxDB for collecting the results is up and running.
3. Nginx web server for VoD service is up and running.
4. 5G RAN is operational. Both the n7 coverage and n78 capacity cell are active with no energy saving features enabled.
5. Carlo Gavazzi measurements for all the components (video server, baseband, radios, video client) are operational, and the results are collected in the database.
6. All 5G UEs are connected to the higher priority capacity cell. Only data traffic from the video server is routed through the 5G interface. All other traffic related to measurements, such as measurement forwarding to InfluxDB and time synchronization, is routed over the Ethernet interface.
7. Otii Ace measurements of Sierra EM9293 power consumption are running and forwarded to the database.
8. Qosium Probes are active at each video client and at the video server.
9. Qosium Scopes at the video clients forward the results to the QMCP listener, which in turn forwards them to InfluxDB.
10. Pre-generated week-long video session schedule is available at each video client.

Test scenario

The purpose of this test is to get the baseline values for energy consumption, energy efficiency, OPEX from electricity, CO_2 emissions, and the number of video cache threshold violations when there is no integrated green energy production, no RAN energy saving features, and no video resolution adaptation. Because some factors affecting the performance, such as electricity price, change slowly on an hourly basis, a several-day-long test scenario is targeted.

1. Start the process at the video clients that trigger downloading the video clip according to the session schedule.
2. Energy consumption, data amount, and QoS parameters are collected automatically.
3. Test runs up to 7 days, but if the video clients request video download for at least 48 hours over the 5G network, the test is considered successful.
4. Result post-processing to form the baseline values for KPIs.

Test variables

- Video session inter-arrival times follow an exponential distribution such that the mean value changes according to the daily traffic profile (see Table 19)
- Radio channel conditions vary in time (although the UEs are stationary)
- Electricity price varies per hour
- CO_2 emission factor varies per 15-minute period

Expected behavior/Target Values

- Requesting download of video clips over 5G network has been running for at least 48 hours for all video clients.
- All the measurements have been successfully collected in the database.

VTT	**E2E application and 5G RAN optimization based on green energy availability**		
Test Case Name	Baseline (UC5.BL)		
Test Execution Date	29.10.2025 – 31.10.2025		
Test Executed By	VTT (Mikko Uitto, Olli Apilo, Mikko Hongisto, Seppo Rantala)		
Number of repetitions	1		
Test's comments	There were instability issues with wwan interface of 5G devices. The duration of the test had to be reduced to 48 hours.		
Verification Points (VP)			
Checkpoint ID	**Description of Validation Criteria for the checkpoint**		
ID #1	Download of video clips has been successful for all three clients over the 5G network, at least for 48 hours.		
ID #2	Measurement collection to the database has been successful during the video download (Checkpoint ID #1).		
ID #3	Total energy consumption for the test run.		
ID #4	Total transmitted video data amount for the test run.		
ID #5	Energy efficiency for the test run.		
ID #6	Total OPEX from electricity for the test run.		
ID #7	Total CO_2 emissions for the test run.		
ID #8	Percentage of video clips with empty cache during download (avg. of three clients).		
Test Validation Conditions	Checkpoints ID #1 and #2 have passed. Single numerical values and related time series have been collected for Checkpoints #3-#8.		
Test results	**Test run**	**Description**	**Result**
ID #1	1	Figure 86	Pass
ID #2	1	Measurement collection was successful during 29.10.2025 00:00 – 31.10.2025 00:00. The corresponding 48-h period to collect electricity cost and CO_2 emission data is 14.5.2025 00:00 – 16.5.2025 00:00.	Pass
ID #3	1	Total energy consumption = 75.97 kWh, Figure 87	Pass
ID #4	1	Amount of transmitted video data from the server = 3677 GB, Figure 86	Pass
ID #5	1	Total energy efficiency = 107.5 kbit/J, Figure 86, Figure 87	Pass
ID #6	1	Total OPEX from electricity = 3.58 €, Figure 88, Figure 87	Pass
ID #7	1	Total CO_2 emissions = 1.452 kg, Figure 89, Figure 86	Pass
ID #8	1	Percentage of video clips with empty cache = 26.3%, Figure 90	Pass

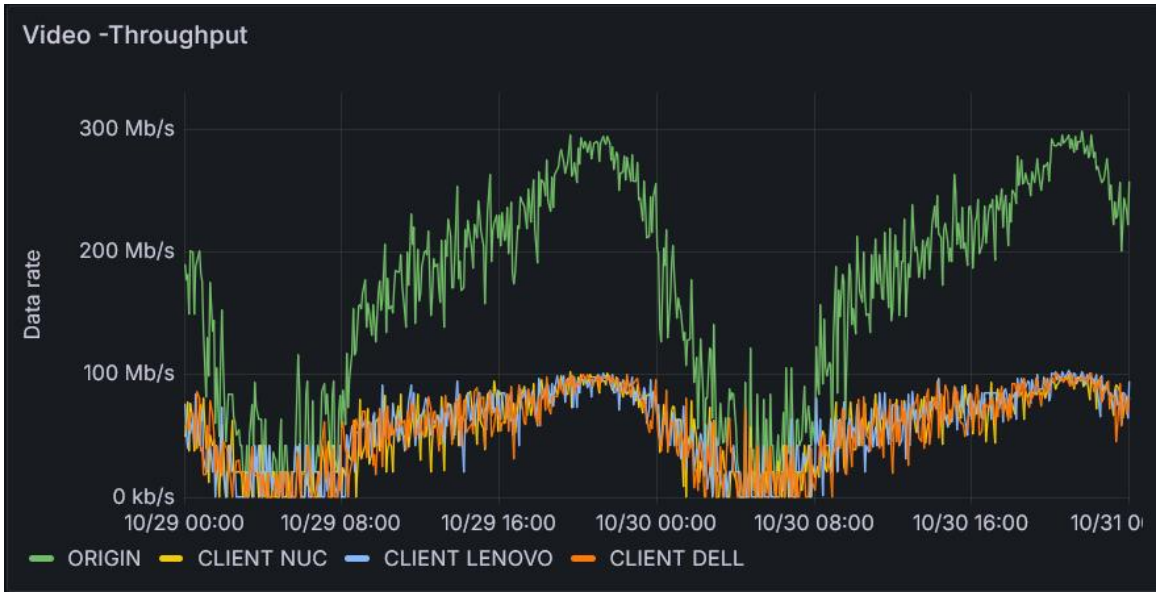

Figure 86: Video throughput from the server to the clients during the baseline test.

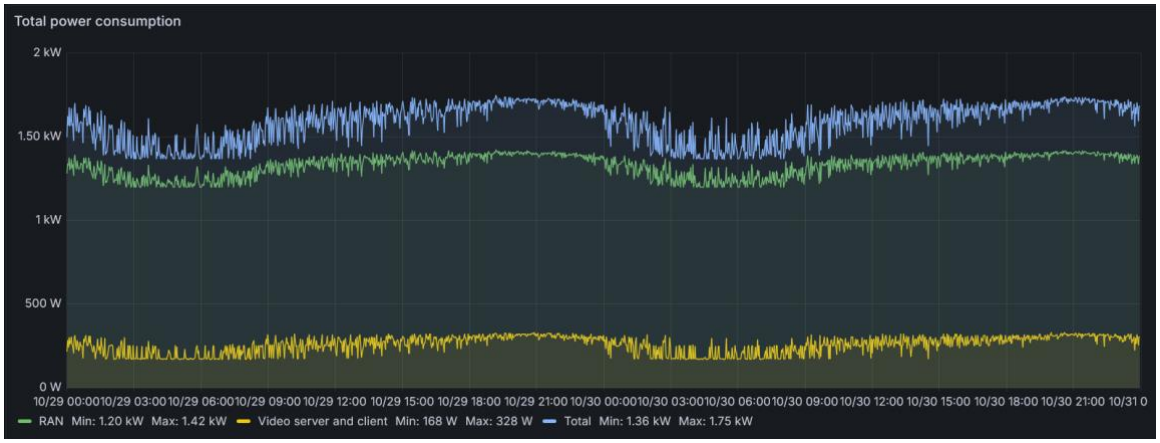

Figure 87: Total power consumption during the baseline test.

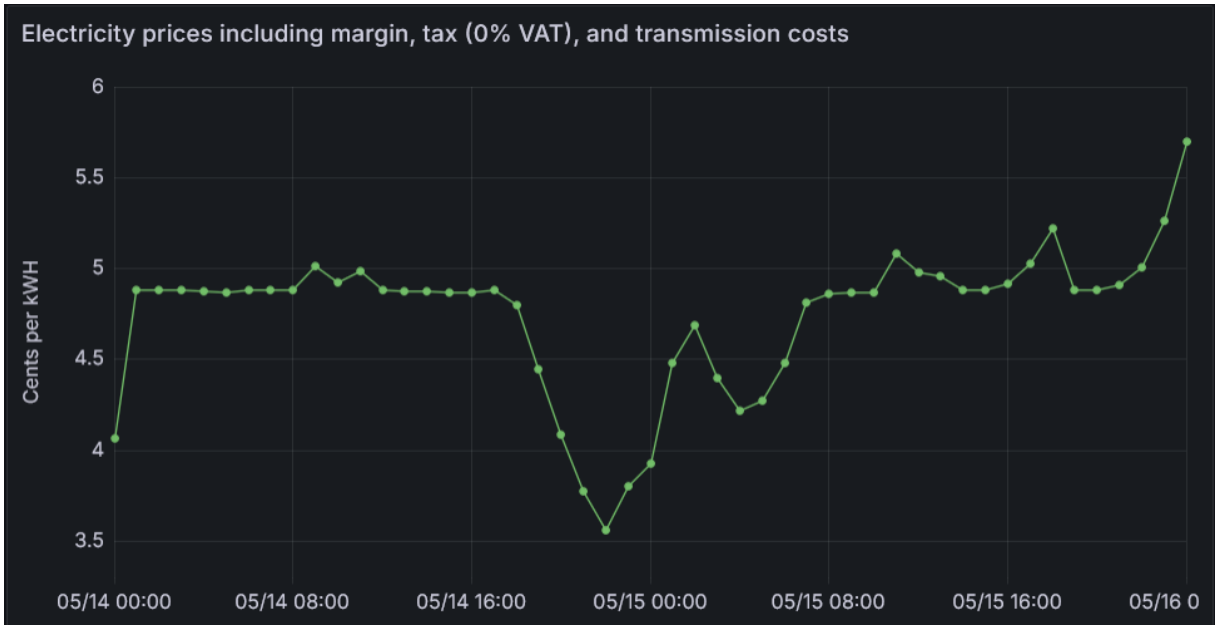

Figure 88: Electricity price between 14.5. 00:00 and 16.5. 00:00.

Figure 89: CO2 emission factor between 14.5. 00:00 and 16.5. 00:00.

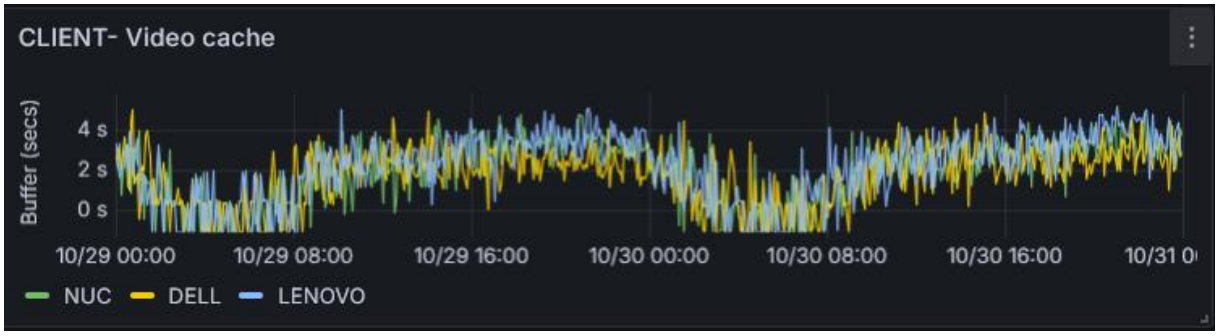

Figure 90: Video cache sizes for the three clients during the baseline test.

7.4.2 Adaptive test case

VTT	E2E application and 5G RAN optimization based on green energy availability

Test Case Name	Adaptive (UC5.AD)						
Test Case Objective	To show that integrated green energy production with joint RAN and video quality optimization can improve all the relevant KPIs (energy consumption, energy efficiency, OPEX from electricity, CO_2 emissions, and number of video cache threshold violations).						
Test Case Category	KPI Measurements						
Test Environment	The test was executed at the VTT laboratory over a self-operated 5G SA network with an integrated energy production system.						
Test Deployment Setup	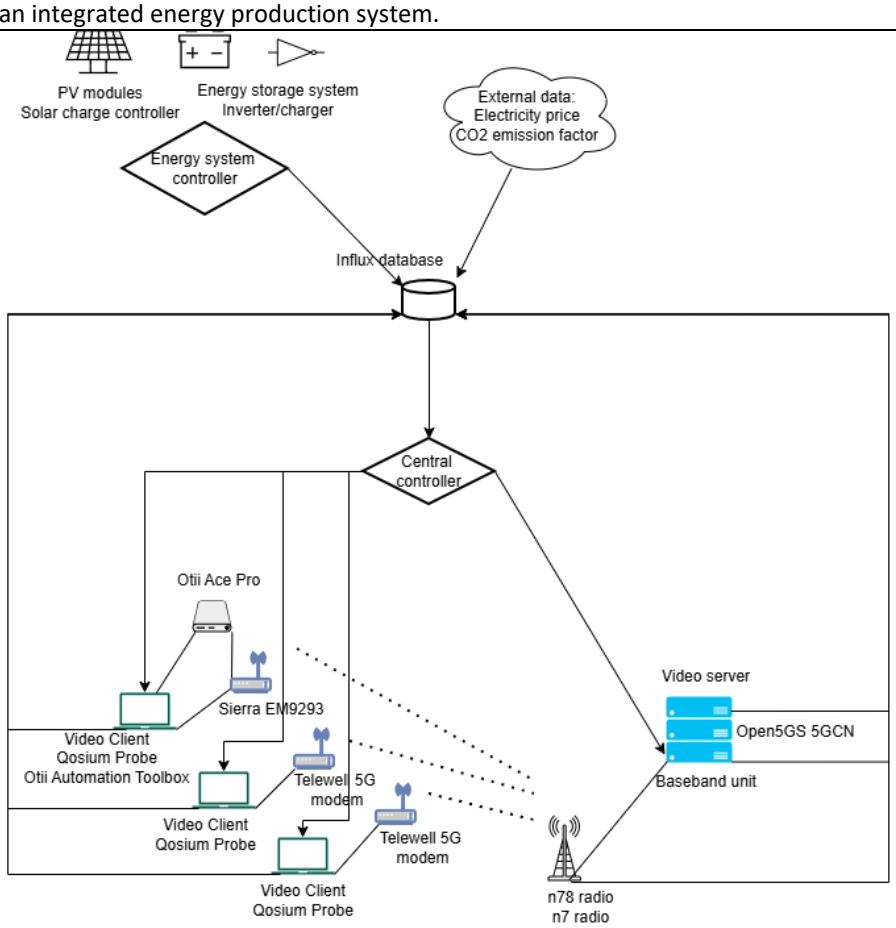						
Network Setup	**RAN:**	Commercial carrier-grade: n78 mMIMO radio, n7 macro radio	**5G Core:**	Open5GS	**Edge:**	Video server	**Band:** n78 and n7 **Bandwidth:** 60MHz and 10MHz
Test Configuration	**Components Under Test:**	Nginx web server (VoD service), gNB baseband unit, n78 mMIMO radio, n7 macro radio, Sierra EM9293 5G module, Telewell 5G	**Test Software:**	Qosium, Otii 3, Otii Automation Toolbox, mpv	**Test Devices:**	Carlo Gavazzi energy meters, Otii Ace Pro	**Testing Payload Data:** H264-encoded 60 s video clips over DASH

		modem, Intel NUC mini-PC					

Initial Conditions/Prerequisites

1. External data, including hourly electricity price and CO_2 emission factors, are available for the selected period of time.
2. InfluxDB for collecting the results is up and running.
3. Nginx web server for VoD service is up and running.
4. 5G RAN is operational. Both the n7 coverage and n78 capacity cell are active in State A.
5. Carlo Gavazzi measurements for all the components (video server, baseband, radios, video client) are operational, and the results are collected in the database.
6. All 5G UEs are connected to the higher priority capacity cell. Only data traffic from the video server is routed through the 5G interface. All other traffic related to measurements, such as measurement forwarding to InfluxDB, is routed over the Ethernet interface.
7. Otii Ace measurements of Sierra EM9293 power consumption are running and forwarded to the database.
8. Qosium Probes are active at each video client and at the video server.
9. Qosium Scopes at the video clients forward the results to the QMCP listener, which in turn forwards them to InfluxDB.
10. Pre-generated week-long video session schedule is available at each video client.
11. The energy system controller and central controller are up and running.

Test scenario

The purpose of this test is to evaluate how much the baseline values for KPIs can be improved when the central controller adapts the RAN states and video resolution such that the hourly energy budget is not exceeded. Because some factors affecting the performance, such as electricity price, change slowly on an hourly basis, a several-day-long test scenario is targeted. The traffic generation is done according to the same video session schedule as in the baseline case. In addition, the energy budget is calculated based on the same days from week 20 as in the baseline case.

1. Start the process at the video clients that trigger downloading the video clip according to the session schedule.
2. The energy budget is calculated for each hour.
3. Central controller adapts the RAN energy saving states and video resolution based on the energy budget.
4. Energy consumption, data amount, and QoS parameters are collected automatically.
5. Test runs up to 7 days, but if the video clients request video download for at least 48 hours over the 5G network, the test is considered successful.
6. Result post-processing to form the absolute KPI values and the relative values compared to the baseline.

Test variables

- Video session inter-arrival times follow an exponential distribution such that the mean value changes according to the daily traffic profile (see Table 19)
- Radio channel conditions vary in time (although the UEs are stationary)
- Electricity price varies per hour
- CO_2 emission factor varies per 15-minute period
- Target maximum energy consumption per hour, i.e., hourly energy budget varies per hour
- RAN power saving state is selected on an hourly basis

• Video resolution is selected on an hourly basis
Expected behavior/Target Values
• Requesting download of video clips over 5G network has been running for at least 48 hours for all video clients. • All the measurements have been successfully collected to the database. • Hourly energy budget has been successfully calculated and transmitted to the central controller. • RAN power saving state and video resolution have been adapted several times during the measurement. • KPIs total energy consumption, OPEX from electricity, and CO_2 emissions have lower values than in the baseline case.

VTT	**E2E application and 5G RAN optimization based on green energy availability**		
Test Case Name	Adaptive (UC5.AD)		
Test Execution Date	05.11.2025 – 07.11.2025		
Test Executed By	VTT (Mikko Uitto, Olli Apilo, Mikko Hongisto, Seppo Rantala)		
Number of repetitions	1		
Test's comments	There were instability issues with wwan interface of 5G devices. The duration of the test had to be reduced to 48 hours.		
Verification Points (VP)			
Checkpoint ID	**Description of Validation Criteria for the checkpoint**		
ID #1	Download of video clips has been successful for all three clients over the 5G network, at least for 48 hours.		
ID #2	Measurement collection to the database has been successful during the video download (Checkpoint ID #1). This time period, during which both the video clients and measurement collection have been working as expected, is referred to as the test run.		
ID #3	The hourly energy budget calculation has been successful for the test run.		
ID #4	RAN power saving states have been adapted during the test run.		
ID #5	Video resolution has been adapted during the test run.		
ID #6	Total energy consumption for the test run.		
ID #7	Total transmitted video data amount for the test run.		
ID #8	Energy efficiency for the test run.		
ID #9	Total OPEX from electricity for the test run.		
ID #10	Total CO_2 emissions for the test run.		
ID #11	Percentage of video clips with empty cache during download (avg. of three clients).		
ID #12	Energy self-sufficiency during the test run.		
Test Validation Conditions	Checkpoints ID #1-#5 have passed. Single numerical values and related time series have been collected for Checkpoints #6-#12.		
Test results	**Test run**	**Description**	**Result**
ID #1	1	Figure 91	Pass
ID #2	1	Measurement collection was successful during 05.11.2025 00:00 – 07.11.2025 00:00. The corresponding 48-h period to collect	Pass

		electricity cost and CO_2 emission data and to calculate hourly energy budget is 14.5.2025 00:00 – 16.5.2025 00:00.	
ID #3	1	Figure 92	Pass
ID #4	1	Figure 93, Table 20	Pass
ID #5	1	Figure 91	Pass
ID #6	1	Total energy consumption = 48.04 kWh, reduction by 36.8%, Figure 93	Pass
ID #7	1	Amount of transmitted video data from the server = 553.6 GB, Figure 91	Pass
ID #8	1	Total energy efficiency = 25.6 kbit/J, Figure 91, Figure 93	Pass
ID #9	1	Total OPEX from electricity 0.47 €, Figure 88, Figure 93, Figure 94, reduction by 86.9%	Pass
ID #10	1	Total CO_2 emissions 0.224 kg, Figure 89, Figure 93, reduction by 84.6%	Pass
ID #11	1	Percentage of video clips with empty cache = 1.56 %, Figure 95	Pass
ID #12	1	Energy self-sufficiency = 76.5%, Figure 93, Figure 94	Pass

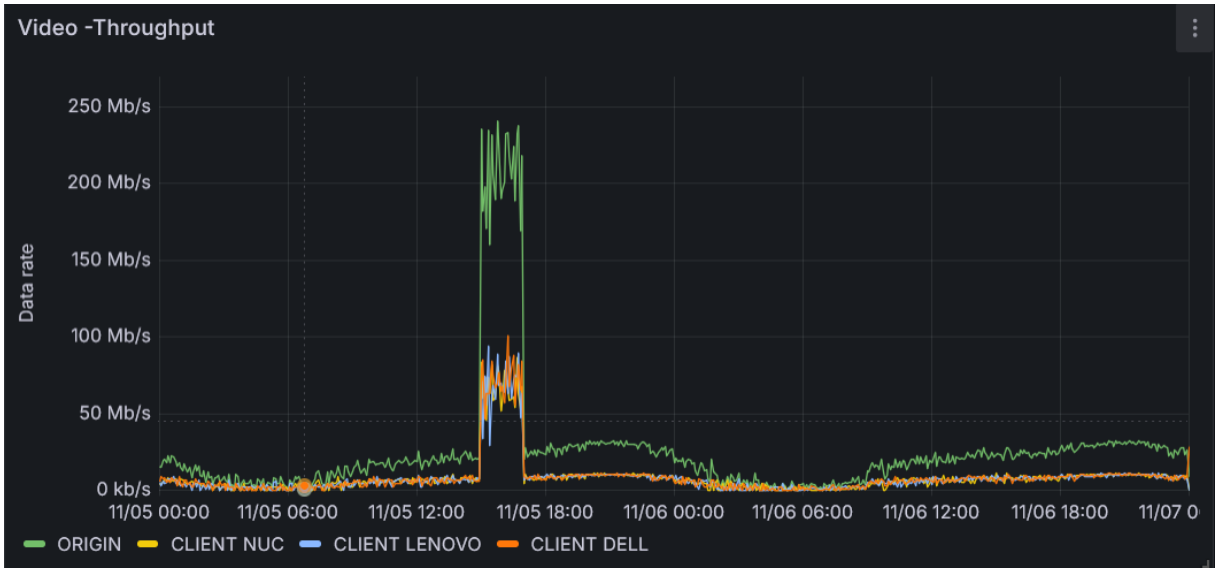

Figure 91: Video throughput from the server to the clients during the adaptive test.

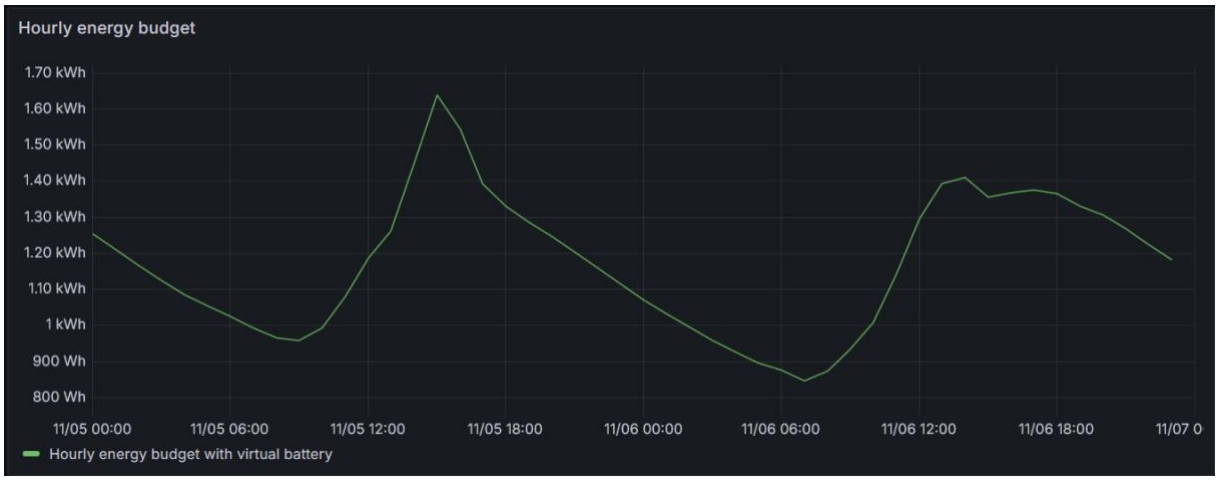

Figure 92: Hourly energy budget during the adaptive test.

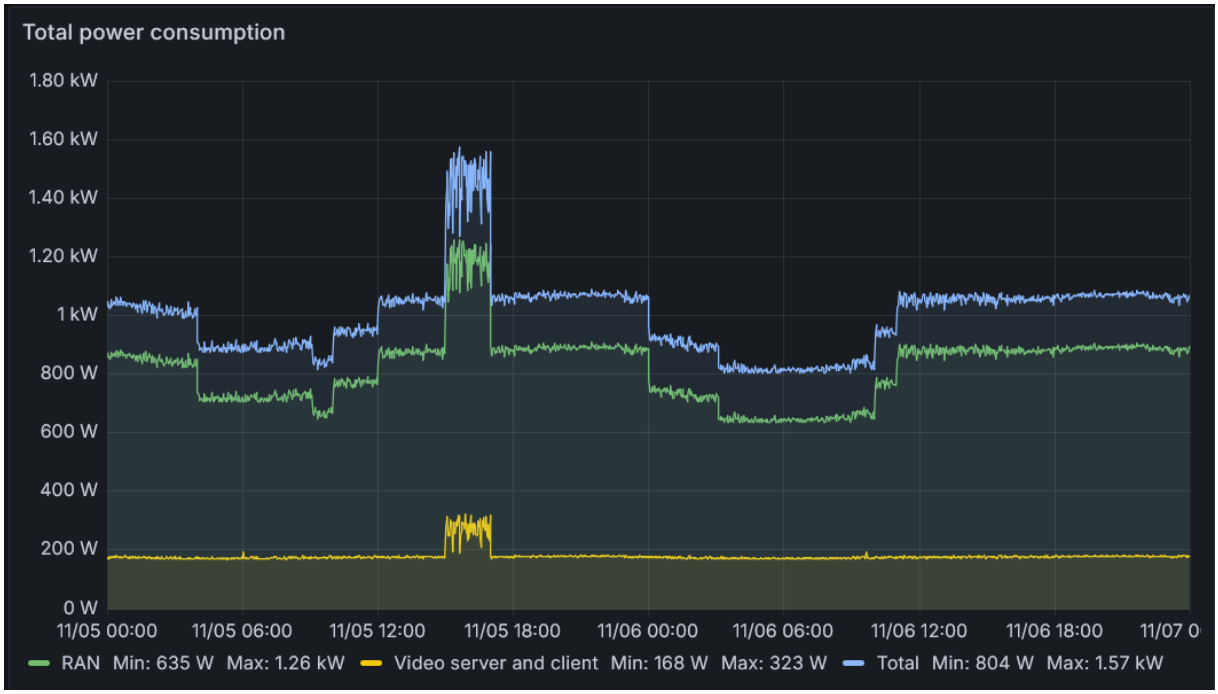

Figure 93: Total power consumption during the adaptive test.

Table 20: RAN states and their relative power consumption during the adaptive test.

Time	05.11 00:00-04:00	05.11 04:00-09:00	05.11. 09:00-10:00	05.11. 10:00-12:00	05.11. 12:00-15:00	05.11. 15:00-17:00	05.11. 17:00-23:59	06.11. 00:00-03:00	06.11. 03:00-10:00	06.11. 10:00-11:00	06.11. 11:00-00:00
RAN state	BBC	BCC	BDC	BCC	BBC	BAC	BBC	BCC	BDC	BCC	BBC
Avg. RAN power consumption relative to the baseline avg.	64%	54%	51%	58%	66%	89%	67%	55%	49%	58%	67%

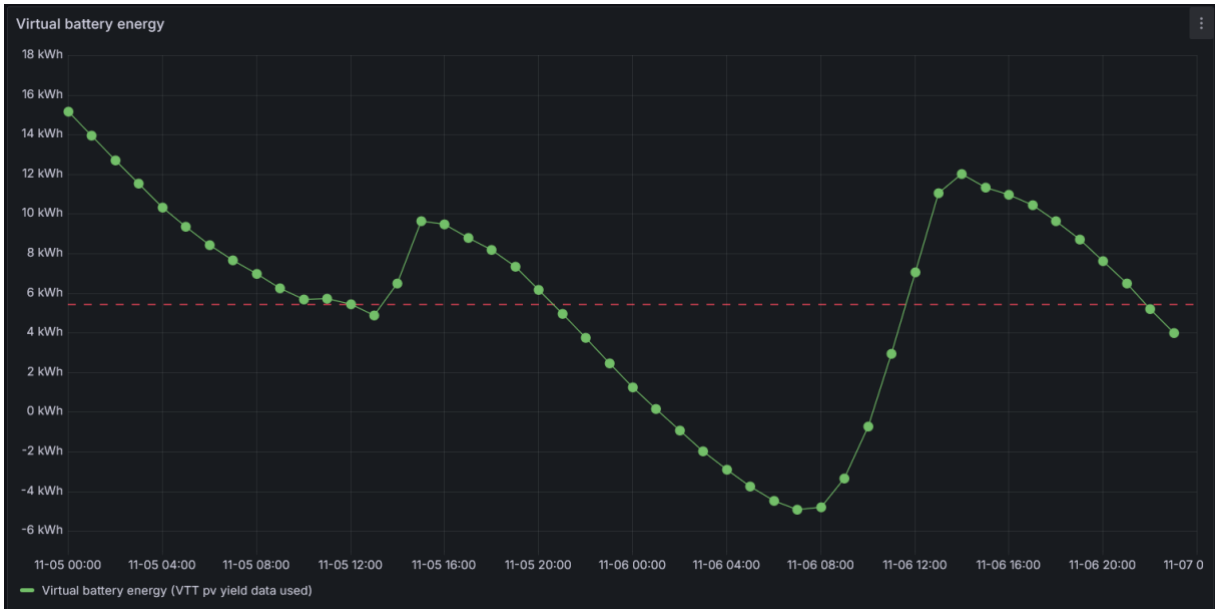

Figure 94: Virtual battery energy content during adaptive test.

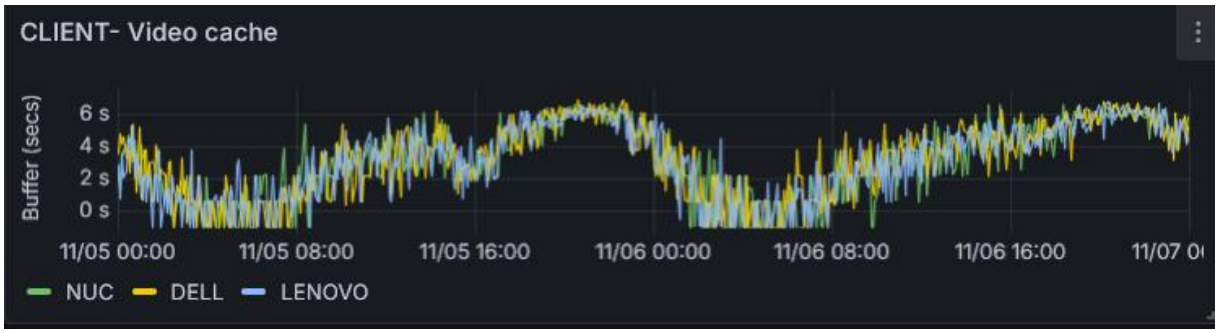

Figure 95: Video cache sizes for the three clients during the adaptive test

7.5 RESULT ANALYSIS

The validation tests at UOULU demonstrate that adjusting the RAN parameters in the OAIBOX gNB has a significant impact on energy consumption, electricity costs, and CO_2 emissions. Comparing the two power modes, full power and power saving mode, shows that optimizing the RAN configuration can reduce total power consumption by 15.4% (Figure 82). These configurations also resulted in daily CO_2 reductions of 55–72 g (Figure 85) and provided noticeable energy cost savings when selecting the right power mode based on negative or positive energy pricing (Figure 83). This highlights that selecting the appropriate RAN parameters, when integrated with energy budgeting strategies, can substantially enhance both operational efficiency and sustainability.

The validation tests show that energy consumption was reduced by 36.8% when RAN power saving states and video resolution were adapted to fit the energy budget. This significant energy saving is mostly due to the RAN state adaptation; each abrupt change in total power consumption in Figure 93 corresponds to a change in the RAN state, see Table 20. The logic for selecting the RAN states is explained in Section 5.3.3.4. Other factors affecting energy consumption are the reduced traffic load in the adaptive case due to video resolution reduction and the use of DTX in the adaptive case. From the video application perspective, the advantage of centralized control in our system is to equalize the

video quality for all the clients to guarantee a satisfying quality of service with reduced energy consumption.

Due to reduced energy consumption and well-dimensioned solar energy production and storage, we were able to reach significant savings in terms of operational costs and CO_2 emissions. Additionally, the hourly energy budget was calculated such that higher energy consumption was allowed only when the solar yield was high, and the battery was clearly above its minimum state of charge. The OPEX from electricity and CO_2 emissions reduced by 86.9% and 84.6%, respectively. The energy self-sufficiency of the adaptive system was at the level of 76.5%, which is very good for a system operating in Finland. Higher levels of self-sufficiency tend to be impractical to reach in terms of CAPEX and return on investment.

The video clips are downloaded with a cache of 10 s. In practice, this means that when the cached video content becomes empty, the user experiences stalling of the video playback. According to the baseline results where the highest 8k video resolution with 100 Mbps data rate is used, empty cache is quite common (26.3% of the video clips) occurring when all three clients attempt to download the video clip at the same time (300 Mbps DL sum rate). This indicates that even though the maximum DL capacity of our 60-MHz TDD cell is typically 600-800 Mbps, the clients during the test run were located close to the cell edge with capacity occasionally dropping below 300 Mbps. The variation in capacity is due to time-varying nature of wireless channels, especially in our outdoor-to-indoor case, which results in rank and channel quality variation for the clients. In the adaptive case, the central controller aims to select the video resolution such that the capacity in the chosen RAN state is enough for the video traffic. According to the results, this adaptation is successful as the percentage of video clips with empty cache is only 1.56%. The video clips with empty cache occur on 5.11. 15:00 – 17:00 when the RAN state A is selected for the capacity cell. Based on the results, we can claim that E2E adaptation not only improves energy-related KPIs in terms of reduced energy consumption but also improves the service quality experienced by the users as the probability of video stalling is reduced.

8 CONCLUSIONS (WP5 IN GENERAL)

The main result of Task T5.1 is the construction of the operative electricity monitoring research infrastructure covering both local PV-production, battery energy storage, monitoring and control systems, and consumption measurement systems capable of operating on almost real-time 1/s -level and store a vast amount of obtained datapoints. The energy measurement framework was successfully applied together with a flexible data infrastructure in other tasks of this project, as well as in several open call projects remotely. Methodologies to derive long-term performance indicators as well as to execute shorter-term trial-oriented test runs were developed and used to validate savings.

The results of T5.2 'Autonomous Base Station Energy Conservation Technologies' are summarized in Section 3. Based on our extensive gNB feature evaluation and measurements, the most potential energy saving methods are DTX, MIMO muting, cell blocking, and cell sleep modes. The measurements were performed using our reference RAN architecture of one coverage and two capacity cells. In the case of the empty system with no connected UEs, it is possible to reduce power consumption by up to 51% by energy-saving methods. In order to allow external control of RAN energy consumption, per-cell power saving states were defined, and the RAN controller was implemented for converting external commands for changing the RAN power saving states into gNB configuration changes. RAN controller was integrated as part of the E2E energy optimization framework (Section 5.3). We show that by adapting the RAN power saving states to the typical daily traffic pattern, it is possible to achieve considerable energy savings (26% reduction in a system with a macro coverage cell and a macro capacity cell).

The results of T5.3 "ENERGY PRODUCTION: AI TOOLS FOR 48 H ENERGY WEATHER" are summarized in Section 4, where the evaluation identifies the updated FMI Open PV forecast, improved with the new configuration file, as the most effective forecasting API for energy weather prediction for the next 48 hours, providing strong correlation with the real-time PV production. The simulated PV outputs achieved an MAE of 217.25 and an RMSE of 413.71 (27.86% RMSE), while the high MAPE of 77.97% reflects large relative errors under rapidly changing weather conditions. Despite this, the correlation coefficient of 0.974 confirms that the forecast reliably follows the curves and dynamic changes of actual PV production, enabling dependable energy budgeting with minor real-time adjustments using on-site sensors and DL/RNN models, such as solar irradiance sensors and LSTM, respectively. The average daily accumulated accuracy remained within ±8% for the next 48 hours, providing a robust platform for planning base station consumption and energy profiling adjustments. Compared to traditional third-party methods and cloud services that rely heavily on historical data and struggle with short-term dynamics or site specificity, the FMI-based approach continuously updates atmospheric variables (irradiance, temperature, wind, albedo, cloud cover) and can simulate virtual production even for sites without installed panels. This makes FMI-powered forecasting a highly adaptable, cost-effective, and reliable solution for energy-aware network operations and energy budgeting/planning.

Section 5 introduced T5.4 'E2E Energy Efficiency', focusing on the test environments for optimized E2E evaluation with partial results as an introduction for the validation results presented in Section 7. Subsection 5.3 presented the implementation for controlling 5G RAN and video streaming applications dynamically in North-Node according to the availability of green energy and network capacity. The basis of this adaptive system relied on an accurate energy measurement framework as a result of T5.1, which enabled initial power measurement campaigns both for RAN and applications to identify different power saving states. From the video application perspective, the highest energy savings were achieved by lowering video resolution alongside bitrate at the cost of lower video quality. The long-term measurements show 43% energy savings for a single video client when using adaptive control.

Similarly, one of the identified QoE indicators, video cache remains at an acceptable level where only 1.6% of watched video clips suffer from video stalls compared baseline 26%.

Additionally, in T5.4, the ORAN setup at the UOULU site was used to perform energy conservation techniques for validation and KPI assessments presented in section 7. The evaluation of different combinations of RAN configurations, including restricting the used bandwidth, restricting the modulation constellation, TDD frame structure selection, and changing the antenna selection from MIMO to SISO, showed that each parameter adjustment has a significant impact on the overall energy consumption of the ORAN setup. In most cases, radio configurations that provided higher bitrates caused more power consumption during non-traffic periods and during TCP/UDP speed tests (UL and DL traffics). It seems that all the tested radio configuration changes. Based on the measurement results, it seems that the lowering of bandwidth is the most efficient method to reduce power consumption for OAIBOX MAX, and changing from MIMO to SISO antenna configuration is the most efficient method to save energy for USRP N310. The validation tests at UOULU demonstrate that adjusting the RAN parameters in the OAIBOX gNB has a significant impact on energy consumption, electricity costs, and CO_2 emissions. Comparing the two power modes, full power and power saving mode, shows that optimizing the RAN configuration can reduce total power consumption by 15.4%. These configurations also resulted in daily CO_2 reductions of 55–72 g and provided noticeable energy cost savings when selecting the right power mode based on negative or positive energy pricing. This highlights that selecting the appropriate RAN parameters, when integrated with energy budgeting strategies, can substantially enhance both operational efficiency and sustainability.

T5.4 also developed an energy-aware AI orchestration framework for scheduling tasks across the three-tier, edge cloud continuum. Tasks were classified by urgency, resource needs, and constraints, and dynamically placed using real-time monitoring, load balancing, and energy-efficient resource selection. Functional requirements included energy availability, pricing, computational demand, QoS, and scalability. A rule-based AI approach using FMI energy-weather forecasts and ELSPOT pricing was applied to schedule 100 mixed tasks, prioritizing execution during high PV production and low electricity prices. Results show that this method significantly reduces overall energy cost compared to baseline random scheduling.

The E2E validation tests executed at the VTT site reported in Section 7 show that adaptive control of RAN power saving states and video resolution based on the energy availability budget results in significant gains in all main KPIs. Energy consumption was reduced by 36.8% when compared to the baseline case with no RAN energy saving features and maximum video resolution. In addition, due to clever energy budgeting, which allowed high RAN capacity only when excess energy was available, OPEX from electricity and CO_2 emissions also reduced by 86.9% and 84.6%, respectively.

Also obtained PV hybrid based power supply system's KPI results and trial simulations for sunny periods indicate that even 70-80% of the procured energy (in the form of electricity intake from the grid) can be saved or substituted by local energy by means of applied multifunctional and bi-directional inverter/charger technology and well dimensioned PV-hybrid power supply system with LiFEPO4-battery energy storage and flexible and controllable grid interface.

REFERENCES

[1] E. Kolta and T. Hatt, “Going green: Measuring the energy efficiency of mobile networks,” GSMA Intelligence, Tech. Rep., 2024. [Online]. Available: https://data.gsmaintelligence.com/research/research/research-2024/going-green-measuring-the-energy-efficiency-of-mobile-networks

[2] E. A. Walelgne, A. S. Asrese, J. Manner, V. Bajpai, and J. Ott, “Understanding data usage patterns of geographically diverse mobile users,” *IEEE Transactions on Network and Service Management*, vol. 18, no. 3, pp. 3798–3812, 2021.

[3] D. López-Pérez, A. De Domenico, N. Piovesan, G. Xinli, H. Bao, S. Qitao, and M. Debbah, “A survey on 5G radio access network energy efficiency: Massive MIMO, lean carrier design, sleep modes, and machine learning,” *IEEE Commun. Surveys Tuts.*, vol. 24, no. 1, pp. 653-697, Jan. 2022.

[4] W. Chen, X. Lin, J. Lee, A. Toskala, S. Sun, C. F. Chiasserini, and L. Liu, ”5G-Advanced toward 6G: Past, present, and future,” *IEEE J. Sel. Areas Commun.*, vol. 41, no. 6, pp. 1592-1619, Jun. 2023.

[5] L. M. P. Larsen, H. L. Christiansen, S. Ruepp, and M. S. Berger, “Toward greener 5G and beyond radio access networks – A survey,” *IEEE Open Journal of the Communications Society*, vol. 4, pp. 768-797, Mar. 2023.

[6] *Study on network energy savings for NR*, 3GPP TR38.864, V18.1.0, Mar. 2023.

[7] X. Lin, “The bridge toward 6G: 5G-Advanced evolution in 3GPP Release 19,” *IEEE Commun. Standards Mag.*, vol. 9, no. 1, pp. 28-35, Mar. 2025.

[8] (2025, May) 5G NR Throughput calculator. 5G Tools for RF Wireless. [Online]. Available: https://5g-tools.com/5g-nr-throughput-calculator/.

[9] Techplayon, “5G Mobility Scenarios – Handovers,” https://www.techplayon.com/5g-mobility-scenarios-handovers/, 2023. accessed: 2025-03-19.

[10] “Energy efficiency analysis of the reference systems, areas of improvements and target breakdown,” EARTH Deliverable D2.3 V2.0, 2012. [Online]. Available: https://cordis.europa.eu/docs/projects/cnect/3/247733/080/deliverables/001-EARTHWP2D23v2.pdf

[11] *Metrics and measurement method for energy efficiency of wireless access network equipment; Part 2: Energy efficiency – dynamic measurement method*, ETSI TS 102 706-2, V1.7.1, Jul. 2024.

[12] J. Navarro-Ortiz, P. Romero-Diaz, S. Sendra, P. Ameigeiras, J. J. Ramos-Munoz and J. M. Lopez-Soler, "A Survey on 5G Usage Scenarios and Traffic Models," in *IEEE Communications Surveys & Tutorials*, vol. 22, no. 2, pp. 905-929, Second quarter 2020.

[13] 6G-XR Consortium, D5.1 – “Description of sustainability experimentation framework”, 6G-XR project report, Jun. 2024. Available at: https://www.6g-xr.eu/wp-content/uploads/sites/96/2024/09/D5.1-Description-of-sustainability-experimentation-framework.pdf

[14] M. Uitto, O. Apilo, J. Koivisto and N. Gupta, ”Towards energy-aware video streaming in 5G/B5G - application perspective”, in Proc. of EuCNC/6G Summit, June 2025.

[15] *Extended reality (XR) in 5G*, 3GPP TR26.928, V16.1.0, Dec. 2023

[16] J. Koivisto, “Evaluation of the energy consumption in secure HTTP video streaming over 5G”, Master’s Thesis, University of Oulu, June 2025.

[17] 6G-XR Consortium, D1.1 – Requirements and Use Case Specifications, Version 1.0, October 2023.

Available at: https://www.6g-xr.eu/wp-content/uploads/sites/96/2023/10/D1.1-Requirements-and-use-case-specifications-V1.0.pdf

[18] 6G-XR Consortium, D1.2 – Reference Architecture Description V1.0, September 2024. [Online]. Available: https://www.6g-xr.eu/wp-content/uploads/sites/96/2024/09/D1.2-Reference-architecture-description-V1.0-1.pdf

[19] ITP 2018; Lithium-ion Battery Testing, Public Report 4. March 2018. ITP Renewables O, Australia. Available: https://arena.gov.au/knowledge-bank/itp-battery-test-centre-reports/

[20] European Union / 6G-VERSUS Project. (2025). Finland – 6G-VERSUS Finnish Pilot: Sustainable operations for a remote (Arctic Circle) base station. 6G-VERSUS. https://6g-versus.eu/finland/

[21] Finnish Meteorological Institute. (2025). Numerical weather prediction. FMI – Ilmatieteen laitos. https://en.ilmatieteenlaitos.fi/numerical-weather-prediction.

[22] Nord Pool. Day-Ahead Market (ELSPOT) – Market Rules and Price Data. Nord Pool Group. Available at: https://www.nordpoolgroup.com/en/

[23] Fingrid. (2025). Real-time CO_2 emissions estimate. Retrieved from https://www.fingrid.fi/en/electricity-market-information/real-time-co2-emissions-estimate

[24] Finnish Meteorological Institute (FMI). (2024). fmi-open-pv-forecast: Weather forecast aware solar PV forecasting application (GitHub repository) https://github.com/fmidev/fmi-open-pv-forecast

[25] ITP 2020, Lithium-ion Battery Testing, Public Report 9. September 2020. ITP Renewables O, Australia. Available: https://arena.gov.au/knowledge-bank/itp-battery-test-centre-reports/

[26] ITP 2022, Lithium-ion Battery Testing, Public Report 12 (Final Report). March 2022. ITP Renewables O, Australia. All previous test reports are available here: https://arena.gov.au/knowledge-bank/itp-battery-test-centre-reports/

[27] Carlo-Gavazzi, Datasheet: Energy Management, Energy Analyzer, Type EM111. EM111 DS,070323,Available: https://www.gavazziautomation.com/fileadmin/images/PIM/DATASHEET/ENG/EM111_DS_ENG.pdf

[28] Ettus Research. (2025). Ettus Research website. Retrieved January, 2025: https://ettus.com/

[29] VTT 2019, M. Hongisto, S. J. Rantala, J. Mäkelä, M. Lasanen, J. Huusko, M. Savela, J. Penjala, “Building blocks towards energy self-sufficient / sustained 5G”, 5GTN-demo seminar poster, Published 1.11.2019.

[30] Trina Solar’s datasheet: Honey module TSM-PD05, 2017 (checked 2011.2025), available: https://static.trinasolar.com/sites/default/files/EN_TSM_PD05_datasheet_B_2017_web.pdf

[31] Victron Energy’s blog 2023: Introducing Solar Production Forecast https://www.victronenergy.com/blog/2023/07/05/new-vrm-solar-production-forecast-feature/

[32] Victron Energy 23.4.2024: Dynamic Energy Storage System: save energy costs – automatically - What is Dynamic ESS and how does it work? https://www.victronenergy.com/blog/2024/04/23/dynamic-energy-storage-system-save-energy-costs-automatically/

[33] H. Malik and A. Pouttu, "Integration of LSTM based Model to guide short-term energy forecasting for green ICT networks in smart grids," *2022 IEEE International Conference on Communications, Control, and Computing Technologies for Smart Grids (SmartGridComm)*, Singapore, Singapore, 2022, pp. 290-295, doi: 10.1109/SmartGridComm52983.2022.9960992.

[34] Dimitris Tsolkas, Anastastios-Stavros Charsmiadis, Dionysis Xenakis, and Lazaros Merakos. Service and network function placement in the edge-cloud continuum. In 2022 IEEE Conference on Standards for Communications and Networking (CSCN), pages 188–193. IEEE, 2022.

[35] H. F. Shahid and E. Harjula, ‘‘Resource-aware orchestration of iot applications in edge-cloud continuum with 6g,’’ in 2024 IEEE International Conference on Pervasive Computing and Communications Workshops and other Affiliated Events (PerCom Workshops), pp. 245–246, 2024.

[36] Erkki Harjula, Pekka Karhula, Johirul Islam, Teemu Lepp¨anen, Ahsan Manzoor, Madhusanka Liyanage, Jagmohan Chauhan, Tanesh Kumar, Ijaz Ahmad, and Mika Ylianttila. Decentralized iot edge nanoservice architecture for future gadget-free computing. IEEE Access, 7:119856–119872, 2019.

[37] Johirul Islam, Erkki Harjula, Tanesh Kumar, Pekka Karhula, and Mika Ylianttila. Docker enabled virtualized nanoservices for local iot edge networks. In 2019 IEEE Conference on Standards for Communications and Networking (CSCN), pages 1–7, 2019.

[38] H. F. Shahid, J. Islam, I. Ahmad, and E. Harjula, ‘‘Optimizing resource-aware service orchestration in edge-cloud continuum,’’ in 2025 IEEE Intelligent Mobile Computing (MobileCloud), pp. 44–50, 2025.

[39] H. F. Shahid and C. Pahl, ‘‘Enhanced particle swarm optimisation and multi objective optimization for the orchestration of edge cloud clusters.,’’ in IJCCI, pp. 155–162, 2019.

APPENDIX A

The template presented below refers to Test Cases descriptions used in the 6G-XR, within which the validation methodology is executed. It contains the test cases specification part and the results presentation part.

1. ANNEX A:

UOULU	**User Story/Scenario**						
Test Case Name	*Active energy counter Test case validation*						
Test Case Objective/KPI	*Active energy counter for real-time energy monitoring of OAIBOX gNB+Core, USRP n310 and UE*						
Test Execution Date	29/10/2025						
Test Executed By	UOULU						
Test Environment	*Laboratory Indoor /OAIBOX, Netio Powerbox, USRP n310, Quectel Modem, 5GTN Server*						
Test Deployment Setup	*Figure1…*						
Network Setup	**RAN:**	*OAIBOX, USRP n310*	**5G Core:**	Open5GS	**EDGE**	*Nokia OpenEdge Blade*	**Band:** *3.8-4.0GHz* **Bandwidth:** *100MHz*
Test Configuration	**Traffic**	**Iperf3**	**Mobility**	**Low**	**RAN Configurations**		**BW, MCS, TDD frame, MIMO**
Initial Conditions/Prerequisites							
OAIBOX MAX + USRP N310 communicates with 1 UE (Quectel modem +Win laptop), (No traffic, Downlink: base station transmits to UE, Uplink: UE transmits to base station)							
Test scenario							
The OAIBOX is connected to an external power meter (Netio Powerbox). The absolute power values are measured using MQTT and stored in a central database using a central controller (Nokia OpenEdge Blade server).							
Test variables							
Power values of OAIBOX and USRP n310 with different RAN parameters							
Expected behaviour/Target Values							
Setup time: 1 hour, measurements, Numerical values for power measurements based on RAN configurations stored in the central database and visualized using Grafana							
Verification Points (VP)							
Checkpoint ID	**Description of Validation Criteria for the checkpoint**						
ID #1	***Bandwidth 100 MHz**, MCS = 256 QAM (max_mcs=28), TDD= 3*DD-F-1*UU, MIMO2x2*						
ID #2	***Bandwidth 80 MHz**, MCS = 256 QAM (max_mcs=28), TDD= 3*DD-F-1*UU, MIMO2x2*						
ID #4	***Bandwidth 60 MHz**, MCS = 256 QAM (max_mcs=28), TDD= 3*DD-F-1*UU, MIMO2x2*						
ID #4	***Bandwidth 40 MHz**, MCS = 256 QAM (max_mcs=28), TDD= 3*DD-F-1*UU, MIMO2x2*						
ID #5	***Bandwidth 20 MHz**, MCS = 256 QAM (max_mcs=28), TDD= 3*DD-F-1*UU, MIMO2x2*						
Test Validation Conditions	All checkpoints have passed in all the repetitions						
Naming convention	**Define log file naming logic**						
Test results	**Test run 1**	**Test run 2**	**Test run 3**	**Diagrams**			
Checkpoint ID #1	*logfileA*	*logfileD*	*logfileG*	*System architecture for energy measurement framework*			

Checkpoint ID #2	*logfileB*	*logfileE*	*logfileH*	
Checkpoint ID #3	*logfileC*	*logfileF*	*logfileI*	
Final Diagrams				

2. ANNEX B:

Preliminary processed test data for UOULU and VTT, PV yields, gCO2/kWh, €/MWh, FMI energy weather forecast, VRM forecasts, virtual battery simulation (to week 20 tests)

						UOULU'S	PV-installation		Notes, if h shifts
		Scaled-up	Realized	Emissions	ELSPOT	PV-yield prognoses (1=VRM afterwards)			
		Real	PV-Yield		in the context data?	Yes, hour shift but already adjusted in values.			
Week 20		PV-Yield	PV-Yield	gCO2/kWh,prev.h	€/MWh,prev.h				
		Downloaded VRM-prognosis to next hour				PV-yield	Prognoses		
		D1-24h F	D2-48h F	D3-72h F					
12/05/2025	00:00:00	0	10	96.5	26.35	0		0	0
12/05/2025	01:00:00	0	0	98.1	38.18	0		0	0
12/05/2025	02:00:00	0	0	102	52.04	0		0	0

12/05/2025	03:00:00	0	0	103.4	62.75	0	0	0
12/05/2025	04:00:00	0	0	105.4	58.01	82.69	0	0
19.93	19.93							
12/05/2025	05:00:00	38	10	107.1	53.92	80.6	53	
106.26	106.26	106.26						
12/05/2025	06:00:00	114	40	106.7	104.23	70.61	157	
196.57	196.57	196.57						
12/05/2025	07:00:00	228	60	107.9	125.94	180.56	495	
742.47	742.47	742.47						
12/05/2025	08:00:00	304	90	108.7	115.06	333.74	1352	
1725.49	2023.34	2023.34						
12/05/2025	09:00:00	1064	280	107.4	111.55	600.03	2691	
2725.87	3281.7	3281.7						
12/05/2025	10:00:00	2660	700	104.2	74.81	881.57	3973	
4245.57	4245.57	4245.57						
12/05/2025	11:00:00	4066	1080	100.5	36.68	1012.25		
4707	4751.81	4751.81	4751.81					
12/05/2025	12:00:00	5054	1330	99.4	40.01	1435.87		
5136	5129.93	5129.93	5129.93					
12/05/2025	13:00:00	5510	1470	90.4	33.62	1251.92		
5208	5242.44	5438.29	5242.44	5242.44				
12/05/2025	14:00:00	5624	1480	86.4	16.92	1209.79		
4949	4923.99	5166.83	4923.99	4923.99				
12/05/2025	15:00:00	5282	1390	82.4	19.5	818.46	4403	
4410.61	4792.25	4410.61	4410.61					
12/05/2025	16:00:00	4598	1190	81.1	32.89	900.61	3393	
4025.1	4025.1	2655.8	2655.8					
12/05/2025	17:00:00	3116	830	82	40.98	644.78	2374	
2827.88	2827.88	2474.75	2474.75					
12/05/2025	18:00:00	1900	500	85.6	19.29	359.24	972	
1343.86	1343.86	1580.22	1580.22					
12/05/2025	19:00:00	608	170	89.5	40	98.52	533	
413.91	413.91	396.52	396.52					
12/05/2025	20:00:00	418	110	91.7	42.71	0	109	
209.84	209.84	232.83	232.83					

12/05/2025	21:00:00	152	40	94.5	31.07	0	64	
69.93	69.93	74.45	74.45					
12/05/2025	22:00:00	114	30	94.7	48.06	0	0	0
12/05/2025	23:00:00	0	0	91.8	21.85	0	0	0
13/05/2025	00:00:00	0	0	91.7	9.08	0	0	0
13/05/2025	01:00:00	0	0	92.4	5.11	0	0	0
13/05/2025	02:00:00	0	0	92.3	5.8	0	0	0
13/05/2025	03:00:00	0	0	92	4.51	0	0	0
13/05/2025	04:00:00	0	0	90.6	1.76	0	0	0
14.11	23.81							
13/05/2025	05:00:00	38	10	86.3	2	0	0	0
105.74	142.35							
13/05/2025	06:00:00	38	10	84	1.26	0	42	
35.76	35.76	365.55						
13/05/2025	07:00:00	76	30	82.4	20.04	0	455	
349.87	349.87	97.99	788.5					
13/05/2025	08:00:00	456	130	86.4	69.76	133.99	385	
327.15	327.15	254.13	552.17					
13/05/2025	09:00:00	342	90	91.1	100.34	66.96	834	
567.81	567.81	549.44	230.4					
13/05/2025	10:00:00	722	190	94.4	74.82	234.95	964	
1303.11	520.57	1303.11	74.25					
13/05/2025	11:00:00	798	210	118.4	25.9	377.78	2439	
1986.26	1361.83	1986.26	298.3					
13/05/2025	12:00:00	2470	690	100.4	5.99	597.7	5128	
2937.87	2036.8	2937.87	490.49					
13/05/2025	13:00:00	5586	1470	142.6	5.82	746.56	5127	
3365.8	3365.8	3130.86	998.38					
13/05/2025	14:00:00	5548	1470	129.3	4.93	819.21	4978	
5240.28	5240.28	3130.58	1327.08					

13/05/2025	15:00:00	5244	1390	84.1	5.65	816.18		4437	4388.12	4388.12	2465.78	2019.75
13/05/2025	16:00:00	4636	1200	85.5	3.59	1025.63		3561	3592.16	3592.16	2823.78	2099.49
13/05/2025	17:00:00	3382	880	80.7	3.92	614.34		2389	2899.71	2899.71	2449.5	1822.17
13/05/2025	18:00:00	1824	490	78.5	1.26	348.42		1099	1144.71	1596.59	1144.71	1080.27
13/05/2025	19:00:00	570	160	77.8	5.3	67.11		411	444.48	444.48	496.7	506.94
13/05/2025	20:00:00	342	90	77	2.98	0		289	279.15	279.15	265.02	325.42
13/05/2025	21:00:00	342	90	79.4	0	0		22	64.36	64.36	83.59	66.69
13/05/2025	22:00:00	75.99999999	20	85.6	-0.01	0		0	0			
13/05/2025	23:00:00	38	20	83.4	-5	0		0	0			
14/05/2025	00:00:00	0	0	79.6	-10.24	0		0	0			
14/05/2025	01:00:00	0	0	81.6	-0.02	0		0	0			
14/05/2025	02:00:00	0	0	84.1	-0.01	0		0	0			
14/05/2025	03:00:00	0	0	84.7	-0.02	0		0	0			
14/05/2025	04:00:00	0	0	85.8	-0.07	0		0	0	26.3	15.16	
14/05/2025	05:00:00	0	0	86.1	-0.15	35.59		29	15.16	226.87	64.88	
14/05/2025	06:00:00	76	20	84	-0.01	78.96		44	292.14	457.7	292.14	
14/05/2025	07:00:00	114	30	82.6	-0.01	53.65		253	568.24	850.02	800.77	
14/05/2025	08:00:00	266	70	79.9	0.01	133.41		386	1051.55	2098.87	1438.79	

14/05/2025	09:00:00	342	90	79	1.29	230.07	436	
895.76		3385.78		1051.55				
14/05/2025	10:00:00	342	100	81.5	0.39	189.7	482	
346.36		3850.18		1206.85				
14/05/2025	11:00:00	456	110	84	1.06	187.56	1266	
963.05		4236.99		895.76				
14/05/2025	12:00:00	1140	300	77.2	-0.02	404.25	984	
922.27		1781.5	346.36					
14/05/2025	13:00:00	874	230	75.8	-0.11	248.67	802	
877.89	877.89	963.05	212.22					
14/05/2025	14:00:00	684	190	77.8	-0.11	379.22	2675	
1046.17		1046.17		922.27	428.29			
14/05/2025	15:00:00	2850	750	77.4	-0.21	895.95	4313	
2741.12		2741.12		1456.74		1067.57		
14/05/2025	16:00:00	4408	1160	75.9	-0.17	1200.87		
1758	1959.35		832.51	1959.35		1694.06		
14/05/2025	17:00:00	1596	420	74.7	-0.01	403.6	1304	
1620.8	986.49	2543.31		1620.8				
14/05/2025	18:00:00	1064	280	73.6	-1.06	231.5	965	
868.86	868.86	728.92	1501.04					
14/05/2025	19:00:00	608	180	74.9	-5.46	87.89	481	
505.35	505.35	663.22	595.45					
14/05/2025	20:00:00	456	120	74.8	-10.01	7.88	68	
95.46	95.46	220.69	194.96					
14/05/2025	21:00:00	114	30	74.9	-13.91	0	13	
38.15	91.49	38.15	83.36					
14/05/2025	22:00:00	38	10	75.9	-16.59	0	0	0
2.49	5.76	6.35						
14/05/2025	23:00:00	38	10	75	-13.52	0	0	0
15/05/2025	00:00:00	0	0	76.6	-11.97	0	0	0
15/05/2025	01:00:00	0	0	79.1	-5	0	0	0
15/05/2025	02:00:00	0	0	78.7	-2.42	0	0	0

15/05/2025	03:00:00	0	0	77.9	-6.04	0	0	0
15/05/2025	04:00:00	0	0	79.9	-8.35	7.85	3	
21.35		25.71	21.35					
15/05/2025	05:00:00	37.99999999	10	80.9	-7.6	45.41		65
89.69		117.37	89.69					
15/05/2025	06:00:00	114	40	83.2	-5.01	83.52	225	
285.81		316.1	285.81					
15/05/2025	07:00:00	228	70	83.4	-0.88	63.32	655	
664.54		931.24	664.54					
15/05/2025	08:00:00	532	140	81.2	-0.29	239.48	1385	
1593.68			1917.98		1593.68			
15/05/2025	09:00:00	1064	280	75.3	-0.2	544.95	2522	
2496.6		2961.38		2496.6				
15/05/2025	10:00:00	2432	640	73.6	-0.2	775.44	3707	
3224.53			3224.53		3009.15			
15/05/2025	11:00:00	3610	950	78.5	1.99	1056.61		
4667	4032.31			3027.71		4032.31		
15/05/2025	12:00:00	4826	1270	66.7	0.94	1336.35		
5176	4550.51			2333.66		4550.51		
15/05/2025	13:00:00	5396	1420	64.9	0.77	1457.82		
4785	4466.08		4466.08		546.46	4643.07		
15/05/2025	14:00:00	5244	1380	63.3	0	1314.9	2344	
2486.67		2486.67		448.45	3919.27			
15/05/2025	15:00:00	2318	620	64.5	0	458.67	637	
824.98	824.98	835.17	2666.53					
15/05/2025	16:00:00	570	160	64.3	0.37	97.67	955	
900.11	900.11	1467.82		1491.88				
15/05/2025	17:00:00	874	230	63.9	1.48	140.54	816	656
656	1524.63		1052.37					
15/05/2025	18:00:00	760	190	64.5	3.36	143.37		
1342.338539	983.16		536.6	983.16	726.47			
15/05/2025	19:00:00	456	120	66.9	-0.01	90.3		
1338.281648	474.36		338.26	474.36	489.87			
15/05/2025	20:00:00	304	90	73.2	0.01	31.64		
1334.224757	246.34		192.23	246.34	291.33			

15/05/2025	21:00:00	190	70	76.6	0.26	0			
1330.167866	54.55		53.51	54.55	74.92				
15/05/2025	22:00:00	114	40	80.3	1.24	0		0	2.27
3.97	2.27	5.07							
15/05/2025	23:00:00	0	0	82.2	3.83	0		0	0
16/05/2025	00:00:00	38	10	80.1	8.19	0		0	0
16/05/2025	01:00:00	0	0	76.2	10.33	0			0
16/05/2025	02:00:00	0	0	74.2	6.17	0			0
16/05/2025	03:00:00	0	0	78.6	4.53	0		0	0
16/05/2025	04:00:00	0	0	82.6	4.62	11.03		3	
32.72		32.72	37.77						
16/05/2025	05:00:00	75.99999999	20	85.7	5.19	63.01			69
118.91		118.91	188.69						
16/05/2025	06:00:00	114	50	87.5	20.59	152.38		172	
204.19		204.19	519.32						
16/05/2025	07:00:00	228	60	90.9	71.98	286.65		519	
724.52	724.52	742.63	1150.96						
16/05/2025	08:00:00	342	90	120.1	150	412.17		1344	
1976.41		1976.41		2002.69		2007.03			
16/05/2025	09:00:00	1026	280	34.4	102.6	421.71		2695	
3212.8	3212.8	3248.31		3045.63					
16/05/2025	10:00:00	2584	690	0	55.32	856.93		3957	
4205.94		4205.94		4258.8	3693.97				
16/05/2025	11:00:00	4028	1050	44.7	41.52	1214.1		4731	
4979.3	4979.3	5041.58		3894.68					
16/05/2025	12:00:00	5016	1320	83.4	10.5	934.35		5175	
5426.79		5426.79		5531.82		5068.69			
16/05/2025	13:00:00	5510	1450	77.8	8.27	956.6		5264	
5599.48		5599.48		5711.39		5660.51			
16/05/2025	14:00:00	5548	1460	76.8	10.13	1250.49			
5044	5450.72		5450.72		5555.56		5506.44		

16/05/2025	15:00:00	5206	1370	78	4.27	892.77	4438	
4952.8	4952.8	5062.75		5008.4				
16/05/2025	16:00:00	4408	1160	78.3	4.17	506.86	3537	
4156.2	4156.2	4221.34		4102.4				
16/05/2025	17:00:00	3230	860	76.9	5.29	524.91	2292	
3039.75		3039.75		3080.25		2931.13		
16/05/2025	18:00:00	1710	450	77.1	25.01	283.84	1063	
1618.26		1618.26		1642.78		1630.41		
16/05/2025	19:00:00	456	120	79.4	38.04	229.37	353	
331.63	331.63	342.44	351.4					
16/05/2025	20:00:00	266	70	81.2	27.94	134.76	150	
168.08	168.08	180.79	309.12					
16/05/2025	21:00:00	228	60	82.1	15.67	42.85	49	
82.36	82.36	89.61	114.09					
16/05/2025	22:00:00	76	20	81.3	15.21	1.94	0	9.26
9.26	8.97	10.33						
16/05/2025	23:00:00	38	10	78.9	13.27	0	0	0
17/05/2025	00:00:00	38	10	76.8	10.95	0	0	0
17/05/2025	01:00:00	0	0	75.9	7.84	0		0
17/05/2025	02:00:00	0	0	76.6	6.86	0		0
17/05/2025	03:00:00	0	0	76.9	4.04	0	0	0
17/05/2025	04:00:00	0	0	77.1	2.91	0	6	
20.18		20.18	25.69					
17/05/2025	05:00:00	76	20	79	2.99	0	101	
122.32		122.32	76.78					
17/05/2025	06:00:00	152	50	78.1	3.86	0	312	
345.95		345.95	237.92					
17/05/2025	07:00:00	342	90	77.2	7.99	0	602	
682.62		925.44	682.62					
17/05/2025	08:00:00	418	110	81	15.74	0	1358	
1489.48			2031.78		1489.48			

17/05/2025	09:00:00	950	280	83.9	12.94	434.57	2597	
2319.55		3275.76		2319.55				
17/05/2025	10:00:00	2546	670	77.9	4.22	829.87	3967	
3815.43		3815.43		3720.21		3324.34		
17/05/2025	11:00:00	3914	1020	76.8	2.2	861.66	4774	
4816.47		3659.71		4816.47		3779.24		
17/05/2025	12:00:00	4940	1300	76.2	-0.01	960.37	4755	
5144.94		3514	5628.21		5144.94			
17/05/2025	13:00:00	5016	1320	92.1	-0.33	955.51	5271	
5641.6	4013.8	5775.45		5641.6				
17/05/2025	14:00:00	5586	1470	90.9	-0.3	918.05	4957	
5473.4	3680.3	5473.4	5513.24					
17/05/2025	15:00:00	5092	1350	84.8	-0.01	804.45	4397	
4931.35		3585.19		4931.35		5017.06		
17/05/2025	16:00:00	4370	1140	75.4	1.29	658.67	3486	
3303.85		3303.85		4186.95		4230.7		
17/05/2025	17:00:00	3154	830	73.6	3.1	513.32	2270	
2344.6	2344.6	3049.76		3106.93				
17/05/2025	18:00:00	1672	440	70.6	7.82	356.03	1061	
1559.18		1559.18		1630.38		1668.74		
17/05/2025	19:00:00	456	130	71.2	15.93	244.45	352	
375.49	805.67	339.24	375.49					
17/05/2025	20:00:00	266	70	69.7	12.9	152.21	147	
183.72	403.74	183.72	203.61					
17/05/2025	21:00:00	228	60	71.5	9.29	51.72	53	
90.82	130.37	90.82	98.75					
17/05/2025	22:00:00	76	30	71.6	8.53	3.31	0	
10.56	12.08	10.56	9.44					
17/05/2025	23:00:00	38	0	65.7	7.47	0	0	0
18/05/2025	00:00:00	38	10	62.9	4.18	0	0	0
18/05/2025	01:00:00	0	0	61.5	2	0		0
18/05/2025	02:00:00	0	0	62.6	1.4	0		0

18/05/2025	03:00:00	0	0	64.9	1.51	0	0	0
18/05/2025	04:00:00	0	0	65.1	1.99	11.99	1	
28.81		28.81	35.79					
18/05/2025	05:00:00	75.99999999	20	65.5	3.62	57.63		115
119.67		119.89	119.67					
18/05/2025	06:00:00	152	50	66.7	3.69	111.94	260	
305.63		305.63	208.91					
18/05/2025	07:00:00	304	80	72.6	5	235.54	608	
917.07		917.07	973.82					
18/05/2025	08:00:00	456	120	77.9	6.02	390.19	1371	
1272.64			1272.64		1984			
18/05/2025	09:00:00	1026	280	78.5	6.37	569.81	2730	
2682.74			2343.59		2682.74			
18/05/2025	10:00:00	2584	680	72.8	5.04	750.17	4048	
3956.18		3956.18		3061.1	2971.43			
18/05/2025	11:00:00	3990	1040	67.6	2.32	901.28	3968	
4281.82		4281.82		3150.59		3733.32		
18/05/2025	12:00:00	3800	1000	67.2	1.86	984.51	4133	
3923.98		3923.98		3643.44		4594.91		
18/05/2025	13:00:00	4674	1240	68.9	0.24	986.27	4721	
4722.98		3788.31		4722.98		5227.56		
18/05/2025	14:00:00	4940	1290	69	-1.96	939.97	4513	
3704.7	3704.7	5486.57		5518.37				
18/05/2025	15:00:00	4522	1190	73.7	-2.23	832.8	4245	
3210.24		3210.24		5083.81		5088.56		
18/05/2025	16:00:00	4218	1110	74.7	-0.02	737.74	3454	
3760.51		3760.51		4271.77		4267.44		
18/05/2025	17:00:00	3154	830	72.6	2.46	548.78	2261	
3077.95		3077.95		3119.25		3133.51		
18/05/2025	18:00:00	1672	440	71.3	7.1	380.12	1069	
1650.07		1650.07		1672.2	1695.87			
18/05/2025	19:00:00	456	120	72.5	9.87	237.91	377	
355.91	355.91	369.49	381.42					
18/05/2025	20:00:00	304	90	75.2	12.86	152.15	158	
191.38	191.38	193.5	206.87					

18/05/2025	21:00:00	190	50	77.6	13.71	53.24	59	
101.39	101.39	104.44	110.64					
18/05/2025	22:00:00	114	30	81.2	13.3	4.56	1	
12.51	12.51	12.67	13.9					
18/05/2025	23:00:00	38	10	78.9	10.43	0	0	0
18/05/2025	00:00:00	0	10	78.3	8.06	0	0	0